PROCEEDINGS
of the

Twelfth
International Tissue Elasticity Conference™

Lingfield, UK
October 1 – 4, 2013

PROCEEDINGS

of the

Twelfth International Tissue Elasticity Conference™

Lingfield, UK
October 1–4, 2013

Table of Contents

QUESTIONS OR COMMENTS ARE WELCOME AT ANY TIME AT <secretariat@elasticityconference.org>

FOREWORD

By the year 2000, it was clear that a small but highly innovative international group of researchers were making rapid progress toward the goal of imaging the elastic properties of tissue. So planning began for the First International Conference on the Ultrasonic Measurement and Imaging of Tissue Elasticity™ (now ITEC, International Tissue Elasticity Conference™) with an exciting set of results waiting to be discussed, but great uncertainty as to how many scientists and clinicians would actually register and attend the inaugural session in Niagara Falls, Canada, in October 2002. In fact nearly 100 delegates, including academicians, students, physicians and commercial representatives attended and the 3 days of presentations displayed a high level of scientific rigor, innovation and diagnostic promise. The stated goals of the First International Conference were "to advance the field of measurement and imaging of the elastic attributes of soft tissues through tutorials and scientific presentations of the state of the art in the field". Furthermore, it was stated that "we expect that the conference will provide a unique and unified forum that will bring together researchers from several countries and that it will ultimately contribute to the rapid development and clinical introduction of this new medical imaging technology".

The subsequent years have seen a robust forward movement from laboratory developments, to specialized platforms, to clinical trials, and ultimately to approved devices in the hands of clinicians, for the benefit of the patients they serve. The fact that we are gathering for the 12th ITEC is a testimony to the growing impact of the field, and the usefulness of this unique forum for disseminating the newest developments and research directions.

Many volunteers and colleagues worked diligently to make each of the past 12 Conferences a success including this year's. We are grateful to all those individuals and entities that have participated and served as organizers, sponsors, reviewers, session chairs, and contributors.

At 12, ITEC is entering adolescence, just as the research and clinical developments in our field are likewise coming out of "early childhood". For organizations, this phase is the ideal time to establish new leadership and fresh energy and ideas. Thus, it is our great pleasure to welcome our distinguished colleague, Dr. Jeffrey Bamber, as the new ITEC Organizer. With the continued growth of the field, along with your participation and Dr. Bamber's leadership, we are more optimistic than ever for the positive and unique role of ITEC and for its continued future success.

Jonathan Ophir
Founding Organizer

Kevin J. Parker
Founding Organizer

Lingfield, UK, October 1, 2013

Welcome

Dear Conference Delegate:

On behalf of the local and general organizing teams, welcome to the 12th annual International Tissue Elasticity Conference™ (ITEC™) and to the tranquil village of Lingfield, Surrey, England. We started planning this conference in March 2013, as you may have been able to tell by some of the very short deadlines that we gave you, for abstract submission etc. Thank you for adjusting to this exceptionally short timescale and thus proving that ITEC remains a priority in your scientific calendar. The result has been that ITEC this year will be as successful as ever, which has typically varied around a 100 delegates, continuing the tradition of bringing together academics, students, physicians and commercial representatives for three and a half days of high quality presentations and discussions at the forefront of the subject in a friendly atmosphere that stimulates discussion, innovation and collaboration.

Past ITECs have been held in varying types of location: near waterfalls, mountain ski resorts, by lakesides and at the seaside. This time, we have chosen an off–season race course not far from London, to provide a peaceful and spacious view from the conference centre and hotel rooms. Lingfield is 27 miles south of central London in the county of Surrey, close to the border with the neighboring county of Kent. Both counties are rich in history, documented through Saxon and Roman times. However, the many Tudor buildings provide a characteristic "look" to the villages, and Lingfield is no exception. The landscape is undulating with woodland and green fields. Moving into Kent, known as the garden of England, one increasingly finds orchards and hop farms; if you wonder what the buildings are that have a typically conical appearance with a little white tilted cone on top, they are called oast houses, and they are used for drying hops in the manufacture of ale and beer. We hope that you will find the time to explore some of the woodland walks and the rich density of historic buildings in the area such as Hever Castle (on our front cover this year), Knole (15th century country house) and Chartwell (family home and garden of Sir Winston Churchill). For the free evening this year we are providing buses to Royal Tunbridge Wells, a lively Georgian spa town rich in history with characteristic architecture in "The Pantiles" which used to house a spa of spring waters containing salts of iron. We hope you enjoy the experience.

As mentioned in the Foreword from Jonathan Ophir and Kevin Parker on the previous page, this 12th ITEC is a transitionary conference, representing a hand–over of leadership. I am certain that you will join me in thanking Jonathan and Kevin for conceiving this fantastic meeting and nurturing "their baby" to become the exciting annual event that it now is, succeeding in achieving the worthy values so eloquently expressed in their Foreword. I am most grateful for their vote of confidence, and I will do my utmost to uphold these values and traditions, as well as, with your help and guidance, explore new ways in which ITEC can best serve researchers and practitioners in the field tissue elasticity measurement and imaging. ITEC's role will evolve as we move from a period of exploration of concept, seeking evidence of clinical value and commercial availability of first–generation devices, towards refinement, extension of capability, consolidation in application and a greater understanding of how best to use elasticity methods in clinical practice. Therefore, please complete the feedback forms in this Proceedings book. They will be of immense value to us as we plan future ITECs.

I am delighted to welcome this year's first–day tutorial speakers: Andy Evans (Ninewells Hospital and University of Dundee, Dundee, Scotland, UK) and Jonathan Ophir (University of Texas Medical School, Houston, Texas, USA). Jonathan and his group invented a method for imaging strains in tissues which he named Elastography; in later years, the term elastography was broadened to include many types of elasticity imaging. However, his role as ITEC organizer interfered with his giving a tutorial. It is wonderful that he can now teach us some of the finer details and likely future of elastography. Andy will complement this with a look at shear wave speed imaging of the breast from a clinical perspective, in which he has gained great experience and insight. It is a substantial task to prepare an ITEC tutorial, and I am grateful to them both for agreeing to pass on their knowledge and experience.

For this transitionary Conference, Jonathan has also accepted my invitation to briefly review the past eleven ITECs, reminding us of were we began, the aims of ITEC and providing us with an opportunity to take stock of how ITEC has developed, so that we may consider future directions. You will find this in the program at 11:30am on Day 3.

Our Conference dinner will be accompanied by jazz standards and close harmony singing from The London Moonlight Trio, and followed by a special interest presentation from Francis Duck on the life and work of renaissance scientist Giovanni Alfonso Borelli, "father of biomechanics". Many of you will know Francis' work on Doppler, tissue characterization, ultrasound safety and non–linear effects, as well as his book on the Physical Properties of Tissue, and his extensive contribution to medical physics (for which he was awarded an MBE in the 2007 Queen's Birthday Honours List). Now you will discover his contagious interest in the history of medical physics. I am very excited that Francis has agreed to give this lecture.

Many volunteers and colleagues have helped to bring about this conference, especially our new conference secretary, Cheryl Taylor. She has worked tirelessly, having to learn as well as do and has achieved it all in an incredibly short time. Please do me a favor and stop by the Conference desk, chat with Cheryl and tell her that "Jeff said thanks!" Also, don't be fooled by the stated hand–over of leadership. We could not have run ITEC 2013 without the so–called past organizers who have been heavily involved in "showing us the ropes" by example. In particular, without Karen Ophir's generous volunteering of her personal time, inexhaustible energy and painstaking attention to detail, this conference would not have been possible. Karen, thank you so much! Sadly, Karen will not be able visit the UK this year. However, as last year, we hope and expect that she will be able to attend some ITEC events via Skype.

It is a pleasure also to acknowledge contributions from the administration of the Institute of Cancer Research, especially Emily Bushby and Alan Hill for assistance in financial and legal matters and Neil Walford and James Storey for audio–visual assistance. Finally, we are grateful to all those who have participated as helpers, sponsors, reviewers, session chairs, award judges and contributors.

The local and general organizing teams hope that you will be inspired by the presentations and discussions during the 12th ITEC, make new friends, establish productive collaborations and renew old acquaintances in the restful and pleasant surroundings of the English countryside.

Jeffrey Bamber
Chair of the Local Organizing Team and General Conference Organizer
Lingfield, UK, October 1, 2013

CONFERENCE–AT–A–GLANCE

Twelfth International Tissue Elasticity Conference™

Lingfield Park Marriott Hotel – Lingfield, UK October 1–4, 2013

Tuesday, October 1		**9:00A – 8:00P**	
9:00A – 12:00P	**Set Up:**	Oral Presenters load presentations (CD or jump drive)	Pavilion Ste 1 & 2
		Poster Presenters set up presentations	Pavilion Suite 3 & 4
9:00A – 8:00P		Registration Desk Open	Pavilion Suite Foyer
11:00A – 8:00P	**Session EEX:**	Equipment Exhibit *(during breaks & Reception)*	Pavilion Suite 3 & 4
12:00P – 2:00P	**Session TUT:**	**Tutorials: Medical and Scientific Challenges in Elastography**	Pavilion Suite 1 & 2
2:00P – 2:30P		*Coffee Break*	Pavilion Suite 3 & 4
2:30P – 4:30P	**Session SAS:**	**Oral Presentations of Finalists for Student Awards Session**	Pavilion Suite 1 & 2
4:30P – 5:00P		*Recess*	
5:00P – 6:00P	**Session POS:**	**Poster Session – Live Oral Summaries**	Pavilion Suite 3 & 4
6:00P – 8:00P		*Opening Dinner Reception*	Trackside Restaurant
Wednesday, October 2		**8:30A – 10:00P**	
8:30A – 5:30P		Registration Desk Open	Pavilion Suite Foyer
8:30A – 5:30P	**Session POS:**	Posters	Pavilion Suite 3 & 4
8:30A – 5:30P	**Session EEX:**	Equipment Exhibit	Pavilion Suite 3 & 4
8:30A – 8:45A		**Opening Remarks**	Pavilion Suite 1 & 2
8:45A – 10:30A	**Session MIP–1:**	**Methods for Imaging Elastic Tissue Properties**	Pavilion Suite 1 & 2
10:30A – 11:00A		*Coffee Break*	Pavilion Suite 3 & 4
10:11A – 11:45A	**Session SIP:**	**Signal and Image Processing**	Pavilion Suite 1 & 2
11:45A – 1:15P		*Group Lunch*	Track Side Restaurant
1:15P – 3:15P	**Session MPT:**	**Mechanical Properties of Tissues – I**	Pavilion Suite 1 & 2
3:15P – 3:45P		*Coffee Break*	Pavilion Suite 3 & 4
3:45P – 5:23P	**Session CAA–1:**	**Clinical and Animal Applications – I**	Pavilion Suite 1 & 2
7:00P – 10:00P		*Conference Dinner featuring The London Moonlight Trio and Invited Presentation by Francis Duck*	Pavilion Suite 1 & 2
Thursday, October 3		**9:00A – 5:00P**	
9:00A – 4:00P		Registration Desk Open	Pavilion Suite Foyer
9:00A – 4:00P	**Session POS:**	Posters	Pavilion Suite 3 & 4
9:00A – 4:00P	**Session EEX:**	Equipment Exhibit	Pavilion Suite 3 & 4
9:00A – 10:15A	**Session CVE:**	**Cardiovascular Elasticity**	Pavilion Suite 1 & 2
10:15A – 10:45A		*Coffee Break*	Pavilion Suite 3 & 4
10:45A – 11:05A		**ITEC at 12** *Invited Presentation*	Pavilion Suite 1 & 2
11:05A – 11:42A	**Session FIP:**	**Forward and Inverse Problems**	Pavilion Suite 1 & 2
11:43A – 1:15P		*Group Lunch*	Track Side Restaurant
1:15P – 1:45P		**ITEC Announcements** including **Student Best Paper Award Recipients**	Pavilion Suite 1 & 2
1:45P – 3:22P	**Session MIP–2:**	**Methods for Imaging Elastic Tissue Properties – II**	Pavilion Suite 1 & 2
3:23P – 4:00P		*Coffee Break*	Pavilion Suite 3 & 4
4:00P – 5:00P		*Group Photo*	TBA
6:00P – 6:30P		*Coach to Royal Tunbridge Wells for free evening*	
Friday, October 4		**9:00A – 10:00P**	
9:00A – 4:30P		Registration Desk Open	Pavilion Suite Foyer
9:00A – 4:30P	**Session POS:**	Posters	Pavilion Suite 3 & 4
9:00A – 4:30P	**Session EEX:**	Equipment Exhibit	Pavilion Suite 3 & 4
9:00A – 10:07A	**Session CAA–2:**	**Clinical and Animal Applications – II**	Pavilion Suite 1 & 2
10:08A – 10:45A		*Coffee Break*	Pavilion Suite 3 & 4
10:45A – 12:22P	**Session MMT:**	**Mechanical Measurement Techniques for Tissue**	Pavilion Suite 1 & 2
12:23P – 2:00P		*Group Lunch*	Track Side Restaurant
2:00P – 3:52P	**Session MIP–3:**	**Methods for Imaging Elastic Tissue Properties – III**	Pavilion Suite 1 & 2
3:53P – 4:30P		*Coffee Break*	Pavilion Suite 3 & 4
6:30P – 10:00P		*Closing Reception (Proceedings Book Signing)*	Pavilion Patio

PROGRAM

Twelfth International Tissue Elasticity Conference™

Lingfield, UK
October 1 – 4, 2013

Tuesday, October 1 9:00A – 8:00P

9:00A – 12:00P Presentation & Exhibit Set Up
All Oral Presenters load presentations onto Conference computers — Pavilion Suite 1 & 2
Poster Presenters set up presentations — Pavilion Suite 3 & 4
Exhibitors set up exhibits — Pavilion Suite 3 & 4

9:00A – 8:00P
Registration Desk Open — Pavilion Suite Foyer

11:00A – 12:00P 2:00P – 2:30P 4:30P – 5:00P 6:00P – 8:00P
Session EEX: Equipment Exhibit — Pavilion Suite 3 & 4

Tuesday 12:00P – 2:00P
Session TUT: Tutorials: Medical and Scientific Challenges in Elastography

Chair: W Weitzel, USA *Co–Chair: E Brusseau, France* Pavilion Suite 1 & 2

Page No.

12:00P – 12:45P

085 SHEAR WAVE ELASTOGRAPHY OF THE BREAST IN PRACTICE AND BEYOND THE OBVIOUS. 22
A Evans[1].*
[1]Ninewells Hospital & Medical School, University of Dundee, Dundee, Scotland, UK.

12:45P – 1:00P Discussion

1:00P – 1:45P

083 ELASTOGRAPHY: OLDIE–BUT–GOODIE AND GETTING BETTER. 23
J Ophir[1].*
[1]University of Texas Medical School, Houston, TX, USA.

1:45P – 2:00P Discussion

2:00P – 2:30P
COFFEE BREAK — Pavilion Suite 3 & 4

Tuesday 2:30P – 4:30P
Session SAS: Oral Presentations of Finalists for Student Awards Session

Chair: J Ophir, USA *Co–Chair: JL Gennisson, France* Pavilion Suite 1 & 2

Page No.

2:30P – 2:45P

009 ULTRAFAST PLANE WAVE ELASTOGRAPHY USING TRANSVERSE OSCILLATIONS FOR THE NON–INVASIVE MECHANICAL CHARACTERIZATION OF CAROTID PLAQUE. 24
J Porée[1,2], B Chayer[1], J Ohayon[3], D Garcia[1,2], G Cloutier[1,2].*
[1]University of Montréal Hospital Research Center, Montréal, Québec, CANADA; [2]University of Montréal, Montréal, Québec, CANADA; [3]University Joseph–Fourier, Grenoble, FRANCE.

(Session SAS continues on next page)

(Session SAS continued from previous page)

2:45P – 3:00P

015 ABDOMINAL AORTIC ANEURYSM FOLLOW–UP AFTER ENDOVASCULAR REPAIR IN A CANINE MODEL WITH NON–INVASIVE VASCULAR ELASTOGRAPHY. 25
E Salloum[1], A Bertrand–Grenier[1], S Lerouge[2], C Kauffmann[1], G Cloutier[1], G Soulez[1].*
[1]University of Montréal Hospital Research Center, Montréal, Québec, CANADA; [2]École de Technologie Supérieure, Montréal, Québec, CANADA.

3:00P – 3:15P

034 ABDOMINAL AORTIC ANEURYSM FOLLOW–UP BY DYNAMIC ELASTOGRAPHY AFTER ENDOVASCULAR REPAIR. 26
A Bertrand–Grenier[1,2], E Salloum[1,2], S Lerouge[1,2], P Lequoy[1,2], C Kauffmann[1,2], G Cloutier[1,2], G Soulez[1,2].*
University of Montréal Hospital Research Center, Montréal, Québec, CANADA; University of Montréal, Montréal, Québec, CANADA.

3:15P – 3:30P

036 ASSESSMENT OF CUTANEOUS SCLEROTIC DISORDERS USING ARFI SWEI. 27
SY Lee[1], AR Cardones[2], J Hooten[2], JR Doherty[1], KR Nightingale[1], ML Palmeri[1].*
[1]Duke University, Durham, NC, USA; [2]Duke Medical Center, Durham, NC, USA.

3:30P – 3:45P

052 ESTIMATING ELECTROMECHANICAL WAVE VELOCITY VECTOR FIELDS WITH ELECTROMECHANICAL WAVE IMAGING: AN *IN VIVO* FEASIBILITY STUDY. 28
A Costet[1], EE Konofagou[1].*
[1]Columbia University, New York, NY, USA.

3:45P – 4:00P

053 SHEAR STRAIN IMAGING IN PROSTATE MR ELASTOGRAPHY. 29
RS Sahebjavaher[1], M Honarvar[1], A Bylinski[1], G Nir[1], H Moradi[1], LO Gagnon[1], R Sinkus[2], SE Salcudean[1].*
[1]University of British Columbia, Vancouver, CANADA; [2]Kings College London, London, England, UK.

4:00P – 4:15P

056 ACCOUNTING FOR MASS IN VISCOELASTIC STRAIN RESPONSE (ViSR) ULTRASOUND. 30
MR Scola[1], TJ Czernuszewicz, CM Gallippi[1].*
[1]The University of North Carolina at Chapel Hill, Chapel Hill, NC, USA.

4:15P – 4:30P

060 ELECTROMECHANICAL WAVE IMAGING IDENTIFIES BIVENTRICULAR PACING AND TREATMENT RESPONSE/NONRESPONSE IN HEART FAILURE PATIENTS UNDERGOING CARDIAC RESYNCHRONIZATION THERAPY. 31
EA Bunting[1], LK Lambrakos[1], F Sera[1], EE Konofagou[1].*
[1]Columbia University, New York, NY, USA.

4:30P – 5:00P

Recess

Tuesday 5:00P – 6:00P

(Posters will be available for viewing and Coffee Break Discussion through the afternoon Coffee Break, Friday, October 4)

Session POS: Poster Session – Live Oral Summaries

Chair: R Souchon, France *Co–Chair: M Fatemi, USA* Pavilion Suite 3 & 4

Page No.

5:00P – 5:02P

004 DEVELOPMENT OF A SET OF PHANTOMS MIMICKING THE STIFFNESS OF HUMAN BIOLOGICAL SOFT TISSUES USING MAGNETIC RESONANCE ELASTOGRAPHY (MRE). 32
GE Leclerc[1], SF Bensamoun[1].*
[1]Université de Technologie de Compiègne, Compiègne, FRANCE.

5:02P – 5:04P

5:04P – 5:06P

5:06P – 5:08P

5:08P – 5:10P

5:10P – 5:12P

5:12P – 5:14P

5:14P – 5:16P

5:16P – 5:18P

5:18P – 5:20P

(Session POS continues on next page)

** indicates Presenter*

(Session POS continued from previous page)

5:20P – 5:22P

040 SHEAR WAVE VISCOELASTICITY MEASUREMENT BY LASER SPECKLE CONTRAST DETECTION. 42

Y Cheng[1], S Li[1], RJ Eckersley[2], DS Elson[1], MX Tang[1].*
[1]Imperial College London, London, England, UK; [2]King's College London, London, England, UK.

5:22P – 5:24P

076 QUANTITATIVE MICROELASTOGRAPHY USING A MULTI–CHANNEL OPTICAL COHERENCE TOMOGRAPHY. 43

E Elyas[1,2], JT Erler[3], SP Robinson[2], TR Cox[3], D Woods[4], PClowes[1], JC Bamber[1,2].*
[1,2]The Institute of Cancer Research and The Royal Marsden NHS Foundation Trust, Sutton, Surrey, England, UK; [3]University of Copenhagen, Copenhagen, DENMARK; [4]Michelson Diagnostics Ltd, Orpington, Kent, England, UK.

5:24P – 6:00P **Discussion**

Tuesday 6:00P – 8:00P
Opening Dinner Reception

Pavilion Suite 3 & 4

Wednesday, October 2 8:15A – 10:00P

8:30A – 5:30P

Registration Desk Open — Pavilion Suite Foyer

8:30A – 5:30P **Session POS: Posters** — Pavilion Suite 3 & 4

Session EEX: Equipment Exhibit — Pavilion Suite 3 & 4

Wednesday 8:15A – 8:30A
OPENING REMARKS

J Ophir, JC Bamber — Pavilion Suite 1 & 2

Wednesday 8:45A – 10:30A
Session MIP–1: Methods for Imaging Elastic Tissue Properties – I

Chair: TJ Hall, USA *Co–Chair: A Milkowski, USA* — Pavilion Suite 1 & 2

8:45A – 9:00A

011 NON–INVASIVE QUANTIFICATION OF LIVER FIBROSIS, ACTIVITY AND STEATOSIS STAGING BY USING SHEAR WAVE ELASTICITY AND VISCOSITY: A FEASBILITY STUDY. 44

T Deffieux[1], J–L Gennisson[1], L Bousquet[2], D Amroun[2], M Corouge[2], S Tripon[2], V Mallet[2], M Fink[1], P Sogni[2], S Pol[2], M Tanter[1].*
[1]Institut Langevin – Ondes et Images, Paris, FRANCE; [2]Université René Descartes Paris V, Hôpital Cochin, Paris, FRANCE.

9:00A – 9:15A

001 MAGNETIC RESONANCE ELASTOGRAPHY THROUGH ATHEROSCLEROSIS: THE PROGRESSION FROM COMPUTATIONAL SIMULATIONS TO EXPERIMENTAL FEASIBILITY. 45

L Thomas–Seale[1], P Kennedy[1], D Klatt[2], T Anderson[1], S Hammer[3], S Semple[1], S Mirsadraee[1], I Sack[2], P Pankaj[1], N Roberts[1], P Hoskins[1].*
[1]The University of Edinburgh, Edinburgh, Mid–Lothian, UK; [2]Charité–University Medicine Berlin, Berlin, GERMANY; [3]Heriot–Watt University, Edinburgh, Mid–Lothian, UK.

9:15A – 9:30A

016 A METHOD FOR DETERMINING TISSUE VISCOELASTICITY VIA SINGLE TRACK LOCATION ACOUSTIC RADIATION FORCE IMPULSE IMAGING. 46

JH Langdon[1], EC Elegbe[1], SA McAleavey[1].*
[1]University of Rochester, Rochester, NY, USA.

Page No.

9:30A – 9:45A

018 DYNAMIC ELASTOGRAPHY AND HYPER–FREQUENCY VISCOELASTIC SPECTROSCOPY OF A LIVER MIMICKING PHANTOM. 47

A Tang[1], E Montagnon[2], C Schmitt[3], AH Henni[3], D Olivié[1], H Castel[1], G Cloutier[2].*

[1]Hôpital St–Luc, University of Montréal, Montréal, Québec, CANADA; [2]University of Montréal Hospital Research Center (CRCHUM), Montréal, Québec, CANADA; [3]Rheolution Inc., Montréal, Québec, CANADA.

9:45A – 10:00A

022 IMAGING OF SHEAR WAVE INDUCED BY LORENTZ FORCE IN SOFT TISSUE. 48

P Grasland–Mongrain[1], R Souchon[1], F Cartellier[1], A Zorgani[1], JY Chapelon[1], C Lafon[1], S Catheline[1].*

[1]INSERM, U1032, Université de Lyon, Lyon, FRANCE.

10:00A – 10:15A

024 PASSIVE SHEAR WAVE ELASTOGRAPHY USING AN ULTRAFAST ULTRASOUND SCANNER. 49

A Zorgani[1], R Souchon[1], S Catheline[1].*

[1]INSERM, U1032, Université de Lyon, Lyon, FRANCE.

10:15A – 10:30A

025 A NEW DEVICE FOR MEASURING PROSTATE ELASTICITY *IN VIVO* COMBINING ACOUSTIC RADIATION FORCE AND MAGNETIC RESONANCE IMAGING: SIMULATION RESULTS. 50

H Latorre–Ossa[1], F Chavrier[1], S Chatelin[2], J–L Gennisson[2], AH Dinh[1], S Catheline[1], O Rouvière[3], R Souchon[1].*

[1]INSERM, U1032, Université de Lyon, Lyon, FRANCE; [2]Institut Langevin – Ondes et Images, Paris, FRANCE; [3]Hôpital Edouard Herriot, Lyon, FRANCE.

10:30A – 11:00A

COFFEE BREAK — Pavilion Suite 3 & 4

Wednesday 11:00A – 11:45A
Session SIP: Signal and Image Processing

Chair: R Daigle, USA — *Co–Chair: J Fromageau, UK* — Pavilion Suite 1 & 2

Page No.

11:00A – 11:15A

045 LATERAL DISPLACEMENT ESTIMATION USING MOMENTUM EQUATION CONSTRAINTS. 51

OA Babaniyi[1], PE Barbone[1], AA Oberai[2].*

[1]Boston University, Boston, MA, USA; [2]Rensselaer Polytechnic Institute, Troy, NY, USA.

11:15A – 11:30A

077 RSNA/QIBA: ULTRASOUND SHEAR WAVE SPEED ELASTIC PHANTOM RESULTS. 52

A Milkowski[1], TJ Hall[2], BS Garra[3].*

[1]Siemens Medical Solutions SA, Inc., Issaquah, WA, USA; [2]University of Wisconsin–Madison, Madison, WI, USA; [3]Food and Drug Administration, Silver Spring, MD, USA

11:30A – 11:45A

067 LOCALISED VIBRATION TAGGING (LOVIT) FOR CLUTTER REDUCTION IN EPIPHOTOACOUSTIC AND OTHER IMAGES. 53

M Jeager[1,2], M Frenz[2], JC Bamber[1].*

[1]The Institute of Cancer Research and The Royal Marsden NHS Foundation Trust, Sutton, Surrey, England, UK; [2]University of Bern, Bern, SWITZERLAND.

11:45A – 1:15P

GROUP LUNCH — Trackside Restaurant

** indicates Presenter*

Wednesday 1:15P – 3:15P
Session MPT: Mechanical Properties of Tissues

Chair: E Mazza, Switzerland *Co–Chair: H Latorre–Ossa, France* Pavilion Suite 1 & 2

Page No.

1:15P – 1:30P

006 ASSESSMENT OF THE RHEOLOGICAL MODEL OF COAGULATING BLOOD OVER A VERY LARGE BANDWIDTH BY COMBINING SWE AND CLASSICAL RHEOMETRY MEASUREMENTS. 54

M Bernal[1], JL Gennisson[1], M Fink[1], P Flaud[2], M Tanter[1].*

[1]Institut Langevin – Ondes et Images, Paris, FRANCE; [2]Université Paris VII Denis Diderot, Paris, FRANCE.

1:30P – 1:45P

007 GENERATION OF ADAPTIVE SHEAR WAVES WITH RADIATION FORCE USING OCTAGONAL PHASED ARRAY FOR BREAST CANCER CHARACTERIZATION: PROOF OF CONCEPT. 55

A Ouared[1,2], E Montagnon[1,2], A Hadj–Henni[1,3], G Cloutier[1,2,4].*

[1]University of Montréal, Montréal, Québec, CANADA; [3]Rheolotion Inc, Montréal, Québec, CANADA.

1:45P – 2:00P

019 ANALYTICAL AND NUMERICAL SIMULATIONS OF WAVE PROPAGATION USING VISCO–ELASTIC ANISOTROPIC GREEN'S FUNCTION FOR CARDIAC REMOTE ULTRASONIC ELASTOGRAPHY. 56

S Chatelin[1], C Papadacci[1], M Fink[1], M Tanter[1], J–L Gennisson[1], M Pernot[1].*

[1]Institut Langevin – Ondes et Images, Paris, FRANCE.

2:00P – 2:15P

031 MODELING RADIATION FORCE AND SHEAR WAVE PROPAGATION USING FRACTIONAL KELVIN–VOIGT MODEL. 57

W Zhang[1], S. Holm[1].*

[1]University of Oslo, Blindern, Oslo, NORWAY.

2:15P – 2:30P

032 CHANGES IN SHEAR WAVE SPEED PRE– AND POST–INDUCTION OF LABOR. 58

LC Carlson[1], H Feltovich[1,2], ML Palmeri[3], S Romero[2], TJ Hall[1].*

[1]University of Wisconsin–Madison, Madison, WI, USA; [2]Intermountain Healthcare, Intermountain Medical Center, Murray, UT, USA; [3]Duke University, Durham, NC, USA.

2:30P – 2:45P

003 CHARACTERIZATION OF THE DUCHENNE SKELETAL MUSCLE WITH MAGNETIC RESONANCE ELASTOGRAPHY (MRE). 59

SF Bensamoun[1], F Charleux[2], L Debernard[1], C Themar–Noel[3].*

[1]Université de Technologie de Compiègne, Compiègne, FRANCE; [2]ACRIM–Polyclinique Saint Côme, Compiègne, FRANCE; [3]Centre de Référence des Maladies Neuromusculaires Paris–Est, GH Pitié–Salpêtrière, FRANCE.

2:45P – 3:00P

005 THE USE OF ULTRASOUND ELASTOGRAPHY TO MONITOR THE EFFECTS OF NEOADJUVANT CHEMOTHERAPY ON LOCALLY ADVANCED BREAST CANCER. 60

A Di Battista[1], R English[2], L Winter[2], RF Adams[2], JA Noble[1].*

[1]Oxford University, Oxford, England, UK; [2]Oxford University Hospitals NHS Trust, Oxford, England, UK.

3:00P – 3:15P

017 *IN VIVO* EVALUATION OF THE ELASTIC ANISOTROPY OF THE HUMAN ACHILLES TENDON USING SHEAR WAVE SPECTROSCOPY. 61

J Brum[1], M Bernal[1], J–L Gennisson[1], M Tanter[1].*

[1]Institut Langevin – Ondes et Images, Paris, FRANCE.

3:15P – 3:45P
COFFEE BREAK Pavilion Suite 3 & 4

Wednesday 3:45P – 5:23P
Session CAA–1: Clinical and Animal Applications – I

Chair: EE Konofagou, USA *Co–Chair: F Duck, UK* Pavilion Suite 1 & 2

Page No.

3:45P – 4:00P

002 *IN–VIVO* ASSESSMENT OF THE BIOMECHANICAL PROPERTIES OF THE PREGNANT CERVIX. 62
S Badir[1], E Mazza[1], M Bajka[2].*
[1]Swiss Federal Institute of Technology Zurich, SWITZERLAND; [2]University Hospital Zurich, SWITZERLAND.

4:00P – 4:15P

020 CERVIX ELASTOGRAPHY: A NEW METHOD FOR THE PREDICTION OF PRETERM DELIVERY. 63
RL Maurice[1,2], P Delachartre[2], G Dubernard[3], C Huissoud[3], J Caloone[3].*
[1]Université de Montréal, Montréal, Québec, CANADA; [2]Université de Lyon, CREATIS, Lyon, FRANCE; [3]Croix Rousse University Hospital, Lyon, FRANCE.

4:15P – 4:30P

071 PROPOSITION OF A MULTIPARAMETRIC MODEL–BASED METHOD FOR BREAST LESION DIFFERENTIATION: A FEASIBILITY STUDY. 64
RL Maurice[1,2], E Brusseau[2], A Coulon[3], E Maissiat[3], M Devouassoux–Shisheboran[3], N Boublay[3], L Boussel[2,3].*
[1]Université de Montréal, Montréal, Québec, CANADA; [2]Université de Lyon, CREATIS, Lyon, FRANCE; [3]Hospices Civils de Lyon, Lyon, FRANCE.

4:30P – 4:37P

072 AXIAL SHEAR STRAIN ELASTOGRAPHY IN BENIGN AND MALIGNANT BREAST DISEASE: PRELIMINARY PROSPECTIVE FREEHAND *IN VIVO* DATA. 65
EG Khalil[1], AK Thittai[1], BS Garra[2], J Ophir[1].*
[1]The University of Texas Health Science Center at Houston, Houston, TX, USA; [2]Food and Drug Administration, Silver Spring, MD, USA.

4:38P – 4:53P

063 3D *IN VIVO* ARFI IMAGING OF THE PROSTATE USING A SIDE–FIRING ENDORECTAL ARRAY. 66
ML Palmeri[1], SJ Rosenzweig[1], SL Lipman[1], K Garcia–Reyes[1], A Buck[1], J Madden[1], T Polascik[1], ZA Miller[1], KR Nightingale[1].*
[1]Duke University, Durham, NC, USA.

4:53P – 5:08P

029 ASSISTING MRI–GUIDED PERCUTANEOUS PROCEDURES WITH ELASTOGRAPHY: DEVELOPMENT OF AN INTERVENTIONAL MR–ELASTOGRAPHY PROTOCOL. 67
N Corbin[1], Q Boehler[1], E Breton[1], L Barbé[1], P Renaud[1], M de Mathelin[1], J Vappou[1].*
[1]University of Strasbourg–CNRS, Strasbourg, FRANCE.

5:08P – 5:23P

051 ARFI SURVEILLANCE OF SUBCUTANEOUS HEMOSTASIS (ASSH) AT FEMORAL ARTERIOTOMY IN ASPIRIN–TREATED VERSUS NAIVE DOGS. 68
RE Geist[1], TC Nichols[1], MC Caughey[1], EP Merricks[1], CM Gallippi[1].*
[1]University of North Carolina at Chapel Hill, Chapel Hill, NC, USA.

Wednesday 7:00P – 10:00P
Conference Dinner, Musical Event & Interest Presentaion Pavilion Suite 1 & 2
Proceedings Book Signing

8:30P – 9:00P
Musical Event: *Selections performed by The London Moonlight Trio* Page No.

9:10P – 9:45P Invited Presentation

086 GOIVANNI ALFONSO BORELLI: RENAISSANCE ASTROPHYSICIST AND BIOENGINEER. 69
Francis Duck[1], MBE, Visiting Professor.*
[1]University of Bath, Bath, England, UK.

Thursday, October 3 9:00A – 5:00P

9:00A – 4:00P
Registration Desk Open Pavilion Suite Foyer
9:00A – 4:00P Session POS: Posters Pavilion Suite 3 & 4
Session EEX: Equipment Exhibit Pavilion Suite 3 & 4

Thursday 9:00A – 10:15A
Session CVE: Cardiovascular Elasticity
Chair: W Svensson, UK *Co–Chair: P Hoskins, UK* Pavilion Suite 1 & 2
Page No.

9:00A – 9:15A

035 THERMAL EXPANSION IMAGING FOR REAL–TIME LESION DEPTH ASSESSMENT DURING RF CATHETER ABLATION. 70
P Baki[1], G Székely[1], O Göksel[1].*
[1]Computer Vision Laboratory, ETH, Zurich, SWITZERLAND.

9:15A – 9:30A

037 A NOVEL 3D STRAIN RECONSTRUCTION AND EJECTION FRACTION ESTIMATION TECHNIQUE: *IN VIVO* FEASIBILITY. 71
SJ Okrasinski[1], JL Grondin[1], EE Konofagou[1].*
[1]Columbia University, New York, NY, USA.

9:30A – 9:45A

026 EFFECTS OF THE SAC GEOMETRY AND MODULUS CONTRAST ON THE REGIONAL PULSE WAVE PROPAGATION ALONG THE ANEURYSMAL ARTERIAL WALL *IN SILICO*. 72
D Shahmirzadi[1], I Jourard[1], EE Konofagou[1].*
[1]Columbia University, New York, NY, USA.

9:45A – 10:00A

041 PIECE–WISE PULSE WAVE VELOCITY MAPPING IN MURINE ATHEROSCLEROTIC AND ANEURYSMAL AORTAS USING PULSE WAVE IMAGING (PWI). 73
IZ Apostolakis[1], SD Nandlall[1], EE Konofagou[1].*
[1]Columbia University, New York, NY, USA.

10:00A – 10:15A

050 PULSE WAVE IMAGING OF STENOTIC CAROTID ARTERIES *IN VIVO* – A FEASIBILITY STUDY. 74
RX Li[1], P Narayanan[1], JK Salomon[1], JF McKinsey[1], EE Konofagou[1].*
[1]Columbia University, New York, NY, USA.

10:15A – 10:45A
COFFEE BREAK Pavilion Suite 3 & 4

Thursday 10:45A – 11:05P
ITEC at 12

Chair: JC Bamber, UK Pavilion Suite 1 & 2

Page No.

10:45A – 11:05A Invited Presentation

084 ITEC AT 12: AGAINST ALL ODDS. 75
J Ophir[1], KJ Parker[2], K Ophir[3].*
[1]University of Texas Medical School, Houston, TX, USA; [2]University of Rochester, Rochester, NY, USA; [3]ITEC, Austin, TX 78734, USA.

Thursday 11:05A – 11:42A
Session FIP: Forward and Inverse Problems

Chair: PE Barbone, USA *Co–Chair: T Shiina, Japan* Pavilion Suite 1 & 2

Page No.

11:05A – 11:20A

013 ROBUST SHEAR WAVE VELOCITY RECONSTRUCTION FROM MULTI–RESOLUTION TIME–OF–FLIGHT ESTIMATES. 76
PJ Hollender[1], NB Bottenus[1], GE Trahey[1].*
[1]Duke University, Durham, NC, USA.

11:20A – 11:35A

058 COMPARISON OF MR ELASTOGRAPHY INVERSION TECHNIQUES USING *EX–VIVO* TISSUE AND AN INDENTATION SCAN. 77
M Honarvar[1], RS Sahebjavaher[1], R Rohling[1], SE Salcudean[1].*
[1]The University of British Columbia, Vancouver, CANADA.

11:35A – 11:42A

054 IMPROVING FEM INVERSE PROBLEM RECONSTRUCTIONS BY INCORPORATING ALL DISPLACEMENT OBSERVATIONS USING ELEMENT SHAPE FUNCTION INTERPOLATIONS. 78
O Göksel[1], G Székely[1].*
[1]Computer Vision Laboratory, ETH, Zurich, SWITZERLAND.

11:43A – 1:15P

GROUP LUNCH Trackside Restaurant

Thursday 1:15P – 1:45P
ITEC Announcements including the Student Best Paper Award Recipients

Pavilion Suite 1 & 2

Thursday 1:45P – 3:22P
Session MIP–2: Methods for Imaging Elastic Tissue Properties – II

Chair: S Catheline, France *Co–Chair: C Gallippi, USA* Pavilion Suite 1 & 2

Page No.

1:45P – 2:00P

033 *IN VIVO* 3D BAYESIAN SHEAR WAVE SPEED RECONSTRUCTION OF THE PROSTATE. 79
S Rosenzweig[1], NC Rouze[1], B Byram[1], ML Palmeri[1], T Polascik[2], KR Nightingale[1].*
[1]Duke University, Durham, NC, USA; [2]Duke University Medical Center, Durham, NC, USA.

2:00P – 2:15P

039 SHEAR WAVE TRACKING WITH AN OPTO–ELASTOGRAPHY SYSTEM: SIMULATION AND EXPERIMENT. 80
S Li[1], Y Cheng[1], RJ Eckersley[2], DS Elson[1], M–X Tang[1].*
[1]Imperial College London, London, England, UK; [2]King's College London, London, England, UK.

2:15P – 2:30P

043 USING 3D SPATIO–TEMPORAL FILTERS TO REMOVE OUT OF PLANE REFLECTION ARTIFACTS FROM SHEAR WAVE IMAGES. 81
SL Lipman[1], NC Rouze[1], MH Wang[1], ML Palmeri[1], KR Nightingale[1].*
[1]Duke University, Durham, NC, USA.

(Session MIP–2 continues on next page)

** indicates Presenter*

(Session MIP–2 continued from previous page)

2:30P – 2:45P

081 THE WFUMB GUIDELINES AND RECOMMENDATIONS ON THE CLINICAL USE OF ULTRASOUND ELASTOGRAPHY–PART 1: BASIC PRINCIPLES AND TERMINOLOGY. 82
T Shiina[1], KR Nightingale[2], ML Palmeri[2], TJ Hall[3], JC Bamber[4] et al. for the Guidelines Working Group.*
[1]Kyoto University, Kyoto, JAPAN; [2]Duke University, Durham, NC, USA; [3]University of Wisconsin–Madison, Madison, WI, USA; [4]Institute of Cancer Research and Royal Marsden NHS Foundation Trust, Sutton, Surrey, England, UK.

2:45P – 3:00P

057 THE INFLUENCE OF 3D VERSUS 2D TRACKING FOR THE ESTIMATION OF VOLUMETRIC–STRAIN RELAXATION TIME IN PATIENTS WITH CHRONIC LYMPHOEDEMA. 83
J Fromageau[1], P Mortimer[2,3], JC Bamber[1].*
[1]The Institute of Cancer Research and Royal Marsden Hospital, Sutton, Surrey, England, UK; [2]St. George's and Royal Marsden Hospitals, London, England, UK; [3]The University of London, London, England, UK.

3:00P – 3:15P

038 REAL–TIME MONITORING OF HIFU ABLATION USING AXIAL STRAIN AND AXIAL–SHEAR STRAIN ELASTOGRAMS. 84
R Xia[1], AK Thittai[1].*
[1]The University of Texas Medical School, Houston, TX, USA.

3:15P – 3:22P

042 REAL–TIME 2–D VISCOELASTICITY IMAGING AND MONITORING OF HIFU TREATMENT USING HARMONIC MOTION IMAGING FOR FOCUSED ULTRASOUND (HMIFU). 85
GY Hou[1], J Provost[1], JL Grondin[1], S Wang[1], F Marquet[1], EE Konofagou[1].*
[1]Columbia University, New York, NY, USA.

3:23P – 4:00P

COFFEE BREAK — Pavilion Suite 3 & 4

Thursday 4:00P – 5:00P

Group Photo — TBA

6:00P – 6:30P — *Coach to Tunbridge Wells for free evening* — TBA

After 5:00P — *No Conference Activities*

Friday, October 4 9:00A – 10:00P

9:00A – 4:30P

Registration Desk Open — Pavilion Suite Foyer

9:00A – 4:30P **Session POS: Posters** — Pavilion Suite 3 & 4

Session EEX: Equipment Exhibit — Pavilion Suite 3 & 4

Friday 9:00A – 10:07A

Session CAA–2: Clinical and Animal Applications – II

Chair: ML Palmeri, USA *Co–Chair: H Feltovich, USA* Pavilion Suite 1 & 2

9:00A – 9:15A

010 CORTICOMEDULLARY STRAIN RATIO: A QUANTITATIVE MARKER IN ASSESSMENT OF RENAL ALLOGRAFT CORTICAL FIBROSIS. 86
J Gao[1], R Min[1], JM Rubin[2], J Lee[1], D Dahdania[1], J Hamilton[3], W Weitzel[2].*
[1]Weill Cornell Medical College, New York, NY, USA; [2]University of Michigan, Ann Arbor, MI, USA; [3]Epsilon Imaging, Ann Arbor, MI, USA.

Page No.

9:15A – 9:30A

028 SINGLE TRACKING LOCATION ARFI ASSESSMENT OF LIVER FIBROSIS PROGRESSION IN A RAT MODEL. 87

EC Elegbe[1,2], J Langdon[1,2], J Castañeda[1], SA McAleavey[1,2].*

[1]University of Rochester, Rochester, NY, USA; [2]Rochester Center for Biomedical Ultrasound, Rochester, NY, USA.

9:30A – 9:45A

080 FEASIBILITY OF A NEW TRANSIENT ELASTOGRAPHY EXAMINATION OPTIMIZED FOR SPLEEN STIFFNESS MEASUREMENT. 88

C Bastard[1], D Festi[2], H Stefanescu[3], S Audière[1], L Sandrin[1], V Miette[1].*

[1]Echosens, Paris, FRANCE; [2]University of Bologna, Bologna, ITALY; [3]University of Medicine and Pharmacy, Cluj–Napoca, ROMANIA.

9:45A – 10:00A

021 FAST AND TARGETED VISCOELASTIC EVALUATION OF THYROID NODULES: PRELIMINARY *IN VIVO* STUDY. 89

M Mehrmohammadi[1], P Song[1], CA Carrascal[1], MW Urban[1], MR Callstrom[2], JC Morris[2], S Chen[1], JF Greenleaf[1], M Fatemi[1], A Alizad[1].*

[1]Mayo Clinic, Rochester, MN, USA.

10:00A – 10:07A

069 CROSS–VALIDATION OF ELASTICITY IMAGING USING MAGNETIC RESONANCE ELASTOGRAPHY AND ULTRASOUND SHEAR WAVE ELASTOGRAPHY IN POST–MORTEM MOUSE BRAINS. 90

HW Chan[1,3], J Li[1], C Cummings[1], R Sinkus[2], C Uff[3], A Chakraborty[4], N Dorward[3], S Robinson[1], Y Jamin[1], JC Bamber[1].*

[1]Institute of Cancer Research and the Royal Marsden Hospital, Sutton, Surrey, England, UK; [2]St. Thomas' Hospital, King's College London, London, England, UK; [3]The National Hospital for Neurology and Neurosurgery, Queen Square, London, England, UK; [4]Southampton General Hospital, Southampton, England, UK.

10:08A – 10:45A

COFFEE BREAK — Pavilion Suite 3 & 4

Friday 10:45A – 12:22P
Session MMT: Mechanical Measurement Techniques for Tissues

Chair: YP Zheng, China — *Co–Chair: AK Thittai, USA* — Pavilion Suite 1 & 2

Page No.

10:45A – 11:00A

062 DYNAMIC OPTICAL COHERENCE TOMOGRAPHY (OCT) BASED AIR JET INDENTATION TO ESTIMATE CORNEAL ELASTIC PROPERTY. 91

L Wang[1], J Zhang[1,3], Y Hon[2], T Li[1], Y Huang[1], A Lam[2], YP Zheng[1].*

[1,2]Hong Kong Polytechnic University, Hong Kong, CHINA; [3]Eye Hospital China Academy of Chinese Medical Sciences, Beijing, CHINA.

11:00A – 11:15A

012 INVESTIGATING THE EFFECT OF CROSS–LINKING ON THE MECHANICAL PROPERTIES OF PORCINE CORNEAS BY INFLATION TEST. 92

S Matteoli[1], A Virga[1], I Paladini[2], R Mencucci[2], A Corvi[1].*

[1,2]University of Florence, Florence, ITALY.

11:15A – 11:30A

065 COMPARISON BETWEEN CRAWLING WAVE SONOELASTOGRAPHY AND STL–ARFI IN BIOMATERIALS. 93

J Ormachea[1], A Salo[2], A Lerner[2], S McAleavey[2], B Castañeda[1].*

[1]Pontificia Universidad Católica del Perú, Lima, PERU; [2]University of Rochester, Rochester, NY, USA.

(Session MMT continues on next page)

** indicates Presenter*

(Session MMT continued from previous page) Page No.

11:30A – 11:45A

068 FINITE ELEMENT ANALYSIS OF SHEAR WAVE PROPAGATION IN SOFT MEDIA WITH PLATE–LIKE GEOMETRY IN A RIGID CONTAINER. 94

R De Luca [1,2], J Fromageau[1], E Elyas[1], F Marinozzi[2], JC Bamber[1].*
[1]Institute of Cancer Research and Royal Marsden Hospital, Sutton, Surrey, England, UK; [2]Sapienza University of Rome, Rome, ITALY.

11:45A – 12:00P

078 A SIMPLE STRAIN MEASUREMENT TECHNIQUE THAT UTILIZES PHOTON ATTENUATION. 95

T Alrefae[1].*
[1]Kuwait University, Khaldia, KUWAIT.

12:00P – 12:15P

079 INVESTIGATION OF A GOLD STANDARD PHANTOM AND MEASUREMENT TECHNIQUE TO ESTIMATE ELASTIC PROPERTIES IN ELASTOGRAPHY. 96

J Oudry[1], T Lynch[2], J Vappou[3], L Sandrin[1], V Miette[1].*
[1]Echosens, Paris, FRANCE; [2]CIRS Inc., Norfolk, Virginia, USA; [3]ICube, CNRS–Université de Strasbourg, Strasbourg, FRANCE.

12:15P – 12:22P

030 PERFORMANCE EVALUATION OF RHEOLOGICAL MODELS APPLIED TO LOCAL CHARACTERIZATION OF BIOMIMETIC MATERIALS IN A CREEP TEST EXPERIMENT. 97

B Galaz[1], R Acevedo[1].*
[1]University of Santiago of Chile, Santiago, CHILE.

12:23P – 2:00P

GROUP LUNCH Trackside Restaurant

Friday 2:00P – 3:52P

Session MIP–3: Methods for Imaging Elastic Tissue Properties – III

Chair: J Vappou, France Pavilion Suite 1 & 2

Page No.

2:00P – 2:15P

055 SHEAR WAVE DISPERSION MEASUREMENTS ON TISSUE–MIMICKING PHANTOM AND *EX–VIVO* HUMAN BRAIN. 98

E Nicolas[1], S Callé[1], R Ternifi[1], E Simon[1], JP Remenieras[1].*
[1]Université François–Rabelais de Tours, Tours, FRANCE.

2:15P – 2:30P

027 OPTICAL COHERENCE ELASTOGRAPHY. 99

S Wang[1], J Li[1], S Aglyamov[2], S Emelianov[2], MD Twa[1], KV Larin[1,3].*
[1]University of Houston, Houston, TX, USA; [2]University of Texas, Austin, TX, USA; [3]Baylor College of Medicine, Houston, TX, USA.

2:30P – 2:45P

064 CRAWLING WAVE SPEED ESTIMATION BASED ON DOMINANT COMPONENT ANALYSIS AM–FM DEMODULATION. 100

R Rojas[1], J Ormachea[1], A Salo[2], P Rodríguez[1], A Lerner[2], KJ Parker[2], B Castañeda[1].*
[1]Pontificia Universidad Católica del Perú, Lima, PERU; [2]University of Rochester, Rochester, NY, USA.

2:45P – 3:00P

066 COMBINING AXIAL MEAURES TO ESTIMATE 3D MOTION OVER AN ULTRASOUND VOLUME. 101

JM Abeysekera[1], M Honarvar[1], SE Salcudean[1], R Rohling[1].*
[1]Univeristy of British Columbia, Vancouver, BC, CANADA.

3:00P – 3:15P

073 INFERRING STROMAL MICROSTRUCTURE PROPERTIES VIA NONLINEAR ELASTICITY IMAGING. 102

E Rodrigues Ferreira[1], T Liu[2], PE Barbone[3], AA Oberai[2], TJ Hall[4].*

[1]University of Minnesota, Minneapolis, MN, USA; [2]Rensselaer Polytechnic Institute, Troy, NY, USA; [3]Boston University, Boston, MA, USA; [4]University of Wisconsin–Madison, Madison, WI, USA.

3:15P – 3:30P

044 CELLULAR DISPLACEMENT ESTIMATION USING MITOCHONDRIA IMAGES. 103

DT Seidl[1], E Canović[1], AA Oberai[2], PE Barbone[1], D Stamenović[1], ML Smith[1].*

[1]Boston University, Boston, MA, USA; [2]Rensselaer Polytechnic Institute, Troy, NY USA.

3:30P – 3:45P

082 QUANTITATIVE ASSESMENT OF SOFT EMBALMED HUMAN CADAVERS WITH ULTRASOUND SHEAR WAVE ELASTOGRAPHY. 104

J Joy[1], C Demore[1], N Lee[1], L Cui[1], S Munirama[2], S Vinnicombe[2], R Eisma[1], G Corner[2], G McLeod[2], S Cochran[1].*

[1]University of Dundee, Dundee, Angus, Scotland, UK; [2]Ninewells Hospital & Medical School, Dundee, Angus, Scotland, UK.

3:45P – 3:52P

061 MAPPING VISCOELASTIC PROPERTIES USING ACOUSTIC RADIATION FORCE. 105

M Gomyo[1], K Kondo[2], M Yamakawa[3], T Shiina[1].*

[1]Kyoto University, Kyoto–City, Kyoto, JAPAN; [2]Center for the Promotion of Interdisciplinary Education and Research, Kyoto–City, Kyoto, JAPAN; [3]Advanced Biomedical Engineering Research Unit, Kyoto–City, Kyoto, JAPAN.

3:53P – 4:30P

COFFEE BREAK — Pavilion Suite 3 & 4

Friday **6:30P – 10:00P**

Closing Reception *Proceedings Book Signing* TBA

Session EEX: Equipment Exhibit

Pavilion Suite 3 & 4

Hitachi Medical Systems Europe Holding AG.
Zug, SWITZERLAND.

HITACHI
Inspire the Next

ALOKA
illuminate the change

Verasonics, Inc.
Redmond, WA, USA.

Verasonics®

* *indicates Presenter*

The London Moonlight Trio

The London Moonlight Trio is formed of three Jazz musicians, all graduates of the London Guildhall School of Music and Drama, where they studied and performed with many great musicians, including Kirk Lightsey, Henry Lowther, Stan Sulzman, Jean Toussaint, Mike Westbrook, Pete Churchill, and Nikki Isles, to name a few. They are each members of several different musical groups, such as The London Vocal Project (LVP), the Spike Orchestra, and Jazzbomb, and have performed in London at well known venues such as The Royal Festival Hall (with Sir John Dankworth and Dame Cleo Lane), the Barbican (with Bobby McFerrin), the Royal Albert Hall, the Vortex Jazz Club, 606 Club, and Ronnie Scott's. The LVP, an innovative jazz choir, is worth a special mention, as it was the focal point of regular meeting of our three, and the spark that encouraged them to form the London Moonlight Trio. The three regularly come together because of their common love of performing jazz standards and close harmony singing. Their formal musical education allows them to give a performance that is not as limited as that of many function–jazz trios and is a sophisticated mixture of instrumental (piano, bass and saxophone) and occasional a capella three–part harmony vocals. They are equally at home providing understated background music as well as accomplished virtuoso entertainment, and for us they will provide a little of both.

A detailed program will be available at the Conference Dinner.
Wednesday, October 2nd, 2013
Performance will start at 8:30 pm

On the Cover:
Hever Castle and grounds, Hever, Kent
not far from the Conference Venue.

Hever Castle dates from the 13th Century as a country house, although it is most famous for being the childhood home of Anne Boleyn, the second queen consort of King Henry VIII of England and later owned by Anne of Cleves, King Henry VIII's forth wife.

The castle and grounds are open for public viewing. The picture is reproduced with the kind permission of Visit Kent Limited, England for all of ITEC's Conference materials.

AUTHOR INDEX

AUTHOR INDEX

Session TUT: Tutorials: Medical and Scientific Challenges in Elastography

Tuesday, October 1 12:00P – 2:00P

085 **SHEAR WAVE ELASTOGRAPHY OF THE BREAST IN PRACTICE AND BEYOND THE OBVIOUS.**

Andy Evans[1].*

[1]Ninewells Hospital & Medical School, University of Dundee, Dundee, Scotland, UK.

Shearwave elastography provides quantitative, qualitative and reproducible information which when combined with greyscale imaging improves the accuracy of benign/malignant differentiation of solid breast masses. Maximum and mean elasticity values give similar results when used to evaluate breast lesions. In UK practice the most obvious use of shearwave will be to increase negative predicative value of ultrasound to allow women with benign solid breast lesions to be reassured and discharged with the need for percutaneous breast biopsy or short term follow–up.

Peri–lesional stiffness has strong correlations with poor prognostic factors such as invasive size, high histological grade, vascular invasion and lymph node involvement. We have recently shown that stiffness is an independent predictor for lymph node involvement in a multivariate analysis including the classical predictors of nodal involvement (invasive size, histological grade and vascular invasion).

Peri–tumoural stiffness at diagnosis has also been found to predict response of breast cancer to neo–adjuvant chemotherapy. The role of shearwave elastography in assessing early response to chemotherapy has not yet been established.

3D shearwave elastography is not superior to 2D in benign malignant/differentiation. However early work suggests that the volume of peri–tumoural stiffness is related to pathological indictors of systemic spread (vascular invasion and lymph node metastasis).

083 **ELASTOGRAPHY: OLDIE–BUT–GOODIE AND GETTING BETTER.†**

Jonathan Ophir[1]*.

[1]Ultrasonics and Elastographics Laboratory, Diagnostic and Interventional Imaging Department, University of Texas Medical School, 6431 Fannin Street, MSMB 6.168, Houston, TX, USA.

Unlike sonography which is based on an *acquired* image of tissue backscatter and reflection which generate image contrast, strain elastography is based on a *computed* image of the strain distribution in tissues in response to some kind of a mechanical load, which is based on several different kinds of contrast mechanisms. While sonography has been around in clinics for more than 50 years, strain elastography as an imaging technique has been around for more than 20 years and has been widely adopted clinically only in the last decade. In order to bring about the clinical utility of elastography, many theoretical, engineering and clinical innovations and investigations were undertaken by research groups, clinics and commercial entities.

This presentation starts from the basic principles of 'traditional' strain elastography. Simple observations of tissue shear elastic, viscoelastic and poro–elastic properties are given. The interaction of sound waves with deforming tissues are shown to affect the echo signals. Some of the changes in the signal due to deformation are useful and essential for the estimation of tissue displacement (via 'speckle tracking') and strain, while other changes are simultaneously corrupting and therefore limiting the ability to obtain high quality estimates. The compromises that must be made among several ultrasonic, mechanical, signal processing and statistical parameters dictate the ultimate attainable image quality.

The basic imaging of axial strains in tissues is the harbinger of a much richer imaging field that lies ahead. Other elastic parameters that have been shown to be promising candidates for elastographic imaging are the modulus distribution, stress/strain nonlinearity, Poisson's ratio and its time dependence, shear strain effects near or within boundaries, and others. Each one of these parametric images may become useful for different specialized medical applications in the detection, classification and monitoring of diseases and treatments.

Acknowledgements: I. Céspedes, R. Righetti, E.E. Konofagou, A.K. Thittai, S. Srinivasan, T. Varghese, S.K. Alam, N. Maklad, F. Kallel, B.S. Garra, R. Chandrasekhar, A. Patil, H. Ponnekanti, R. Zahiri and E. Khalil have contributed to the material in this presentation.

†This work was supported in part by the National Institutes of Health (NIH) grants R01–CA60520, P01–CA064597, P01–EB 002105, R21–CA127291, R21–153373 and R21–CA135580, the State of Texas and the John S. Dunn Foundation.

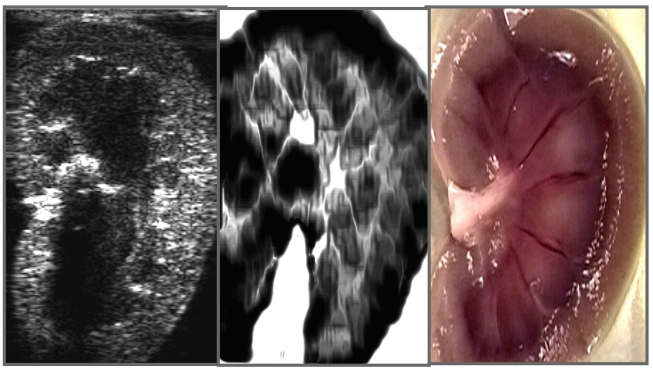

Figure 1: A triptych showing simultaneously–obtained sonogram (left) and an elastogram (center) and a photo of a longitudinal cut surface of an ovine kidney *in vitro* (right). Note that the sonogram and the elastogram depict different information.

009 **ULTRAFAST PLANE WAVE ELASTOGRAPHY USING TRANSVERSE OSCILLATIONS FOR THE NON–INVASIVE MECHANICAL CHARACTERIZATION OF CAROTID PLAQUE.**

Jonathan Porée[1,3], Boris Chayer[1,2], Jacques Ohayon[5], Damien Garcia[2,3,4], Guy Cloutier[1,3,4].*
[1]Biorheology and Medical Ultrasonics Laboratory (LBUM), [2]Biomechanics and Imaging in Cardiology Research Unit, University of Montréal Hospital Research Center (CRCHUM), Montréal, Québec, CANADA; [3]Biomedical Engineering Institute, [4]Radiology Department, Radio–Oncology and Nuclear Medicine, University of Montréal, Montréal, Québec, CANADA; [5]Laboratory TIMC/IMAG, University Joseph–Fourier, Grenoble, FRANCE.

Background: Cardiovascular diseases, attributed to atherosclerosis and vulnerable plaque rupture, are rated as the leading cause of death in western countries. Studies revealed that vulnerability depends on plaque tissue composition and their biomechanical properties [1]. The feasibility of evaluating mechanical properties of carotid plaques with ultrasound (US) elasticity imaging has been demonstrated. However, due to the limited lateral resolution of external US scans, lateral components of the strain tensor cannot be accurately estimated. Furthermore, the low temporal resolution (~60Fps) tends to increase decorrelation artifacts. Recent developments on ultrafast plane wave imaging and synthetic aperture methods have led to improved image quality and high frame rates (~1000Fps) [2].

Aims: We propose to use high speed plane wave imaging (PWI) and transverse oscillations (TO) to improve the non–invasive vascular elastography (NIVE) capability.

Methods: High frame rate US sequences were obtained through tilted plane wave emissions. RF–lines were recovered using coherent compounding [2] combined with transverse oscillation beamforming [3]. Strain fields were computed from pre– and post–compression PWI and combined PWI–TO images using the Lagrangian Speckle Model Estimator [4]. High frame rate images (~1000Fps) were obtained using the SonixTouch scanner and DAQ system (Ultrasonix, Vancouver, Canada). We used a multilayered PVA–C tubular phantom mimicking a vulnerable plaque geometry. This phantom was dynamically pressurized using a blood pump (Model 1421, Harvard Apparatus, Holliston, USA) and a water column.

Results: Both PWI and combined PWI–TO showed promising strain tensor estimations compared to conventional focus imaging (Figure 1). The higher frame rate in PWI mode allowed decreasing local variability of elastograms, whereas the lateral phase information introduced using TO increased lateral sensitivity. These results were confirmed using finite element modeling and US simulations.

Conclusions: This study highlighted the potential of plane wave imaging and transverse oscillation beamforming to provide high quality strain elastograms at high frame rates.

Acknowledgements: This research was supported by a strategic grant (#STPGP–381136–09) and a discovery grant (#138570–11) of the Natural Sciences and Engineering Research Council of Canada. We also acknowledge the scholarship support of MEDITIS (Institute of Biomedical Engineering).

References:

[1] Finet et al.: Morphological and Biomechanical Aspects of Vulnerable Coronary Plaque. Arch Mal Coeur Vaiss, 2007.
[2 Montaldo et al.: Coherent Plane–Wave Compounding for Very High Frame Rate Ultrasonography and Transient Elastography. IEEE UFFC, 2009.
[3] Liebgott et al.: Transverse Oscillations for Tissue Motion Estimation. Physics Procedia, 2010.
[4] Maurice et al.: Noninvasive Vascular Elastography: Theoretical Framework. IEEE TMI, 2004.

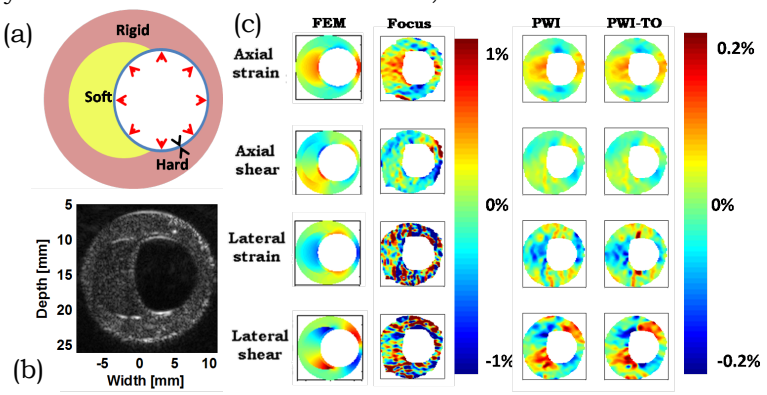

Figure 1: (a) PVA–C vulnerable plaque geometry; (b) B–mode image; and (c) Corresponding *in vitro* elastograms (axial strain, axial shear, lateral strain and lateral shear) computed from finite element modeling, standard focusing, PWI and PWI combined with transverse oscillations.

* *indicates Presenter*

015 **ABDOMINAL AORTIC ANEURYSM FOLLOW–UP AFTER ENDOVASCULAR REPAIR IN A CANINE MODEL WITH NON–INVASIVE VASCULAR ELASTOGRAPHY.**

E Salloum[1,2], A Bertrand–Grenier[1,2], S Lerouge[3], C Kauffmann[4], G Cloutier[1,2,5], G Soulez[2,4,5].*

[1]Biorheology and Medical Ultrasonics Laboratory, University of Montréal Hospital Research Center, Montréal, Québec, CANADA; [2]Biomedical Engineering Institute, University of Montréal, Montréal, Québec, CANADA; [3]École de Technologie Supérieure, Montréal, Québec, CANADA; [4]Radiology Department, University of Montréal Hospital, Montréal, Québec, CANADA; 5Radiology, Radio–Oncology and Nuclear Medicine Department, University of Montréal, Montréal, Québec, CANADA.

Background: Non–invasive vascular elastography (NIVE) using the Lagrangian Speckle Model Estimator (LSME) may become a complementary follow–up imaging technique for endovascular aneurysm repair (EVAR). NIVE [1] has the capability of providing important information on the thrombus organization within the aneurismal sac and on the detection of endoleaks. A previous study [2] tested the LSME in a Type I endoleak canine model. It was possible to characterize the strain of the aneurysm wall and differentiate the venous patch used to create the aneurysm from the native artery. The characterization of the thrombus organization was not possible in the latter study. A limitation was the absence of CT examinations as gold standard for endoleak diagnosis.

Aims: We aimed to apply and optimize NIVE of abdominal aortic aneurysm (AAA) after (EVAR) with stent–graft (SG) in a canine model to detect endoleaks and characterize thrombus organization.

Methods: SGs were implanted in a first group of 3 dogs with an aneurysm created in iliac arteries (6 aneurysms) and in a second group of 3 dogs in the abdominal aorta. Type I endoleak was created in 6 iliac and 1 aortic aneurysms and Type II endoleak in two aortic aneurysms. Duplex ultrasound (Supersonic Imagine, Aix–en–Provence, France) and NIVE elastography examinations (Sonix RP, Ultrasonix, Vancouver, Canada) were performed at baseline, 1 week, 1 month, 3 month (first group) and at 6 month (second group) follow–up. Angiography (Koordinat 3D II, Siemens Erlengen, Germany), CT scan and histology (Exakt Gmbh, Norderstedt, Germany) were also performed at sacrifice. Ultrasonic raw RF data were acquired on longitudinal and three axial planes (proximal, mid and distal parts of the aneurysm) to generate with NIVE time–varying strain curves. Elastograms of zones of interest were computed using the LSME. Areas of endoleaks, liquid thrombus (non–organized) and solid thrombus (organized) were identified and segmented by comparing results of CT scan and histology (Figure 1). Strain values in areas with endoleaks, liquid and solid thrombus were compared.

Results: Five iliac and one aortic aneurysm had confirmed Type I endoleaks. A Type II endoleak was observed in two aortic aneurysms, whereas one iliac aneurysm was sealed. Maximal axial strain values in endoleak, liquid and solid thrombus areas were, respectively, estimated at 0.73±0.14%, 0.22±0.04% and 0.11±0.04%. Strain values were significantly different between endoleaks and liquid or solid thrombus areas (p=5,136E–09) and between solid and liquid thrombus areas (p=0.00063). All endoleak areas were clearly identified on elastography examinations using axial and shear strain parameters (Ffigure 1).

Conclusions: Non–invasive elastography using the LSME is capable of detecting endoleaks and characterizing the thrombus organization as liquid or solid. Further developments are needed to enable real time elastograms optimized for AAA follow–up after EVAR.

References:

[1] Maurice R.L. et al.: Noninvasive Vascular Elastography: Theoretical Framework. IEEE Trans Med Imaging, 23(2), pp. 164–80., 2004.

[2] Fromageau J. et al.: Noninvasive Vascular Ultrasound Elastography Applied to the Characterization of Experimental Aneurysms and Follow–Up after Endovascular Repair. Phys Med Biol, 53(22), pp. 6475–90, 2008.

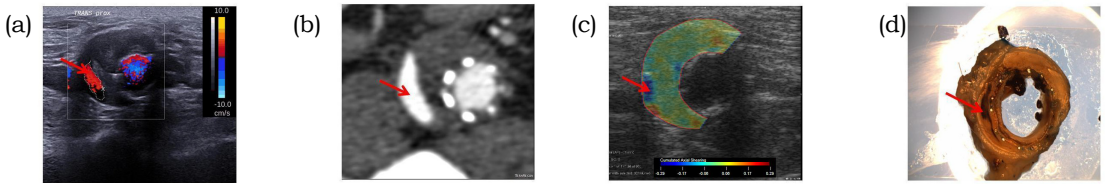

Figure 1: The red arrow on each image indicates the endoleak region for the same proximal axial acquisition of the first dog. (a) Duplex US, (b) CT scan, (c) Cumulated axial shear strain NIVE, (d) Macroscopic section.

* *indicates Presenter*

034 **ABDOMINAL AORTIC ANEURYSM FOLLOW–UP BY DYNAMIC ELASTOGRAPHY AFTER ENDOVASCULAR REPAIR.**

Antony Bertrand–Grenier[1,2,4], Elie Salloum[1,2,5], Sophie Lerouge[3], Pauline Lequoy[3], Claude Kauffmann[2], Guy Cloutier[1,5,6], Gilles Soulez[2,5,6,7].*

[1]Biorheology and Medical Ultrasonics Laboratory, [2]Central Image Processing Laboratory, [3]EndoVascular Biomaterials Laboratory, University of Montréal Hospital Research Center (CRCHUM), Montréal, Québec, CANADA; [4]Physics Department, [5]Biomedical Engineering Institute, [6]Radiology, Radio–Oncology and Nuclear Medicine Department, University of Montréal, Montréal, Québec, CANADA; [7]Radiology Department, University of Montreal Hospital, Montréal, Québec, CANADA.

Background: Surgical treatment of abdominal aortic aneurysms (AAA) is increasingly being replaced by endovascular aneurysm repair (EVAR) using stent–grafts (SGs) [1]. However, the efficacy of this approach is jeopardized by the incidence of endoleaks leading to aneurysm rupture [2]. A lifelong surveillance by CT–scan on an annual basis is required, increasing the cost of EVAR, and exposing the patient to ionizing radiation and nephrotoxic contrast agent [3]. A relatively new method, supersonic shear–wave imaging (SSI) measures the tissue elasticity in real–time [4]. We hypothesize that this technique can help to detect endoleaks, sac pressurization and grade the fibrous evolution of the thrombus around the SG.

Aims: Our goal was to characterize mechanical properties of AAA after endovascular EVAR in a canine model (properties of walls, thrombus and endoleaks) with SSI and correlate results with Doppler ultrasound (DUS), computed tomography (CT) and pathologic findings.

Methods: SGs were implanted in 2 groups of dogs after creation of iliac or aortic aneurysms. The first group of 3 dogs (6 iliac arteries) had creation of Type I endoleak and the second group of 3 dogs (3 aortic arteries) had creation of Type I or Type II endoleaks. DUS and SSI were performed at baseline, implantation, 1–week, 1–month, 3–month (Groups 1 and 2) and 6–month (Group 2) follow–up. CT–scan, angiography and histology were also performed at sacrifice to evaluate the presence, the type and the size of endoleaks and the characterization of thrombus organization. Areas with endoleak, solid thrombus (organized) and liquid thrombus (non–organized) were identified and segmented on histology images. Elasticity modulus values in areas with endoleak, solid thrombus and liquid thrombus were compared on longitudinal and three axial plane images (proximal, mid and distal parts of the aneurysm).

Results: Five iliac and one aortic aneurysms had confirmed Type I endoleaks, two aortic aneurysms had Type II endoleaks and one iliac aneurysm was sealed. Elasticity moduli of 0.2±0.3kPa were found in endoleak regions, 63.4±66.3kPa in solid thrombi and 3.0±2.0kPa in liquid thrombi. Elasticity moduli were significantly different between areas of endoleak and solid thrombus (p=0.0002), of endoleak and liquid thrombus (p=0.0009), and of liquid thrombus versus solid thrombus (p=0.0003). SSI detected endoleaks in which DUS failed (n=3) and detected liquid thrombus (*possibility of endotension).

Conclusions: Results showed that SSI is able to detect endoleaks, characterize thrombus organization and possibly endotension. The next objective is to evaluate the feasibility and efficacy of this approach in a clinical study. This new technique could reduce the cost, the exposition to ionizing radiation and nephrotoxic contrast agents of surveillance CT–scan follow–up of AAA after EVAR. It is note that CEUS have not been used considering its requirement for intravenous contrast, incremental time and cost [5].

Acknowledgements: Funding of FRQ–S–ARQ and Canadian Institutes of Health Research (MOP–115099).

References:

[1] Eli et al.: Endovascular Treatment of Aortic Aneurysms: State of the Art. Curr Treat Options Cardiovasc Med. 2009.
[2] Rosen et al.: Endoleak Management Following Endovascular Aneurysm Repair. J Vasc Interv Radiol., 2008.
[3] White et al.: Estimating Risk Associated with Radiation Exposure during Follow–Up after Endovascular Aortic Repair. J Cardiovasc Surg (Torino), 2010.
[4] Bercoff et al.: Supersonic Shear Imaging: A New Technique for Soft Tissue Elasticity Mapping. IEEE Trans Ultrason Ferroelectr Freq Control., 2004.
[5] Wilson et al.: CEUS: What Is the Evidence and What Are the Obstacles? A J Roent., 2009.

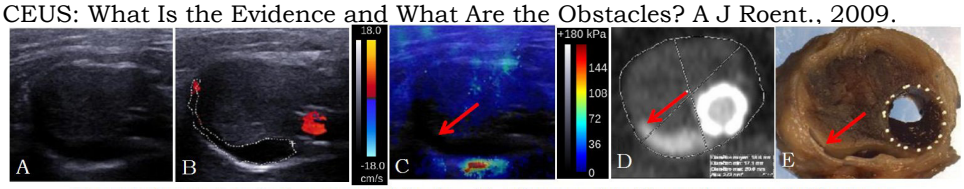

Figure 1: Comparison of techniques used in Dog #1 of Group 1. The red arrow indicates a Type 1 endoleak: (A) B–mode, (B) DUS, (C) SSI, (D) CT–scan, (E) histo–macroscopy.

* *indicates Presenter*

036 **ASSESSMENT OF CUTANEOUS SCLEROTIC DISORDERS USING ARFI SWEI.**

Seung Yun Lee[1], Adela R Cardones[2], Joanna Hooten[2], Joshua R Doherty[1], Kathryn R. Nightingale[1], Mark L. Palmeri[1].*

[1]Biomedical Engineering Department, Duke University, Durham, NC, USA; [2]Duke University Medical Center, Durham, NC, USA.

Background: Cutaneous sclerotic disorders are histologically characterized by increased fibrosis and collagen hyalinization in the dermis and deeper soft tissue. These conditions can be a significant source of morbidity, but there is no reliable measure to quantify disease severity in both the clinical and research setting [1]. Acoustic Radiation Force Impulse (ARFI) and Shear Wave Elasticity Imaging (SWEI) use ultrasound waves to make micron level transient deformation in soft tissue and measure the its dynamics to directly quantify material properties such as elasticity and viscosity [2]. They are sensitive to the functional pathology of sclerosis, making them ideal for assessing fibrotic conditions [3]. Already proven useful in evaluating fibrosis of the liver [4], this technology can be translated for use in cutaneous sclerosis to answer the clinical gaps in this field.

Aims: This study aims to determine the potential for employing ARFI/SWEI in the clinical evaluation of cutaneous sclerosis, testing the hypothesis that the diseased skin is stiffer than the normal skin.

Methods: Using the 14L5 transducer on the Siemens S2000 scanner with custom designed beam sequences and processing, ARF was generated at a 0.55cm focus using a F/1 7.2MHz pushing excitation and was tracked at the first harmonic frequency of 12.2MHz on and off–axis. We recruited patients with sclerotic disease and imaged them using ARFI/SWEI on lesionous and normal skin on various body sites. Along with standard B–mode, on–axis displacement (averaged over 1.7mm) and off–axis shear wave propagation (ROI size 1.7mm x 7.2mm) was measured using normalized cross–correlation on rf–data. A total of 12 patients have been imaged to date but only 2 patients' data were analyzed for this abstract.

Results: Computed Shear Wave Speed (SWS) and mean ARFI displacement magnitude were normalized to their controls. Metrics from lesionous skin were normalized by those acquired from normal skin laterally opposite to the affected region, and those of normal skin were normalized by dividing the metrics from the left side of the body to the right side. Normalized SWS and mean ARFI displacement inside the lesionous skin and inside the normal skin for two patients are shown in Figure 1. SWS inside the lesionous skin is significantly greater than that inside the normal skin ($p=0.03$); mean ARFI displacement inside the lesionous skin is significantly smaller than that inside the normal skin ($p=0.007$).

Conclusions: As hypothesized, the SWS was greater and mean ARFI displacement smaller in lesionous skin compared to those in normal skin. Although the speed and displacement magnitude are impacted by both the material stiffness and geometry, the results show that there are significant differences in these metrics due to stiffness alone. We are continuing patient accrual and exploring ways for robust analyses.

Acknowledgements: This work has been supported by NIH grants EB002132 and Dermatology Foundation. We thank the Ultrasound Division at Siemens Medical Solutions, USA, Inc. for their technical and in–kind support. We also thank Dr. Veronica Rotemberg for her help with patient imaging.

References:

[1] Fett N, et al: Academy of Dermatology, 64(2), pp. 231–242, quiz 243–234, 2011.
[2] Palmeri ML, et al: Interface Focus, 1(4), pp. 553–564, 2011.
[3] Nezafati KA, et al.: Archives of Dermatology, 147(9), pp. 1112–1115, 2011.
[4] Palmeri ML, et al.: Journal of Hepatology, 55(3), pp. 666–672, 2011.

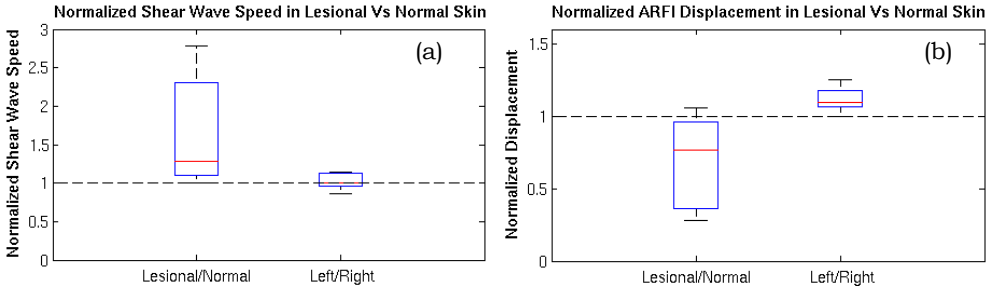

Figure 1:
(a) comparison of normalized SWS in lesionous skin to normal skin; (b) comparison of normalized mean ARFI displacement inside lesionous skin to normal skin. In both cases, the two populations were significantly different from each other with $p<0.05$ using Mann–Whitney U test.

052 **ESTIMATING ELECTROMECHANICAL WAVE VELOCITY VECTOR FIELDS WITH ELECTROMECHANICAL WAVE IMAGING: AN *IN VIVO* FEASIBILITY STUDY.**

Alexandre Costet[1], Elisa E. Konofagou[1,2].*
[1]Biomedical Engineering Department, [2]Radiology Department, Columbia University, New York, NY, USA.

Background: The conduction velocity describes the local magnitude and direction of propagation of the wavefront of electrical activity as it moves across all four cardiac chambers. Arrhythmias and ischemic heart disease have both been shown to affect the magnitude and direction of propagation of the electrical activation wavefront [1–3]. Electromechanical Wave (EW) Imaging (EWI) [4,5] is a direct ultrasound–based imaging technique that can map the transmural electromechanical activation in all four chambers *in vivo*. Previous studies have shown that the EW closely followed the electrical activation wavefront [6]. In this study, the estimation of the EW velocity was assessed as it could provide a quantitative measure of electromechanical, and thereby electrical, activity.

Aims: In this study, we introduce an automated technique of estimating the EW propagation velocity vector fields, transmurally and in all four chambers of the heart. We then explore the EW propagation velocity in normal and ischemic canine hearts *in vivo* during sinus rhythm and pacing.

Methods: A Verasonics system (Verasonics, Redmond, WA) with a 2.5MHz phased array was used to perform EWI transthoracically in both healthy and ischemic hearts (n=10) in all four chambers, using an unfocused sequence at 2000 frames/s, in the standard apical views during sinus rhythm and pacing at the apex of the right ventricle at 60 bpm. In the four–chamber, two–chamber and apical long axis views, axial incremental displacements and strains were estimated using RF cross–correlation with a window size of 9.2mm and a window shift of 0.385mm, and a least–squares kernel size of 5.0mm, respectively. EW, or the wavefront of electromechanical activation, was defined as the point in time where axial incremental strain transitioned from positive (relaxation) to negative values (contraction), i.e. zero–crossings. Each point on the wavefront of the activation was thus labeled by its coordinates in space and time: $z_i=[x_i,y_i,t_i]$. The velocity vector at a point z_i on the wavefront was estimated by using a least–squares algorithm to fit a smooth second order 2D polynomial surface to the point z_i and its active neighbors on the front, $t_i=P(x_i,y_i)$. Both speed and direction of propagation were then computed from the gradient of the local polynomial surface,

$$\nabla P = \left[\frac{\partial P}{\partial x}, \frac{\partial P}{\partial y}\right] \text{[7]}.$$

Results: In the normal heart, during sinus rhythm, the mean EW propagation velocity in all four chambers of the heart was found to be 0.72±0.31m/sec. During pacing from the apex of the right ventricle, the mean propagation velocity of the EW in all four chambers of the heart decreased to 0.45±0.23m/sec. Finally, 15–30 minutes after total occlusion of the left anterior descending (LAD) artery, the mean EW velocity in all four chambers of the heart was found to be 0.51±0.23m/sec.

Conclusions: In this feasibility study we introduced an automated method to compute vector fields of propagation velocity of the EW from EWI data. We found that EW propagation velocities for healthy animals in sinus rhythm were comparable to previously reported conduction speeds [7]. Furthermore, EW propagation velocity was found to be reduced on average by 37.5% during pacing at the apex of the right ventricle at 60 bpm, and by 29% in ischemic cases. Because both slowed conduction and velocity heterogeneity have been shown to be a basis for arrhythmogenesis in the heart [8,9], these findings further indicate the potential of EWI to serve as a simple, direct and non–invasive imaging tool capable of providing quantitative measures of the electromechanical, and thus electrical, activation.

Acknowledgements: Supported in part by NIH funding (R01EB006042 & R01HL094410).

References:

[1] Akar FG, Nass RD, Hahn S, et al.: Am J Physiol – Heart Circ Physiol, 293(2), pp. H1223–H1230, 2007.
[2] Kléber AG, Janse MJ, Wilms–Schopmann FJ, Wilde AA, Coronel R: Circulation, 73(1), pp. 189–198, 1986.
[3] Verheule S, Wilson E, Banthia S, et al.: Am J Physiol – Heart Circ Physiol, 287(2), pp. H634–H644, 2004.
[4] Provost J, Nguyen VT–H, Legrand D, et al.: Phys Med Biol, 56(22), pp. 1–11, 2011.
[5] Provost J, Lee W–N, Fujikura K, Konofagou EE: Proc Natl Acad Sci., 108(21), pp. 8565–8570, 2011.
[6] Provost J, Gurev V, Trayanova N, Konofagou EE: Heart Rhythm, 8(5), pp. 752–759, 2011.
[7] Bayly PV, KenKnight BH, Rogers JM, et al.: IEEE Trans Biomed Eng, 45(5), pp. 563–571, 1998.
[8] Yamashita T, Oikawa N, Inoue H, et al.: Am Heart J, 127(2), pp. 353–9, 1994.
[9] Sims JJ, Miller AW, Ujhelyi MR: J Cardiovasc Pharmacol, 41(5), pp. 795–803, 2003.

* *indicates Presenter*

056 **ACCOUNTING FOR MASS IN VISCOELASTIC STRAIN RESPONSE (ViSR) ULTRASOUND.**

MR Scola[1], TJ Czernuszewicz, CM Gallippi[1].*
[1]The University of North Carolina at Chapel Hill, Chapel Hill, NC, USA.

Background: Viscoelastic Strain Response (ViSR) ultrasound is a method for quantitatively assessing the viscoelastic properties of tissue. Using two successive ARF impulses and monitoring induced displacements in the region of excitation, ViSR fits displacements to a mechanical model to measure the relaxation time constant, τ, given by the ratio of viscosity to elasticity. We have previously demonstrated ViSR for characterizing the mechanical properties of gelatin phantoms and muscle by fitting displacements using the Voigt model [1,2], however the Voigt model assumes a massless material. We hypothesize that a modified version of the Voigt model, consisting of an inertial component in series with the Voigt model [3], will more accurately model tissue displacement and better estimate ViSR τ measurements.

Aims: This work investigates the relevance of a modified Voigt model for modeling ARF induced displacements and measuring the relaxation time constant, τ, for ViSR ultrasound.

Methods: Imaging was performed using a Siemens ACUSON Antares (Siemens Medical Solutions USA) imaging system specially equipped for research purposes and a VF7–3 linear array transducer. ViSR was implemented using two 300–cycle ARF excitations administered to the same region of excitation and separated by 0.6ms in time, and was performed in an agar/gelatin tissue mimicking phantom with a xanthan gum additive for increased viscosity. ViSR displacement profiles were fit to the Voigt model with added inertial component to calculate τ, and compared to τ measurements derived from fitting displacement profiles to the classical Voigt model. Two different focal configurations of the ARF excitations were employed (F/1.5 and F/3) in order to vary the volume of displaced tissue and investigate the effect of material mass on calculations.

Results: The Voigt model with added inertial component was better able to predict displacement profiles than the classical Voigt model, given by the R^2 statistic and illustrated in Figure 1. R^2 values for the Voigt model with added inertial component were 0.96±0.05 and 0.97±0.03 for the F/1.5 and F/3 focal configurations respectively, whereas R^2 values for the classical Voigt model were 0.83±0.18 using F/1.5 and 0.79±0.15 using F/3. Further, τ values for the different focal configurations were not statistically significantly different when derived from the Voigt model with added inertial component (F/1.5: 0.34±0.04 ms, F/3: 0.35±0.07 ms, p=0.38), but were statistically significantly different when derived from the classical Voigt model (F/1.5: 0.18±0.04 ms, F/3: 0.23±0.11 ms, p=0.002).

Conclusions: Results showed better closeness of fit between experimental and predicted displacement profiles when using the Voigt model with added inertial component. In addition, τ measurements derived using the Voigt model with added inertial component were not significantly different for the two focal configurations despite an increase in the volume of the displaced tissue, suggesting that the model is able to compensate for differences in mass.

Acknowledgements: This work was supported by NIH grants R01–NS074057, R01–HL092944, and K02–HL105659.

References:

[1] M.R. Scola, CM Gallippi: Abstract in Proceedings of the 37th International Symposium on Ultrasonic Imaging and Tissue Characterization, Arlington, VA, June 11–13, 2012.
[2] M.R. Scola, JN Kornegay, JF Howard, CM Gallippi: Abstract in Proceedings of the 38th International Symposium on Ultrasonic Imaging and Tissue Characterization, Arlington, VA, June 10–12, 2013.
[3] F. Viola, W.F. Walker: IEEE Transactions on Ultrasonics, Ferroelectrics, and Frequency Control, Vol. 50, No. 6, pp. 736–42, Jun. 2003.

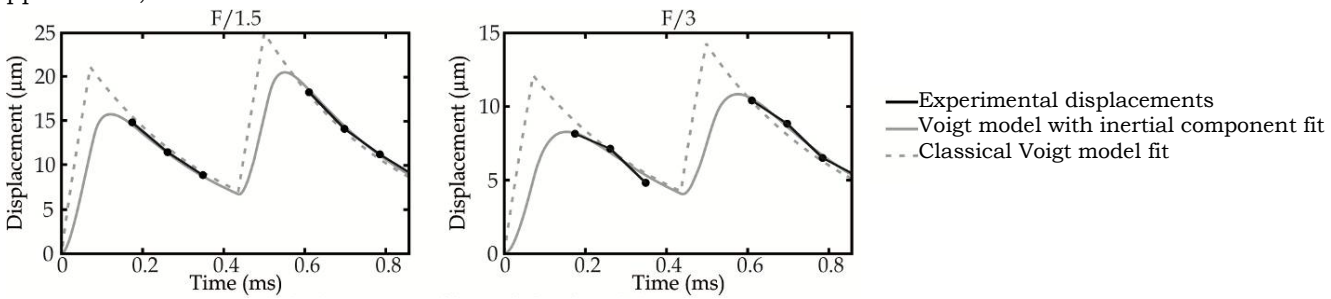

Figure 1: Experimental displacement profiles with fitted models.

* *indicates Presenter*

060 **ELECTROMECHANICAL WAVE IMAGING IDENTIFIES BIVENTRICULAR PACING AND TREATMENT RESPONSE/NONRESPONSE IN HEART FAILURE PATIENTS UNDERGOING CARDIAC RESYNCHRONIZATION THERAPY.**

Ethan A. Bunting[1], Litsa K. Lambrakos[1], Fusako Sera[1], Elisa E. Konofagou[1].*
[1]Columbia University, 630 West 168th Street, New York, NY, 10032 USA.

Background: Cardiac resynchronization therapy (CRT) is a promising treatment for patients with mid– to late–stage heart failure (HF) which uses electrical pacing in each of the ventricular chambers to resynchronize the electromechanical activity of the heart. Although CRT has been shown to decrease mortality and HF–related hospitalizations, several studies have found that approximately 30–50% of patients do not derive significant benefit from CRT [1]. This nonresponse rate is especially alarming considering the cost and invasive nature of the treatment itself. Electromechanical wave imaging (EWI), a technique developed previously in our lab, has been shown to be able to estimate healthy and pathologic cardiac strains *in vivo* through the use of precise strain estimation at very high spatial (<1mm) and temporal (2000Hz) resolutions [2]. Furthermore, the measured electromechanical wave has been shown to be closely correlated with the electrical activation sequence [3]. Clinically, EWI is also appealing since it offers full–view imaging of the cardiac electromechanics within a single heartbeat.

Aims: Previous work has demonstrated the capability of EWI to identify single pacing sites in CRT subjects. In this work, EWI was used to identify the electromechanical activation sequence of sinus rhythm and biventricular pacing in HF patients. Patients have also been separated into two groups, responders and non–responders, and the electromechanical activation sequences of patients in each group are compared.

Methods: Six patients in NYHA Stage III or IV heart failure were imaged transthoracically using a 2.5MHz phased array transducer and an ultrasound system capable of sampling radiofrequency signals directly from each of the 64 transducer elements (Verasonics, Inc., Redmond, WA). A diverging beam sequence was used in order to achieve a frame rate of 2000Hz. Each subject was scanned in the 4– and 2–chamber views in sinus rhythm and in their preprogrammed biventricular pacing protocol. Three of the subjects were designated as responders by a trained cardiologist using a ≥25% increase in ejection fraction. EWI was performed using a 1D cross–correlation method on the RF signals, which generated electromechanical activation isochrones for the full view of the heart as previously described [2].

Results: EWI isochrones showed that in sinus rhythm, electromechanical activation started in the septum before propagating to the right ventricular (RV) and left ventricular (LV) walls. Biventricular pacing caused different activation origins compared to sinus rhythm, with origins occurring in the LV lateral wall as well as the RV apex. Complete activation of both ventricles occurred within 150–300ms in sinus rhythm, with the LV lateral wall being activated the latest. Responders experienced a 50–150ms reduction in total activation time, while non–responders saw significantly decrease or no improvement in activation.

Conclusions: For the first time, EWI has been used to identify the presence and location of biventricular pacing in patients *in vivo*. Furthermore, EWI has been shown to be capable of imaging the recovery in electromechanical activation in CRT patients. These initial findings indicate the potential of EWI to monitor CRT and distinguish responders from non–responders.

Acknowledgements: This study was partly supported by NIH EB006042 and NIH HL114358.

References:

[1] Birnie, D. and Tang, A.: The Problem of Non–Response to Cardiac Resynchronization Therapy. Curr. Opin. Cardiol., 21, pp. 20–26, 2006.
[2] Provost, J., et al.: A Clinical Feasibility Study of Atrial and Ventricular Electromechanical Wave Imaging. Heart Rhythm, 10(6), pp. 856–862, 2013.
[3] Provost, J., et al.: Imaging the Electromechanical Activity of the Heart *In Vivo*. Proc. Natl. Acad. Sci. U.S.A., 108(21), pp. 8565–8570, 2011.

004 **DEVELOPMENT OF A SET OF PHANTOMS MIMICKING THE STIFFNESS OF HUMAN BIOLOGICAL SOFT TISSUES USING MAGNETIC RESONANCE ELASTOGRAPHY (MRE).**

GE Leclerc[1], SF Bensamoun[1].*
[1]BioMécanique et BioIngénierie, UMR CNRS 7338, Université de Technologie de Compiègne, Compiègne, FRANCE.

Background: Non–invasive imaging technologies, such as Magnetic Resonance Elastography, have been developed to characterize the mechanical properties of soft tissues. The development of these technologies will be improved by the creation of phantoms, with similar mechanical properties of biological soft tissues, allowing the set–up of new MRE protocols and to assess its feasibility. In the literature, different kinds of phantoms have been developed with wirosil, agar, or bovine gels [1–3].

Aims: The purpose of this study was to develop a set of phantoms, composed of plastisol, mimicking the stiffness of different biological soft tissues (healthy and fibrotic livers, spleen, kidney, skeletal muscles) using magnetic resonance elastography (MRE).

Methods: Five homogeneous phantoms (14x5x7cm) were created with different concentrations of liquid plastic (Plastileurre, Bricoleurre, France) and softener (Assouplissant, Bricoleurre, France). The mixture was adjusted from 30–70% in order to progressively increase the stiffness of the media. The density of the phantom was evaluated as similar to the biological tissues (1000kg/m^3). Subsequently, MRE tests were performed for each phantom which was placed inside a head coil in a 1.5T MRE machine (Signa HDx, General Electric). The driver (Figure 1) was the one used for clinical liver exam realized at 60Hz and is positioned under the phantom [4,5]. Coronal MRE phase images were collected using a motion sensitizing gradient echo sequence, a flip angle of 45°, a 20 x 20 cm FOV, a 256 x 64 acquisition matrix, TE/TR=27.9/50ms and four offsets. The cartography of the shear modulus (μ) was generated with LFE (Local Frequency Estimate) algorithm, and the elastic properties were measured within a region of interest (ROI) located in the same area for each phantom.

Results: Phase images show clear shear wave propagation inside all the phantoms. An increase of the shear modulus was obtained as a function of the plastic liquid concentration. The shear modulus varied from 1–8kPa as represented in the following Figures.

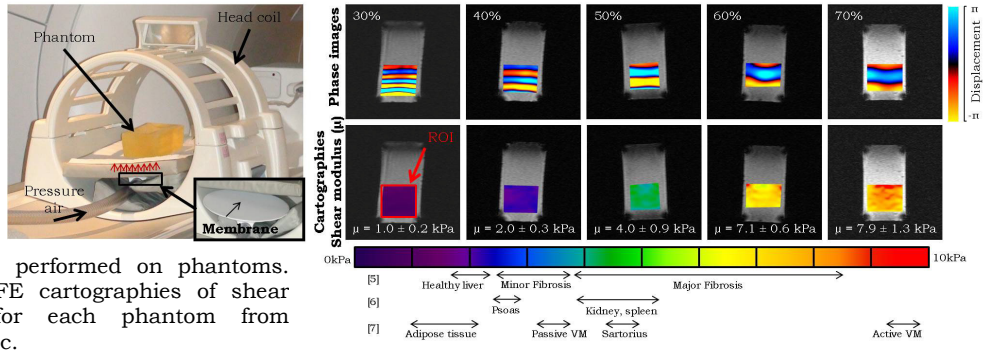

Figure 1: Set up of MRE tests performed on phantoms. Phase images and LFE cartographies of shear modulus obtained for each phantom from 30–70% of liquid plastic.

Conclusions: In the literature, mechanical properties of liver, abdominal and muscular tissues are represented by a shear modulus in a range of 1–9kPa [5–7], which is similar to the present phantom behaviors. These results confirmed the feasibility of this set of phantoms to mimic healthy and pathological human soft tissues. Furthermore, these phantoms could be used to develop a finite element identification method based on simulated shear wave propagation in order to set up of future clinical MRE protocols [8]. In addition, the viscoelastic properties of these phantoms could be further characterized with multifrequency MRE tests in order to represent the true soft tissue behaviors.

References:

[1] Oudry et al.: JMRI, 30(5), pp. 1145–1150, 2009a.
[2] Chen et al.: JB, 38(4), pp. 959–963, 2005a.
[3] Hamhaber et al.: Magnetic Resonance in Medicine, 49(1), pp. 71–77, 2003.
[4] Leclerc et al.: JB, 6(6), pp. 952–957, 2012.
[5] Leclerc et al.: JMRI, in press.
[6] Bensamoun et al.: CI, 35(4), pp. 284–287, 2011.
[7] Debernard et al.: JMR, in press.
[8] Leclerc et al.: CMBBE, in press.

* *indicates Presenter*

008 **INFLUENCE OF REGION OF INTEREST SIZE ON THE PERFORMANCE OF SHEAR WAVE ELASTOGRAPHY IN SOLID BREAST MASSES.**

Katrin Skerl[1], Kim Thompson[1], Sarah Vinnicombe[1], Patsy Whelehan[1], Andrew Evans[1].*
[1]Dundee Cancer Centre, University of Dundee, Dundee, Scotland, UK.

Background: Ultrasound shear wave elastography (SWE) has been shown to be useful for refining benign/malignant differentiation in solid breast masses [1–3]. During scanning, a region of interest (ROI) is selected, and the mean and max elasticity values of the area are measured. Previously validated threshold values (mean 50kPa [3], max 80kPa [1]) to differentiate benign and malignant masses were used. To date there are no published studies indicating what size of ROI gives optimal diagnostic performance.

Aims: To identity which of three ROI diameters provides optimal accuracy and whether this varies with lesion size.

Methods: 2D SWE images of 137 solid breast masses (median size: 16mm) were reviewed. Eighty–eight (88) lesions were malignant and 49 lesions were benign. The images had been acquired using the Aixplorer ultrasound machine (Supersonic Imagine, Aix–en–Provence, France). The ROI was moved around the elastography color map until it was over the area of greatest stiffness. The mean and max stiffness values were assessed using ROI's of 1mm, 2mm and 3mm in diameter. The assessment of the SWE images was made blinded to the pathological results and the assessor was not experienced in the interpretation of grey scale ultrasound imaging (B–mode imaging). The gold standard was the results of core biopsy or surgical excision. The analysis was performed for all the lesions and for separate subsets of small (<15mm) and large≥(15mm) lesions. The sensitivity, specificity and diagnostic accuracy were calculated and compared, using chi squared and chi squared for trend tests.

Results: For mean stiffness values in all the masses, sensitivity for a ROI of 1mm (98%) was significantly better than for a ROI of 2mm (93%) or 3mm (88%) (p=0.031). Sub–analysis of small lesions also show superior performance of a 1mm ROI compared to 2mm and 3mm (96%, 88%, 80%, p=0.048). For large lesions, no significant differences were found. There were no significant differences in specificity or diagnostic accuracy using different sizes of ROI. Maximum stiffness values were similar whichever ROI size was used.

Conclusions: The results indicate that SWE assessment of mean stiffness in solid breast masses should be performed with the smallest possible ROI (1mm), especially when small lesions are being examined.

Acknowledgements: This work was funded by Supersonic Imagine and the EPSRC.

References:

[1] Berg et al.: Shear–Wave Elastography Improves the Specificity of Breast US: The BE1 Multinational Study of 939 Masses. Radiology, Volume 262, Number 2, February 2012.
[2] Chang et al.: Clinical Application of Shear Wave Elastography (SWE) in the Diagnosis of Benign and Malignant Breast Diseases. Breast Cancer Res Treat, 129, pp. 89–97, 2011.
[3] Evans et al.: Quantitative Shear Wave Ultrasound Elastography: Initial Experience in Solid Breast Masses. Breast Cancer Res [serial on the Internet] 12(6). Available at http://breast-cancer-research.com/content/12/6/R104.

014 **A GPU–BASED IMPLEMENTATION OF ITERATIVE SHEAR VELOCITY IMAGE RECONSTRUCTION.**

Sua Bae[1], Jae Hee Song[1], Yangmo Yoo[1], Tai–Kyong Song[1], Jin Ho Chang[1].*
[1]Sogang University, Seoul, REPUBLIC OF KOREA.

Background: Shear wave (SW) imaging provides quantitative stiffness information in the tissue, and thus it allows for improving diagnostic performance. The SW images can be reconstructed using a simple direct inversion method [1]. However, the method is susceptible to noise due to its double derivative operations. To overcome the problem, a few iterative image reconstruction algorithms were proposed [2]. It is challenging to implement the algorithms for real–time operation because of its high computational cost.

Aims: This paper presents GPU–based implementation of an iterative image reconstruction algorithm and evaluates its performances in terms of accuracy and computational speed.

Methods: In the iterative method, an initial displacement field is obtained by solving the forward problem with a homogeneous velocity map. The displacement field is updated using a modified velocity map computed with the previously calculated displacement field and measured one. This process should be repeated until the final velocity map is obtained. This is the main reason why the iterative method requires high computational cost. The whole pixel values of one frame in the displacement field can be independently computed for the updating, which allows for parallel computing by multithreaded GPU; the number of threads is equal to the number of pixels in one frame. Each thread simultaneously executes a kernel producing one displacement frame. The backward problem in the iterative image reconstruction is also solved in the same way. The GPU program was run on Nvidia´s GeForce GTX–560Ti GPU chips. Its computational speed and accuracy are measured. For this, 250–frame simulation displacement data are generated; one frame consists of 90 scanlines, and each scanline has 90 samples. The simulation displacement data contains -35dB white Gaussian noise.

Results: Figure 1 shows velocity SW images reconstructed with the simulation displacement data. The execution time for an iteratively reconstructed image was 93.2msec that corresponded to about 10 frames per second. The error between the true SW velocity and the computed one by GPU was 2.21% while the error of the direct inversion method was 10.03% due to the noise.

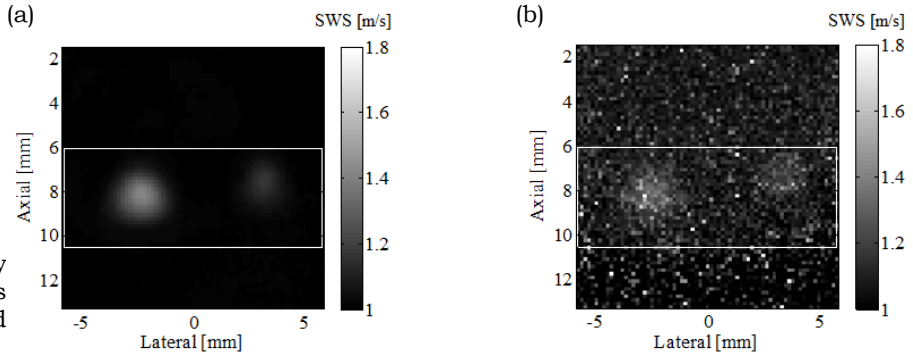

Figure 1: SW images reconstructed by the iterative methods implemented by (a) GPU and (b) direct inversion.

Conclusions: The results indicated that the iterative method is robust to noise and can be implemented using GPU for real–time SW image reconstruction.

Acknowledgements: This work was supported by the R&D program of MKE/KEIT(10033627, Ultrasound Imaging Technique of Tissue Elasticity)

References:

[1] J. Bercoff, M. Tanter: Supersonic Shear Imaging: A New Technique for Soft Tissue Elasticity Mapping. IEEE Trans. UFFC, Vol. 51, No. 4, pp. 396–409, 2004.
[2] A. Hossain, M. Cho: A Simulation Study on Iterative Shear Velocity Image Reconstruction for Ultrasound Transient Elastography. Biomedical Engineering Letters, Vol. 2, No. 1, pp. 52–61, 2012.

* *indicates Presenter*

023 **CHIRP MODULATED SHEAR WAVE FOR NOISE–ROBUST IMAGE RECONSTRUCTION: A SIMULATION STUDY.**

Jae Hee Song[1], Sua Bae[1], Tai–Kyong Song[1] and Jin Ho Chang[1].*
[1]Sogang University, Seoul, REPUBLIC OF KOREA.

Background: Shear wave (SW) elastography has become a useful tool for disease diagnosis in breast and thyroid tissues due to its capability of quantitative assessment. Image reconstruction of SW velocity map from displacements induced by SW is performed in two different ways; the iteration method is robust to noise but computationally inefficient while the direct inversion method (DIM) is computationally efficient but very susceptible to noise [1].

Aims: This presentation proposes a new method to increase a signal–to–noise ratio (SNR) of displacement signals by using SW modulation.

Methods: In this presentation, the analytic solution of the displacement was derived using the Kelvin–Voigt model [2] to seek an external force function suitable for SNR improvement. The displacement as a function of time, *t*, can be expressed as

$$x(t) = \frac{1}{c} e^{-\frac{k}{c}t} \cdot u(t) * f(t) \qquad \text{Equation 1}$$

where *c* is the viscous constant (6Pa•s in the simulation), *k* is the elastic constant (6kPa), *u(t)* is the step function and *f(t)* is the arbitrary external force. When *f(t)* is defined, Equation 1 can be numerically calculated using MATLAB. In the study, step and chirp functions were used as external forces. Note that the step function corresponds to the conventional external force. Also, SW propagation on 2–D plane was simulated using a finite difference time domain method. White Gaussian noise with -40dB magnitude was added to displacement signals obtained at each time step. Out–of–band noise in displacement signals generated by the step function was suppressed with a low pass filter. For the chirp function, pulse compression was conducted on displacement signals by using time inverted replica before reconstruction. Other imaging processing was not used. From resultant displacement signals, velocity map was reconstructed using the DIM.

Results: Figure 1 shows reconstructed SW velocity maps. Velocities of round and square inclusions were set to be 2m/s and 1.5m/s, respectively, while background velocity was 1m/s. By comparing two maps, it was seen that the proposed method could effectively improve the accuracy of reconstructed SW velocity because of its higher SNR.

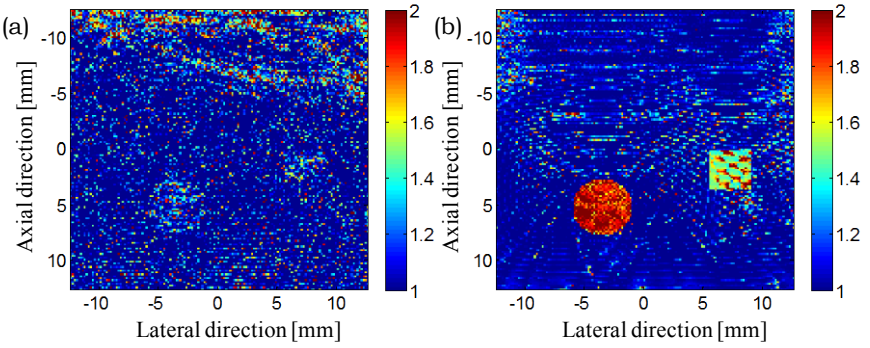

Figure 1: Shear wave velocity maps reconstructed by the conventional (step function, (a)) and the proposed (chirp, (b)) methods.

Conclusions: We derived the analytic solution of the displacement induced by SW. From this, it was proposed that the chirp function as an external force could increase SNR of the displacement signals and thus the drawback of DIM could be overcome. Although simulation results were successful, it should be further verified through phantom and *in vitro* experiments.

Acknowledgements: This work was supported by the R&D program of MKE/KEIT(10033627, Ultrasound Imaging Technique of Tissue Elasticity)

References:

[1] J. Bercoff, M. Tanter and M. Fink: Supersonic Shear Imaging: A New Technique for Soft Tissue Elasticity Mapping. IEEE Trans Ultrason. Ferroelectr. Freq. Control, Vol. 51, No. 4, pp. 396–409, 2004.
[2] W.F. Walker, F.J. Fernandez and L.A. Negron: A Method of Imaging Viscoelastic Parameters with Acoustic Radiation Force. Phys. Med. Biol., Vol. 45, pp. 1437–1447, 2000.

046 **HIGH SPEED BEAMFORMING ON ARBITRARY ORTHOGONAL COORDINATE SYSTEM THROUGH FOURIER'S TRANSFORM WITH NO APPROXIMATE CALCULATIONS.**

Chikayoshi Sumi[1], Naoto Yamazaki[1].*
[1]Sophia University, 7–1, Kio–cho, Chiyoda–ku, Tokyo, JAPAN.

Background: Recently, raid tissue motions are measured ultrasonically with high frame rates in various manners (e.g., parallel processing etc.), for instance, shear wave propagation, carotid blood flow, heart motion etc. For such measurements, we previously proposed to use steered plane wave transmissions (e.g., [1]) in conjunction with the use of the lateral modulation (LM) method (e.g., [2]) and a steering angle (ASTA) method (e.g., [3]). The transmissions are performed respectively or simultaneously. The respectively received echo plane waves with different steering angles can also be coherently superposed to yield high spatial resolution echo data (e.g., [1]). For such plane wave generations, as far, other two groups from us have reported fast beamforming methods using Fourier's transforms [4,5].

Aims: A new Fourier's transform–based beamforming method is reported. In other methods, a wave number matching is performed approximately by interpolating spectra in a frequency domain [4] or using a special Fourier's transform with non–uniform sampling intervals [5]. In contrast, the new method permits to carry out the beam steering on an arbitrary coordinate system without any approximate calculations. For the echo data generation, a high accuracy and a high speed are achieved. Accordingly, the accuracy of displacement measurements using an echo signal phase is also improved.

Methods: As shown in Figure 1 Steps 2 and 4, the wave number matching is performed through the two complex exponential multiplication steps for the respective lateral and depth directions. Step 4 also performs the calculation of angular spectra at respective depths simultaneously. Although these calculations are performed through the conventional one–dimensional Fast Fourier's transform (1D FFT) in Steps 1 and 3, the last two–dimensional (2D) inverse Fourier's transform to be performed is carried out by the faster processing using the conventional 1D inverse FFT reported for a synthetic aperture [6] (Steps 5 and 6). When plural steered plane waves are transmitted simultaneously, respective echo waves separated in a frequency domain in advance are similarly processed, and Steps 5 and 6 are performed on superposed data. Simulations are performed to confirm the feasibility of the new method. An array type–transducer is simulated using Field II [7].

Results: For instance, with respect to the simulation phantom shown in Figure 2a, a linear array type transducer (3MHz; pitch, 0.1mm; kerf, 0.025mm; 128 elements) yields echo data with no steering (Figure 2b) and with 10° steering angle (Figure 2c). Figure 2d shows the echo data obtained through the superposition of echo data with less than ±10° steering angles.

Conclusions: We developed a new high speed Fourier's transform–based beamforming method for plane wave transmissions. The feasibility and accuracy are confirmed through such simulations. The method permits the echo generation without performing any approximations on an arbitrary orthogonal coordinate system. That is, various scanning can be performed (e.g., sector, radial, convex, fan etc.). At the Conference, such advantageous properties of the method will be demonstrated on simulations and experiments through the comparisons with other methods.

1 FFT with respect to time t.
2 Matching on lateral kx.
3 FFT with respect to lateral x.
4 Matching on depth ky and calculation of angular spectra with respective depths.
5 Summation with respect to k.
6 IFFT with respect to kx.

Figure 1: Steps of beamforming.

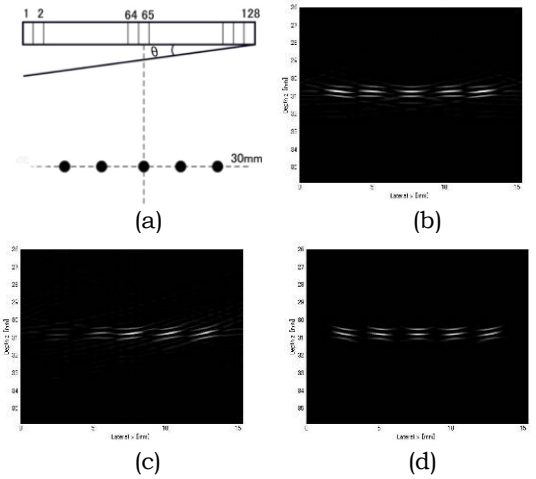

Figure 2: Simulations. (a) Phantom. (b) No steering; (c) 10° steering; (d) Coherent superposition.

References: [1] C. Sumi et al.: Proc 11th ITEC, 2012.
[2] C. Sumi et al.: IEEE Trans. UFFC, Vol. 55, pp. 24–43, 2008.
[3] C. Sumi et al.: Rep Med Imag, Vol. 5, pp. 23–50, 2012.
[4] J. Cheng, et al.: IEEE Trans UFFC, Vol. 53, pp. 880–899, 2006.
[5] P. Kruizinga et al.: IEEE Trans. UFFC, Vol. 59, pp. 2684–2691, 2012.
[6] L. J. Busse: IEEE Trans. UFFC, Vol. 39, pp. 174–179, 1992.
[7] J. A. Jensen: Proc Med Biol Eng Comp, 10th Nordic–Baltic Conf Biomed Imag, pp. 351–353, 1996.

* *indicates Presenter*

047 **BEAM STEERING WITH POST–INCREASING LATERAL BANDWIDTH FOR HIGH SPATIAL RESOLUTION ECHO IMAGING AND HIGH ACCURACY DISPLACEMENT MEASUREMENT: DEMONSTRATION ON SMALL INCLUSION AGAR PHANTOMS.**

*C*hikayoshi *Sumi*[1]*, *Ryo Araki*[1], *Tsuyoshi Shimoyama*[1], *Daiki Kikunaga*[1], *Miki Sakai*[1].
[1]Sophia University, 7–1, Kio–cho, Chiyoda–ku, Tokyo, JAPAN.

Background: When performing beam steering for such as a sector or our proposed lateral modulation (LM) scanning (e.g., [1,2]), if an ultrasound (US) element pitch or a beam pitch is large, or if a steering angle is made too large to obtain a large field of view or a large lateral frequency and bandwidth, aliasing occurs. A properly generated large steering angle increases a lateral spatial resolution and measurement accuracies of a lateral displacement/strain. Then, we previously proposed a method for increasing a lateral bandwidth, i.e., through performing zero spectra padding in a frequency domain after physically completing beamforming [1,2]. As far, we showed only B–mode images obtained using the method [1].

Aims: The method was used for high spatial resolution measuring displacements/elasticity (strains, etc.) using a special transducer and beamforming parameters, particularly on agar phantoms having very small cylindrical stiff inclusions (i.e., dia. 3 and 5mm) that were laterally compressed.

Methods: The transducer was specially manufactured to have a small element pitch (0.1mm) rather than commercial ones. Experiments were performed using three kinds of beams generated through synthetic aperture processing with respect to same raw echo data (US frequency, 7.5MHz; wavelength, λ). (i) Echo data were generated with the same pitch as the element pitch, and a lateral wavelength (LW) 2λ was achieved with no aliasing; (ii) For echo data aliased with respect to LW 2λ, which were generated with the twofold pitch (0.2mm) through addition of adjacently received raw echo data, 2λ was achieved using the method; (iii) Echo data with LW λ were generated using the method with the half pitch (0.05mm). For comparison, other echo data were also generated through the coherent superposition (e.g., [3]) of echo data (i) and (iii), and over–determined systems were also generated from echo data (i) and (iii), i.e., the least squares method (LST) and averaging of measurements (AVE) were performed (e.g., [3]).

Results: The measurement accuracies depend on various parameters such as a window size, an echo SNR, etc. For instance, when our previously developed multidimensional autocorrelation method (MAM) [4] was used with a window size, $1.0\times2.4mm^2$, the measurement accuracies of strains and shear moduli were evaluated statistically. For echo data (i), without the method, accurate measurements were achieved (the small circular inclusions was detected). With the method, the echo data (ii) were not useful for the measurements (the inclusion shapes were distorted). However, LM echo imaging was achieved. For echo data (iii), the method was effective in yielding large lateral frequency and bandwidth echo images (wavelength, λ) and high measurement accuracies. However, the larger lateral frequency decreased the measurement accuracies due to decreasing an echo SNR. The order of accuracies was LST>coherent superposition=AVE>(iii)>(i)>(ii) [for lateral strains in a 5mm inclusion, about mean, -0.5%, SDs, 0.23, 0.24, 0.24, 0.28, 0.30, 0.70%]. When using a smaller window, the order changed, and for instance, for $0.5mm\times2.4mm^2$, the method was not effective, i.e., (i)>AVE>LST>coherent superposition>(iii)>(ii). As previously confirmed in [3], when local echo data had a low echo SNR, AVE was more effective than LST; and coherent superposition had a trend in yielding a lower measurement accuracy than such over–determined systems, although a higher spatial resolution echo imaging was performed. Moreover, MAM allowed measuring a high accuracy lateral displacement but also a higher accuracy axial displacement than a conventional axial measurement.

Conclusions: Using the method, even when performing spatially sparsely beamforming or the Nyquist theorem was not satisfied with, such a large steering angle was achieved; high frame rate echo imaging and accurate measurements were also achieved. The uses of plural beams were also effective. In addition, other previously developed methods were also used, e.g., steered plane wave transmissions (e.g., [3,4]). Combinational high spatial resolution echo imaging was also effective. The uses of spectra frequency division method (e.g., [3]) will also be reported together. These methods will be effectively used for measurements of various rapid and complex tissue motions and shear wave propagations etc.

References:

[1] C. Sumi et al.: Proc. 7th ITEC, 2008.
[2] C. Sumi et al.: IEICE US Meeting, Vol. 2013–5, pp. 23–28, (in Japanese) May 2013.
[3] C. Sumi et al, Proc. 11th ITEC, 2012.
[4] C. Sumi, IEEE Trans on UFFC, Vol. 55, pp. 24–43, Jan 2008.

048 **SIMULTANEOUS ECHO IMAGING AND ELASTICITY/DISPLACEMENT MEASUREMENT WITH HIGH INTENSITY FOCUS ULTRASOUND TREATMENT AND/OR ACOUSTICAL RADIATION FORCE IMAGING.**

Chikayoshi Sumi[1], Yuto Hirabayashi[1], Naoto Yamazaki[1].*
[1]Sophia University, 7–1, Kio–cho, Chiyoda–ku, Tokyo, JAPAN.

Background: The developments of useful ultrasound (US)–echo–based tissue displacement measurement methods and beamforming methods increase the applications of displacement/strain measurements (e.g. various blood flow, motions of the heart, liver, etc.). For instance, our previously developed combination of the multidimensional autocorrelation method (MAM) and lateral modulation (LM) methods (e.g. [1]) or a single beam method (e.g. [2]) resulted in accurate two– or three–dimensional displacement vector/strain tensor measurements. We have also been developing combined digital US diagnosis/treatment systems (e.g. [3]), in which (i) a diagnostic US echography can be performed, (ii) a high intensity focus US (HIFU) treatment can also be performed for an echo–based and/or radiation–force–based diagnostic measurement/imaging, as well as the combination used with diagnostic ultrasounds, (iii) a radiation force can also be used for an echo–based measurement/imaging. Last year, various useful applications of coherences of ultrasound and low frequency waves are reported [4]. Specifically, spectral frequency divisions and/or coherent superpositions of spectra or echo signals are performed with weighting for yielding (1) a high spatial resolution imaging/treatment, (2) accurate displacement vector/strain tensor measurements, (3) desired mechanical and/or thermal sources, (4) desired low frequency deformations or low frequency wave propagations and (5) accurate temperature measurements, etc. Interferences of US or low frequency beams/waves are properly used for synthesizing new beamforming/wave parameters such as a wavefront, a propagation direction, a steering angle, frequencies, bandwidths, focuses etc. Quasi–beams/quasi–waves can also be generated by signal processing (i.e., not physically generated ones). A temporal and/or spatial filtering can also be performed in the frequency domain to change beam/wave properties or separate signals or waves (e.g. plural crossed beams/waves, and mechanical and thermal strains, etc.).

Aims: In this presentation, simultaneous a high spatial resolution echo imaging and accurate elasticity/displacement measurements are performed through the same spatial filtering of spectra [4] with respect to HIFU transmissions for a thermal treatment or an acoustical radiation force imaging (simulations).

Methods: Performing the spectra filtering with respect to a large spatial bandwidth echo data obtained using concave transducers (aperture dia., 12mm, focus depth, 35mm, 5MHz). The transducers are simulated using Field II [5]. Echo data are also simulated for same scattering tissue with same uniform axial and lateral strains (0–3%). A strong scatter is set in a region of interest. Two cases are simulated for the same deformed tissue: (i) One transducer is used to obtain non–steered echo data and (ii) Two transducers are laterally, symmetrically steered (0–45°) and received echo data are superposed to achieve an LM. For Case (ii), the spatial filtering can be performed with respect to superposed, separated, or respectively received echo data. The point spread functions (PSFs) are made to be circular. These effect qualities of echo images and measurement accuracies of strains. Displacement vector measurements are performed using MAM.

Results: For respective (a) non–steering (0°) and (b) LM with steering, B–mode images are obtained from non–filtered and filtered spectra. For the filtered spectra, the strong scatter and speckle patterns are visualized to be circular. Measurement accuracies (statistics) of axial and lateral displacements are evaluated. For the non–steering case with axial and lateral strains larger than 2%, the reshaping PSF increases the measurement accuracy of a lateral displacement (for instance, for 3% strains, when means are about 5.36 vs 5.27×10^{-2}mm, SDs are 0.78 vs 0.83×10^{-2}mm).

Conclusions: For echo imaging and displacement/elasticity measurement/imaging, the reshaping of PSFs through the spectra filtering is confirmed to be effective with respect to the use of concave transducers. At the Conference, results obtained for other steering angles will be specifically reported. The same approach will also be used for a microscopic imaging using the concave aperture type transducer.

References:

[1] C. Sumi et al.: IEEE Trans. on UFFC, Vol. 55, pp. 24–43, 2008.
[2] C. Sumi et al.: Reports in Medical Imaging, Vol. 5, pp. 57–101, 2012.
[3] C. Sumi: Proc 1st ITEC, p. 23, 2002.
[4] C. Sumi: Proc 11th ITEC, 2012.
[5] J. A. Jensen: Proc Med Biol Eng Comp, 10th Nordic–Baltic Conf Biomed Imag, pp. 351–353, 1996.

* *indicates Presenter*

049 **ACCURACY OF SHEAR MODULUS RECONSTRUCTION DEPENDS ON IGNORING MEAN NORMAL STRESS DISTRIBUTION.**

C. Sumi[1].*
[1]Sophia University, 7–1, Kio–cho, Chiyoda–ku, Tokyo, JAPAN.

Background: Mechanical properties such as viscoelasticities (e.g., [1]) are estimated using various mechanical sources such as a heart motion, a low frequency compression/stretching, an applied vibration, an acoustically radiated force etc. Such estimation is performed through measurements of deformations, shear wave propagations etc. The properties can also be reconstructed numerically or via signal processing. A stress tensor, internal mechanical sources and a mean normal stress can also be reconstructed simultaneously. However, various artifacts possibly occur under various assumptions such as an incompressibility, a low dimensionality of the mechanical property distributions (e.g., [2–4]), etc.

Aims: Recently, for the reconstruction of a shear modulus distribution, the distribution of a mean normal stress is ignored. In this presentation, the effects of ignorance are investigated through simulations. Theoretically, an assumption of a uniform mean normal stress distribution leads to reconstruction errors.

Methods: Various linear numerical cubic phantoms (50mm sides) are dealt with. For instance, a Poisson's ratio is assumed to be uniform or non–uniform (~0.49). The phantoms have a stiff or soft spherical inclusion (10mm dia.). The respective phantoms are compressed/stretched or vibrated in a depth direction using large external sources generated at the top planes of the phantoms. The forward calculation is performed using the successive–over–relaxation (SOR) method. Using the reconstruction Method B described in [3], the shear modulus distribution is reconstructed together with the mean normal stress distribution; and the shear modulus is also reconstructed using the method ignoring a mean normal stress distribution. The means and standard deviations (SDs) of reconstructed shear moduli are estimated in inclusions.

Results: For instance, for both phantoms having uniform Poisson's ratios 0.48 and 0.47 and an inclusion with a shear modulus higher than the surrounding region (2.0 vs 1.0×10^5N/m^2), as theoretically predicted, the shear moduli of the inclusion is estimated to be larger than the original value, i.e., inaccurate [for respective Poisson's ratios 0.48 and 0.47, means (SDs) are 2.07 (0.16) vs 2.02 (0.07) and 2.07 (0.15) vs 1.99 (0.06)$\times10^5$N/m^2]. The SDs also becomes larger (i.e., unstable). For soft inclusion phantoms, as theoretically predicted, the shear modulus is estimated to be smaller than the original value (for instance, for a half shear modulus, 0.5×10^5N/m^2 and Poisson's ratio, 0.47, means and SDs are respectively 0.19 (0.01) vs 0.52 (0.02)$\times10^5$N/m^2. When an inclusion has a smaller Poisson's ratio than that of the surrounding region (smaller than 0.43 vs 0.47), the twofold shear modulus is estimated to be smaller than that of the surrounding under the same assumption (for instance, when Poisson's ratio is 0.42, a mean is 0.73×10^5N/m^2). For the respective same phantoms, completely the same results are obtained in compression and stretching cases.

Conclusions: The effects of ignoring a mean normal stress distribution are investigated. Theoretically predicted results are numerically obtained. Similar artifacts are generated when ignoring internal mechanical sources, viscosity, nonlinear properties, isotropic properties. Occasionally performed assumption of a local homogeneity also affects the reconstruction (e.g., decrease in a spatial resolution). The limitations caused by such assumptions will also be reported at the Conference.

References:

[1] C. Sumi et al.: Usefulness of Ultrasonic Strain Measurement–Based Mechanical Properties Imaging Technique: Toward Realization of Short–Time Diagnosis/Treatment. in Research and Development in Breast Ultrasound, New York, Springer, pp. 16–43, 2005.
[2] C. Sumi et al.: J Med Ultrasonics, Vol. 34, pp. 171–188, 2007.
[3] C. Sumi: IEEE Trans on UFFC, Vol. 53, pp. 2416–2434, 2006.
[4] C. Sumi: Therm Med, Vol. 25, pp. 89–103, 2009.

070 **ELASTOGRAPHIC VERSUS B–MODE DIMENSIONAL ANALYSIS OF BREAST TISSUE LESIONS.**

Elisabeth Brusseau[1], Valérie Detti[1], Agnès Coulon[2], Emmanuèle Maissiat[2], Mojgan Devouassoux–Shisheboran[3], Nawele Boublay[4,5,6], Loïc Boussel[1,2], Jérémie Fromageau[7], Nigel Bush[7], Jeffrey Bamber[7].*

[1]Université de Lyon, CREATIS, CNRS UMR5220, Inserm U1044, INSA–Lyon, Université Lyon 1, FRANCE; [2]Service de Radiologie et [3]Anatomie et Cytologie Pathologiques, Hôpital de la Croix–Rousse, Hospices Civils de Lyon, FRANCE; [4]Pôle Information Médicale Evaluation Recherche, Hospices Civils de Lyon, FRANCE; [5]Université Lyon 1, EA 4129, FRANCE; [6]CMRR, Hôpital des Charpennes, Lyon, FRANCE; [7]Joint Department of Physics, Institute of Cancer Research and Royal Marsden NHS Foundation Trust, Sutton, Surrey, England, UK.

Background and Aims: The objective of elastography is to complement mammography and ultrasound to better differentiate between benign and malignant breast lesions. In this aim, strain–related criteria have been introduced, based on axial strain imaging [1,2] but also shear strain imaging [3]. In this study, size and shape of fibroadenomas and cancers between B–mode and axial strain images are compared. To quantify the size differences observed, the area of the lesions in elastograms and sonograms were determined and the strain/B–mode area ratios computed.

Methods: Twelve cancer cases and eight fibroadenoma cases were examined. In this two–center study, data were acquired at the Hôpital de la Croix–Rousse, Lyon, France, with an Ultrasonix (Sonix RP or MDP) ultrasound scanner equipped with a L14–5W/60 probe and at the Royal Marsden Hospital, London, England, with an Acuson 128XP ultrasound system, working with a L7EF probe. RF data were sampled at 40MHz and processed off–line. The manual delineation of the lesion was performed by a radiologist with 5 years of experience in breast imaging for the B–mode images and by a researcher specializing in elastography for strain images. In three cases, poorly defined boundaries prevented the lesions from being delineated and the corresponding area ratios are therefore not reported.

Results: Fibroadenomas tend to be stiffer than the surrounding tissues and similarities in size, shape and margin can be observed between the lesions in elastograms and sonograms, with a mean strain/B–mode lesion area ratio assessed at 1.04±0.26. Carcinomas also appear stiffer than the surrounding tissues, but the stiffer region is frequently much larger in the elastogram than the corresponding lesion in the sonogram and with a different overall shape. For these cases, the mean lesion area ratio obtained is 3.26±3.00.

Conclusions: The differences observed between B–mode and strain images are consistent with published findings [4] and underscore the interest of a further analysis of the size differences to help discriminating between the two lesion classes.

References:

[1] Yerli et al.: Qualitative and Semiquantitative Evaluations of Solid Breast Lesions by Sonoelastography. J Ultrasound Med, 30, pp. 179–186, 2011.
[2] Itoh et al.: Breast Disease: Clinical Application of US Elastography for Diagnosis. Radiology, 239, pp. 341–350, 2006.
[3] Xu et al.: *In Vivo* Classification of Breast Masses using Features Derived from Axial–Strain and Axial–Shear Images. Ultrason Imaging, 34, pp. 222–236, 2012.
[4] Hall et al.: *In Vivo* Real–Time Freehand Palpation Imaging. Ultrasound Med Biol, 29, pp. 427–435, 2003.

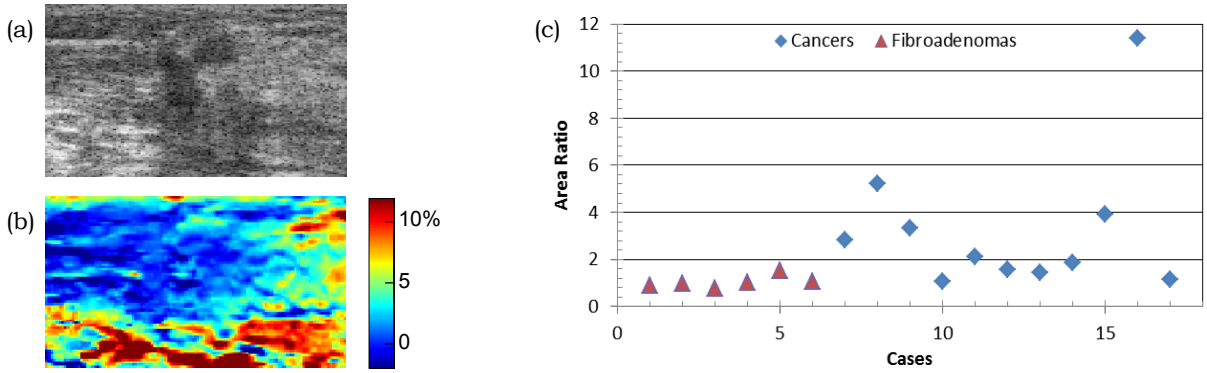

Figure 1: Example of a B–mode image (a) and elastogram (b) obtained with a carcinoma; (c) Elastogram–to–sonogram area ratios for fibroadenomas and cancers.

* *indicates Presenter*

074 **DYNAMIC FRAME–PAIRING IN REAL–TIME FREEHAND ELASTOGRAPHY.**

R Xia[1] and AK Thittai[1].*
[1]The University of Texas Health Science Center at Houston, Houston, TX, USA.

Background: Quasi–static ultrasound (US) elastography is now a well–established technique that involves acquiring US (RF/envelope) signals from an imaging plane before (pre–) and after (post–) a small quasi–static compression to form axial strain elastograms (ASE). The image quality of the elastograms is a function of the applied axial strain. This relationship was extensively investigated and reported in the literature in mid to late 1990s and formalized in terms of the strain filter [1]. Most of the work in elastography has exploited this information and formed elastograms by choosing pre– and post–compression frames separated by a desired compression strain. While this is possible in simulations or tissue mimicking phantom, *in vitro* or *in vivo* experiments that involve controlled compression, it has been a challenge to do this in real–time during freehand compression. Nevertheless, for elastography to be effective in clinical conditions, the importance of selecting the RF–frame pairs appropriately in real–time to yield quality elastograms is understood [2].

Aims: In this work we aim to develop a method that selects pre– and post–compression frames dynamically in real–time based on the axial strain level to form an elastogram. We aim to employ a novel predictive selection approach that allows for implementing this method for real–time elastogram formation.

Methods: Our proposed approach dynamically pairs frames using the frame–average axial strain (FAAS) as an estimate of the applied axial strain. In order to minimize the number of different possible computations required to identify appropriate RF–frame pairing, we propose a 1–prediction–1–correction approach. Essentially, the method predicts the minimum number of frames that need to be skipped (number of frames preceding the current incoming frame) such that the FAAS crosses a 1% strain threshold. After generating the ASE based on the predicted skip frames, a 1–time correction (or reselection) of the frame–pair is allowed. The major steps of our method are shown as block diagram in Figure 1. We validate and demonstrate the advantages of the method with the help of freehand acquired data from tissue–mimicking phantom experiments and an example *in vivo* breast elastography data.

Results: The results show that the method provides most of the frames with similar axial strain levels and specifically rescue frames that otherwise would have been unusable had an in appropriate fixed frame selection was employed. The results also demonstrate that this method can be implemented without sacrificing the ability to perform real–time elastography.

Conclusions: We have reported a method that selects pre– and post–compression RF frames dynamically to form an elastogram based on the axial strain level. We showed that by employing a novel predictive selection approach it is feasible to implement this method for real–time elastogram formation.

Acknowledgements: This work was supported in part by NIH grant R21–CA135580–01 and by the John S. Dunn foundation.

References:

[1] Varghese T, Ophir J: A Theoretical Framework for Performance Characterization of Elastography: The Strain Filter. IEEE Trans Ultrason Ferroelect Freq Control, 44 (1), pp. 164–172, 1997.
[2] Jiang J, Hall TJ, Sommer AM: A Novel Image Formation Method for Ultrasonic Strain Imaging. Ultrasound Med Biol, 334, pp. 643–652, 2007.

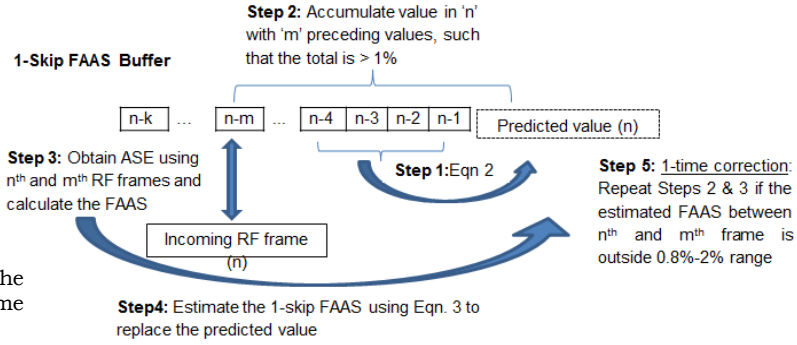

Figure 1: A block diagram representing the important steps of the dynamic frame pairing method

* *indicates Presenter*

040 **SHEAR WAVE VISCOELASTICITY MEASUREMENT BY LASER SPECKLE CONTRAST DETECTION.**

Yi Cheng[1], Sinan Li[1], Robert J Eckersley[2], Daniel S Elson[3] and Meng–Xing Tang[1]*

[1]Bioengineering Department, Imperial College London, London, England, UK; [2]Biomedical Engineering Department, King's College London, London, England, UK; [3]Surgery and Cancer Department, Imperial College London, London, England, UK.

Background: Shear wave speed and attenuation are related to tissue viscoelasticity which could be an indicator for pathological changes. In this abstract, we reported an opto–elastography system that tracks transient shear wave speed at cm depth in tissue mimicking phantoms with laser speckle contrast detection [1]. We also extended our method to continuous shear wave detection so that both elasticity and viscosity could be derived from the shear wave dispersion.

Aims: To study shear wave detection with laser speckle contrast detection and evaluate viscoelasticity property of tissue mimicking phantoms.

Methods: Tissue mimicking phantoms with varied elasticity and viscosity were made. A green coherent laser illuminated phantoms and formed laser speckle patterns were received on a CCD camera that aligned with laser. Time–resolved speckle contrast difference was calculated as shear wave signal. Shear waves were generated with ultrasound at two positions which had different distances to laser axis. By comparing signals of shear wave from two positions, shear wave speed and attenuation between the two positions can be calculated.

Results: By tracking transient shear waves, local shear wave speed was calculated. Elasticity of phantoms were estimated and agreed with independent mechanical compression test. However, fitting both elasticity and viscosity from Voigt's model by measuring shear wave attenuation dispersion from speckle contrast signal is challenging due to a number of factors such as shear wave reflection from phantom boundaries and large volume where optical measurements are sensitive to shear waves. Nevertheless, given a constrained elasticity range, e.g. providing a reference elasticity value by measuring transient shear wave speed, the viscosity of phantoms was inverted from Voigt's model. The estimated viscosity values agree well with those in previous study.

Conclusions: In this study we have demonstrated the feasibility of an optical system to evaluate the elasticity of phantom and extended our opto–elastography system to viscosity measurement by estimating shear wave dispersion from laser speckle contrast analysis. As this system is also able to imaging tissue optical properties it offers the potential of an integrated dual–modality system.

Acknowledgements: We acknowledge the fruitful discussion and suggestion from Prof. David O Cosgrove and the funding from EPSRC (EP/H02316X/1).

Reference:

[1] Y. Cheng, R. Li, S. Li, C. Dunsby, R.J. Eckersley, D.S. Elson, and M.X. Tang: Ultrasound. Med. Biol., 38, p. 1637, 2012.

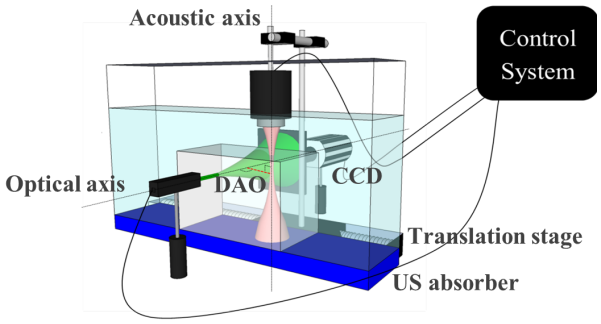

Figure 1: Experiment set up.

* *indicates Presenter*

076 **QUANTITATIVE MICROELASTOGRAPHY USING A MULTI–CHANNEL OPTICAL COHERENCE TOMOGRAPHY**

E. Elyas[1,2], J.T. Erler[3], S.P. Robinson[2], T.R. Cox[3], D. Woods[4], P.Clowes[1], J.C. Bamber[1,2].*

[1]Joint Department of Physics ,[2]CR–UK and EPSRC Cancer Imaging Centre, The Institute of Cancer Research and The Royal Marsden NHS Foundation Trust, Sutton, Surrey, England, UK; [3]Biotech Research and Innovation Centre (BRIC), University of Copenhagen, Copenhagen, DENMARK; [4]Michelson Diagnostics Ltd, Orpington, Kent, England, UK.

Background: Determination of elastic and viscoelastic tissue's features has a broad medical application in diagnosis of many types of malignancies, among them atherosclerotic lesions and various types of solid cancers. There is current interest in extending elastographic methods from the macroscopic, using clinical ultrasound (US) or magnetic resonance technology, to the microscopic, where optical techniques provide the new information on soft tissue mechanobiology with highest resolution.

Aims: This work aims to demonstrate the application of a novel method for quantitative OCT–based microelastography, which takes advantage of unique capabilities of a particular OCT system to simultaneously acquire four parallel spatially–separated optical backscatter A–lines.

Methods: A vibrating needle was used to generate bursts of 5 cycles of 500Hz shear waves within gelatine phantoms of varying stiffness that mimicked a 3D cell–culture matrix. Shear displacements were measured as a function of time and distance from the needle, using four M–mode images acquired simultaneously by modifying a commercial four–channel OCT system (Michelson Diagnostics VivoSight™ model TP1301, UK). Shear wave time–of–arrival (TOA) was detected for each channel and at each distance from the needle by tracking the transverse OCT–speckle motion using cross–correlation methods. Shear–wave speed was then calculated automatically from inter–channel differences of shear–wave arrival time.

Results: Previously we have shown that the speed of the shear wave increases in proportion with gelatine concentration. To measure the resolution of the system a 1.5mm diameter stiff inclusions (15% gelatin) was introduced into soft background (5% gelatin). The propagation waves through the inclusion showed an alternation in their speed over the range of about 200µm as shown in Figure 1.

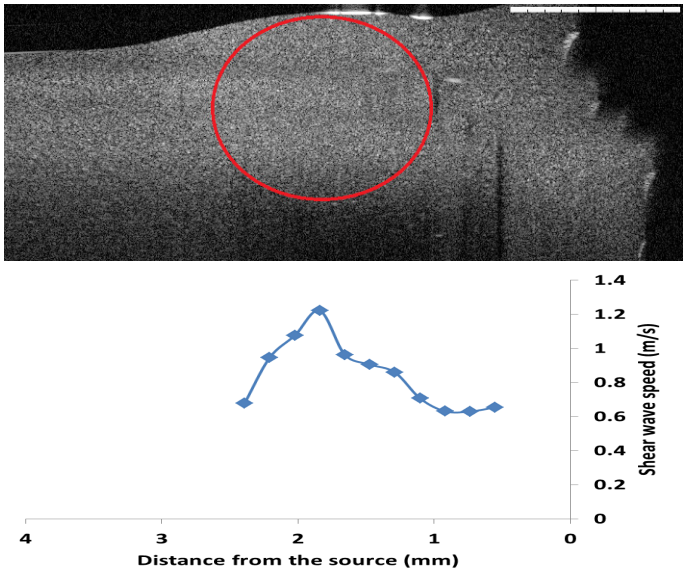

Conclusions: Shear–wave speed of homogeneous gelatin phantoms was measured using novel 4–channel method. Stiff inclusion was successfully detected and a resolution of about 200µm was established. Further work is required to create three dimensional elastograms.

011 **NON–INVASIVE QUANTIFICATION OF LIVER FIBROSIS, ACTIVITY AND STEATOSIS STAGING BY USING SHEAR WAVE ELASTICITY AND VISCOSITY: A FEASBILITY STUDY.**

Thomas Deffieux[1], Jean–Luc Gennisson[1], Laurence Bousquet[2], Dalila Amroun[2], Marion Corouge[2], Simona Tripon[2], Vincent Mallet[2], Mathias Fink[1], Philippe Sogni[2], Stanislas Pol[2], Mickaël Tanter[1].*
[1]Institut Langevin – Ondes et Images, ESPCI ParisTech, CNRS UMR7587, INSERM U979, 1 rue Jussieu, 75005 Paris, FRANCE; [2]Service d'hépathologie, INSERM U1016, Université René Descartes Paris V, Hôpital Cochin, 27 rue du Faubourg Saint–Jacques, 75014 Paris, FRANCE.

Background: Quantitative elastography has been established as an efficient tool for chronic liver diseases non–invasive diagnosis and staging. By estimating shear wave velocity in the liver, the local shear modulus can be estimated and used for non–invasive fibrosis staging since it is correlated to the fibrosis level. However, shear wave propagation also yields information on the viscosity and other medium properties than can be assessed under the assumption of a rheological model which could be interesting for diagnosis.

Aims: The aim of this study is to compare Shear Wave Spectroscopy (SWS) [1], giving access to viscosity, with fibrosis, steatosis and activity assessed by liver biopsies.

Methods: After conflicting Fibroscan and blood–tests results, 120 patients with chronic liver diseases (68 patients with viral hepatitis, 14 patients with alcoholic liver disease, 9 patients with Nash, 7 patients with autoimmune diseases, 22 others or unknown) were selected for a liver biopsy and subsequently included in the study. Among them 117 patients had a Shear Wave Elastography (SWE) exam (Aixplorer with curved probe SC6–1, 3MHz), 110 patients had a Fibroscan (FS) and 94 patients had Apri, Fib4, and Forn's index blood tests. The fibrosis score was assessed using the biopsy according to Metavir (F0–1: n=63, F2: n=18, F3: n=21, F4: n=18). We then assessed the performances of SWE, blood tests and FS using receiver operator characteristic (ROC) curves analysis. We also estimated the liver viscosity using the SWS technique and compared the results not only to the fibrosis levels but also to activity and steatosis levels.

Results: On all patients, results show that fibrosis can be reliably estimated from the shear wave group velocity as well as from the shear wave dispersion curve by estimating the Young's moduli at 50Hz and 150Hz using phase velocities or by the Voigt shear modulus and Voigt viscosity (Table 1). The areas under the ROC curves based on blood tests results were found to be 0.74 F≥2, 0. 70 for F≥3, and 0.70 for F=4 using Apri, 0.76 F≥2, 0. 71 for F≥3, and 0.77 for F=4 using Fib4 and 0.79 F≥2, 0.74 for F≥3, and 0.83 for F=4 using Forn's index. Activity can be also estimated from those same parameters albeit with lower areas under the curve respectively. Steatosis is not correlated to any parameters tested in the study including Voigt viscosity or dispersion curve slope.

Conclusions: SSI was thus found to give equivalent performance to Fibroscan on this particular population with superior results to all blood tests used here. Viscosity as well as elasticity were found to be average predictors for the fibrosis level and found to be not related to steatosis and activity.

	Fibrosis			Activity		Steatosis	
	F>F1	F>F2	F>F3	A>A0	A>A1	S>20 %	S>35%
Young's modulus from group velocity	0.82	0.82	0.87	0.64	0.78	0.58	0.47
Young's modulus @ 50 Hz	0.79	0.83	0.87	0.7	0.8	0.63	0.58
Young's modulus @ 150 Hz	0.81	0.82	0.86	0.67	0.8	0.59	0.43
Voigt Shear modulus	0.75	0.79	0.79	0.67	0.76	0.64	0.6
Voigt viscosity	0.76	0.77	0.82	0.62	0.75	0.62	0.57
Dispersion slope	0.7	0.72	0.8	0.52	0.69	0.55	0.47

Table 1: Areas under the curve for the separation of different fibrosis, activity and steatosis stages versus different parameters estimated from shear wave dispersion curves. Grey background denotes area under the curve >0.8.

References:

[1] T. Deffieux, G. Montaldo, M. Tanter, M.Fink: Shear Wave Spectroscopy for *In Vivo* Quantification of Human Soft Tissues Viscoelasticity. IEEE Trans. Med. Im., 28 (3), pp. 313–322, 2009.

* *indicates Presenter*

001 **MAGNETIC RESONANCE ELASTOGRAPHY THROUGH ATHEROSCLEROSIS: THE PROGRESSION FROM COMPUTATIONAL SIMULATIONS TO EXPERIMENTAL FEASIBILITY.**

Lauren Thomas–Seale[1], Paul Kennedy[1], Dieter Klatt[2], Tom Anderson[1], S.Hammer[3], Scott Semple[1], Saeed Mirsadraee[1], Ingolf Sack[2], Pankaj Pankaj[1], Neil Roberts[1], Peter Hoskins[1].*

[1]The University of Edinburgh, Edinburgh, Mid–Lothian, UK; [2]Charité–University Medicine Berlin, Berlin, GERMANY; [3]Heriot–Watt University, Edinburgh, Mid–Lothian, UK.

Background: It is widely acknowledged that the biomechanical properties of atherosclerotic plaques may provide a better indication of rupture risk than the current criteria for surgery, a measurement of lumen reduction. It is hypothesised that magnetic resonance elastography (MRE) could be used to image the stiffness of atherosclerotic plaques. MRE employs phase contrast MRI to image the propagation of externally excited, low frequency shear waves through tissue [1]. These images are then inverted using an inversion algorithm into an image of stiffness, known as an elastogram [1]. To date, the concept of arterial MRE has been investigated in terms of vessel wall stiffness [2] and shear wave propagation through atherosclerotic plaques [3].

Aims: To explore the feasibility of applying MRE to atherosclerosis through arterial phantoms, healthy volunteers and peripheral artery disease (PAD) patients in comparison to simulated MRE results.

Methods: Ten (10) phantoms containing various size and stiffness plaques were created using the vessel mimicking material polyvinyl alcohol cryogel. MRE was conducted through the arterial phantoms and peripheral arteries of 2 healthy volunteers and 3 PAD patients on a 3 Tesla Magnetom Verio MRI research scanner (Siemens, Germany). Harmonic waves at frequencies of 75Hz, 100Hz and 125Hz were synchronized with the imaging sequence, generated by a subwoofer (Monacor, Germany) and transmitted using a carbon–fiber piston. Simulations of MRE through idealised atherosclerotic plaques were created using the computer aided design software RHINO (McNeel, USA) and run in the finite element analysis software ABAQUS (Simulia, USA). The inversion of the simulated and experimental wave images into elastograms was conducted using the Helmholtz algorithm [1] on MATLAB (MathWorks, USA).

Results: Simulating MRE through idealised atherosclerotic plaques at 100Hz shows that under optimum conditions, local plaque stiffness falls with increasing lipid volume, Figure 1. Figure 2 shows examples of the wave images and elastograms through an arterial phantom and healthy volunteer conducted at 100Hz. The wave images and elastograms through the phantoms and *in–vivo* vessels give visibility of the vessel as a whole, however the technique struggles to delineate between the lumen, wall and plaque. Noise is also significantly higher in the *in–vivo* images. Consequently comparisons between the phantom, healthy volunteer and PAD patient results do not show any definitive changes in stiffness with the presence of a plaque.

Conclusions: Computational studies show that under ideal conditions, changes in local plaque stiffness with composition are quantifiable. However experimental MRE through vessels leads to poor quality results due to the challenges of resolution, wall motion and flow artefacts. Further development of this technique could have the potential to image the local stiffness of atherosclerotic plaques.

Acknowledgements: The authors would like to acknowledge the following funding bodies: EPSRC, SINAPSE, The Edinburgh Campaign and CHSS.

References:

[1] Manduca, A, et al.: Magnetic Resonance Elastography: Non–Invasive Mapping of Tissue Elasticity. Med Image Anal, 5, pp. 237–254, 2001.

[2] Kolipaka, A, et al.: MR Elastography of the *In Vivo* Abdominal Aorta: A Feasibility Study for Comparing Aortic Stiffness Between Hypertensives and Normotensives. J Magn Reson Imaging, 3, pp. 582–586, 2012.

[3] Thomas–Seale, LEJ, et al.: A Simulation of the Magnetic Resonance Elastography Steady State Wave Response through Idealised Atherosclerotic Plaques. IAENG International Journal of Computer Science, 38, pp. 394–400, 2011.

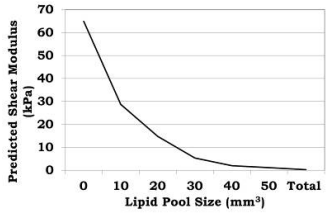

Figure 1: The variation of predicted shear modulus with lipid pool size through MRE simulations.

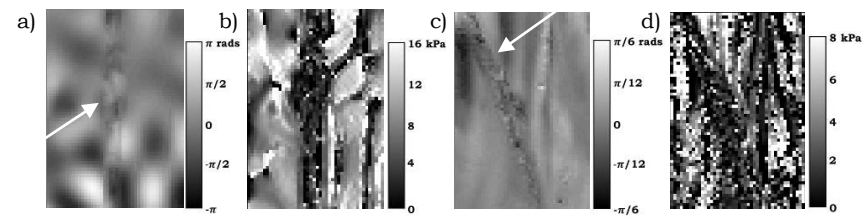

Figure 2: The experimental MRE a) wave image and b) elastogram through a 70% stenosis, lipid plaque, arterial phantom. The experimental MRE c) wave image and d) elastogram through the peripheral artery of a healthy volunteer.

016 **A METHOD FOR DETERMINING TISSUE VISCOELASTICITY VIA SINGLE TRACK LOCATION ACOUSTIC RADIATION FORCE IMPULSE IMAGING.**

JH Langdon[1], EC Elegbe[1], SA McAleavey[1].*
[1]University of Rochester, Rochester, NY, USA.

Background: Single Track Location (STL) Acoustic Radiation Force Impulse (ARFI) imaging is a method for determining the elasticity of tissue that has been shown to suppress speckle noise [1] and assumes a linear elastic model. Here we show that failure to account for viscosity in STL–ARFI can lead to an over–estimation of the shear modulus. This is significant because tissues such as liver [2] and breast [3] are known to be viscoelastic and shear modulus is known to change in disease states [2,3]. While shear viscosity may also vary (as in liver [2]), a viscoelastic model is desirable even when contrast only exists in the shear modulus because of the aforementioned over–estimation. Techniques such as Shearwave Dispersion Ultrasound Vibrometry (SDUV) [4] and direct Helmholtz inversion [5] have been used for determining the viscoelastic parameters of tissues. However, both these techniques use a monochromatic wave source and require interrogations at multiple frequencies. We propose a new reconstruction technique, denoted STL Viscosity Estimation (STL–VE), that utilizes the speckle suppressing properties of STL–ARFI to achieve a simple and effective estimation of the viscoelastic parameters.

Aims: The objective of this project is to mathematically develop, implement and validate a technique for determining the viscoelastic parameters of tissue via data generated using the STL–ARFI technique.

Methods: We developed a formulation of the STL–VE inversion problem using the Kelvin–Voigt viscoelastic model. A viscoelastic Finite Difference Time Domain (FDTD) simulation, based on [6], was used to simulate the propagation of shear waves of a form typical of STL–ARFI over a range of viscosities (0–1 Pa·s). Added white noise and a tracking location error simulates the finite SNR and "speckle bias" of the simulated displacement estimates. The shear wave data from our simulations were used to validate our reconstruction software. Finally, we reconstructed the viscoelastic parameters of a rat liver (*in vivo* and *ex vivo*) using data acquired from our on–going rat liver fibrosis study. These data were collected using a Siemens Antares ultrasound system with a VF10–5 linear array transducer operating at 5.7MHz.

Results: The simulations showed good agreement between the input viscoelastic parameters and the value reconstructed by our STL–VE software. There was much better agreement between the actual shear modulus and that determined using STL–VE than that determined using a linear model. In fact, for shear modulus of μ=2kPa and a shear viscosity of η=1.0Pa·s, the purely elastic reconstruction yielded a μ that was 65% higher than the actual value. The STL–VE method yielded a value within 10% of the actual value even in the presence of noise. In the absence of viscosity, both methods yielded values within 1% of the actual modulus. Using this method, healthy control rats in our study were found a shear viscosity of η=0.49±0.12Pa·s, which agrees well with values previously reported in the literature [2].

Conclusions: The results demonstrate the validity of the STL–VE method both through simulations and tissue measurement. Advantages of this technique include insensitivity to speckle noise and straightforward implementation on a standard ultrasound scanner. This new technique is limited by a greater sensitivity to noise than our linear elastic reconstruction. However, this increased noise sensitivity is traded for a greatly increased accuracy in viscous materials. Since liver [2] and breast tissue [3] are viscous, the STL–VE algorithm may be applicable to both ARFI imaging scenarios.

Acknowledgements: The authors gratefully acknowledge the support of the NIH (R03 EB016127).

References:

[1] Elegbe EC, McAleavey SA: Single Tracking Location Methods Suppress Speckle Noise in Shear Wave Velocity Estimation. Ultrasonic Imaging, 35, pp. 109–125, 2013.
[2] Salameh N, Peeters F. et al.: Hepatic Viscoelastic Parameters Measured with MR Elastography: Correlations with Quantitative Analysis of Liver Fibrosis in the Rat. J. of Magn. Reson. Im., 26, pp. 956–962, 2007.
[3] Sinkus R, Tanter M, Xydeas T, Catheline S, Bercoff J, Fink M: Viscoelastic Shear Properties of *In Vivo* Breast Lesions Measured by MR Elastography. Magnetic Resonance Imaging, 23, pp. 159–165, 2005.
[4] Shigao C, Urban MW, et al.: Shearwave Dispersion Ultrasound Vibrometry (SDUV) for Measuring Tissue Elasticity and Viscosity. IEEE Trans. Ultrason., Ferroelectr., Freq. Control, 56, pp. 55–62, 2009.
[5] Orescanin M, Wang Y, Insana MF: Shear Modulus Eastimation with Vibrating Needle Stimulation. IEEE Trans. Ultrason., Ferroelectr., Freq. Control, 57, pp. 1385–1367, 2010.
[6] Orescanin M, Wang Y, Insana MF: 3–D FDTD Simulation of Shear Waves for Evaluation of Complex Modulus Imaging. IEEE Trans. Ultrason., Ferroelectr., Freq. Control, 58, pp. 389–398, 2011.

* *indicates Presenter*

018 **DYNAMIC ELASTOGRAPHY AND HYPER–FREQUENCY VISCOELASTIC SPECTROSCOPY OF A LIVER MIMICKING PHANTOM.**

A Tang[1], E Montagnon[2], C Schmitt[3], A Hadj Henni[3], D Olivié[1], H Castel[1], G Cloutier[2].*
[1]Hôpital St–Luc, University of Montréal, Montréal, Québec, CANADA; [2]Biorheology and Medical Ultrasonics Laboratory, University of Montréal Hospital Research Center (CRCHUM), Montréal, Québec, CANADA; [3]Rheolution Inc., Montréal, Québec, CANADA.

Background: Dynamic elastography methods are used for liver stiffness measurement, a noninvasive biomarker of liver fibrosis. However, there are discrepancies between published stiffness thresholds for different elastographic methods, which may be attributable to different frequencies used, shear wave generation techniques and inversion algorithms. Thus, there is a need to harmonize elastographic measurements with an independent measurement instrument. Hyper–frequency viscoelastic spectroscopy performed with RheoSpectris™ can characterize properties of synthetic and biological materials between 10–1000Hz [1], a range suitable for validation of elastographic measurements.

Aims: The first objective was to evaluate the elasticity of phantoms using two radiation force–based shear wave generation techniques (SSI and ARFI with spectral analysis and time–to–peak post–processing) and RheoSpectris™ to measure shear storage modulus as a function of frequency. The second objective was to compare the elasticity of the same phantoms as measured by 4 commercial systems (Aixplorer, ARFI, FibroScan, and MRE) with our previous measurements.

Methods: Two phantoms composed of 2% agar and 3% gelatin (Phantom A), and 2% agar and 4% gelatin (Phantom B) were built to mimic the liver elasticity encountered in mild and advanced liver fibrosis, respectively. The phantoms were evaluated with acoustic radiation force impulse (ARFI) and supersonic shear imaging (SSI) pulses implemented on a Verasonics (WA) ultrasound system equipped with an L7–4 probe (Philips, MA) probe at 5MHz. The shear modulus was estimated with spectral analysis (SSI–Vera–SA, ARFI–Vera–SA) algorithms between 150–400Hz and with time–to–peak (SSI–Vera–TTP, ARFI–Vera–TTP) algorithms. The phantoms were also evaluated with Aixplorer (SuperSonic Imagine S.A., France), ARFI (Siemens Acuson S2000, CA), FibroScan (Echosens, France), and MRE (Discovery MR450, GE, WI). Temperature of phantom was controlled. Time and depth (between 2–5cm) of measurements were recorded. The same agar–gelatin mixtures were molded in cylindrical holders for characterization using RheoSpectris™ C500 (Rheolution Inc., Canada). All measurements were performed within 6 hours.

Results: The elastic spectra measured by RheoSpectris™ indicate minimal frequency dependence of the two agar–gelatin phantoms (Figure 1a). There is an effect of shear wave generation method on elasticities measured on Phantoms A and B with a trend toward higher elasticity measurements with SSI–Vera–SA than ARFI–Vera–SA over most of the frequency range from 150–400Hz. All commercially available elastography systems as well as SSI–Vera–TTP and ARFI–Vera–TTP reported higher shear storage moduli for Phantom B than A (Figure 1b). Elasticities measured by elastographic methods on Phantom A were systematically higher than RheoSpectris™ measurements.

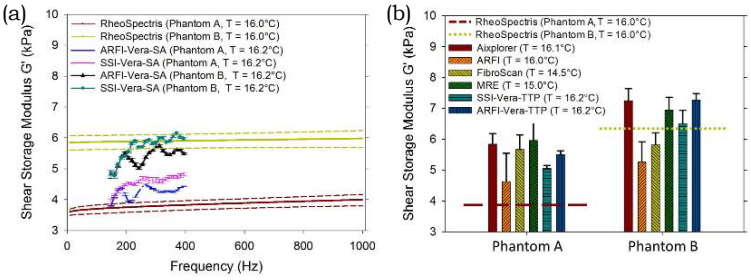

Figure 1: (a) Shear storage modulus (G') of Phantom A (2% agar and 3% gelatin) and Phantom B (2% agar and 4% gelatin) measured between 10–1000Hz by RheoSpectris™, and between 150–400Hz by spectral analysis with two shear wave generation techniques (SSI and ARFI) implemented on a Verasonics ultrasound system. (b) Shear storage modulus measured by RheoSpectris™, SSI (Aixplorer), ARFI (Siemens), Fibroscan (Echosens), MRE (GE), SSI and ARFI (implemented on Verasonics).

Conclusions: This study highlights two important observations: 1) commercial and research elastography methods are in good agreement, regardless of the material stiffness and 2) a systematic bias is observed between elastography methods and reference measurements with RheoSpectris™ at low stiffness values. The study does not explicitly show that the bias depends on the elastography method. It will be important to understand the origin of this bias to achieve accurate and consistent elastography results.

Acknowledgements: Funding was provided by grants of the Natural Sciences and Engineering Research Council of Canada (NSERC CHRP–365656–09) and Canadian Institutes of Health Research (CIHR CPG–95288 and MOP–84358).

Reference:

[1] Hadj Henni, A., Schmitt, C., et al.: Hyper–Frequency Viscoelastic Spectroscopy of Biomaterials. J. Mech. Behav. Biom. Mater., Vol. 4, pp. 1115–1122, 2011.

* *indicates Presenter*

022 **IMAGING OF SHEAR WAVES INDUCED BY LORENTZ FORCE IN SOFT TISSUES.**

P Grasland–Mongrain[1], R Souchon[1], F Cartellier[1], A Zorgani[1], JY Chapelon[1], C Lafon[1], S Catheline[1].*
[1]INSERM, U1032, LabTau, Lyon, F–69003, FRANCE; Université de Lyon, Lyon, F–69003, FRANCE.

Background: The Lorentz force induced by the application of a current in a soft conductive tissue within a magnetic field can create mechanical waves. At frequencies higher than a few hundred kHz, shear waves are quickly attenuated and only compressional waves are created. This is used in an imaging method called "Magneto–Acoustic Imaging with Magnetic Induction" which creates electrical conductivity pictures of the tissue [1–3]. However, at frequencies around a few hundred hertz, shear waves should also be present.

Aims: In this study, we conducted experiments to detect the presence of a shear wave due to Lorentz force in conductive soft phantoms and in *ex–vivo* tissue (ovine kidney).

Methods: The experiment used a generator which was emitting an 80V peak–to–peak, 100Hz electrical signal on two electrodes in contact with a sample placed in a 300mT magnetic field. Tested samples were (a) a gelatin phantom with an electrical conductivity of 1S/m, close to human soft tissue conductivity, (b) two layers of PVA (polyvinyl alcohol) phantom with same conductivity but different stiffness and (c) ovine kidney. Ultrafast ultrasound imaging was performed with a Verasonics scanner operating at 1000frames/sec. Movement of the phantom was measured with a speckle–tracking technique.

Results: Results showed that a movement about a micrometer was induced by Lorentz force. This motion initiated shear waves propagating at different speeds depending on the tissue: 1.3m/s in the gelatin phantom, at 2.5 and 5.1 respectively in the soft and hard PVA layers, and 5m/s in the kidney.

Conclusions: The Lorentz force can induce shear waves. Foreseen applications of this new approach could be shear wave imaging in deep organs or soft tissues protected by bones such as brain.

Acknowledgements: No conflict of interest is declared.

References:

[1] Y Xu, B He: Magnetoacoustic Tomography with Magnetic Induction. Physics in Medicine and Biology, 2005.
[2] X Li, Y Xu, B He: Imaging Electrical Impedance from Acoustic Measurements by Means of Magnetoacoustic Tomography with Magnetic Induction (MAT–MI). IEEE Transactions on Biomedical Engineering, 2007.
[3] X Li, X Li, S Zhu, B He: Solving the Forward Problem of Magnetoacoustic Tomography with Magnetic Induction by Means of the Finite Element Method. Physics in Medicine and Biology, 2009.

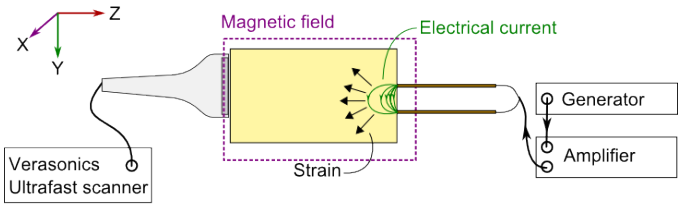

Figure 1: An electrical current is injected by two electrodes in a conductive phantom submitted to a magnetic field. Displacements are observed with an ultrasound probe.

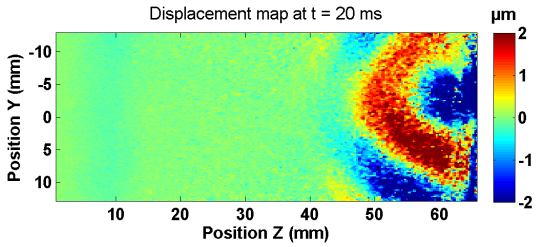

Figure 2: Displacement map 20ms after current injection. A shear wave is appearing and propagates at 1m/s.

* *indicates Presenter*

024 **PASSIVE SHEAR WAVE ELASTOGRAPHY USING AN ULTRAFAST ULTRASOUND SCANNER.**

Ali Zorgani[1], Rémi Souchon[1], Stefan Catheline[1].*
[1]LabTAU, INSERM U1032. University of Lyon 1, 151 Cours Albert Thomas, 69424 Lyon, FRANCE.

Background: Transient elastography techniques use shear wave propagation in biological tissues to measure their elasticity. In order to generate shear waves, the majority of these techniques use external active sources (e.g., mechanical vibrator or acoustical radiation force (ARF)). The efficiency of this technique (ARFI) was demonstrated in breast cancer, but it is substantially reduced when used to generate shear waves inside deep organs or in organs with high muscular activity. In this study, an alternative technique called "Passive Elastography" was proposed. Inspired from the techniques developed in seismology, to obtain a tomography of the earth's mantle by the correlation of the seismic noise, passive elastography aims to replace the external active sources by the physiological noise (muscular activity, heartbeat, breathing, etc.). With this approach, extracting elasticity of soft tissues was demonstrated in [1] using an ultrafast ultrasound scanner. Transposed to conventional ultrasound scanner, the passive elastography method can also convey a qualitative elastogram [2].

Aims: Using an ultrafast scanner in this work, we carefully study the ability of passive elastography to reconstruct quantitative tomography of the shear elasticity in an elastic medium from a diffuse wave field.

Methods: Our experiments were performed on a CIRS® phantom (Model 049), containing four inclusions with 10mm diameter and elastic moduli ranging from 8–80 kPa and 25kPa for the background. The steps of the experiment are as following: (1) A diffuse wave field is created inside the phantom by a random finger's impacts during 2 and a half seconds. The shear wave propagation is imaged with a 10MHz ultrasonic array (128 channels) and a pulse repetition frequency of 500images/second using an ultrafast scanner. (2) The 2D displacement field is then measured using the classical speckle tracking algorithm developed in elastography. (3) Quantitative shear wave speed tomography is retrieved from the computation of the particle velocity field (i.e., the time derivative of the displacement field), and of the strain field (i.e., the gradient of the displacement field). More precisely, the shear wave tomography results from the ratio between the time reversal velocity field and the time reversal strain field.

Results: Ultrafast imaging allows us to continuously follow the propagation of the diffuse shear wave field. The displacement field measured using the ultrafast scanner and the speckle tracking algorithm Figure 1a, shows a typical diffuse field. A wave front (dashed lines) was propagated and distorted in the direction of arrows. Afterward, a time reversal algorithm [2] was used to compute the local shear wave speed, Figure 1b. The inclusion is clearly distinguished from the background, but with a slight overestimation of the shear wave speed compared to the characteristics given by the phantom's manufacturer. The measured shear waves speed is 7m/s in the inclusion instead 5m/s and 6m/s in the background instead of 2m/s. This overestimation will be discussed.

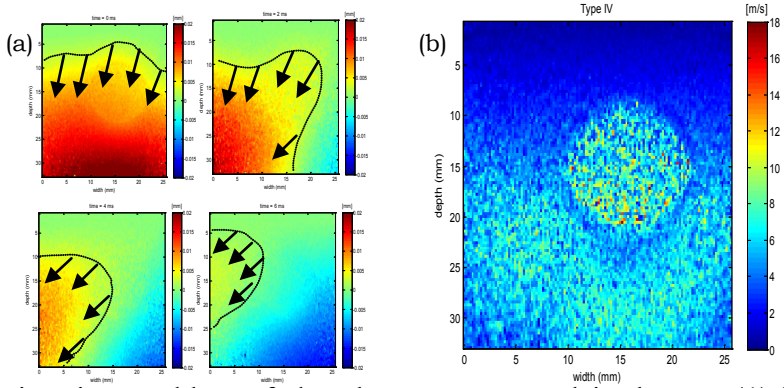

Figure 1: (a) An experimental diffuse wave field is represented in these four consecutive snapshots. (b) The local shear wave speed map shows the 80kPa inclusion.

Conclusions: We suspect that the overestimation problem of the shear wave speed is due to: (1) The imperfect isotropic nature the diffuse field; because a wave speed gradient is observed from the top to the bottom of Figure 1b. (2) Wave diffraction may also be the reason of this overestimation.

References:

[1] T. Gallot, S. Catheline, P. Roux, J. Brum, N. Benech, and C. Negreira: Passive Elastography: Shear–Wave Tomography from Physiological–Noise Correlation in Soft Tissues. IEEE Trans. Ultrason. Ferroelec. Freq. Contr., 58(6), p. 1122, 2011.
[2] S. Catheline, R. Souchon, M. Rupin, J. Brum, A.H Dinh, and J–Y Chapelon: Tomography from Diffuse Waves: Passive Shear Wave Imaging using Low Frame Rate Scanners. Appl. Phys. Lett. 103, 014101, 2013.

* *indicates Presenter*

025 **A NEW DEVICE FOR MEASURING PROSTATE ELASTICITY *IN VIVO* COMBINING ACOUSTIC RADIATION FORCE AND MAGNETIC RESONANCE IMAGING: SIMULATION RESULTS.**

Heldmuth Latorre–Ossa[1], Françoise Chavrier[1], Simon Chatelin[2], Jean–Luc Gennisson[2], Au Hoang Dinh[1], Stefan Catheline[1], Olivier Rouvière[3], and Rémi Souchon[1].*

[1]Therapeutic Applications of Ultrasound Laboratory–LabTAU, INSERM U1032, Lyon, FRANCE; [2]Institut Langevin – Ondes et Images, ESPCI ParisTech, CNRS UMR7587, INSERM U979, Paris, FRANCE; [3]Hospices Civils de Lyon, Hôpital Edouard Herriot, Lyon, FRANCE.

Background: Prostate cancer is one of the leading causes of cancer related deaths in men worldwide. Nevertheless, detecting prostate cancer and assessing its degree of malignancy continue to be challenges which none of the existing medical imaging techniques have been able to successfully overcome.

Aims: Here, we propose a new device to measure noninvasively *in vivo* the elasticity of the prostate combining Magnetic Resonance (MR) imaging and acoustic radiation force.

Methods: Unlike conventional magnetic resonance elastography methods [1–3], which use an external vibrator to induce shear waves within the tissue, our prototype will employ transient acoustic radiation force as a shear wave source [4]. The resulting shear waves will be tracked using a MR scanner. In our device, the acoustic radiation force will be generated by two spherically focused ultrasound transducers positioned against the perineum of the volunteer. A MR echo–planar sequence will be used to track the displacement of the generated shear waves. Numerical simulations of the acoustic and the shear displacement fields were performed for spherically focused transducers with a diameter of 30mm, a radius of curvature of 80mm and resonance frequencies of 2, 4, 6 and 8MHz. The simulations took into account tissue attenuation values ranging from 0.3–0.7dB/cm/MHz and assumed a linear shear wave propagation in a purely elastic medium. A 100µs duration burst was used as the shear wave source.

Results: The simulation results show that for a peak acoustic pressure of 4MPa at the focal point and a medium attenuation of 0.3dB/cm/MHz displacements of up to 24, 23 and 20µm are induced at resonance frequencies of 2, 4 and 6MHz, respectively. For these parameters, the mechanical index is expected to be ~1.6–2.8, and the focal length at -6dB, 23.4mm. Figure 1 contains the simulated acoustic pressure field for a 2MHz transducer with 0.3dB/cm/MHz medium attenuation.

Conclusions: The simulations suggest that our device will induce tissue displacement of some tens of µm sufficient to allow accurate tracking with MRI [4,5] with a mechanical index within an acceptable range. In addition, the focal length is long enough to generate shear waves in the whole gland in a single shot.

Acknowledgements: This project is funded by the French National Cancer Institute (INCA).

References:

[1] Kemper J et al.: MR Elastography of the Prostate: Initial *I*n–Vivo Application. Rofo, 176(8), pp. 1094–9, 2004.
[2] Li S et al.: A Feasibility Study of MR Elastography in the Diagnosis of Prostate Cancer at 3.0T. Acta Radiol. 52(3), pp. 354–8, 2011.
[3] Sahebjavaher RS et al.: Transperineal Prostate MR Elastography: Initial *In Vivo* Results. Magn Reson Med.; 69(2), pp. 411–20, 2013.
[4] Souchon R. et al.: Transient MR Elastography (t–MRE) using Ultrasound Radiation Force: Theory, Safety, and Initial Experiments *In Vitro*. Magn Reson Med., 60, pp. 871–881, 2008.
[5] Souchon R et al.: Measurement of Pulsatile Motion with Millisecond Resolution by Magnetic Resonance Imaging. Magn Reson Med, 67(6), pp. 1787–1793, 2012.

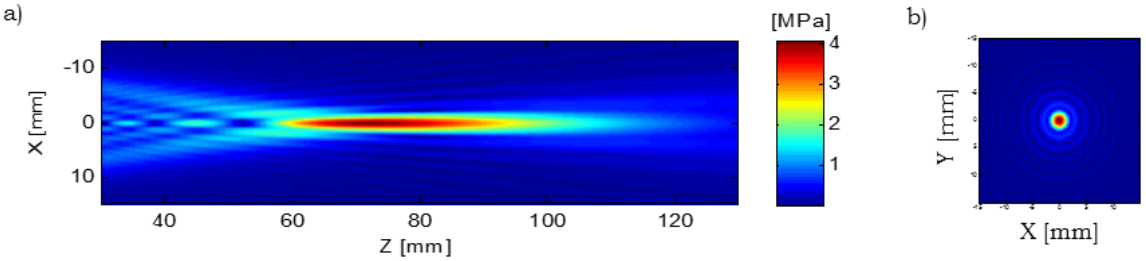

Figure 1: Simulation of the acoustic pressure field generated by a 2MHz spherically focused ultrasonic transducer (0.3dB/cm/MHZ attenuation): a) XZ Plane; b) XY plane. Z is the axis of sound propagation. The peak acoustic pressure at the focal region is ~4MPa. Both figures share the same color bar.

* *indicates Presenter*

045 **LATERAL DISPLACEMENT ESTIMATION USING MOMENTUM EQUATION CONSTRAINTS.**

Olalekan A. Babaniyi[1], Paul E. Barbone[1], Assad A. Oberai[2].*
[1]Mechanical Engineering Department, Boston University, 110 Cummington St., Boston, MA 12180, USA; [2]Mechanical, Aerospace and Nuclear Engineering Department, Rensselaer Polytechnic Institute, 110 8th Street, Troy, NY, 12180, USA.

Background: Conventional ultrasound beam forming enables highly precise axial displacement estimates but provides image data that contains relatively little information about lateral displacements. Two approaches to obtaining precise lateral displacement estimates dominate the literature: 1) Novel signal processing to extract the little signal present (c.f. [1,2]), 2) Novel beam forming strategies to increase sensitivity to lateral displacements (c.f. [3]). Here we evaluate a third approach: post–processing the displacement measurements using physical constraints in a piecewise homogeneous material.

Aims: The aim here is to develop a new processing scheme that can be used to reconstruct high precision displacement vector and strain tensor fields from a single component of the measured displacement field.

Methods: The goal was achieved by using the following functional to calculate the filtered displacements:

$$\pi[\boldsymbol{u},\boldsymbol{\epsilon}] = \frac{1}{2}\int (\boldsymbol{u}-\boldsymbol{u}_m)\cdot\boldsymbol{T}(\boldsymbol{u}-\boldsymbol{u}_m)d\Omega + \frac{\beta}{2}\int\left(\boldsymbol{\epsilon}-\frac{1}{2}(\nabla\boldsymbol{u}+(\nabla\boldsymbol{u})^T)\right)^2 d\Omega + \alpha\int|\nabla\cdot(tr(\boldsymbol{\epsilon})\boldsymbol{I}+\boldsymbol{\epsilon})|d\Omega$$

where u_m is the measured displacements, u is the filtered displacements, ϵ is the strain, T is a weighting tensor that allows more emphasis to be placed on the more accurate component of the displacement field, β is a constant that regulates how strongly the strain displacement relation is enforced, and α is a constant that regulates how strongly the equilibrium equation for a material with a piecewise homogeneous shear modulus distribution is enforced. Minimizing this functional with respect to the independent variables results in filtered displacements and strains that are more precise than the measurements and that satisfy the equilibrium equations.

Results: Validation of the method was performed using simulated displacement data in which one of the displacement components was corrupted by approximately 50% additive noise. The full vector displacement field was reconstructed within 2%, and the full 2D strain tensor field was reconstructed within 3% of the target values for this test. Further testing was performed with ultrasound measured displacement data from a tissue mimicking phantom, and *in vivo* displacement data measured from patients with breast masses. In these tests, precise estimates of the full displacement and strain fields were recovered as demonstrated in Figure 1. Iterative reconstructions of modulus and displacement fields served as benchmark results against which to compare the filtered lateral displacements.

Conclusions: We have developed a new processing scheme that can be used to reconstruct high precision displacement and strain tensor fields from low precision measurements.

Acknowledgements: The authors are grateful to T.J. Hall (University of Wisconsin) and J. Jiang (Michigan Technological University) for providing displacement fields measured in the phantom.

References:

[1] E. Brusseau, J. Kybic, J. Deprez, and O. Basset: 2–D Locally Regularized Tissue Strain Estimation from Radio–Frequency Ultrasound Images: Theoretical Developments and Results on experimental Data. IEEE Transactions on Medical Imaging, 27, pp. 145–160, 2008.
[2] E. Konofagou, and J. Ophir: A New Elastographic Method for Estimation and Imaging of Lateral Displacements, Lateral Strains, Corrected Axial Strains and Poisson's Ratios in Tissues. Ultras in Med & Biol, 24, pp. 1183–1199, 1998.
[3] S. Korukonda, and M. Doyley: Estimating Axial and Lateral Strain using a Synthetic Aperture Elastographic Imaging System. Ultras in Med & Biol, 37, pp. 1893–1908, 2011.

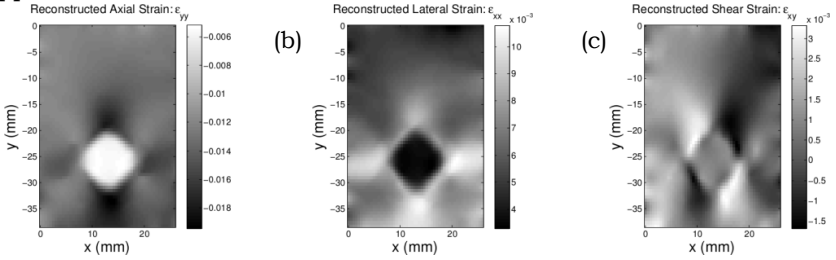

Figure 1: Reconstructed axial (a), lateral (b) and full–tensor (c) shear strains within a tissue mimicking phantom.

077 **RSNA/QIBA: ULTRASOUND SHEAR WAVE SPEED ELASTIC PHANTOM RESULTS.**

A Milkowski[1], TJ Hall[2], BS Garra[3].*

[1]Siemens Medical Solutions SA, Inc., Issaquah, WA, USA; [2]University of Wisconsin–Madison, Madison, WI, USA; [3]Food and Drug Administration, Silver Spring, MD, USA.

Background: The Radiological Society of North America (RSNA) created the Quantitative Imaging Biomarker Alliance (QIBA) to advance the concept of converting imaging systems to measurement systems. The Ultrasound Committee is working through a process to develop a protocol that would allow direct comparison of shear wave speed (SWS) measurements for liver fibrosis staging.

Aims: An interlaboratory study of shear wave speed estimation in elastic phantoms was performed. This study was designed to assess the impact different systems, operators and sites had on shear wave speed.

Methods: Commercially available shear wave elastography systems from Echosens, Philips, Siemens and Supersonic Imagine, as well as several custom laboratory systems, were used in the study. Fifteen sites with one or more of the systems performed the study. CIRS manufactured and donated 11 pairs of 'soft' and 'stiff' custom phantoms designed for this investigation. All phantoms were initially measured at one site. Then each investigating site used three operators to acquire ten repeated SWS measures three times in a randomized fashion. The mean of each 10 measures was analyzed in a variety of ways.

Results: The results of this study demonstrate good agreement among SWS estimation systems; however, there are statistically and clinically significant differences between systems, phantoms and depths.

Conclusions: Several sources of bias and variance should be addressed to enable comparison of measurement results and liver fibrosis staging.

067 **LOCALISED VIBRATION TAGGING (LOVIT) FOR CLUTTER REDUCTION IN EPIPHOTOACOUSTIC AND OTHER IMAGES.**

Michael Jeager[1,2], Martin Frenz[2], Jeffrey C. Bamber[1].*

[1]The Institute of Cancer Research and The Royal Marsden NHS Foundation Trust, Downs Road, Sutton, Surrey, SM2 5PT, England, UK; [2]University of Bern, Sidlerstrasse 5, 3012 Bern, SWITZERLAND.

Background: For clinical photoacoustic (PA) imaging to be applied in a versatile way to many organs, an epiphotoacoustic (ePA) technique is preferred, so as to avoid strongly attenuating media such as bone or gas and to integrate easily with conventional echography. Unfortunately, the ePA approach causes severe clutter from strong PA emissions close to the probe, which limits useful clinical imaging to depths of 1cm or less. We have reported previously on deformation compensated averaging, a technique which exploits clutter decorrelation during tissue strain, and this has achieved signal–to–clutter ratio (SCR) improvements in clinical ePA imaging of about three [1]. Larger gains than this are needed, however, if the noise–limited imaging depth is to be reached.

Aims: The aim of this study was to test, in phantoms, a new method for clutter reduction, which uses vibration–induced localized displacements to "tag" PA signals at their place of origin, and which should, in theory, enable true signal identification and full clutter cancellation if ideal conditions are met.

Methods: Experiments were conducted with gelatine phantoms containing TiO2 optical scatterers, cellulose ultrasound scatterers and India ink for optical absorption. Localised vibration tagging (LOVIT) was induced by acoustic radiation force (ARF) using a custom cylindrical 2MHz transducer. Sequences of pairs of PA images were acquired using a Zonare z.one™ ultrasound (US) scanner with an ELEN 1064nm–wavelength 7ns–pulse Q–switched Nd:YAG laser, a first image prior to an ARF push, and a second with an ARF push to produce a localized displacement. Different pairs were for different locations of the push focus, scanned in steps of 2mm laterally and 5mm axially.

Results: An example result is shown in the figure. (a) is a phantom section corresponding to the imaging plane, showing 2mm diameter optically–absorbing (India ink) and hypoechoic (no cellulose) gelatine cylinders, which are seen to imitate blood vessels on the ultrasound echogram shown in (b). (c) is the best ePA image that could be obtained without clutter reduction. (d) is a LOVIT image obtained by mosaicing results from many push–focus locations where, at each location, a difference (push minus no–push) image was calculated with normalization to ensure equal noise level for conventional and LOVIT images.

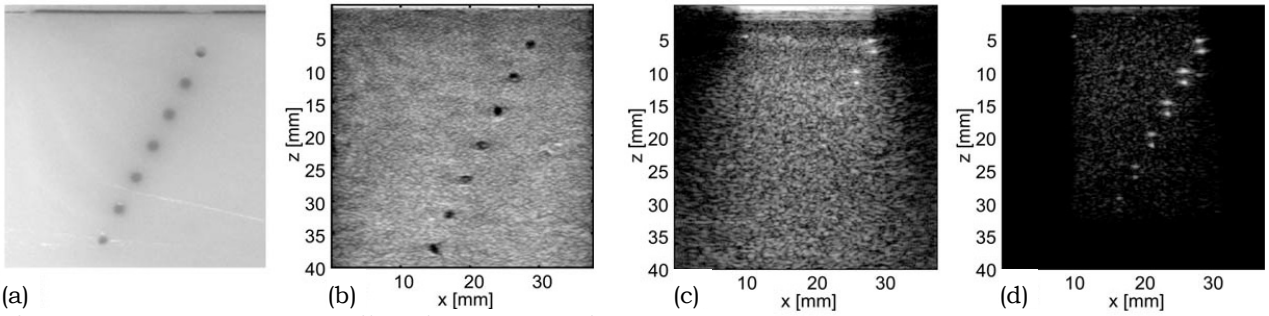

Conclusions: LOVIT repeatedly demonstrated greatly improved SCR and imaging depth over conventional ePA imaging. Many implementations are possible and the method may offer benefits in conventional US and other images, such as those from some types of optical coherence tomography, if clutter limits image contrast.

Acknowledgements: Funding received from Cancer Research UK and the Engineering & Physical Sciences Research Council (Joint Grant No. C1060/A10334), and the Swiss National Science Foundation (No. 205320–103872). We thank Zonare Medical System Inc., USA, for providing equipment and technical support.

References:

[1] M. Jaeger, D. Harris–Birtill, A. Gertsch, E. O'Flynn, J. Bamber: Deformation Compensated Averaging for Clutter Reduction in Epiphotoacoustic Imaging *In Vivo*. J. Biomed. Opt., 17, 066007–1–8, 2012.

** indicates Presenter*

006 **ASSESSMENT OF THE RHEOLOGICAL MODEL OF COAGULATING BLOOD OVER A VERY LARGE BANDWIDTH BY COMBINING SWE AND CLASSICAL RHEOMETRY MEASUREMENTS.**

Miguel Bernal[1], Jean–Luc Gennisson[1], Mathias Fink[1], Patrice Flaud[2], Mickaël Tanter[1].*
[1]Institut Langevin – Ondes et Images, ESPCI ParisTech, CNRS UMR7587, INSERM U979, 1 rue Jussieu, 75005 Paris, FRANCE; [2]Matière et Systèmes Complexes, CNRS UMR7057, Université Paris VII Denis Diderot, 10 rue Alice Domon et Léonie Duquet, 75205 Paris Cedex 13, FRANCE.

Background: Deep venous thrombosis (DVT) affects millions of people worldwide. Its diagnosis and treatment depends on clot's age which is closely related to its viscoelastic properties [1,2). These properties could be assessed noninvasively using Shear Wave Elastography (SWE) and Shear Wave Spectroscopy (SWS) [3] cross validation.

Aims: The aim of this study is to study the best rheological model fitting the blood coagulation and at to validate SWE and SWS with classical rheometry during this process.

Methods: Classical rheometry and SWE were used in this study to the viscoelastic properties of blood clots. Blood was collected from pigs and anticoagulated using EDTA. Coagulation was initiated using calcium ions. Shear waves over a bandwidth between 70–300Hz were induced with 100µs tonebursts of 8MHz. The displacements generated were measured using ultrafast imaging at a rate of 2kHz. Shear wave speed was recovered using a time of flight algorithm. Simultaneously, classical rheometry using a Haake Mars II was done on the same blood sample (2.9ml) in a frequency range between 0.25–30Hz. A low amplitude (5%) oscillatory shear was imposed to insure the linearity of the viscoelastic response. Using the values for G' and G" the theoretical shear wave speeds were calculated for frequencies between 0.25–30Hz. Maxwell, Voigt and Zener models were fitted to the dispersion data, obtained by suing SWS technique, combined with rheological data to retrieve the viscoelastic parameters.

Results: Shear wave speed showed a marked increase with time of coagulation for all the frequencies, from around 0.5m/s at the beginning of coagulation to 0.9 after 2 hours. The Zener model (μ_1, μ_2, η) showed the best fit on the data out of the 3 models (Figure 1). Even though the Maxwell (μ_M, η_M) and Voigt (μ_V, η_V) models did a good job at higher frequencies (70Hz and higher), both models failed to characterize the lower frequencies. For the Zener model, the shear elasticity and viscosity increased with coagulation time from μ_1=167kPa, μ_2=138kPa and η=1.38Pa·s at minute 10 of coagulation to 341kPa, 391kPa and 1.59Pa·s, respectively, after 50 minutes of coagulation. After two hours, the values had increased to 351kPa, 472kPa and 1.56Pa·s, respectively.

Conclusions: Combination of SWE and classical rheometry allowed the characterization of the viscoelastic properties of blood clots in a very large frequency range between 0.25–300Hz. The two techniques showed very good agreement suggesting that SWE could be used to study the rheological properties of soft solids

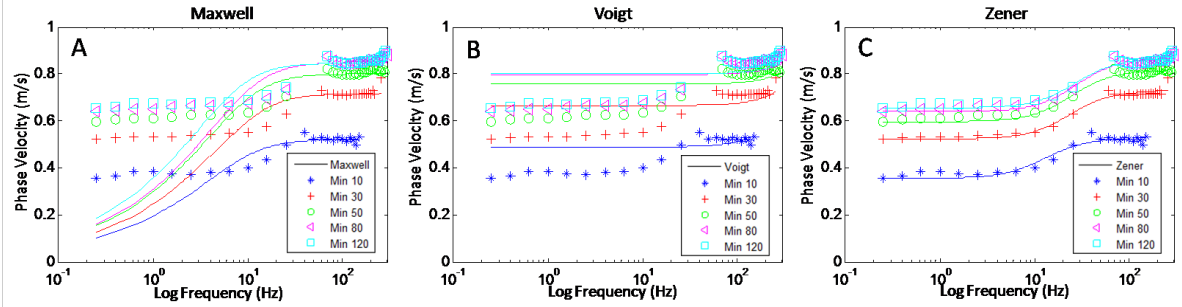

Figure 1: Maxwell, Voigt and Zener models fitted to dispersion values obtained by SWE and classical rheometry.

References:

[1] Emelianov, S.Y., Chen, X., O'Donnell, M., Knipp, B., Myers, D., Wakefield, T.W., Rubin, J.M.: Triplex Ultrasound: Elasticity Imaging to Age Deep Venous Thrombosis. Ultrasound in Medicine & Biology, 28(6), pp. 757–767. 2002.
[2] Xie, H., Kim, K., Aglyamov, S.R., Emelianov, S.Y., O'Donnell, M., Weitzel, W.F., Wrobleski, S.K., et al.: Correspondence of Ultrasound Elasticity Imaging to Direct Mechanical Measurement in Aging DVT in Rats. Ultrasound in Medicine & Biology, 31(10), pp. 1351–9, 2005.
[3] T. Deffieux, G. Montaldo, M. Tanter, M. Fink: Shear Wave Spectroscopy for *In Vivo* Quantification of Human Soft Tissues Viscoelasticity. IEEE Trans. Med. Im., 28 (3), pp. 313–322, 2009.

* *indicates Presenter*

007 **GENERATION OF ADAPTIVE SHEAR WAVES WITH RADIATION FORCE USING OCTAGONAL PHASED ARRAY FOR BREAST CANCER CHARACTERIZATION: PROOF OF CONCEPT.**

Abderrahmane Ouared[1,2], Emmanuel Montagnon[1,2], Anis Hadj–Henni[1,3], Guy Cloutier[1,2 4].*
[1]Biorheology and Medical Ultrasonics Laboratory, University of Montréal Hospital Research Center, Montréal, H2L 2W5, Québec, CANADA; [2]Biomedical Engineering Institute, University of Montréal, Montréal, H3C 3J7, Québec, CANADA; [3]Rheolotion Inc, Montréal, H2S 2X3, Québec, CANADA; [4]Radiology, Radio–Oncology and Nuclear Medicine Department, Montréal, H3T 1J4, Québec, CANADA.

Background: Dynamic elastography is a promising technique due to its additional contribution for the diagnosis of breast cancer [1]. However, one of the main problems of dynamic elastography techniques using remote palpation (i.e., acoustic radiation force) is the strong attenuation of shear waves [2]. In order to overcome such limitation, we propose an approach based on adaptive torsional shear waves (TSW) generated by an octagonal phased array for breast cancer characterization.

Aims: The objective was to increase the amplitude of displacements and improve the signal–to–noise ratio (SNR) for an accurate estimation of viscoelasticity. The second objective was to induce resonance of structures to improve further the displacement contrast between the heterogeneity and its surrounding medium [3]. The resonance can also be used as a parameter to estimate mechanical properties.

Methods: In our experiments, a homogeneous agar–gelatin (3–4% mass ratio) phantom and a heterogeneous agar–gelatin (3–4% surrounding medium and 2–3% inclusion) phantom with a 5mm cylindrical soft inclusion were prepared. To mimic the octogonal phased array of [4], assuming that TSW is obtained by the linear combination of plane wavefronts (PW) around a closed path (e.g. a circle), each PW was generated separately, and TSW was formed in post–processing as for crawling waves [5]. A finite element method (FEM) model was developed to compare TSW obtained by the combination of delayed PW generated a several positions in the closed path. TSW were experimentally generated by geometrically combining each single plane wavefront obtained using three radiation force foci along the ultrasound beam using a Verasonics V1 scanner (Redmond, USA).

Results: The FEM model shows an excellent fitting (R^2=0.97 and relative error ~1%) between displacement profiles of the two simulated TSW cases (Figure 1). Displacement amplitudes generated by TSW were close to two fold greater than the amplitude of tissue motion generated by a PW (Figure 2), and the SNR of estimated displacements (using cross–correlation) were significantly improved (from 2.5 for PW to 6.6 for TSW). In the case of the heterogeneous phantom, adaptive torsional waves produced resonance of the inclusion (i.e. at 190Hz), which increased significantly the displacement contrast (Figure 3).

Conclusions: In this work, it has been proven experimentally that TSW generated by radiation force enhance the amplitude of displacements and can make resonate inclusions. SNR of estimated displacements was also greatly improved. The next step will be to develop the inverse problem for the quantification of the viscoelasticity based on TSW. Results will be compared with other works.

References:

[1] Berg, W.A., et al.:. Radiology, 262(2), pp. 435–449, 2012.
[2] Deffieux, T., et al.: IEEE Transactions on UFFC, 59(11), pp. 2390–2410, 2012.
[3] Hadj Henni, A., et al.: Applied Physics Letters, 100(13), pp. 133702–133702–5, 2012.
[4] Ekeom, D., et al.: IEEE Transactions on UFFC, 60 (3), pp. 552–561, 2013.
[5] Hazard, C., et al.: Ultrasound in Med. & Bio., 38(2), pp. 296–311, 2011.

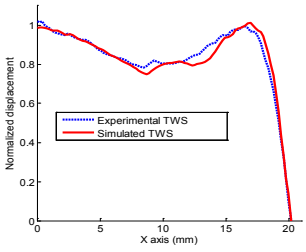

Figure 1: Comparison between displacement amplitudes of reconstructed torsional waves (solid red) and simulated (FEM) torsional waves (dashed blue) as a function of the traveled distance.

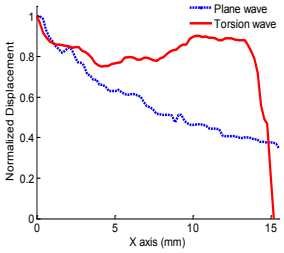

Figure 2: Displacement amplitudes as a function of the traveled distance for plane waves (dashed line) and torsional waves (solid line) in a homogeneous phantom.

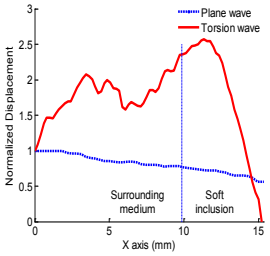

Figure 3: Comparison between displacement amplitudes of a plane wavefront (dashed line) versus torsional waves (solid line) in a heterogeneous phantom at resonance (i.e., at 190Hz). The vertical dashed line represents the interface between the surrounding medium and inclusion (mechanical heterogeneity).

* *indicates Presenter*

019 **ANALYTICAL AND NUMERICAL SIMULATIONS OF WAVE PROPAGATION USING VISCO–ELASTIC ANISOTROPIC GREEN'S FUNCTION FOR CARDIAC REMOTE ULTRASONIC ELASTOGRAPHY.**

Simon Chatelin[1], Clément Papadacci[1], Mathias Fink[1], Mickaël Tanter[1], Jean–Luc Gennisson[1], Mathieu Pernot[1].*

[1]Institut Langevin – Ondes et Images, ESPCI ParisTech, CNRS UMR7587, INSERM U979, 1 rue Jussieu, 75005 Paris, FRANCE.

Background: The generation of shear waves from an ultrasound focused beam has been developed as a major concept for remote palpation. For myocardial application, the characteristics of the focal spot and the resulting shear wave profile will depend on both the design of the transducer and the presence of the cardiac fibers.

Aims: The aim of this study is to provide complete numerical tools allowing simulation of a shear wave front in anisotropic media from the description of an ultrasonic transducer.

Methods: The first part of this study consists of generating the pressure focusal spot from a concave transducer (diameter: 20mm, focal distance: 40mm) by the use of FieldII ultrasound simulation software [1,2]. The second part is to derive the exact visco–elastodynamic Green's Functions from the focal spot for homogeneous transversely isotropic material [3]. The transversely isotropic Green's function for a punctual source consists of the combination of a far–field term (compression wave), two near–singularities terms (longitudinal and transverse shear waves), a near–field term (combining compression and shear waves along the direction of the fibers) and a near–singularities term (combining the two shear waves). The 3D displacement field is then calculated by summation of all the contributions from the focal spot and convolution by a 300µs rectangular time function. The simulation is performed in a quasi–incompressible isotropic medium of 2.25kPa in stiffness and 1Pa.s for dynamic viscosity. The Green's function is estimated in 14 planes (2mm in thickness) of 20x20mm² in size (0.2x0.2mm² in resolution) orthogonally to the focal axis. Transverse isotropy is added through a shear modulus of 9kPa (1Pa.s for dynamic viscosity) along a unique orientation (orthogonal to the focal axis, representing an orientation of fibers in the material).

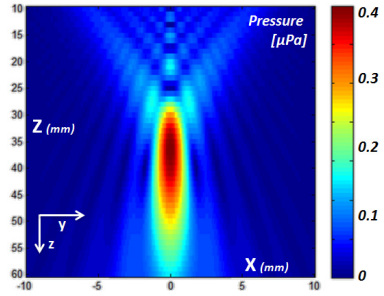

Figure 1: Total 3D pressure field (transverse view) simulated from a 10mm diameter concave source with 40mm in focalization.

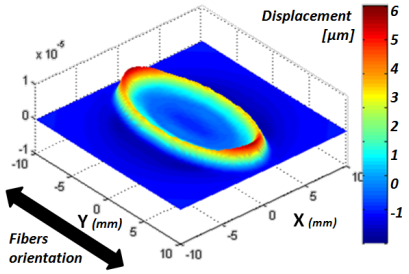

Figure 2: Green's function formalism simulation in a transversely isotropic medium. Longitudinal displacements induced in the focal plane (Z=40mm) by the acoustic radiation force at 30ms sampling times.

Results: The focal spot is illustrated in Figure 1 in the transverse plane. Figure 2 illustrates the shear wave propagation calculated from the focal spot 30ms after its generation for the transversely isotropic case. The shear wave speed is significantly increased along the direction of the fibers. The amplitude and the width of the shear wave front are shown as extremely dependent on the shape and duration of the focal spot.

Conclusions: The results show the feasibility of numerically combining both focal spot simulation and tridimensional displacement field calculation. It plays a major role for the optimization of new ultrasonic transducers dedicated to remote elastography in isotropic and fibrous tissue, such as muscle or myocardium.

Acknowledgements: This work was supported by a grant to M.P. from the European Research Council (FP7–IDEAS–ERC).

References:

[1] J.A. Jensen: Med and Biol Eng and Comp, Volume 34 (1–1), pp. 351–353, 1996.
[2] J.A. Jensen and N.B. Svendsen: IEEE Trans Ultras Ferroelec Freq Contr 39, pp. 262–267, 1992.
[3] V. Vavrycuk: Stud Geophys Geod, 45, pp. 67–84, 2001.

* *indicates Presenter*

031 **MODELING RADIATION FORCE AND SHEAR WAVE PROPAGATION USING FRACTIONAL KELVIN–VOIGT MODEL.**

W. Zhang[1], S. Holm[1].*
[1]Informatics Department, University of Oslo, PO Box 1080, NO–0316 Blindern, Oslo, NORWAY.

Background: Elastography is an important tool for detecting cancer. Many researchers have studied the shear wave propagation in tissue generated by acoustic radiation force such as SWEI, ARFI and SSI. It is well known that wave attenuation in biological tissue obeys power law frequency dependency which cannot be described by the classical lossy wave equations [1].

Aims: We choose a new model to get more accurate results than the classical equation.

Methods: In recent decades, many researchers have found that wave attenuation in biological tissue follows a power law frequency dependency [1,5] which can be modeled with fractional wave equations, and fractional models have better agreement with experimental data than classical models [4]. For example, the following fractional wave equation is based on the fractional Kelvin–Voigt model:

$$\nabla^2 u - \frac{1}{c_0}\frac{\partial^2 u}{\partial t^2} + \tau^\alpha \frac{\partial^\alpha}{\partial t^\alpha}\nabla^2 u = 0 \qquad \text{Equation}$$

u displacement, α fractional order, τ time constant which characterizes the medium. The classical Stokes equation is just a special case of Equation 1 if the fractional order α =1. We choose Equation 1 to describe the shear wave propagation in human tissue.

Results: We demonstrate a practical case where a cylindrically symmetric Gaussian beam is considered, just as in [2,3]. The fractional model is able to take into account tissue property and transducer parameters. We found a value of α =0.25 for freshly excised prostate [4] and compare the deformation response with the non–fractional model with Figure 1 in [2] and Figure 13 in [3]. It shows that the fractional wave equation gives different rise time, $t_{\max}$, and this affects the estimation of the shear modulus in the acoustic radiation force impulse method.

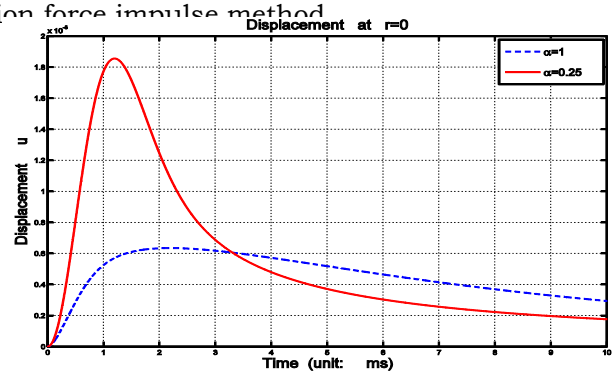

Conclusions: A more accurate wave equation with a fractional derivative loss term is used to model shear wave propagating in biological tissue exhibiting power law attenuation. Numerical result shows that the fractional equation can give more accurate information about wave propagation, and it is useful for the reconstruction of shear modulus.

References:

[1] S. Holm, S. P. Näsholm, F. Prieur, R. Sinkus: Deriving Fractional Acoustic Wave Equations from Mechanical and Thermal Constitutive Equations. Computer and Mathematics with Applications, in press.
[2] Lev Ostrovsky, Alexander Sutin, Yuri Ilinskii, Oleg Rudenko, and Armen Sarvazyan: Radiation Force and Shear Motions in Inhomogeneous Media. The Journal of the Acoustical Society of America, 121, p. 1324, 2007.
[3] Armen P Sarvazyan, Oleg V Rudenko, Scott D Swanson, J Brian Fowlkes, and Stanislav Y Emelianov: Shear Wave Elasticity Imaging: A New Ultra–Sonic Technology of Medical Diagnostics. Ultrasound in Medicine & Biology, 24(9), pp. 1419–1435, 1998.
[4] Man Zhang, Benjamin Castaneda, Zhe Wu, Priya Nigwekar, Jean V Joseph, Deborah J Rubens, and Kevin J Parker: Congruence of Imaging Estimators and Mechanical Measurements of Viscoelastic Properties of Soft Tissues. Ultrasound in Medicine & Biology, 33(10), pp. 1617–1631, 2007.
[5] Sven Peter Nasholm and Sverre Holm: On a Fractional Zener Elastic Wave Equation. Fractional Calculus and Applied Analysis, 16(1), pp. 26–50, 2013.

032 **CHANGES IN SHEAR WAVE SPEED PRE– AND POST–INDUCTION OF LABOR.**

Lindsey C. Carlson[1], Helen Feltovich[1,2], Mark L. Palmeri[3], Stephanie Romero[2], Timothy J. Hall[1].*
[1]University of Wisconsin – Madison, 1111 Highland Ave, Ste. 1005, Madison, WI, USA; [2]Intermountain Healthcare, Intermountain Medical Center, 5121 S. Cottonwood St., Murray, UT, USA; [3]Pratt School of Engineering, Duke University, Rm. 136 Hudson Hall, Durham, NC, USA.

Background: During pregnancy, the cervix undergoes significant remodeling and softening [1]. Premature changes that may occur during this process could lead to preterm birth. Currently, there is no objective method to assess the softness of the cervix. Shear wave speed estimation is a non–invasive quantitative method to quantify the mechanical properties of tissue [2]. A recent study of shear wave speed (SWS) estimation on normal nonpregnant hysterectomy specimens suggests that the mid–anterior location was suitable for good sensitivity to changes due to ripening/softening [3]. However, the *in vivo* environment introduces new challenges such as onset of labor/contractions, fetal movement and changes in cervical length.

Aims: The aim of this study is to measure SWS in pregnant women undergoing cervical softening during induction of labor to determine if there is a significant difference in SWS pre– and post–softening.

Methods: Female patients (n=12) scheduled for induction of labor at term with cervical ripening were recruited, and a subset (m=7) of these did not have an onset of labor or fetal movement. Scanning was performed using a Siemens Acuson S2000 Ultrasound system. Each patient was scanned with an EV–8C4 endovaginal probe to determine cervical length and thickness. The softness of each cervix was subjectively determined by a clinician (Romero). A prototype catheter transducer (128 elements, 14mm aperture, 3mm diameter) operated in linear array mode was used to scan the outside of the cervix. The probe was secured to clinician's hand with the active aperture on her fingertip and then placed into a sterile glove filled with gel for acoustic coupling. The clinician's finger was placed on top of the anterior cervix and aligned parallel to endocervical canal in the mid–position along the length of the canal. 10 replicate SWS measures were made at this location before and four hours after cervical ripening agent was administered to the patient.

Results: For the 7 patients that did not exhibit onset of labor or fetal movement, SWS estimates were 2.39±0.76m/s and 1.51±0.31m/s for pre– and post–induction respectively. A paired–t–test showed a significant difference between pre– and post–induction with cervical ripening ($p=0.01$, 0.05 sig. level). The SWS for pre–induction (12 patients) was 2.33±0.69m/s (compared to 2.11±0.45m/s for anterior/mid/ripened hysterectomy data). All shear wave speeds were in accordance with subjective softness observations.

Conclusions: Shear wave speed estimates significantly decreased as a result of softening for induction of labor. Pre–induction SWS values are in good agreement with values from hysterectomy specimens. Shear wave speed shows potential for a research tool for exploration of premature cervical changes during preterm birth.

Acknowledgements: This work was supported by NIH grants R21HD061896, R21HD063031, HD072077 and Intermountain Medical and Research Foundation.

References:

[1] Word RA, Li XH, Hnat M, Carrick K: Dynamics of Cervical Remodeling During Pregnancy and Parturition: Mechanisms and Current Concepts. Semin Reprod Med, 25, pp. 69–79, 2007. [PMID: 17205425]
[2] Doherty JR, Trahey GE, Nightingale KR, Palmeri ML: Acoustic Radiation Force Elasticity Imaging in Diagnostic Ultrasound. IEEE Trans Ultrason Ferrorelectr Freq Control, 60, pp. 685–701, 2013. [PMID: 23549529].
[3] Carlson LC, Feltovich F, Palmeri ML, Dahl JJ, Munoz del Rio A, Hall TJ: Shear Wave Speed Estimation in the Human Uterine Cervix. Ultrasound Obstet Gynecol, 2013.

003 **CHARACTERIZATION OF THE DUCHENNE SKELETAL MUSCLE WITH MAGNETIC RESONANCE ELASTOGRAPHY (MRE).**

SF Bensamoun[1], F Charleux[2], L Debernard[1], C Themar–Noel[3].*

[1]BioMécanique et BioIngénierie, UMR CNRS 7338, Université de Technologie de Compiègne, Compiègne, FRANCE; [2]ACRIM–Polyclinique Saint Côme, Compiègne, FRANCE; [3]Centre de Référence des Maladies Neuromusculaires Paris–Est, Institut de Myologie, GH Pitié–Salpêtrière, FRANCE.

Background: Duchenne muscular dystrophy (DMD) is caused by mutations of the dystrophin gene which lead to the absence of the dystrophin protein in skeletal muscle inducing repetitive cycles of muscle necrosis and regeneration. Magnetic resonance imaging (MRI) is currently used for the monitoring of DMD patients due to their capacity to qualitatively and quantitatively describe muscle tissue changes and patterns of skeletal muscle damage in disease [1]. Magnetic resonance elastography (MRE) is a recent clinical exam used for the diagnosis of liver fibrosis [2]. This method was further developed to characterize the mechanical properties of individual skeletal muscles [3,4].

Aims: The purpose of this study is to characterize the elastic properties of the vastus medialis (VM) muscle in DMD patients compared to healthy controls.

Methods: Six healthy patients (mean age = 10±0.6 yrs, range = 8–12, male, mean BMI = 17.5±1.0kg/m²) with no muscle abnormality or history of muscle disease, and six Duchenne Muscular Dystrophy (DMD) patients (mean age = 9.9±1.4 yrs, range = 8–12, male, mean BMI = 17.2±2.0kg/m²) were recruited. MRE tests were performed on each participant who lay supine inside a 1.5T MRI machine (General Electric HDxt machine) with the right leg resting on a custom MR compatible leg press [5]. Shear waves were generated with a frequency (f) of 90Hz, by using a pneumatic driver (silicone tube) wrapped around the subject's thigh. Phase images were recorded with four offsets and a motion sensitizing gradient echo sequence. Assuming that the muscle was linear elastic, isotropic, homogeneous and incompressible, the local shear stiffness (μ) was calculated using the following equation $\mu=\rho.(f.\lambda)^2$, where ρ is the muscle density fixed to 1000kg/m3 and λ the wavelength. Moreover, an inversion algorithm (LFE) [6] was applied to provide a cartography of the tissue elasticity.

Results: At rest, the DMD stiffness value of the VM was higher (μ_DMD_VM=4.75±0.50kPa) than the healthy (H) control muscle (μ_H_VM=3.06±0.21kPa), suggesting altered elastic properties of the muscle tissue with higher stiffness, most likely due to muscle fibrosis. In a contracted state, the VM stiffness of the DMD was lower than that found in healthy muscle, due to a lack of the muscle contractile properties. In addition, the characteristic of the wave propagation as well as the stiffness mapping revealed qualitative changes in DMD muscle composition.

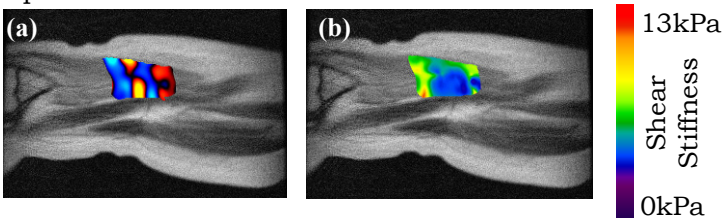

Figure 1: Phase image (a) and cartography of stiffness (b) obtained for DMD

Conclusions: MRE tests performed on DMD children revealed abnormal muscle stiffness in passive as well as in active conditions. The characteristics of this abnormality were revealed with an elevated stiffness value at rest and a weak progression of the muscle stiffness as a function of the level of contraction. This DMD muscle stiffness behavior is probably due to the fibrosis present within the DMD muscle providing changes of the muscle elasticity. This study has demonstrated the capability of the MR elastography technique to quantify muscle altered elastic properties of dystrophic muscle in DMD patients.

References:

[1] Quijano–Roy et al.: Neuromuscul Disord, 2, pp. S68–84, 2012.
[2] Leclerc et al.: JMRI, in press.
[3] Debernard et al.: JMR, in press.
[4] Chen Q et al.: Arch Phys Med Rehabil, 88(12), pp. 1658–1661, 2007.
[5] Bensamoun et al.: JMRI, 23(2), pp. 242–247, 2006.
[6] Manduca et al.: Medical Image Analysis, 5, pp. 237–254, 2001.

005 **THE USE OF ULTRASOUND ELASTOGRAPHY TO MONITOR THE EFFECTS OF NEOADJUVANT CHEMOTHERAPY ON LOCALLY ADVANCED BREAST CANCER.**

A DiBattista[1], R English[2], L Winter[2], RF Adams[2], JA Noble[1].*
[1]Oxford University, Oxford, England, UK; [2]Oxford University Hospitals NHS Trust, Oxford, England, UK.

Background: Neoadjuvant chemotherapy is used as the primary treatment for breast cancer to reduce tumor size and protect against metastatic spread. Significant interaction between tumor and stromal cells occurs during tumor formation and during chemotherapy [1]. In particular, fibrosis and inflammation can modify the biomechanical characteristic of tissue. Ultrasound elastography can estimate the relative stiffness of tissues *in vivo* and is thus well–suited to monitor these particular biological processes.

Aims: To monitor the changes in tissue composition during therapy using elasticity imaging and determine if it can be used as a prognostic indicator.

Methods: Patients were scanned prior to each of their chemotherapy sessions using the Zonare z.one L10–5 probe (Zonare Medical Systems Inc., Mountain View, CA, USA). A quasi–static elastography algorithm [2] was used to generate a set of sequential strain images. All images were normalized relative to the average image strain. The hypoechoic area in the B–mode images was segmented by an expert radiologist to separate tumor and stromal regions. The strain ratio (average stromal strain/average tumor strain) was used as a metric to monitor tissue compositional changes.

Results: Figure 1 depicts the B–mode and corresponding elastography images taken over the course of 6 cycles of chemotherapy of an exemplary responder patient. Note the gradual spread of strain relative to the hypoechoic region in the B–mode image. Figure 2(a) shows the segmentation of tumor and stromal regions and Figure 2(b) exhibits the strain ratio metric compared to tumor size; the strain ratio undergoes a significant drop after the 2nd chemotherapy cycle. This is in contrast to the tumor size which decreases more steadily and is not readily perceivable visually in the B–mode images alone.

Conclusions: Ultrasound elastography is an inexpensive, non–invasive prospective method for monitoring neoadjuvant chemotherapy response that exploits the observable biomechanical processes that coincide with changes in tissue composition during treatment. The strain ratio metric, though intuitive, is subject to the accuracy of the manual segmentation of the B–mode image. Future work will consist of deriving new, less subjective, metrics as well as continuing clinical data collection in an ongoing study.

Acknowledgements: Funding was provided by the NIHR Biomedical Research Centre Programme.

References:

[1] Mueller MM, Fusenig NE: Friends or Foes–Bipolar Effects of the Tumour Stroma in Cancer. Nature Reviews – Cancer, Volume 4, pp. 839–849, Nov. 2004.
[2] Di Battista A, Noble JA: A Fast and Robust 3D Ultrasound Strain Imaging Algorithm for Freehand Scanning. IEEE Proceedings from ISBI, pp. 528–531, 2011.

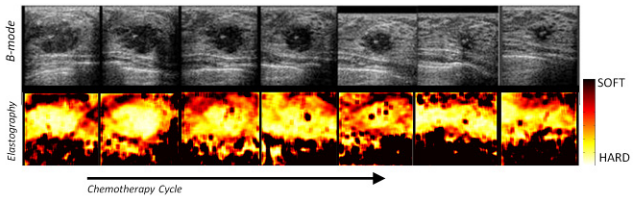

Figure 1: Sequential B–mode and corresponding elastography images taken over 6 cycles of chemotherapy (the first image is pre–treatment). Note the gradual spread of strain relative to the hypoechoic region in the B–mode image.

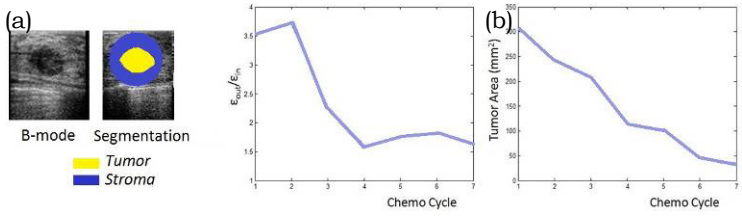

Figure 2: (a) Sample B–mode and resulting separation of tumor and peritumor (stroma) regions obtained from the segmentation of the hypo-echoic area in the B–mode image. (b) The strain ratio, εout/εin (the average stromal strain/average strain inside the tumor) plotted over the course of treatment. The plot to the right depicts the tumor cross sectional area (mm2) over the same period. Note the radical change in the strain ratio after the 2nd chemotherapy cycle is in contrast to the gradual steady change in tumor area.

* *indicates Presenter*

017 *IN VIVO* EVALUATION OF THE ELASTIC ANISOTROPY OF HUMAN ACHILLES TENDON USING SHEAR WAVE SPECTROSCOPY.

Javier Brum[1], Miguel Bernal[1], Jean–Luc Gennisson[1], Mickaël Tanter[1].*
[1]Institut Langevin – Ondes et Images, ESPCI ParisTech, CNRS UMR 7587, INSERM ERL U979, 1 rue Jussieu, 75005 Paris, FRANCE.

Background: Non–invasive evaluation of the tendon's elastic properties is of great importance to predict tendon rupture and in the follow up during recovery treatments. Usually, tendons may be described as a unidirectional arrangement of collagen fibers within a supporting matrix. Thus, the isotropic solid model is no longer valid, and a transverse anisotropic model is more suitable [1]. Aubry et al. measured shear wave speed values of ~15m/s and ~5m/s in the Achilles tendon by applying Shear Wave Elastography (SWE) parallel and perpendicular to the fiber orientation, respectively. Given these values and the frequency range used for SWE (100–800Hz), the shear wavelengths are greater than the mean tendon thickness (~4mm) [2]. Thus, waves may be guided along and across the tendon (Lamb waves). Therefore, to avoid underestimation of the elasticity value calculated from the shear wave speed value, a dispersion analysis is required.

Aims: The aim of this work is to study *in vivo* the wave propagation in human Achilles tendons parallel and perpendicular to the fiber orientation direction by using Shear Wave Spectroscopy (SWS) [3].

Methods: The left and right tendons from two healthy volunteers were studied. For each experiment the volunteer was in a sitting position with a 90° angle between the foot and the tibia as well as between the tibia and the femur. The foot and the ultrasonic probe were submerged in a water tank to avoid pre–compression of the tendon and to facilitate the positioning of the probe. Once a proper echographic image was obtained the probe position was held fixed through an articulated arm. Using the radiation force of a focused 8MHz ultrasound beam, broadband elastic waves (300–800Hz) were generated inside the tendon. The wave propagation parallel and perpendicular to the fiber orientation was then tracked using ultrafast imaging at a 15kHz rate. Finally, the wave dispersion curve (i.e., relation between phase velocity and frequency) was retrieved by performing a 2D Fourier transform to the measured displacement field.

Results: Similar behavior was observed for all four tendons. Phase velocity values between 12.9±1.7m/s and 16.9±2.1m/s were measured for frequencies between 300–800Hz parallel to the fiber orientation (mean value ± standard deviation). In the perpendicular direction the values ranged from 3.1±0.5m/s to 4.3±0.6m/s for the same bandwidth mentioned above. Therefore, non–negligible dispersive effects were observed for wave propagation in both directions Nevertheless, the values obtained in our study coincide with those reported in the literature [2]. Due to the ratio between parallel and perpendicular phase velocities (~3) and the ratio between tendon width and thickness (~3), wave propagation along parallel and perpendicular directions does not interfere with each other. As a consequence, wave propagation along both directions is assumed to take place in a transverse anisotropic plate. Fitting the theoretical dispersion curve given by [4] to the data (assuming the compressional elastic constants to be known from [1]) a parallel mean shear wave speed of 23±6m/s is measured for the four tendons, which greater than the values reported in [2]. Contrary to the parallel direction, dispersion along the perpendicular direction could not be fully explained by Lamb theory. Since along this direction geometrical dispersion is not very strong (wavelength are of the order of plate thickness), it is difficult to establish whether dispersion is mainly due to geometry, viscosity or both. Further studies are being carried out to clarify this point and to establish a more complete model.

Conclusions: In this work wave dispersion was measured *in vivo* in the Achilles tendon in the direction perpendicular and parallel to the fiber orientation, and it was demonstrated that a dispersion model should be taken into account in order to estimate properly the tendon elasticity.

References:

[1] P.L. Kuo, P.C. Li, M.L. Li: Elastic Properties of Tendon Measured by Two Different Approaches. Ultrasound Med. Biol., 27(9), pp. 1275–1284, 2001.
[2] S. Aubry et al.: Biomechanical Properties of the Calcaneal Tendon *In Vivo* Assessed by Transient Shear Wave Elastography. Skeletal Radiol., DOI 10.1007/s00256–013–1649–9, 2013.
[3] T. Deffieux, G. Montaldo, M. Tanter, M. Fink: Shear Wave Spectroscopy for *In Vivo* Quantification of Human Soft Tissues Viscoelasticity. IEEE Trans. Med. Im., 28(3), pp. 313–322, 2009.
[4] V. Dayal, V.K. Kinra: Leaky Lamb Waves in Anisotropic Plate I: An Exact Solution and Experiments. J. Acoust. Soc. Am., 85(6), pp. 2268–2276, 1989.

002 ***IN–VIVO* ASSESSMENT OF THE BIOMECHANICAL PROPERTIES OF THE PREGNANT CERVIX.**

Sabrina Badir[1], Edoardo Mazza[1], Michael Bajka[2].*
[1]Institute of Mechanical Systems, Swiss Federal Institute of Technology, 8092 Zurich, SWITZERLAND; [2]Clinic of Obstetrics, OB/GYN Department, University Hospital Zurich, 8091 Zurich, SWITZERLAND.

Background: A variety of methods for quantitative determination of physical properties of the pregnant cervix have been recently developed [1] and some of them were applied *in–vivo*. Measuring the stiffness of the cervix might be useful in the prediction of preterm delivery or successful induction of labour. Some groups applied quasi–static elastography; others used ultrasound images to determine maximum deformability of the cervix (e.g. quantified with the so called cervical consistency index, CCI [2]). We applied the aspiration technique on the ectocervix.

Aims: We determined mechanical properties of the ectocervix of 50 non–pregnant and 50 pregnant subjects at different gestational ages [3]. Here we present our results and discuss them in view of findings from quasi–static elastography and CCI measurements.

Methods: The aspiration method was developed in order to determine the *in–vivo* stress–strain curve of soft tissues in human organs. The device measured the vacuum (negative pressure) required to deform the tissue into the circular opening of a tube. Measurements on the ectocervix were done such that the (negative) pressure, named "p_{cl}", needed to displace the tissue up to four millimeters was recorded. Lower values of p_{cl} corresponded to lower stiffness [4].

Results: Measurements in 50 pregnant women throughout pregnancy and on non–pregnant subjects (reference, n=50) [3] showed that stiffness in early pregnancy (first trimester) was significantly lower compared to non–pregnant subjects. p_{cl} steadily decreased during gestation, with an initial higher drop in the first two trimesters and subsequent slower decrease in the third trimester. After delivery (average 6 weeks post–partum) the values increased back to the level of early pregnancy. The pressure values are directly proportional to tissue stiffness. Thus, the stiffness of the cervix drops according to the same time function. Based on this assumption, the expected time course of CCI can be estimated. The corresponding prediction of CCI evolution demonstrates that time course of biomechanical properties observed in aspiration measurements [3] and CCI [2] agree to a great extent. In contrast, elastography based assessment of cervical stiffness [5] show weak correlation with gestational age.

Conclusions: There is intensive research going on to characterize the biomechanical and microstructural properties of the cervix during pregnancy. Quasi–static elastography based methodologies cannot provide absolute values of biomechanical properties of the cervix because it is difficult to standardize or measure the applied force. Ultrasound based determination of maximum deformability of the cervix has been more successful. This can be rationalized based on the non–linearity of the force–deformation relationship. The aspiration measurements provided evidence of progressive softening of the ectocervix in pregnancy. Despite the fact that this biomechanical measurement is confined to about 1 cubic cm of tissue at the external surface of the ectocervix, the observed time course of the decrease in stiffness parallels the compliance changes in the entire cervix described by CCI. A multicenter clinical study was started to assess the diagnostic relevance of different biomechanical measurement techniques.

References

[1] Feltovich H, Hall T, Berghella V: Beyond Cervical Length: Emerging Technologies for Assessing the Pregnant Cervix. Am J Obstet Gynecol, 207, pp. 1–10, 2012.
[2] Parra–Saavedra M, Gomez L, Barrero A, et al.: Prediction of Preterm Birth using the Cervical Consistency Index. Ultrasound Obstet Gynecol, 38, pp. 44–51, 2011.
[3] Badir S., Mazza E., Bajka M.: Cervical Softening Occurs Early in Pregnancy: Characterization of Cervical Stiffness in 100 Healthy Women using the Aspiration Technique. Prenatal Diagnosis, in press.
[4] Badir S., Bajka M., Mazza E.: A Novel Procedure for the Mechanical Characterization of the Uterine Cervix during Pregnancy. Journal of the Mechanical Behavior of Biomedical Materials, DOI: 1016/j.jmbbm.2012.11.020, 2012.
[5] Hernandez–Andrade E, Hassan S, Ahn H, et al.: Evaluation of Cervical Stiffness During Pregnancy using Semiquantitative Ultrasound Elastography. Ultrasound Obstet Gynecol, 41, pp. 152–161 2013.

020 **CERVIX ELASTOGRAPHY: A NEW METHOD FOR THE PREDICTION OF THE PRETERM DELIVERY.**

Roch L. Maurice[1,2], Philippe Delachartre[2], Gil Dubernard[3], Cyril Huissoud[3], Jonathan Caloone[3].*
[1]Centre de Recherche, Centre Hospitalier Universitaire Sainte–Justine (CRCHUSJ), Université de Montréal, Montréal, Québec, CANADA; [2]Université de Lyon, CREATIS, CNRS UMR5220, Inserm U1044, INSA–Lyon, Université Lyon 1, FRANCE; [3]Obstetrics and Gynecology Department, Croix Rousse University Hospital, 104 Grande Rue de la Croix Rousse, Lyon, F–69004, FRANCE.

Background: Preterm delivery (PTD) is a major problem in perinatal medicine, which occurs in approximately 7% of cases. PTD is attributed to cervical insufficiency, especially for the internal os which is considered as the weakness area. PTD is responsible for substantial neonatal morbidity and mortality. Current clinical signs or ultrasound measurements of the cervical length are disappointing for the prediction of the PTD in low–risk women. Preliminary studies have demonstrated that the mechanical properties of the uterine cervix could be assessed using elastography [1]. Nevertheless, the predictive value of this approach to prevent PTD remains unknown.

Aims: We here report additional preliminary data supporting the feasibility of the cervix elastography and its potential for the prediction of PTD during pregnancy.

Methods: A singleton pregnancy at 22 weeks gestation, without risk factors of PTD, was evaluated. A transvaginal probe (Voluson E8 Expert, GE Medical Systems, Milwaukee, WI) was applied to the uterine cervix to record B–mode images of the cervical canal, the internal and external os in a sagittal view, during a quick and soft compression. Videoclip sequences were processed off–line using the elastography–based imaging biomarker (ImBioMark) [2] that was adapted to investigate PTD. Four cervical areas were selected (Figure 1a): (A) the superior and internal lip, (B) the inferior and internal lip, (C) the superior and external lip, (D) the inferior and external lip. Strains and displacements were assessed for each area using ImBioMark.

Results: Several sequences were investigated in order to determine the soft pressure varying in time applied to the uterine cervix. Figure 1b shows an example of tissue displacements along time. From this analysis, elastograms were computed. For illustration purposes, Figure 1c displays an axial strain elastogram. Axial strain values of 1.02, 1.40, 1.20 and 1.60% were assessed for A, B, C and D ROI, respectively.

Conclusions: Elastography represents a non–invasive and promising method for the assessment of the mechanical properties of the uterine cervix. It is expected to detect weakness area of the uterine cervix corresponding to higher strains on elastograms. We are looking forward to investigating large high– and low–risk populations to document elastography as a potential method to predict PTD.

Acknowledgements: This work was partially supported by CMIRA Accueil Pro (Rhône–Alpes, France), the Labex CELYA (Lyon, France). The authors are grateful to the "Génie Biomédical" (GBM) of the CHUSJ for their kind support in the achievement of this work.

References:

[1] Molina FS, Gomez LF, Florido J, Padilla MC, Nicolaides KH: Quantification of Cervical Elastography: A Reproducibility Study. Ultrasound Obstet Gynecol, 39, pp. 685–9, 2012.
[2] Maurice RL, Dahdah N and Tremblay J: Imaging–Based Biomarkers: Characterization of Post–Kawasaki Vasculitis in Infants and Hypertension Phenotype in Rat Model. Intnatl J of Vasc Med, ID 364145, 2012.

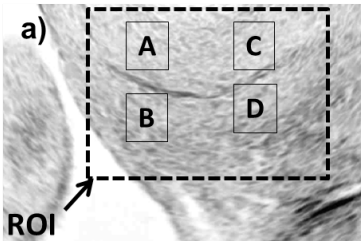

Figure 1a: B–mode image of the uterine cervix including the 4 regions (A–D).

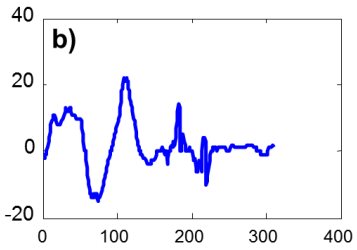

Figure 1b: Global axial translation (in pixels) as a function of the frame number.

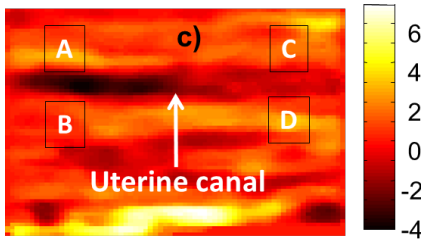

Figure 1c: Axial strain (in %) corresponding to the ROI delimited on Figure 1a.

071 **PROPOSITION OF A MULTIPARAMETRIC MODEL–BASED METHOD FOR BREAST LESION DIFFERENTIATION: A FEASIBILITY STUDY.**

Roch L. Maurice[1,2], Elisabeth Brusseau[2], Agnès Coulon[3], Emmanuèle Maissiat[3], Mojgan Devouassoux–Shisheboran[4], Nawele Boublay[5,6,7], Loïc Boussel[2,3].*

[1]Centre de Recherche, Centre Hospitalier Universitaire Sainte–Justine (CRCHUSJ), Université de Montréal, Montréal, Québec, CANADA; [2]Université de Lyon, CREATIS, CNRS UMR5220, Inserm U1044, INSA–Lyon, Université Lyon 1, FRANCE; [3]Service de Radiologie et [4]Anatomie et Cytologie Pathologiques, Hôpital de la Croix–Rousse, Hospices Civils de Lyon, FRANCE; [5]Pôle Information Médicale Evaluation Recherche, Hospices Civils de Lyon, FRANCE; [6]Université Lyon 1, EA 4129, FRANCE; [7]CMRR, Hôpital des Charpennes, Lyon, FRANCE.

Background: Elastography has been introduced to complement mammography and sonography with the purpose of better differentiating benign from malignant lesions. With this regard, criteria such as elasticity score and strain index, also termed strain ratio (SR), have been introduced [1,2]. SR was defined as the mean strain value of the background divided by the mean strain value within the lesion.

Aims: We previously proposed a multi–parametric model–based elastography method (ImBioMark), devoted to investigate the arterial wall mechanical features [3]. In this study, we adapted this technique to estimate axial strain and axial shear within breast tissues and reported preliminary results for the SR.

Methods: We investigated a tissue–mimicking phantom (n=1), carcinomas (n=3) and fibroadenomas (n=3). The experimental and clinical RF data were recorded with an Ultrasonix ultrasound scanner (Sonix RP or MDP, Ultrasonix Medical Corp., Richmond, BC, Canada). To calculate SR, background regions were manually selected on both sides (left and right) and approximately at the same depth than the lesion.

Results: Figure 1 displays B–mode images (a and d), axial strains (b and e) and axial shears (c and f) for a carcinoma and a fibroadenoma, respectively. Based on SR, carcinomas were found close to 9 times (range 6.4–13.7) stiffer than surrounding tissues, while fibroadenomas were less than 5 times (range 2.9–4.8) stiffer. In axial shear images, characteristic patterns induced by the presence of lesions were also observed.

Conclusions: ImBioMark was found adapted to investigate breast tissues, and resulting SR show higher values for carcinomas than fibroadenomas. These preliminary results were obtained from analyzing elastograms characterized by low strain values (as illustrated in Figure 1), which may potentially impair SR accuracy. This is to be investigated in future works. We also intend to further validate ImBioMark with additional clinical data.

Acknowledgements: This work was partially supported by CMIRA Accueil Pro (Rhône–Alpes, France), the Labex PRIMES and Labex CELYA (Lyon, France). The authors are grateful to the "Génie Biomédical" (GBM) of the CHUSJ for their kind support in the achievement of this work.

References:

[1] Yerli H, Yilmaz T, Kaskati T, Gulay H: Qualitative and Semiquantitative Evaluations of Solid Breast Lesions by Sonoelastography. J Ultrasound Med, 30(2), pp. 179–186, 2011.

[2] Gong X, Xu Q, Xu Z, Xiong P, Yan W, Chen Y: Real–Time Elastography for the Differentiation of Benign and Malignant Breast Lesions: A Meta–Analysis. Breast Cancer Res Treat, 130(1), pp. 11–18, 2011.

[3] Maurice RL, Dahdah N and Tremblay J: Imaging–Based Biomarkers: Characterization of Post–Kawasaki Vasculitis in Infants and Hypertension Phenotype in Rat Model. Interntl J of Vascular Med, ID 364145, 2012.

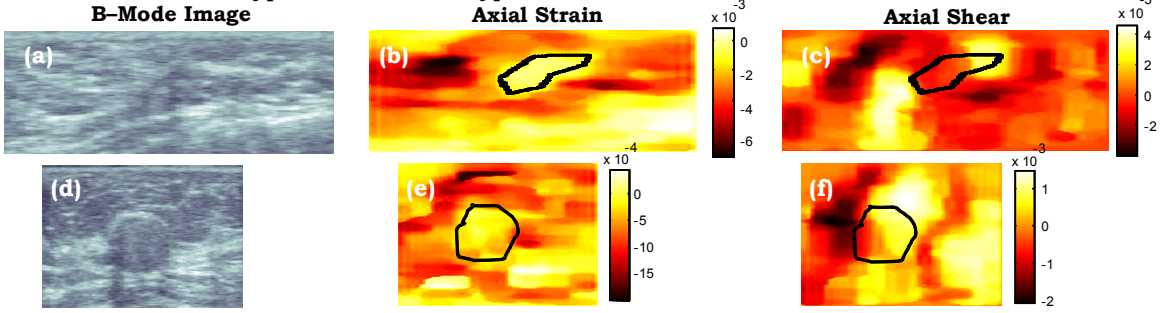

Figure 1: Two examples of results obtained with our technique for a carcinoma (top row) and a fibroadenoma (bottom row). (a, d) B–mode, (b, e) axial strain and (c, f) axial shear images.

* *indicates Presenter*

072 **AXIAL SHEAR STRAIN ELASTOGRAPHY IN BENIGN AND MALIGNANT BREAST DISEASE: PRELIMINARY PROSPECTIVE FREEHAND *IN VIVO* FINDINGS.**

Elaine G. Khalil[1], Arun K. Thittai[1], Brian S. Garra[2], Jonathan Ophir[1].*
[1]The University of Texas Health Science Center at Houston, Houston, TX, USA; [2]Food and Drug Administration, Silver Spring, MD, USA.

Background: There is a 1 in 8 lifetime probability of developing breast cancer. Yet the majority of breast masses are not caused by breast cancer [1]. Ultrasound plays an integral role in the characterization of breast masses. It is used routinely to assess whether or not a mass warrants biopsy based on characteristics deemed suspicious according to the Breast Imaging–Reporting and Data System (BI–RADS) classification. While ultrasound improves the distinction between benign and malignant breast masses, the current BI–RADS criteria still result in many unnecessary benign biopsies [2].

Aims: We are developing and testing ultrasound–based elastographic imaging methods to understand more about the mechanical phenomena occurring at soft tissue boundaries in the breast. We are focusing on axial shear strain fill–in and contrasting margination zones created in slightly compressed breast masses which are suspicious for malignancy by BI–RADS assessment [3]. Our goal is to demonstrate how these elastographic features differ in benign and malignant disease. We hypothesize that these features will contribute additional diagnostic criteria beyond the current BI–RADS criteria for ultrasound, thus improving the sensitivity and specificity of noninvasive classification of benign vs. malignant breast masses *in vivo*.

Methods: To date, 25 patients with suspicious breast masses recommended for biopsy have been recruited to participate. These patients have undergone a standard ultrasound exam followed by a series of freehand elastography acquisitions using a Sonix–500RP scanner, (Ultrasonix® Corp., Richmond, BC, CA). All participants have pathology correlation obtained by core needle biopsy. The Axial Shear Strain Elastograms (ASSE) will subsequently be analyzed via an observer study and evaluated for additive statistical significance when used together with the BI–RADS classification and Axial Strain Elastogram features.

Results: The preliminary results are promising. The biopsy proven benign fibroadenomas, which are usually ovoid and loosely bonded, demonstrate the expected fill–in effect provided the mass is not oriented perfectly parallel to the plane of compression. There are also a few cases which pose challenges to our hypothesis, such as biopsy proven cancers which also demonstrate fill–in or thin margination zones typically associated with benign masses.

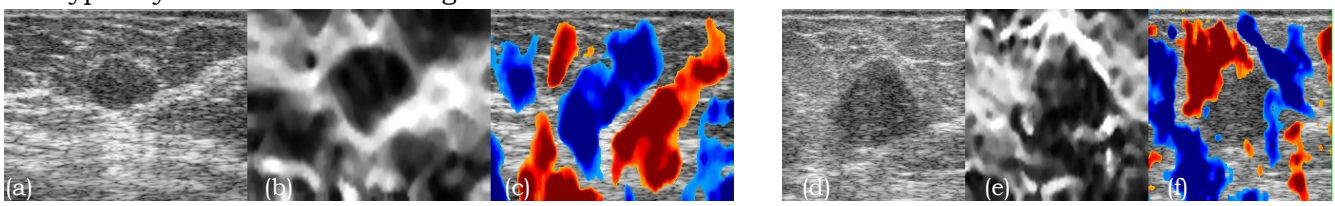

Figure 1: An example frame of (a, d) Sonogram, (b, e) ASE and (c, f) ASSE from a cine–loop of freehand compressed *in vivo* breast lesion data. The data were pathologically confirmed as benign fibroadenoma (a, b, c) (30mm x 38mm); malignant invasive ductal carcinoma (d, e, f) (40mm x 38mm). Observe the presence in the ASSE image of significant non–zero axial–shear strain inside the fibroadenoma (c) only (referred to as "fill–in"), along with high contrast margins of opposite polarity. This characteristic appearance is conspicuously absent in the case of cancer (f).

Conclusions: These novel methods could become important for (1) improving tumor margin visualization for diagnosis and treatment and (2) for differentiation between benign and malignant breast masses *in vivo*, based on their fill–in features.

Acknowledgements: This work was supported in part by NIH grant R21–CA135580–01.

References:

[1] American Cancer Society, Breast Cancer Facts & Figures 2011. Atlanta: American Cancer Society, Inc. Available at: http://www.cancer.org/Research/CancerFactsFigures/CancerFactsFigures/cancer–facts–figures–2011 Date last accessed: March 1, 2012.
[2] Gutwein LG, Ang DN, Liu H, Marshall JK, Hochwald SN, Copeland EM, Grobmyer SR: Utilization of Minimally Invasive Breast Biopsy for the Evaluation of Suspicious Breast Lesions. The American Journal of Surgery, 202, pp. 127–132, 2011.
[3] Thittai, A, Galaz, B and Ophir, J: Axial–Shear Strain Distributions in an Elliptical Inclusion Model: Experimental Validation and *In Vivo* Examples with Implications to Breast Tumor Classification. Ultrasound in Med. and Biol., Vol. 36, No. 5, pp. 814–820, 2010.

063 **3D *IN VIVO* ARFI IMAGING OF THE PROSTATE USING A SIDE–FIRING ENDORECTAL ARRAY.**

ML Palmeri[1], SJ Rosenzweig[1], SL Lipman[1], K Garcia–Reyes[1], A Buck[1], J Madden[1], T Polascik[1], ZA Miller[1], KR Nightingale[1].
[1]Duke University, Durham, NC, USA.

Background: Acoustic Radiation Force Impulse (ARFI) imaging of the prostate to delineate prostate cancer (PCA) has been done *ex vivo* with a linear array [1] and *in vivo* with an endovaginal array [2]. PCA has been shown to appear as regions of decreased displacement, but shortcomings of using the endovaginal array include a limited depth of acoustic energy penetration, restricting evaluation in the poster aspect of the prostate, and a strong radius of curvature that create geometric distortions that need to be compensated for during the image processing.

Aims: The aims of this work include: (1) demonstrating improved ARFI imaging of the anterior aspect of the prostate using a side–firing endorectal imaging array, and (2) evaluating the appearance of PCA, benign prostatic hyperplasia (BPH) and atrophy in ARFI images.

Methods: 3D ARFI imaging was performed using an ER7B (Siemens Medical Solutions, Issaquah, WA) endorectal array on a Siemens ACUSON SC2000® scanner, coupled to a custom–developed, semi–automated rotation apparatus to acquire sequential images to generate a 3D imaging dataset (Figure 1). ARFI imaging was performed immediately prior to radical prostatectomy in 25 patients, and raw IQ data were saved offline. ARFI–induced displacements were calculated using Loupas' algorithm [3] and were correlation–coefficient–thresholded and scan–converted to achieve displacement estimates in a Cartesian coordinate system. Depth–dependent gain was applied using an iterative histogram normalization approach. Structures of appreciable contrast in ARFI images were correlated with whole mount pathology of the excised prostate and/or T2WI/ADC MR images.

Results: Figure 2 shows the characteristic ARFI imaging appearance of BPH, in a coronal view, which has a complex pattern of relatively high displacement regions separated by thin bands of lower displacement (suspected to be fibrotic) tissue. Figure 3 shows a representative example of PCA, in a coronal ARFI imaging view, which is characterized by a region of decreased displacement with contralateral asymmetry. Calcifications in the prostate appear as highly–displacing structures with distal shadowing/decorrelation.

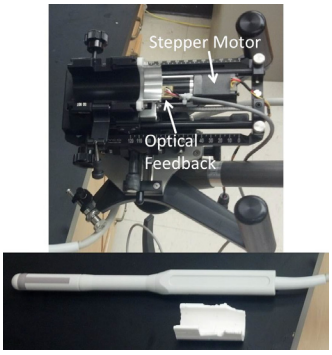

Figure 1: Rotation Setup

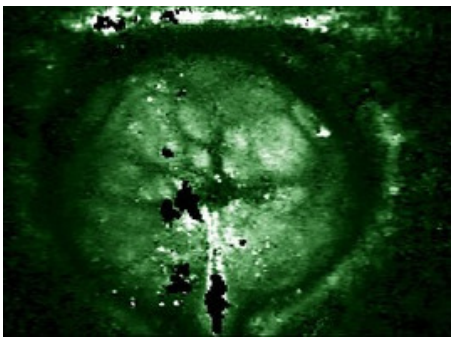
Figure 2: Benign Prostatic Hyperplasia

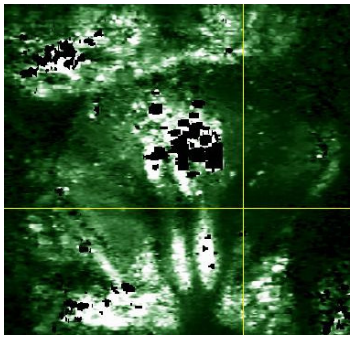
Figure 3: Prostate Cancer

Conclusions: Use of a side–firing endorectal array has improved anterior prostate visualization, though this anterior region is still challenging to visualize in large glands or with significant central gland calcifications. BPH has a very characteristic ARFI imaging appearance, while PCA and atrophy can both appear as asymmetric regions of decreased displacement in coronal view.

Acknowledgements: This work has been funded by NIH R01 CA142824 and the Duke–Coulter Translational Partnership Grant Program. Special thanks to Siemens Medical Solutions for their technical assistance, the Pathology Assistants and Drs. Rajan Gupta and Christopher Kauffman in the Department of Radiology.

References:

[1] http://dx.doi.org/10.1016/j.ultrasmedbio.2009.12.006.
[2] http://www.ncbi.nlm.nih.gov/pubmed/22104533.
[3] Loupas et al.: Experimental Evaluation of Velocity and Power Estimation for Ultrasound. IEEE TUFFC, 42(4), pp. 689–699, 1995.

029 **ASSISTING MRI–GUIDED PERCUTANEOUS PROCEDURES WITH ELASTOGRAPHY: DEVELOPMENT OF AN INTERVENTIONAL MR–ELASTOGRAPHY PROTOCOL.**

Nadège Corbin[1], Quentin Boehler[1], Elodie Breton[1], Laurent Barbé[1], Pierre Renaud[1], Michel de Mathelin[1], Jonathan Vappou[1].*
[1]ICube, University of Strasbourg–CNRS, Strasbourg, FRANCE.

Background: Minimally–invasive, percutaneous interventions offer significant advantages over conventional surgery for several procedures, in terms of patient comfort, reduced hospitalization times and lower complication rates [1,2]. MRI guidance is particularly appreciated by interventional radiologists due to the absence of ionizing radiation and the quality of contrast in soft tissues [3]. However, real–time MRI contrast is not always sufficient to clearly discriminate between healthy and diseased tissue. An additional
elastography–based contrast would clearly help to the targeting in all procedures and would also provide new information for the monitoring of thermal therapies.

Aims: The objective of this study is to develop Magnetic Resonance Elastography (MRE) specifically for assisting MR–guided percutaneous procedures. This requires the development of adequate mechanical excitation devices, ultrafast MRE sequences and ultrafast inverse problem solvers for real–time display of MRE contrast.

Methods: (1) Mechanical exciter: A specific compact exciter was developed that allowed to generate vibrations directly from the needle holder. A piezo–electric vibrator was mounted over a translatable structure, which was itself motorized for easier needle insertion. The whole system was designed to be fully MR–compatible. The achievable excitation frequency range was 50–200Hz. (2) MRE sequences: ultrafast MR–sequences (EPI spin echo, Spoiled GRE sequences with/without real–time slice selection) were implemented and compared. Acquisition times varied between 1.6s and 2s for one full acquisition of 4 images with different phase offsets. (3) Inverse problem: The inverse problem was solved offline at this stage, by performing a 2D inversion of the wave equation. MRE experiments were performed on a 1.5T interventional MRI system (Siemens Aera, Erlangen, Germany). The protocol was tested on gelatin/agar tissue–mimicking phantoms.

Results: No significant artifact could be attributed to the excitation system. Shear waves propagating from the needle could be clearly observed with all MRE sequences. EPI sequences were the fastest but were associated with significant distortion when compared to sequences without EPI readout.

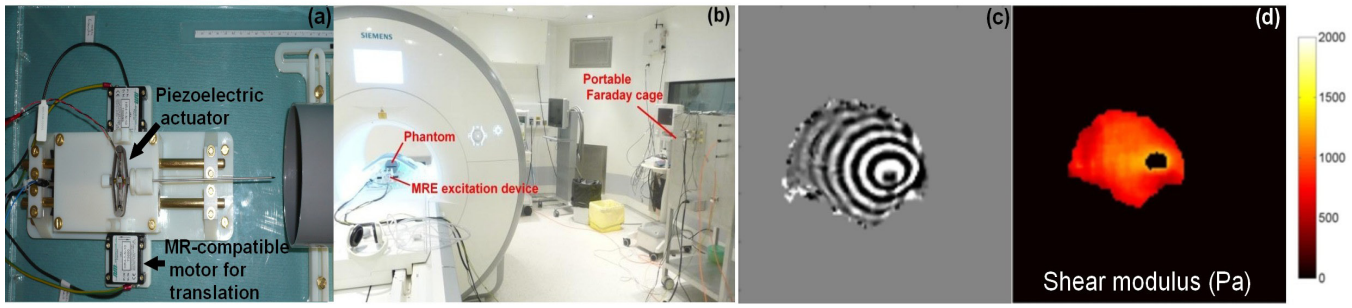

Figure 1: (a) Schematic view of the excitation device; (b) View of the experimental setup; (c) Resulting shear waves propagating away from the needle, encoded with an EPI MRE sequence; (d) Resulting MRE elasticity map in the same phantom.

Conclusions: The feasibility of the interventional MRE protocol was demonstrated here on phantoms, with the use of a dedicated excitation system and sequences. Future developments will focus on integrating the inverse problem solver online for real–time display of the MRE Elastogram and *in vivo* tests with the physicians of the Department of Interventional Radiology of Strasbourg Hospital.

References:

[1] Gazelle et al.: Radiology, 233(3), pp. 729–739, 2004.
[2] Raymond et al.: Colorectal Disease, 12(10), pp. 1001–1006, 2010.
[3] Silverman et al.: Radiology, 217(3), pp. 657–664, 2000.

* *indicates Presenter*

051 **ARFI SURVEILLANCE OF SUBCUTANEOUS HEMOSTASIS (ASSH) AT FEMORAL ARTERIOTOMY IN ASPIRIN–TREATED VERSUS NAIVE DOGS.**

Rebecca E. Geist[1], Timothy C. Nichols[2,3], Melissa C. Caughey[2], Elizabeth P Merricks[3], Caterina M. Gallippi[1].*

[1]Biomedical Engineering NC Joint Department, [2]Medicine Department, [3]Pathology and Laboratory Medicine Department, University of North Carolina at Chapel Hill, Chapel Hill, NC, USA.

Background: Percutaneous coronary intervention (PCI) has reduced coronary heart disease morbidity and mortality, but post–procedural bleeding causes prolonged and recurrent hospitalization, stroke and myocardial infarction (MI), and it is associated with 12.1% of all in–hospital deaths after PCI [1]. On–demand therapies to remedy excessive post–PCI bleeding are easily engaged and proven effective, but their need is often underappreciated due to insufficiencies in the clinically standard bleeding detection method of visual inspection, which is blinded to subcutaneous bleeding [2].

Aims: Our group is developing ARFI Surveillance of Subcutaneous Hemostasis (ASSH) to noninvasively monitor subcutaneous bleeding surrounding femoral artery puncture following PCI. ASSH analyzes tissue reaction after ARFI to determine the region of extravasated blood. This work uses a dog study to test the hypothesis that ASSH discriminates faster bleeding rate (BR) and longer time to hemostasis (TTH) in dogs receiving aspirin anti–platelet treatment versus control following 5F sheath removal from a punctured femoral artery.

Methods: The UNC–CH IACUC approved all procedures. ASSH was performed using a Siemens SONOLINE Antares imaging system in 3 naïve control dogs and in 3 dogs treated for 7 days with 81mg aspirin (ASA)/day (2.7–3.2mg.kg.day po). Platelet inhibition was confirmed by ADP–induced agregometry. Dogs were anesthetized and lying in dorsal recumbancy during B–mode guided femoral puncture and insertion of a 5F sheath (Terumo). Serial ARFI imaging occurred for 15 minutes with the sheath in place, 7 minutes after sheath removal with full arterial occlusion by manual compression, 7 minutes with 70% arterial occlusion, and 11 minutes with no arterial occlusion for a total 40 minutes imaging period. Manual compression was implemented consistently with the clinical standard for achieving hemostasis following PCI, assisted by the ultrasound probe and stereotactic clamp. ASSH BR and TTH were calculated.

Results: ASSH BR was faster ($p<0.05$) in aspirin–treated versus control dogs during 70% and no arterial compression. Mean ASSH TTH was 16 min in control dogs, but complete hemostasis was not observed by ASSH in 2 of the 3 aspirin–treated dogs.

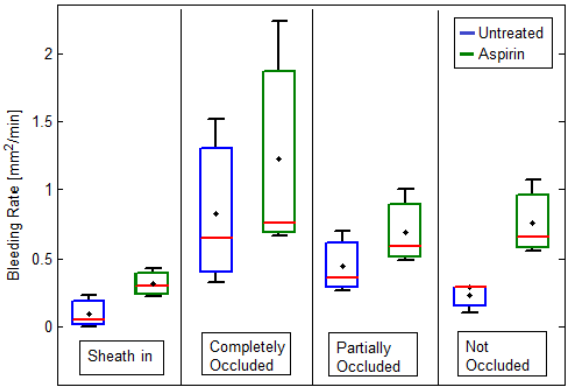

Figure 1: Box plots showing 25th and 75th percentile (box), range (black lines), median (red line) and mean (asterisks) ASSH bleeding rate for aspirin–treated versus naive dogs during 40 minute serial ARFI imaging period.

Conclusions: ASSH delineated faster BR and prolonged TTH in aspirin–treated versus control dogs. These data suggest that ASSH may be relevant to monitoring subcutaneous bleeding with antithrombotic therapy in clinical PCI.

Acknowledgements: Siemens Medical Solutions, USA Inc. Ultrasound Division and the North Carolina Translational and Clinical Sciences (NCTraCS) Institute with UL1TR000083 and HL63098.

References:

[1] A.K. Chhatriwalla, A.P. Amin, K.F. Kennedy, J. a House, D.J. Cohen, S.V. Rao, J.C. Messenger, and S.P. Marso: Association Between Bleeding Events and In–Hospital Mortality after Percutaneous Coronary Intervention. JAMA: The Journal of the American Medical Association, Vol. 309, No. 10, pp. 1022–9, Mar 2013.

[2] Z. Jaffery, C.J. White, T.J. Collins, M. a Grise, J.S. Jenkins, P.W. McMullan, R. a Patel, J.P. Reilly, S.N. Thornton, and S.R. Ramee: Factors Related to a Clinically Silent Peri–Procedural Drop in Hemoglobin with Coronary and Peripheral Vascular Interventions. Vascular medicine (London, England), Vol. 16, No.5, pp. 354–9, Oct. 2011.

* *indicates Presenter*

086 **GIOVANNI ALFONSO BORELLI: RENAISSANCE ASTROPHYSICIST AND BIOENGINEER.**

Francis Duck, MBE, Visiting Professor[1]*.
[1]University of Bath, Bath, England, UK.

Giovanni Borelli (1608–1679) is now recognised as the father of biomechanics. He was born in Naples, studied in Rome and then became professor of mathematics in the University of Messina. In 1656 he moved to Pisa, where his astronomical observations formed a recognized precursor to Newton's theory of gravitation. He also started work on biomechanics and established his own vivisection and dissection laboratory. By the time he left Pisa in 1668 to return to Messina he had accumulated all the experimental material that he required for his later *De Motu Animalium.* He became politically active and, in 1672, he was declared a rebel with a price on his head and had to leave for Rome, where he spent his final years.

He saw physiology as an integral part of physical science, using the rules of mathematics and the concepts of physics to encompass life science, in a manner similar to that so successfully applied to astronomy. Borelli's imagery and the interpretation of his observations of the actions of living beings were exclusively mechanical: forces and moments, gravity and weight, movement and percussion, inflow and outflow, contraction and expansion, volumes and velocities, swelling, binding and wrinkling, ebullition and effervescence, mixing, scraping and separation. His analogies were mechanical, pulleys and scales, goatskin bottles and bladders, wet ropes and balls of string. His text was supported by numerous detailed illustrations. He calculated the forces that various muscles exert during contraction, forces on the spine, and considered the material properties of cartilage. He analysed bipedal walking, jumping, flying and swimming, and included designs for a diving suit and a submarine. He described respiratory function, the pulse, and measurements of intra–cardiac temperature.

In a world in which the Inquisition was still active, he was cautious of the fine line between science and heresy, saying "*The Holy Church teaches such, and such must be believed. We must submit to it'.* He then gave his real belief, quoting Plato: *"God exerts geometry".*

Reference:

[1] Duck FA: Physicists and Physicians. A History of Medical Physics from the Renaissance to Röntgen. IPEM York, Chapter 2: Iatrophysics, 2013.

Figure 1: Giovanni Alfonso Borelli 1608-1679

Figure 2: Borelli's analysis of spinal forces under load.

035 **THERMAL EXPANSION IMAGING FOR REAL–TIME LESION DEPTH ASSESSMENT DURING RF CATHETER ABLATION.**

Péter Baki[1], Gábor Székely[1], Orçun Göksel[1].*
[1]Computer Vision Laboratory, ETH, Zurich, SWITZERLAND.

Background: Since B–mode imaging is not optimal to identify ablated tissue [1], prior studies involve elastography via compressions for post–ablation lesion assessment and thermal strain imaging [2] via changing speed of sound for monitoring pre–coagulation temperature rise. However, real–time assessment of lesion size during tissue coagulation is a less investigated area, although it is essential for achieving desired lesion depth.

Aims: In this study we investigate the feasibility of estimating lesion depth from RF time–series from an A–mode ultrasound transducer custom fit at the tip of the ablation catheter.

Methods: For ablation experiments, 4×4cm^2 samples (N=12) of porcine hearts were positioned on a stainless steel patch immersed in 0.9% saline solution at 25°C. Myocardium thickness among the samples varied from 0.5–1.3cm. RF ablations were performed at 12.5W for ~60s, while imaging the tissue by a single–element 14MHz ultrasound transducer built in the custom design catheter tip, see Figure 1(a). RF data sampled at 80MHz was collected at a frame–rate of 20Hz. To estimate displacements between consecutive RF lines, we used a time–domain cross–correlation method with block length of 0.8mm and 75% overlap. Strains were computed using a 1mm kernel least–squares strain estimator. Above typical thermal coagulation temperatures of ~50°C, the speed of sound does not increase significantly [2]; thus, it is mainly the thermal expansion that contributes to observed ultrasound displacements. Accordingly, we use observed instantaneous strains to monitor the advancing ablation boundary, which we call thermal expansion imaging (TEI) hereafter.

Results: In Figure 1(c) and (d) displacements and strains are plotted after temporal Gaussian smoothing, for a case with ablation from t=2 to t=62s with coagulation starting around t=9s. In the strain image, progression of a high–strain region is observed, which we believe is caused by the expansion of the tissue being coagulated. We thus consider the far end of such high–strain band (as outlined in Figure 1(d)) to mark the boundary of the growing lesion. We utilized manually identified lesion depths from post–ablation visual assessment of cut samples (see Figure 1(b)) in order to evaluate TEI–estimated lesion depth, which were identified in this work automatically using a simple zero–crossing of the axial strain at the termination of ablation. Figure 1(e) shows the correlation of observed and TEI–estimated lesion depths.

Conclusions: Lesion border extracted from TEI was shown to be a good indicator of lesion depth. We will investigate referencing displacements to a distant point to decouple any possible motion–induced strains.

Acknowledgements: This work was supported by the NCCR Co–Me of the Swiss National Science Foundation.

References:

[1] Maleke, C., Konofagou, E.E.: Harmonic Motion Imaging for Focused Ultrasound (HMIFU): A Fully Integrated Technique for Sonification and Monitoring of Thermal Ablation in Tissues. Phys Med Biol, 53(6), pp. 1773–93, 2008.
[2] Seo, C.H., Shi, Y., Huang, S.W., Kim, K., O'Donnell, M.: Thermal Strain Imaging: A Review. Interface Focus, 1(4), pp. 649–664, 2011.

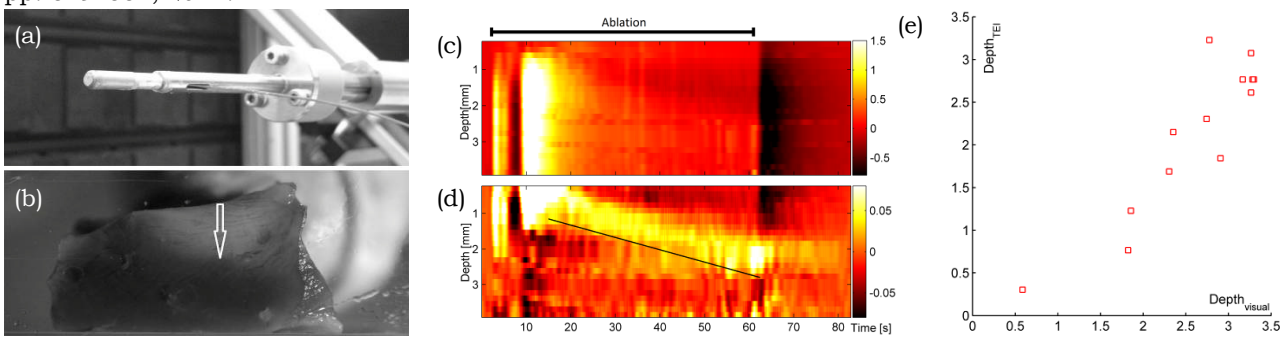

Figure 1: (a) Catheter tip with integrated single–element ultrasound probe; (b) Coagulated tissue sample; (c) Displacements and (d) corresponding instantaneous strains during the ablation procedure. The black line shows the progression of the high–strain band as the lesion grows; (e) TEI–estimated data and the visually observed lesion depths.

* *indicates Presenter*

037 **A NOVEL 3D STRAIN RECONSTRUCTION AND EJECTION FRACTION ESTIMATION TECHNIQUE: *IN VIVO* FEASIBILITY.**

Stanley J Okrasinski[1], Julien L Grondin[1], and Elisa E Konofagou[1,2].*
[1]Biomedical Engineering Department, [2]Radiology Department, Columbia University, 630 W 168th St, P&S 19–405, New York, NY, USA.

Background: Myocardial Elastography (ME) is a high–precision, ultrasound–based 2D imaging modality for estimating myocardial deformation and has been previously validated against sonomicrometry to provide accurate identification of ischemia at various levels of stenosis in humans and canines. While ME is capable of providing information in 2D imaging planes, a more complete analysis of cardiac deformation would consider strain across the whole myocardium. ME requires a technique to reconstruct 2D views into a 3D model.

Aims: In this study, a new image reconstruction technique was developed and applied in an *in–vivo* canine model during both normal and ischemic function to reconstruct a 3D radial strain volume from these 2D radial strain images during a single heartbeat. The volume was also used to automatically estimate the ejection fraction (EF) and characterize the output of the left ventricle.

Methods: In a study approved by the Columbia University Institutional Animal Care and Use Committee, three male mongrel dogs were anesthetized, and the chest was opened by lateral thoracotomy. A snare was placed around the left anterior descending artery (LAD). Images in the standard apical, mid, and basal short axis and apical 2 and 4 chamber views were acquired using diverging beams during sinus rhythm with a Verasonics system (Verasonics, Redmond, WA) and a phased array probe (ATL P4–2) with 64 elements. Images were acquired during both normal and ischemic function, i.e., with and without full LAD ligation. Images were acquired at 2000fps during 2s, followed immediately by the acquisition of a 128 line, 30fps, B–mode during 1.5s. The electrocardiogram (ECG) was acquired simultaneously. RF signals were reconstructed from the element data in a pixel–wise fashion. Inter–frame axial and lateral displacements were estimated at a 500Hz motion–estimation rate and at a 2000Hz motion–sampling rate using normalized cross–correlation (window size: 4.6mm, 90% overlap) and were then accumulated during systole. Axial and lateral Lagrangian strains were estimated using a least–squares estimator (window size: 10.7mm), and then converted to radial and circumferential strains after a centroid was selected. 2D masks of the LV in each imaging plane were manually selected. The 2D masks were registered in MATLAB using anatomical landmarks. A 3D mesh of the LV structure was formed by applying cubic hermite interpolation over the registered masks. A 3D mesh was reconstructed over each frame during systole, and EF was estimated using the meshes at end–diastole and end–systole. Also, EF was estimated from the 2D B–Mode images using the modified Simpson's rule, an established clinical technique, for comparison. In addition, radial strain was interpolated over the 3D mesh using cubic hermite interpolation.

Results: The EF, as estimated from the 3D meshes, was 72±10% and 43±15% in the normal and ischemic cases, while the EF, estimated from the 2D images using the modified Simpson's rule was 68±10% and 50±15% in the normal and ischemic cases. When the reconstruction was applied on the strains estimated from the normal case, radial thickening was observed over the left ventricle, indicating normal function (Figure 1), while in the ischemic case, negative strains were observed in the territory perfused by the LAD.

Conclusions: In this study, 3D meshes were used to automatically estimate EF during both normal and ischemic function and compared against more conventional methods. The estimated EFs from the novel 3D reconstruction technique were similar to the estimates from the modified Simpson's rule, while simultaneously providing a 3D model of the specific anatomy. In addition, 3D reconstructed strains simultaneously depicted uniform radial strain in the normal case, and a region of negative radial strain in the occluded artery's territory of perfusion in the ischemic case. As a result, this technique could be used to assess the output of the left ventricle and present myocardial strains at the same time, in a more intuitive 3D view.

Acknowledgements: This study was funded in part by NIH R01EB006042 and R01HL094410

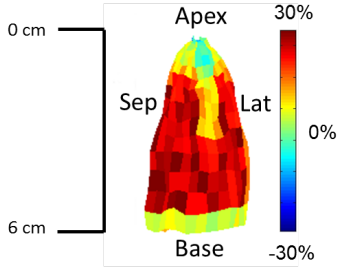

Figure 1: Reconstructed radial strain in the left ventricle of a canine heart during normal function.

026 **EFFECTS OF THE SAC GEOMETRY AND MODULUS CONTRAST ON THE REGIONAL PULSE WAVE PROPAGATION ALONG THE ANEURYSMAL ARTERIAL WALL *IN SILICO*.**

D Shahmirzadi[1], I Jourard[1], EE Konofagou[1].*
[1]Columbia University, PS 19–405, 630 West 168th Street, New York, NY, 10032, USA.

Background: Arterial stiffness has been widely known as an independent indicator of cardiovascular diseases such as aortic aneurysm [1]. Pulse wave imaging (PWI) is a noninvasive method for regional visualization and estimation of pulse wave velocity (PWV) [2,3], which can be related to the wall stiffness through the Moens–Korteweg equation. Fluid–solid interaction (FSI) simulations have previously been shown to serve as an efficient and reliable tool to study pulse propagation in arterial models in healthy [4] and diseased conditions [5,6], where obtaining specimens in vivo could be challenging. FSI simulation results of pulse wave propagation along abdominal aortic aneurysm (AAA) geometry are presented here.

Aims: To identify the effects of sac geometry and modulus contrast on the regional pulse wave propagation along the simulated model of human idealized straight and AAA geometries.

Methods: The Coupled Eulerian–Lagrangian (CEL) explicit solver in Abaqus 6.11–1 (Simulia, RI, USA) was used to perform the fully coupled FSI simulations of fluid–induced wall pulsatile motions along aortas with idealized straight and Eurostar AAA human 3D geometries. Rubber–like hyperelastic wall material parameters were obtained by fitting a 3rd order Ogden model to the tensile and compressive mechanical testing data from similar aortic phantoms. For simulations with stiffer and softer walls, assuming a similar hyperelastic regimen of the material behavior, the same experimental measurements obtained previously were mathematically scaled up (or down), respectively, for hyperelastic parametric modeling. The Lagrangian boundary conditions (BCs) were applied by fixing all 6 DOFs on both ends of the tube. On the Eulerian domain, a free inflow BC was applied on the tube inlet, and a non–reflecting and zero pressure were applied on the tube outlet. A sinusoidal velocity with magnitude 3.63m/s and frequency 5.4Hz was applied as initial condition (IC) on the tube inlet. The vertical component of the wall displacement along the lower wall was extracted, and plotted vs time to obtain the spatio–temporal maps.

Results: Figure 1 illustrates the spatio–temporal maps of the lower wall displacement on the aortas with straight and AAA geometries with different sac modulus. Compared to the results on the straight geometry, where uniform propagation of multiple forward and reflected waves are seen, AAA geometry results show the wave propagation being associated with multiple focal reflections at the sac zone (Figure 1B–D). The post–sac PWVs were thus found to be higher than those in the straight geometry and it decreases as the sac modulus increases. Reflection waves were found to have lower PWVs in particular on the highly reflected waves within the sac zone.

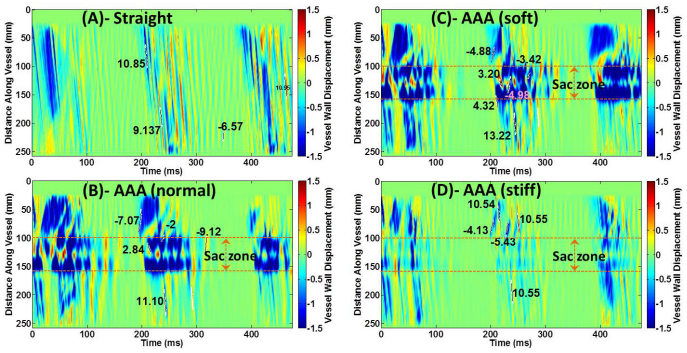

Figure 1: Spatio–temporal maps of the wall displacement aortas with: (A) Straight geometry; (B) AAA geometry with same stiffness sac as the rest of the aortic wall; (C) AAA geometry with 1.5 times softer sac; (D) AAA geometry with 3 times stiffer sac.

Conclusions: The arterial pulse wave simulation results indicated that the regional pulse wave propagation patterns and PWVs, obtained from the spatio–temporal maps of the wall displacement, contain qualitative and quantitative information that can collectively be used to detect and quantify an aneurysmal sac as well as its change in wall modulus. In particular, the saccular region was identified on the spatio–temporal maps as a zone of higher displacements, with diminishing sensitivity with increasing sac modulus. Focal reflected waves, with lower PWV, were also obtained at the sac region. The results obtained here provide additional insights into the effects of AAA geometry and stiffness on the pulse wave propagation that can be used as complementary information for PWI and diagnosis *in vivo*.

Acknowledgements: Funded in part by NIH R01–HL098830; Dr. T. McGloughlin from University of Limerick, Ireland.

References:

[1] Laurent S, et al.: Eur Heart J, 27, pp. 2588–605, 2006.
[2] Fujikura K, et al.: Ult Imag, 29(3), pp. 137–54, 2007.
[3] Vappou J, et al.: Am J Hyp, 23(4), pp. 393–98, 2010.
[4] Shahmirzadi D, et al.: ITEC 2011, Texas, USA, 2011.
[5] Shahmirzadi D, et al.: Artery Res, 6(3), pp. 114–23, 2012.
[6] Shahmirzadi D, et al.: ITEC 2012, Deauville, France, 2012.

* *indicates Presenter*

041 **PIECE–WISE PULSE WAVE VELOCITY MAPPING IN MURINE ATHEROSCLEROTIC AND ANEURYSMAL AORTAS USING PULSE WAVE IMAGING (PWI) *IN VIVO*.**

Iason Z. Apostolakis[1], Sacha D. Nandlall[1], Elisa E. Konofagou[1].*
[1]Columbia University, PS 19–405, 630 West 168th Street, New York, NY, 10032, USA.

Background: Several pathological conditions, such as myocardial infarction, stroke and abdominal aortic aneurysm (AAA), have been shown to be atherosclerosis–related and are some of the major causes of overall morbidity and mortality in Western populations [1]. Atherosclerosis causes the composition of the arterial wall to change compared to its normal state, thereby making the wall tissue less homogeneous [2]. Furthermore, AAAs are known to alter the mechanical properties of the tissue [3]. Therefore, the localized assessment of the local stiffness in different regions of major blood vessels remains of critical importance in the monitoring of the disease. Pulse Wave Imaging (PWI) is a noninvasive technique for tracking the propagation of pulse waves along the wall of the aorta at high spatial and temporal resolutions [3,4]. The velocity of these waves is a well established marker of wall stiffness. Until now only a global pulse wave velocity (PWV) value was obtained for the entire arterial segment imaged.

Aims: The primary aim of this study was to enhance the performance of the PWI technique in order to map the localized stiffness of the arterial wall *in vivo*. These maps may then be used to detect and monitor abnormalities such as atherosclerosis and aneurysms.

Methods: Six–month–old male ApoE$^{-/-}$ mice (n=7; Jackson Laboratory, Bar Harbor, ME) were fed a Western–type diet (Research Diets, New Brunswick, NJ). The suprarenal sections of the abdominal aortas were scanned every 14 days using a Vevo 770 imager (VisualSonics, Toronto, ON, Canada) with axial and lateral resolutions of 55 and 115µm, respectively. Pulse wave propagation was tracked at an effective frame rate of 8kHz using retrospective ECG gating. The displacements induced by the pulse waves were estimated by performing fast 1D cross–correlation on the radiofrequency signals [5]. The same scanning procedure was repeated in the aortas of mice with AAAs using an Angiotensin–II model (n=4). The anterior wall velocities were depicted over time to generate spatio–temporal profiles of the pulse–propagation (Figure 1). The local PWVs were calculated by performing linear regression on the 50% upstroke points of the displacement profiles inside 50% overlapping segments of the imaged arterial wall.

Results: Figure 1 shows three spatio–temporal maps from a normal, an aneurysmal and an atherosclerotic aorta. Also shown on each map are the local piece–wise PWVs and the global PWV, calculated by linear regression over all of the 50% upstroke points. While there is little difference between the global PWV and r^2 of the normal and the aneurysmal cases, the local PWVs increase within the aneurysmal sac, indicating higher stiffness in this region. Furthermore, in the atherosclerotic aorta, after 20 weeks of high fat diet there is an increase in the mean of the local PWVs across all the segments (p=0.01), as well as a decrease in the corresponding mean of r^2 values (p<0.01).

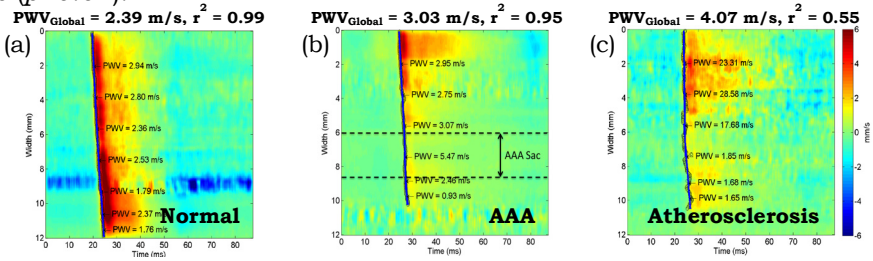

Figure 1: Local PWV maps for a normal (a), aneurysmal (b), and atherosclerotic (c) aorta.

Conclusions: This study demonstrates that the performance of the PWI technique could be enhanced by using piece–wise PWVs, instead of global PWV, in order to obtain local information on the pulse wave propagation and ultimately construct stiffness maps of normal, aneurysmal and atherosclerotic aortas in mice *in vivo*. Based on these maps, aneurysms and the early onset of atherosclerotic plaque could be detected and localized. In particular, the ApoE$^{-/-}$ mice were shown to have significantly higher PWVs as the disease evolved over time.

Acknowledgements: This work was supported in part by R01–HL098830. The work of I. Z. Apostolakis was supported in part by a scholarship from the General Michael Arnaoutis Foundation.

References:

[1] D. Lloyd–Jones, et al.: Circ, 121, pp. 948–954, 2010.
[2] M. Mercuri et al.: Springer, 1997.
[3] J. Luo et al.: IEEE Trans Med Imag, 28(4), pp. 477–486, 2009.
[4] K. Fujikura et al.: Ultra Imag, 29, pp. 137–154, 2007.
[5] J. Luo et al.: IEEE Trans Ultras Ferro Freq Ctrl, 57, pp. 1347–1357, 2010.

* *indicates Presenter*

050 **PULSE WAVE IMAGING OF STENOTIC CAROTID ARTERIES *IN VIVO* – A FEASIBILITY STUDY.**

RX Li[1], P Narayanan[1], JK Salomon[1], JF McKinsey[1], EE Konofagou[1].*
[1]Columbia University, 630 West 168th St., Physicians & Surgeons 19–418, New York, NY, USA.

Background: The capability of Pulse Wave Imaging (PWI) [1,2] to spatio–temporally map the regional arterial wall motion and provide image–guided measurements of the local pulse wave velocity (PWV) has been demonstrated in normal carotid arteries *in vivo* [2]. While the pulse wave propagation is expected to remain uniform over a short arterial segment in healthy subjects, the presence of atherosclerotic plaques may alter the pulse wave behavior [2]. Due to its capability of acquiring multiple wall motion waveforms along an imaged arterial segment over a single cardiac cycle *in vivo*, PWI may serve as a valuable tool for detecting and characterizing carotid plaques.

Aims: The objective of this study was to assess the feasibility of PWI in patients with carotid artery stenosis due to atherosclerotic plaques. Compared to normal carotid arteries, we hypothesize that the uniformity of the pulse wave propagation will be reduced around stenotic regions.

Methods: RF signals were acquired from stenotic carotid arteries of six (N=6) patients (mean age 74.4±7.14 years) using a SonixTouch system (Ultrasonix Medical Corp., Burnaby, Canada) with a 10MHz linear array transducer in a fixed 38mm width x 35mm depth imaging plane. A fast, normalized 1D cross–correlation–based motion estimation method [3] was used on the RF signals to compute the incremental, axial pulse wave–induced wall velocities. The temporal anterior wall velocities were used to generate a spatio–temporal map (Figure 1d) consisting of the wall velocity waveform at each beam location. The PWV and pulse wave propagation uniformity were estimated from the slope and correlation coefficient r^2, respectively, of the linear regression on the spatio–temporal variation of the 50% upstroke of each waveform. For clear visualization of the pulse wave, the posterior and anterior wall velocities estimated from RF data acquired using 32 beam lines (457 fps) was overlaid onto the B–mode image reconstructed from RF data acquired using 256 beam lines (57 fps).

Results: The PWV and r^2 (both averaged over 10 cardiac cycles) measured in all stenotic patients were 2.30±0.98m/s and 0.71±0.16, respectively. Compared to the measurements from the carotid arteries of young, healthy subjects [1], the PWV and r^2 in the older, stenotic subjects were both significantly lower ($p<0.001$). Two recurring phenomena were observed among the cases included in this study. In the case shown in Figure 1, the pulse wave appears to "skip" over the plaque region (white contour in the PWI frame sequence). In other cases, two apparent wall velocity waves originated from the plaque region and subsequently spread out in either direction.

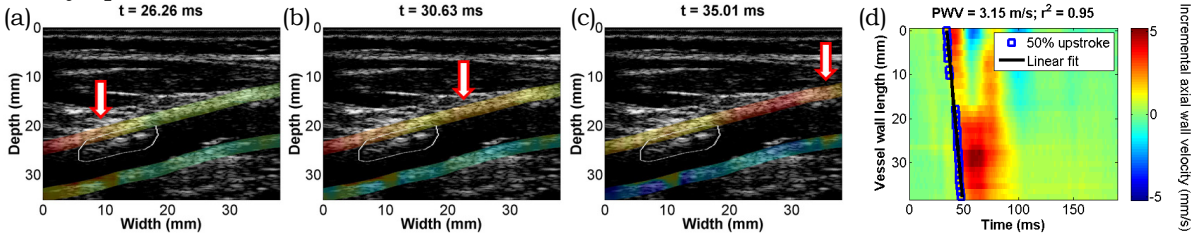

Figure 1: Consecutive PWI frames (a–c) showing the pulse wave propagating along the anterior wall (red/white arrows), and the corresponding 3D spatio–temporal map of the wall velocity waveforms (d). From both the sequence the PWI frames and the spatio–temporal map, the pulse wave appears to "skip" the plaque region (white contour in the PWI frames).

Conclusions: The potential of PWI to differentiate between normal and stenotic carotid arteries both quantitatively (based on the PWV and r^2) and qualitatively (based on the PWI frames and spatio–temporal map) was hereby shown. Future studies will be aimed at increasing the sample size to categorize individual cases based on plaque size and percentage of stenosis.

Acknowledgements: NIH R01–HL098830.

References:

[1] Li RX, Luo J, Balaram SK, Chaudhry FA, Shahmirzadi D, Konofagou EE: Pulse Wave Imaging in Normal, Hypertensive, and Aneurysmal Human Aortas *In Vivo*: A Feasibility Study. Phys Med Biol, 58(13), pp. 4569–62., 2013.
[2] Luo J, Li RX, Konofagou EE: Pulse Wave Imaging of the Human Carotid Artery: An *In Vivo* Feasibility Study. IEEE tUFFC, 59(1), pp. 174–81,. 2012.
[3] Ino–Oka E et al.: Evaluation of Carotid Atherosclerosis from the Perspective of Blood Flow Reflection. Clin Exp Hypertens, 31(3), pp. 188–200, 2009.
[4] Luo J and Konofagou EE: A Fast Normalized Cross–Correlation Calculation Method for Motion Estimation. IEEE Trans Ultrason Ferroelectr Freq Control, 57(6), pp. 1347–57, 2010.

* *indicates Presenter*

084 **ITEC AT 12: AGAINST ALL ODDS.**

Jonathan Ophir[1], Kevin J. Parker[2], Karen Ophir[3].*
[1]Ultrasonics and Elastographics Lab, Diagnostic and Interventional Imaging Department, University of Texas Medical School, Houston, TX 77030, USA; [2]University of Rochester, Rochester, NY, USA; [3]ITEC, Austin, TX 78734, USA.

Background: It has been known for millennia that the elastic properties of tissues are related to disease. These early observations were confirmed by palpation which persisted as standard medical procedures. In the years and even decades that preceded the inauguration of the International Tissue Elasticity Conference (ITEC) in 2002, a few groups were exploring the shear elastic properties of tissues and devising various methods to estimate them. The work of these groups was mostly considered avant–garde in the imaging milieu and was thus allotted minimal 'shelf–space' in the professional journals and conferences. It appeared to us that in spite of the great potential exhibited in the scientific reports, progress continued to be frustratingly sluggish. We hypothesized that by providing a well–focused forum for the exchange of ideas we could accelerate the progress in this area and attract new investigators as well. Dr. Kaisar Alam who did his PhD work in Kevin Parker's lab was doing his postdoctoral work in Jonathan Ophir's lab suggested that we collaborate to create a new conference. In an unrelated visit to the University of Rochester, we discussed this possibility and agreed to work toward this goal.

Aims: The general aims of the Conference were elucidated in the Proceedings published on the occasion of the first meeting in Niagara Falls, Canada in October 2002. Additionally, we have endeavored to adhere to the following principles:

1. The peer–reviewed Conference will be open to basic science and medical investigators in the area of tissue elasticity;
2. There will be no parallel sessions, and meals and breaks will be shared to maximize time for discussion;
3. Emphasis will be placed on student and international participation;
4. Invited special topic tutorial will be given by experts in their respective areas; and
5. Written and oral feedback will be encouraged.

Methods: The cost of staff support to run the Conference turned out to be prohibitive, and so did the financial upfront guarantees demanded by the hotel venues. NIH turned our R13 grant down as well. After some initial difficulties, we were able to rely on many volunteers and on modest industrial support.

Results: The Conference has been successful in defining and leading the new field of elasticity imaging, and many of the pioneering innovations in this field were first discussed there. The Conference is now in its 12th year which coincides with the transfer of organizational leadership to Dr. JC Bamber of the ICR.

Conclusions: The founding organizers are confident in Dr. Bamber's new leadership and his vision for the future of the Conference. We look forward to a continuing expansion of the field and the important role of ITEC in furthering advances.

Acknowledgements: The Conference is indebted to the many volunteers and delegates who have made great contributions to the ongoing success of the Conference.

References:

[1] Proceedings First ITEC, 2002.

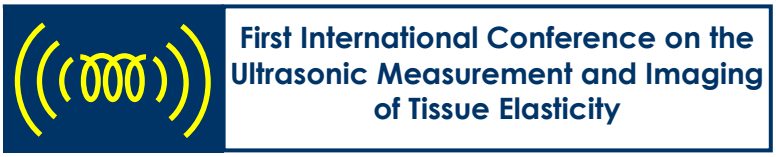

013 **ROBUST SHEAR WAVE VELOCITY RECONSTRUCTION FROM MULTI–RESOLUTION TIME–OF–FLIGHT ESTIMATES.**

PJ Hollender[1], NB Bottenus[1], GE Trahey[1].*
[1]Duke University, 136 Hudson Hall, Box 90281, Durham, NC, USA.

Background: The elasticity of soft tissue can be estimated from the transverse propagation velocity of mechanical shear waves in the tissue. Acoustic Radiation Force (ARF) imaging uses ultrasound both to generate transient shear waves within the tissue of interest and to track the transverse wave propagation. The local shear wave velocity is estimated from the time–of–flight differences between two or more locations in the tissue [1]. Within some field of view (FOV) through which propagation is tracked, images can be formed. The choice of spatial kernel for estimating local velocity has a direct influence on the lateral resolution of the imaging system, with small kernels yielding noisy, high resolution images and large kernels yielding smooth, low resolution images.

Aims: This work presents a generalized framework for the lateral resolution of shear wave imaging, and introduces a multi–resolution method for generating shear wave images.

Methods: Finite Element Method (FEM) simulations of ARF excitations were performed in LS–DYNA (LSTC, Livermore, CA). Excitations were simulated every 0.25mm laterally over a 1cm FOV, with inclusions simulated with elasticity higher, the same as, and lower than the background. FIELD II [2] was used to simulate ultrasonic tracking of the simulated tissue. Progressive normalized cross–correlation was used to estimate tissue axial displacement. The time–of–flight between each pair of tracking locations x_R was computed via cross–correlation of the slow–time axial displacement signals for each pair of excitation locations x_S, from both the ultrasonically–tracked motion estimates and the directly simulated motion (with and without speckle). The time–of–flight was similarly estimated between signals at the same tracking location x_R for different excitation locations x_S, which has been shown to compensate for speckle bias [3]. Using the distance between x_R (or x_S) as the resolution level of each estimate, all estimates were projected onto a consistent set of high resolution estimates by solving the linear system of equations formed by the data. The least–squares solution was computed by classic matrix pseudo–inversion. Regularization of the solution and weighting of estimates were introduced to the estimator to provide additional robustness.

Results: Images formed with high resolution time–of–flight estimates showed good edge definition in the pure simulated data, but were noisy, especially around inclusion boundaries. Images formed with low resolution time–of–flight estimates were smoother but had decreased border definition. The multi–resolution images showed both low noise and good resolution in pure simulations. In the tracked data, the effect of speckle was not reduced for images formed with fixed x_S, but images with a fixed x_R are not subject to speckle bias, resulting in the best images via multi–resolution estimation.

Conclusions: This method of combining multi–resolution time–of–flight estimates uses both the noisy, high resolution estimates and the smooth, low resolution estimates to form accurate, high resolution shear wave images. In ultrasonically tracked data, the effect of speckle bias remains a limiting factor on resolution for fixed–excitation–location images but is eliminated in fixed–track–location images.

Acknowledgements: NIH Medical Imaging Training Grant EB001040, NIH R37HL096023 and NIH R01EB01248.

References:

[1] Sarvazyan, A.P., Rudenko, O.V., Swanson, S.D., Fowlkes, J.B., Emelianov, S.Y.: Shear Wave Elasticity Imaging: A New Ultrasonic Technology of Medical Diagnostics. Ultrasound in Med & Biol, 24(9), pp. 1419–1435, 1998.
[2] Jensen, J.A: Field: A Program for Simulating Ultrasound Systems. Presented at the 10th Nordic–Baltic Conference on Biomedical Imaging, Pub in Med & Biol Eng, & Comp, Vol 34, Sup 1, Part 1, pp. 351–353, 1996.
[3] Elegbe, E.C., McAleavey, S.A.: Single Tracking Location Methods Suppress Speckle Noise in Shear Wave Velocity Estimation. Ultrasonic Imaging, 35(2), pp. 109–125, 2013.

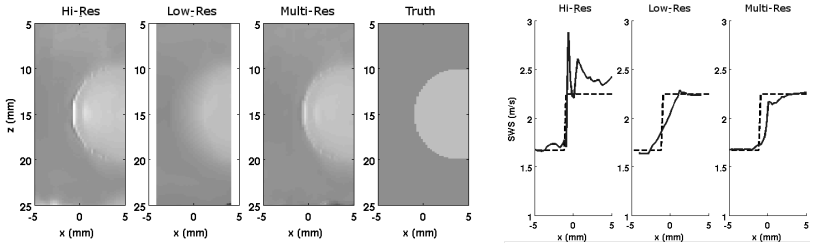

Figure 1: Images and profiles of shear wave velocity images, reconstructed using high resolution estimates, low resolution estimates, and the multi–resolution method. The multi–resolution image is sharper than the low resolution image, but without the edge effects and noise of the high resolution image.

* *indicates Presenter*

058 **COMPARISON OF MR ELASTOGRAPHY INVERSION TECHNIQUES USING *EX–VIVO* TISSUE AND AN INDENTATION SCAN.**

M Honarvar[1], RS Sahebjavaher[1], R Rohling[1], SE Salcudean[1].*
[1]The University of British Columbia, Vancouver, CANADA.

Background: Different techniques have been used in MR elastography (MRE) to create elasticity maps from measured displacement data. While these techniques have been tested and verified using simulations and tissue mimicking phantoms, they still may contain artifacts due to the simplifying assumptions they employ. Previous studies have measured the elasticity independently by methods such as indentation tests and compared the results with elastography results, such as strain images [1] and ARFI images [2]. Other groups have compared absolute elasticity values with indentation results at specific points but not over an entire region. In this study, we attempt to use indentation results to evaluate the elasticity patterns obtained when applying different inversion techniques to *ex–vivo* tissue. We were motivated to do this study by the large differences in elasticity images of *ex–vivo* prostate specimens that we have obtained when using different inversion techniques.

Aims: To compare *ex–vivo* MRE tissue images obtained using different inversion techniques and to evaluate the accuracy of the results using indentation scans of thin tissue slices following the MRE test.

Methods: This study was carried out on a bovine kidney sample with lesions induced by injections of 10% formalin and subsequently kept in 5% formalin for four hours. The sample was embedded in agar gelatin, and the MRE data acquisition was performed using a motion sensitive spin–echo method. Three inversion techniques were used for elasticity reconstruction: 1. c–FEM with sparsity regularization [3], 2. LFE [4] and 3. Curl–based direct inversion (DI) [5]. Following MRE, the sample was sliced into 3mm thick slices and an indentation scan was performed using a custom indenter (Figure 1). The slope of the force–displacement curve at the end of the unloading path was used to estimate the elasticity. In order to further investigate the effects of tissue inhomogeneity, which may explain the wide range of results we obtained, we also created a gelatin phantom with irregular inclusions injected into the background (Figure 3, showing colored inclusions in white substrate). The elasticity maps were then calculated using the three above–mentioned methods for the phantom and for the kidney tissue.

Results: Figure 2 shows the results for the kidney sample. Note that all of the methods detect the kidney sample embedded in the gelatin background, but the c–FEM results show more clearly the boundaries which, due to direct exposure to formalin, exhibit a greater degree of hardening, and its results resemble more closely the indentation results. LFE leads to smooth boundaries and reduced contrast of the softer interior of the kidney. In the DI results, the homogeneity assumption leads to artifacts around boundaries. Similar results can be seen for the gelatin phantom (Figure 3). The c–FEM results best match the shapes of the inclusions which are also detectable in the T2 images. The effect of the local homogeneity assumption is less visible in cases with larger inclusions (Figure 3, second column) but for smaller or narrower inclusions the resulting artifacts may lead to erroneous image interpretation.

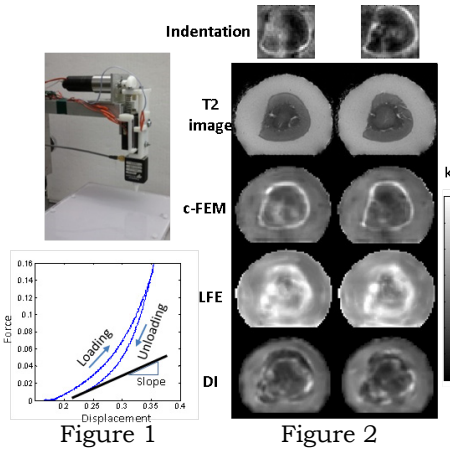

Figure 1

Figure 2

Figure 3

Conclusions: This study shows the importance of the local homogeneity assumption on the results of tissue elasticity reconstructions. These initial tests suggest that the c–FEM method has the potential to improve upon state–of–the–art methods in terms of accuracy and resolution. Further tests are needed.

Acknowledgements: This research was supported by Natural Sciences and Engineering Research Council (NSERC).

References:

[1] S. Srinivasan, et.al.: Ultrasound Med. Biol., 30, p. 329, 2004.
[2] L. Zhai, et.al.: Ultrason. Imaging, 30, p. 95, 2008.
[3] M Honarvar, et.al., Proc. 11th ITEC, France, 2012.
[4] A. Manduca, et.al.: Image Processing, International Conference, 3, p. 527, 1996.
[5] R. Sinkus, et.al.: Magn. Reson. Med., 53, p. 372, 2005.

054 **IMPROVING FEM INVERSE PROBLEM RECONSTRUCTIONS BY INCORPORATING ALL DISPLACEMENT OBSERVATIONS USING ELEMENT SHAPE FUNCTION INTERPOLATIONS.**

Orçun Göksel, Gábor Székely.*
Computer Vision Laboratory, ETH, Zurich, SWITZERLAND.

Background: Viscoelastic parameter reconstruction using the inverse problem (IP) formulation of the finite element method (FEM) involves finding the FEM parameterization that best fits the FEM simulated displacements u to the displacements d^* observed in tissue at the FEM node locations. Numerous techniques in the literature [1] use different forms of excitations (transient wave, harmonic, etc.), FEM parametrizations (nonlinear, dynamic, etc.), constraints (volume preservation, pressure, boundaries, etc.), and regularizations. Nonetheless, most of those commonly involve the obvious cost definition of $|u - d^*|^p$ for fitting their model to observations. Often the displacements d in tissue can be tracked with considerably higher resolution than the FEM nodal grid, due to computational constraints on practical FEM sizes. Then, either a subset of d, for which FEM nodes coincide with tracked displacement samples, is used as d^*, which leads to discarding some observations; or d^* is interpolated in d (possibly with a large kernel to incorporate all data), which perturbs observations by disregarding continuum–mechanics.

Aims: To improve parameter reconstructions, especially with coarse meshes, by leveraging information from all the observed displacements (d) using the FEM framework conformant to continuum–mechanics.

Methods: We reformulate the model fitting over the grid of observed displacements, at which we use the FEM element shape functions to interpolate the simulated deformation. Let the FEM simulated displacements at the tracked locations be $u^*=Lu$ where each row of a sparse matrix L contains the element shape function interpolation weights for one tracked displacement, with its nonzero columns corresponding to the nodes of the element containing the tracked displacement. Then, we solve the IP optimization problem with the objective $|Lu - d|^p$ for reconstructing the model parameters.

Results: A cancerous breast tumor marked in Figure 1(a) was excited harmonically at 92Hz on tissue surface. Displacement phasors were constructed from axial displacements tracked at a spatial resolution of ~480um axially and ~400um laterally. The FEM IP implementation of [2] was used with the objective changed to $min(|Lu - d|^2)$. Young's modulus reconstructions using 9–node quadrilateral elements are presented in Figures 1(b–e) using the traditional (top) and the proposed (bottom) IP objectives at four mesh resolutions. Stiffer tumor is better delineated using our method, in particular at lower mesh resolutions.

Conclusions: The proposed formulation often leads to a larger equation system. Nonetheless, it takes into account all the observations in an FEM–compliant way, therefore yielding better reconstructions.

Acknowledgements: The presented *in–vivo* breast vibro–elastography data were used in this work by courtesy of Tim Salcudean and Hani Eskandari from University of British Columbia, Vancouver, BC, Canada.

References:

[1] M.M. Doyley: Model–Based Elastography: A Survey of Approaches to the Inverse Elasticity Problem. Physics in Medicine and Biology, 57(3), pp. R35–73, 2012.
[2] O. Goksel, H. Eskandari, and S.E. Salcudean: Mesh Adaptation for Improving Elasticity Reconstruction using the FEM Inverse Problem. IEEE Transactions on Medical Imaging, 32(2), pp. 408–418, 2013.

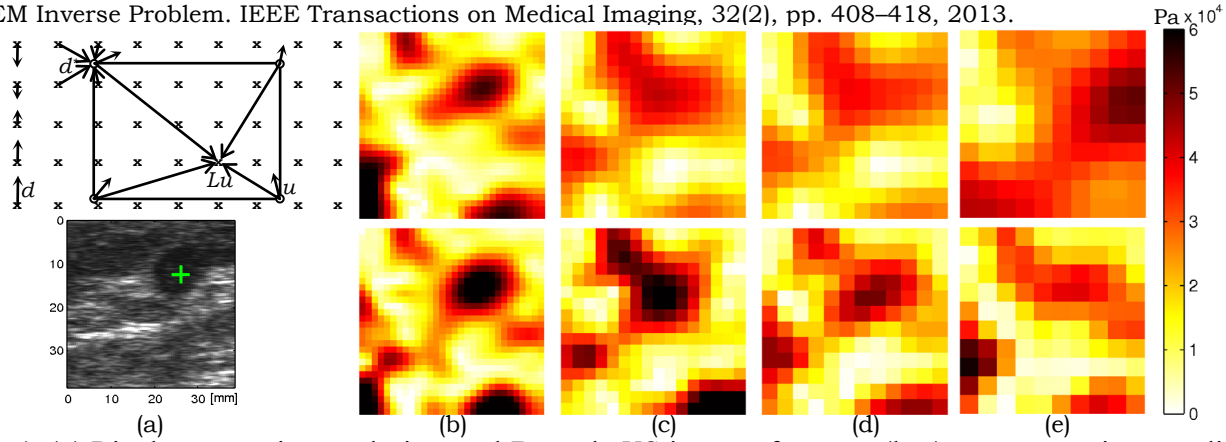

Figure 1: (a) Displacement interpolation and B–mode US image of tumor, (b–e) reconstructions at different mesh resolutions solved (top) with the conventional and (bottom) with the proposed objective function.

* *indicates Presenter*

033 ***IN VIVO* 3D BAYESIAN SHEAR WAVE SPEED RECONSTRUCTION OF THE PROSTATE.**

Stephen Rosenzweig[1], Ned C. Rouze[1], Brett Byram[1], Mark L. Palmeri[1], Thomas Polascik[2], Kathryn R. Nightingale[1].*
[1]Biomedical Engineering Department, Duke University, Durham, NC, USA; [2]Duke University Medical Center, Durham, NC, USA.

Background: Shear wave elasticity imaging (SWEI) has shown promise for visualizing both structure and pathology within the prostate [1]. Many current reconstruction techniques are based on time of flight algorithms, which assume a known direction of wave propagation and homogeneous, isotropic tissue within the reconstruction kernel. Violation of these assumptions can lead to image artifacts generated by reflected waves at structural boundaries [2,3].

Aims: The aim of this work is to utilize a maximum *a posteriori* (MAP) estimator for shear wave speed image reconstruction to reduce the noise and image artifacts in the presence of tissue heterogeneity.

Methods: The MAP estimator is comprised of two parts: the likelihood function, which is the same as least squares linear regression of the wave arrival times versus lateral position, and *a prior* distribution, which is a generalized Gaussian function [4]. The prior distribution provides a spatial continuity constraint for the image. ARFI and SWEI data were collected concurrently from a commercial (CIRS, Norfolk, VA) phantom as well as *in vivo* under an IRB–approved protocol utilizing a modified Siemens Acuson SC2000 ultrasound scanner and Acuson ER7B transducer (Mountain View, CA). The data were analyzed to compare performance of the MAP estimator SWEI reconstruction with the concurrently acquired ARFI data.

Results: Shown below are example ARFI, median filtered linear regression SWEI and MAP estimator reconstructed SWEI images of a phantom data set with a 10mm, 24kPa Young's modulus cylinder in a 8kPa background. The target contrast in the ARFI, linear regression SWEI and MAP SWEI images is 0.46, -0.32, and -0.26, respectively, and contrast to noise ratios are 2.8, -2.0, and -2.9, respectively. Additionally, a reflected wave artifact that appears as a soft region in the right side of the target in the linear regression SWEI image is removed by the use of the MAP estimator algorithm.

Conclusions: We have demonstrated the utility of the MAP estimator to reduce or remove reflected wave artifacts and increase the contrast to noise ratio of SWEI images. We will present the MAP estimator as applied to *in vivo* 3D prostate data.

Acknowledgements: This work has been supported by NIH grants EB001040, EB002132 and CA142824. We thank the Ultrasound Division at Siemens Medical Solutions, USA, Inc. for their technical and in–kind support.

References:

[1] Barr, R et al.: Ultrasound Quarterly, 28(1), pp. 13–20, 2012.
[2] Rouze, N et al.: IEEE UFFC, 59(8), pp. 1729–1740, 2012.
[3] Deffieux, T et al.: IEEE UFFC, 58(10), pp. 2032–2035, 2011.
[4] Bouman, C et al.: IEEE Image Processing, 2, (3), pp. 296–310, 1993.

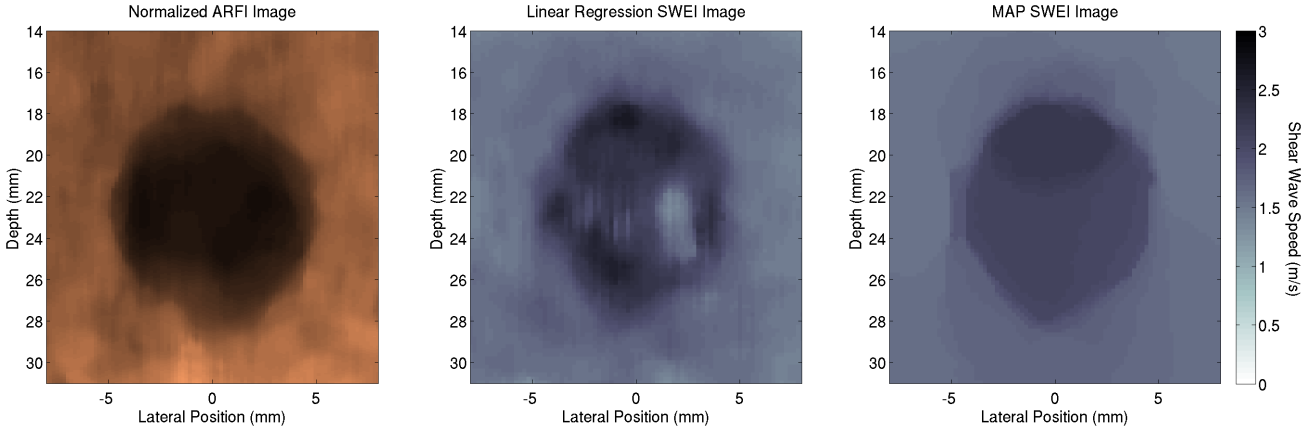

039 **SHEAR WAVE TRACKING WITH AN OPTO–ELASTOGRAPHY SYSTEM: SIMULATION AND EXPERIMENT.**

Sinan Li[1], Yi Cheng[1], Robert J Eckersley[2], Daniel S Elson[3] and Meng–Xing Tang[1].*
[1]Bioengineering Department, Imperial College London, South Kensington Campus, London, England, UK; [2]Biomedical Engineering Department, King's College London, London, England, UK; [3]Surgery and Cancer Department, Imperial College London, London, England, UK.

Background: Tissue elasticity is quantitatively related to shear wave speed. Previously we reported the first opto–elastography system that tracks shear wave propagation at cm depth in tissue mimicking phantoms (TMM) with a laser and a CCD [1]. As the optical wavelength is an order of magnitude smaller than that of ultrasound, using coherent optical detection is highly sensitive to sensing shear waves. Laser speckle patterns are formed when coherent light transverses TMM due to the light scattering. The speckle patterns are blurred when the optical scatterers are displaced, e.g. due to the shear wave propagation. The extent of the blurring can be evaluated by calculating the CCD speckle contrast, defined by the ratio of standard deviation and mean of pixel intensities, which in turn reflects the amplitude of the scatterer movement due to shear waves. We generate shear wave a distance away from laser and calculate CCD contrast values over time after the launch of shear waves. Then the time resolved CCD contrast curve characterizes the evolution of shear wave progression. The shear wave speed can be calculated with the time–of–flight estimation from the curve.

Aims: In this work, we describe the principles of the opto–elastograhy system and develop a simulation tool. We also observe the multiple shear wave interaction with the system in both simulation and experiments and demonstrate that such multiple shear waves can be used to further increase the sensitivity to shear wave sensing.

Methods: In the theoretical study, the interaction between shear wave and coherent light are studied. Light distributions in TMMs are predicted by the Monte Carlo modeling [2]. Shear wave displacements are calculated by the analytical solution given by [3]. We couple the shear wave field with optical field and predict the time–resolved CCD speckle contrast values. In experiment, TMMs (stiffness is controlled by agar concentration; optical scattering property is controlled by intralipid concentration) are exposed to a 532nm laser. The laser speckle patterns are received on a CCD camera with 1ms exposure length. Shear waves are generated by acoustic radiation force using 5MHz–1ms ultrasound bursts with a negative peak pressure of 4.3MPa. Firstly, we demonstrate the shear wave fronts imaged with both spatially and temporally resolved speckle contrast analysis at TMM surface. Then the shear wave is generated at 1.2cm depth, and the progression is tracked with the time–resolved speckle contrast analysis. To measure the local shear wave speed, shear waves are generated at two positions with a different distance (1–3mm) relative to the laser axis. The shear wave speed in the differential distance is estimated from the time shift in the time–resolved CCD contrast curves.

Results: The simulated optical tracking of shear waves matches well with the experimental observations. The shear wave speed measurement on the TMMs agrees well with previous studies. In addition, results suggest that the shear speed measured by dual shear wave signals has smaller standard deviation than individual shear waves.

Conclusions: We report the results of shear wave tracking by an opto–elastography system, including principles, simulation and experiments. The optical system has high sensitivity in shear wave tracking and the shear wave speed estimation agree well with the ultrasound elastography system. The system is limited by light penetration depth and may be applied to relatively shallow structures such as breast and lymph nodes (the penetration depth will be increased by changing to a near infrared laser). The additional optical information intrinsically generated by the system could offer a potential dual mode system with improved sensitivity and specificity for e.g. cancer detection.

Acknowledgements: We acknowledge the fruitful discussion and suggestion from Prof. David O Cosgrove and the funding from EPSRC (EP/H02316X/1).

References:

[1] Y. Cheng, R. Li, S. Li, R.J. Eckersley, D.S. Elson, and M.X. Tang: Ultrasound. Med. Biol., 38, p. 1637, 2012.
[2] L. Wang, S. L. Jacques, and L. Zheng: Comput. Meth. Prog. Bio., 47, p. 131, 1995.
[3] J. Bercoff, M. Tanter, and M. Fink: IEEE. T. Ultrason. Ferr., 51, p. 369, 2004.

* *indicates Presenter*

043 **USING 3D SPATIO–TEMPORAL FILTERS TO REMOVE OUT–OF–PLANE REFLECTION ARTIFACTS FROM SHEAR WAVE IMAGES.**

Samantha L Lipman[1], Ned C. Rouze[1], Michael H. Wang[1], Mark L. Palmeri[1], Kathryn R. Nightingale[1].*
[1]Duke University, 125 Hudson Hall, PO Box 90281, Durham, NC, 27708, USA.

Background: Time of flight methods used to reconstruct shear wave speeds are susceptible to artifacts from constructive interference of wave reflections at boundaries of differences in stiffness. Using a two–dimensional filter in the frequency domain can remove waves travelling in the opposing direction from the assumed direction of propagation[1]; however, this does not account for reflections from the out–of–plane dimension, which can have significant impact on shear wave reconstructions [2]. Using 2D matrix arrays, the elevation dimension can be visualized, and a spatio–temporal filter as described by Manduca et al. can be applied to isolate the shear wave moving in the assumed direction of propagation.

Aims: This work evaluates the feasibility of using a three dimensional directional filter to improve shear wave reconstructions in heterogeneous media, in particular the removal of soft center artifacts from spherical lesions [2,4].

Methods: Field II [5] and LS–DYNA were used to simulate an Acoustic Radiation Force Impulse (ARFI) excitation for Shear Wave Elasticity Imaging (SWEI) focused at 49mm with an F/2 configuration in a 5kPa uniform phantom with a 1cm, 20kPa spherical lesion located at a depth of 49mm, 15mm off–axis. In this 4D data, at the focal depth, a cosine–squared spatial filter and a quadrant–based temporal filter were applied in the frequency domain. The local shear wave speeds were reconstructed using the filtered displacement through time profiles over a lateral kernel of 2mm, using the time to peak slope (TTPS) algorithm to determine wave arrival time. A 2D quadrant–based temporal filter was applied in the frequency domain at an elevation position of 0mm for comparison.

Results: Shear wave speeds were successfully reconstructed from a right–propagating shear wave at all lateral locations after 2D or 3D filtering (Figure 1). Notice the large shear wave speed artifacts near the right lesion boundary that are present in the TTPS and 2D–filtered TTPS reconstructions, which are caused by shear wave reflections off of the lesion boundaries, both in the lateral and elevation dimensions. Application of the 3D filter significantly reduces these reflection–based reconstruction artifacts.

Conclusions: Constructive interference of both in– and out–of–plane reflected waves can cause soft appearing artifacts in stiff inclusions in shear wave speed images. By applying a three dimensional directional filter to ARFI induced displacement fields, these artifacts are removed and more accurate shear wave speed reconstructions can be performed in SWEI.

Acknowledgements: This work has been supported by NIH grants EB002132 and T32–EB001040. We thank the Ultrasound Division at Siemens Medical Solutions, USA, Inc. for their technical and in–kind support.

References:

[1] T. Deffieux, JL Gennison, J Bercoff, M. Tanter: On the Effects of Reflected Waves in Transient Shear Wave Elastography. IEEE transactions on Ultr., Ferro., and Freq. Control., Vol 58, No 10, Oct. 2011.
[2] N. Rouze, M Wang, M. Palmeri, K. Nightingale: Parameters Affecting the Resolution and Accuracy of 2–D Quantitative Shear Wave Images. IEEE transactions on Ultr., Ferro., and Freq. Control., Vol 59, No 8, Oct. 2012.
[3] A. Manduca, D. S. Lake, S. A. Kruse, and L. L. Ehman: Spatiotemporal Directional Filtering for Improved Inversion of MR Elastography Images. Med. Image Anal., Vol. 7, No. 4, pp. 465–473, Dec. 2003.
[4] RG Barr: Shear Wave Imaging of the Breast: Still on the Learning Curve. J Ultrasound Med, 31, pp. 347–350, 2012.
[5] J Arendt Jensen and Dk Lyngby: Field: A Program for Simulating Ultrasound Systems. Medical & Biological Engineering & Computing, 34(1), pp. 351–353, 1996.

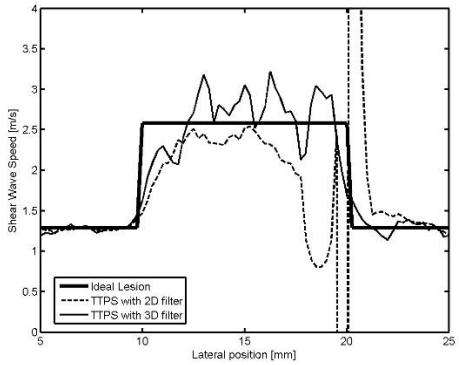

Figure 1: Reconstructed shear wave speeds in a 5kPa phantom with a 20kPa lesion after 2D and 3D directional filtering.

081 **THE WFUMB GUIDELINES AND RECOMMENDATIONS ON THE CLINICAL USE OF ULTRASOUND ELASTOGRAPHY–PART 1: BASIC PRINCIPLES AND TERMINOLOGY.**

Tsuyoshi Shiina[1], Kathryn R. Nightingale[2], Mark L. Palmeri[2], Timothy J. Hall[3], Jeffrey C. Bamber[4] et al. for the Guidelines Working Group.*

[1]Graduate School of Medicine, Kyoto University, Kyoto, JAPAN; [2]Biomedical Engineering Department, Duke University, Durham, NC, USA; [3]Medical Physics Department, University of Wisconsin–Madison, Madison, WI, USA; [4]Joint Department of Physics, Institute of Cancer Research and Royal Marsden NHS Foundation Trust, Sutton, Surrey, England, UK.

Background: Ultrasound–based elasticity imaging (elastography) has been developed as a modality which provides novel diagnostic information regarding differences in the elastic properties of soft tissues (e.g., elasticity and viscosity). Furthermore, the rapid dissemination of ultrasound elastography into the market place, the range of apparently different elasticity imaging methods available and the daunting research literature on the physics and medical applications of elastography has created a potentially confusing situation for those who may be considering using elastography.

Aims: The World Federation for Ultrasound in Medicine and Biology (WFUMB) felt the need to create a set of guidelines and recommendations on the clinical use of ultrasound elastography, with the goal of helping users to understand the different methods, and, to provide guidance as to the appropriate uses, applications, and limitations of each method. Specifically, the goal of Part 1 is to introduce the fundamental physics and associated terminology underlying elastography technologies.

Methods: A plan for publishing the guidelines for standardization and consensus on elastography methods was announced at the conference of WFUMB held in Wien in August 2012. The first meeting was held during the annual RSNA conference in 2013, and the chair and committee members (reviewers) for each section were decided. The guidelines consist of basic principles, and three clinical papers dealing with an existing important application of elastography (liver, breast and thyroid). Draft manuscripts of each section were prepared for the consensus meeting which was held in Washington DC in March, 2013. Here, extensive discussion and document modifications were undertaken to reach consensus on the manuscripts. Revised drafts were reviewed again at the AIUM elastography working group meeting in April, 2013. Final drafts were approved at WFUMB 2013 held at Sao Paulo in May. A similar set of guidelines has been published recently by the European Federation for Ultrasound in Medicine and Biology (EFSUMB) as two papers, i.e., the basic principles and technology [1] and the main clinical applications [2]. The main different points of basics between WFUMB and EFSUMB guidelines is that WFUMB guidelines included a questions and answers section, an extensive appendix, and a glossary of terms. However, terminology and descriptions, although not identical, are broadly compatible across the two sets of guidelines

Results: It is scheduled that the edited final papers will be submitted to UMB (Ultrasound in Medicine and Biology) for publishing this autumn.

Conclusions: We hope that the WFUMB Guidelines on ultrasound elastography will guide users of ultrasound elastography to comprehend the features of equipment and fully utilize them for appropriate diagnosis and therapy.

Acknowledgements: We acknowledge a great debt to Stephanie Hines, Executive Assistant and other staffs of WFUMB.

References:

[1] Bamber J, Cosgrove D, Dietrich CF, et al.: EFSUMB Guidelines and Recommendations on the Clinical Use of Ultrasound Elastography. Part 1: Basic Principles and Technology. Ultraschall in Med., 34(3), pp. 169–184, 2013.

[2] Cosgrove D, Piscaglia F, Bamber J, et al.: EFSUMB Guidelines and Recommendations on the Clinical Use of Ultrasound Elastography. Part 2: Clinical Applications. Ultraschall in Med., 34(3), pp. 238–253, 2013.

** indicates Presenter*

057 **THE INFLUENCE OF 3D VERSUS 2D TRACKING FOR THE ESTIMATION OF VOLUMETRIC–STRAIN RELAXATION TIME IN PATIENTS WITH CHRONIC LYMPHOEDEMA.**

Jérémie Fromageau[1], Peter Mortimer[2], Jeffrey C. Bamber[1].*

[1]The Institute of Cancer Research and Royal Marsden Hospital, 15 Cotswold Road, Sutton, Surrey, SM2 5NG, England, UK; [2]Dermatology Departments, St George's and Royal Marsden Hospitals and the University of London, London, England, UK.

Background: It is known that subjecting a poroelastic object to a sustained unidirectional compression results in a 3D internal volumetric strain that varies with position and time [1], which can be used to estimate tissue properties such as permeability, related to interstitial pressure and the capacity of fluid to diffuse through the elastic porous matrix. In previous work [2], we showed on phantoms that it was possible to estimate the volumetric strain using a 3D probe. In addition, pilot studies using 2D tracking have been performed on patients with lymphoedema, showing ability to distinguish between affected and unaffected limbs but producing noisy strain relaxation curves and highlighting the need for a 3D acquisition.

Aims: In the current work, we investigated clinically whether 3D acquisition, which allows both volumetric strain estimation and out of plane motion tracking, can provide a better poroelasticity estimation that the one observed in 2D.

Methods: Six patients aged from 59 to 78 with chronic unilateral lymphoedema were recruited. Clinical observations were made with an ultrasound scanner (DIASUS, Dynamic Imaging), using a 3D 7MHz probe. The probe itself was used as the compressor, its surface being considered flat on the size of the visualization volume. The probe was connected to a test instrument (Instron 3342), permitting control of its displacement and recording of the applied pressure, and holding the position for 15 minutes to follow fluid motion inside the arm. Both 3D and 2D RF data were recorded, each frame of the volume being recorded with 5 different steered angles to improve the lateral displacement, at the rate of 1 volume every 20s. The volumetric strain in the phantom was estimated from the RF echo signals using both an adaptive 2x2D cross–correlation, where the displacements were calculated on two perpendicular planes, and a full 3D cross–correlation method. Cumulative volumetric strain was observed as a function of time, from which a parametric image of the relaxation time based on a biphasic poroelastic model was created. The results were quantified in terms of quality of the volumetric strain and relaxation time images.

Results: Not surprisingly, the 3D acquisition improved the tracking in general. However the gain in tracking ability was challenged by the drop of image acquisition rate. The choices of the studied pathology and the observed organ were driven by the attempt to minimize rapid movement artifact. Nevertheless, with the current rate of one volume every 20s, these artifacts remained important. This was particularly apparent by the poor quality of the relaxation time parametric image obtained from the 2x2D elastography method. As a result the parametric relaxation time images obtained with 3D tracking were better estimated.

Conclusions: Estimation of the volumetric strain is necessary to estimate quantitatively permeability in poroelastography. While a fast version of the three strain components can be performed using 2D displacement tracking *in vitro*, the time consuming 3D tracking was shown to be more reliable *in vivo*, even in a case where the physiological motion is small. For the future, a compromise solution should be considered, improving the volume rate by altering the size of the region of visualization.

References:

[1] E. Konofagou, TP. Harrigan, J. Ophir, and TA. Krouskop: Poroelastography: Imaging the Poroelastic Properties of Tissues. Ultrasound in Medicine & Biology, 27 (10), pp 1387–1397, 2001.

[2] J. Fromageau, N. Bush, J. Bamber: Reliable Estimation of Permeability from the 4D Strain Distribution in Poroelastic Tissues. Proc. IEEE International Ultrasonics Symposium, 2012.

038 **REAL–TIME MONITORING OF HIFU ABLATION USING AXIAL STRAIN AND AXIAL–SHEAR STRAIN ELASTOGRAMS.**

R Xia[1] and AK Thittai[1].*
[1]The University of Texas Medical School, Houston, TX, USA.

Background: It has been shown previously that Axial Strain Elastograms (ASE) can help visualize sonographically–occult thermal lesions [1,2]. However, most of the studies involving High Intensity Focused Ultrasound (HIFU) induced thermal lesions were subjected to elastography imaging experiments separately at a later time after a lesion was formed.

Aims: In this work, we explore the feasibility of real–time monitoring of tissue elasticity variation during HIFU ablation and immediately thereafter, using quasi–static elastography. Further, in addition to the ASEs we also explore the use of simultaneously–acquired Axial Shear Strain Elastograms (ASSE) for HIFU lesion visualization.

Methods: The experiments were done on commercial porcine liver samples *in vitro*. The HIFU experiments were conducted at two applied acoustic power settings, 35W and 20W. The experimental setup allowed us to interrupt the HIFU–pulse momentarily at several different times during the treatment to perform elastographic compression and data acquisition. At the end of the experiments, the samples were cut along the imaging plane and photographed to compare the size and location of the formed lesion with that which was visualized on ASE and ASSE. Single lesion and multiple–lesion experiments were performed to assess the contribution of ASE and ASSE to lesion visualization and ablation monitoring tasks. The experimental setup is shown in Figure 1.

Results: In the lower power setting case, ASE and ASSE provide accurate lesion size in real–time monitoring (Figure 2). Lesion appearance in ASE and ASSE was affected by the cavitation bubbles produced in the high power setting case. The results further show that the cavitation bubbles influence the lesion appearance in ASE more than they do in ASSE. Both ASE and ASSE provided accurate size information after a waiting period that allowed for the cavitation bubbles to disappear. Figure 3 shows the elastograms before and after a 3rd HIFU ablation at the "thin" untreated gap.

Conclusions: *Ex–vivo* experiments were conducted at two acoustic power settings for HIFU, 35W and 20W. In both power settings, ASE and ASSE provided accurate location information during HIFU ablation. The results further showed that ASSE not only improved the lesion visualization and size measurement of a single lesion, but that it is also able to provide real–time feedback to visualize any untreated region between two lesions in high–contrast and guide additional ablation.

Acknowledgements: This work was supported in part by NIH grant R21–CA135580–01 and by the John S. Dunn foundation. The authors thank Dr. Jonathan Ophir for his valuable insights, comments and suggestions that improved the manuscript.

References:

[1] Kallel F, Stafford R J, Price R E, Righetti R, Ophir J and Hazle J D: The Feasibility of Elastographic Visualization of HIFU–Induced Thermal Lesions in Soft Tissues. Ultrasound Med Biol, 25, pp. 641–647, 1999.
[2] Righetti R, Kallel F, Stafford R J, Price R E, Krouskop T A, Hazle J D and Ophir J: Elastographic Characterization of HIFU–Induced Lesions in Canine Livers. Ultrasound Med Biol, 25, pp. 1099–1113, 1999.

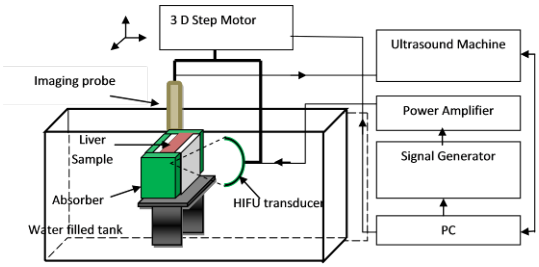

Figure 1: Experimental setup used to generate HIFU lesion and acquire the ultrasound RF raw data.

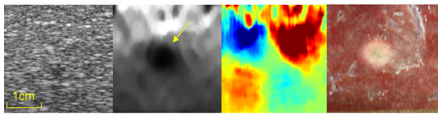

Figure 2: Images of the HIFU lesion obtained without a wait time at an acoustic power setting of 20W and a heating time of 80 seconds.

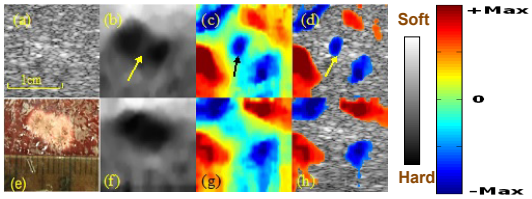

Figure 3: Images from multiple HIFU lesion experiments are shown: Top row: after two HIFU lesions are formed. Bottom row: after the completion of third ablation on the untreated gap. The corresponding photograph after 3rd ablation is shown in (e).

* *indicates Presenter*

042 **REAL–TIME 2–D VISCOELASTICITY IMAGING AND MONITORING OF HIFU TREATMENT USING HARMONIC MOTION IMAGING FOR FOCUSED ULTRASOUND (HMIFU).**

Gary Y. Hou[1], Jean Provost[1], Julien L. Grondin[1], Shutao Wang[1], Fabrice Marquet[1] and Elisa E. Konofagou[1,2].*

[1]Biomedical Engineering Department, [2]Radiology Department, Columbia University, New York, NY, USA.

Background: Harmonic Motion Imaging for Focused Ultrasound (HMIFU) is a recently developed high–intensity focused ultrasound (HIFU) treatment monitoring method. HMIFU utilizes an Amplitude–Modulated (f_{AM}=25Hz) HIFU beam to induce a localized oscillatory motion at its focus, which is simultaneously estimated and imaged by HMI.

Aims: The HMIFU feasibility has previously been shown *in silico*, *in vitro* [1,2], and *in vivo* using both a 1–D and 2–D system for viscoelasticity imaging and monitoring of HIFU treatment. The objective of this study is to develop a new 2–D HMIFU framework with online feedback ability to translate HMIFU towards a clinical setting.

Methods: In this study, a 93–element HIFU transducer (f_{center}=4.5MHz) was used to induce a focal displacement while a coaxially–aligned 64–element phased array (f_{center}=2.5MHz) was operated using a four–board Verasonics ultrasound system for radio–frequency (RF) channel data acquisition and beam–forming. An unfocused transmit sequence was used to perform imaging at 1000 frames/second, in a field of view of 30° with 32 lateral beams. Beamforming was performed using a new method consisting of multiplying a reconstruction matrix by the RF data matrix. The reconstruction matrix is a sparse matrix containing the contribution of each point of the RF data matrix to the points of the beam–formed signals at 80MHz sampling frequency using a delay–and–sum algorithm. Axial HMI displacements were then estimated from the beam–formed RF signals using a 1–D normalized cross–correlation method and streamed to a graphic user interface with a frame rate of up to 5 frames/sec. All the data processing was performed on a Graphical Processing Unit (GPU), and it was shown that the displacement data can be streamed at rate of 1–5 Hz.

Results: A 200ms HMIFU excitation at the acoustic power of 6W was performed in a 15kPa gelatin phantom and a 1 minute ablation monitoring was performed on an *in vitro* canine liver specimen. A focal spot (4mm in axial and 2mm in lateral) at the focusing depth of 7cm was localized, where the HMI displacements estimated in six different locations of the gelatin phantom varied within 47.7±7.4μm. Ablation monitoring also showed a decrease of -2.80±0.32μm after HIFU treatment, indicating the method's capability of estimating and monitoring stiffening in real time.

Conclusion: HMIFU was shown capable of monitoring HIFU ablation based on the associated tissue stiffening in real time. Current ongoing studies include HIFU monitoring in ex vivo canine liver specimens and transgenic pancreatic tumor mice *in vivo*.

Acknowledgements: Supported in part by the NIH R01EB014496.

References:

[1] Maleke C. and Konofagou E.E.: Phys. Med. Biol., Vol. 53, pp. 1773–1793, 2008.
[2] Maleke C and Konofagou EE: IEEE Trans. Biomed. Eng., Vol. 57, pp. 7–11, 2010.

010 **CORTICOMEDULLARY STRAIN RATIO: A QUANTITATIVE MARKER IN ASSESSMENT OF RENAL ALLOGRAFT CORTICAL FIBROSIS.**

Jing Gao[1], Robert Min[1], Jonathan M. Rubin[2], Jun Lee[1], Dadhana Dahdania[1], William Weitzel[2,3].*
[1]Weill Cornell Medical College, 525 East 68th Street, New York, NY 10065, USA; [2]University of Michigan, 1500 Medical Center Drive, Ann Arbor, MI 48109, USA; [3]VA Hospital, Ann Arbor, MI, USA.

Background: In renal transplants, changes in corticomedullary strain may be associated with gradually developing renal cortical fibrosis in chronic allograft nephropathy (CAN), a cause of chronic allograft dysfunction and late transplant graft loss. For estimating kidney hardness in CAN, some normalization method is very useful in improving the reproducibility and accurately of measuring strain. Choosing soft tissue as reference for strain normalization is considered challenging. This is especially true for a transplanted kidney that is usually located between pelvic bones laterally and bladder medially, and surrounded by the bowel. We prospectively assessed an alternative quantitative marker, corticomedullary strain ratio, to assess the cortical fibrosis in renal transplants.

Aims: To assess corticomedullary strain ratio in monitoring cortical fibrosis in renal transplants.

Methods: With Institutional Review Board approval, we prospectively assessed corticomedullary strain ratio in renal allografts with quasi–static ultrasound elasticity imaging (UEI). Written informed consent was obtained from 33 enrolled patients who underwent renal transplant sonography and biopsy from March 2012 to December 2012. We used gentle manual compression similar to deep palpation with the transducer during the ultrasound examination under real time imaging, ensuring the patient remained comfortable during the ultrasound examination. Based on Banff score criteria for renal cortical fibrosis, 33 renal allografts were divided into 2 groups, Group 1 (n=19) with mild (<25%) renal cortical fibrosis and Group 2 (n=14) with moderate (>26%) renal cortical fibrosis. We used two–dimensional speckle–tracking software to perform off–line analysis of strain in the renal cortex and medulla induced by external compression with the ultrasound probe. We used strain in the medulla as reference to normalized renal cortical strain, and then calculated corticomedullary strain ratio (Strain ratio=$Strain_{cortex}$/$Strain_{medulla}$). An unpaired two–tailed t–test was used to determine the differences in strain ratio between the two groups. ROC curve analysis was performed to test the best cutoff value of strain ratio to identify moderate renal cortical fibrosis.

Results: Strain differed between the cortex and medulla (P<0.01). Strain ratio in Group 1 was higher than Group 2 (2.06±1.33 vs 0.70±0.20) (p=0.0007) (Figure 1). The area under ROC curve was 0.964. The sensitivity and specificity of using 0.975 as strain ratio cutoff value to determine a moderate renal cortical fibrosis was 92.9% and 94.7%, respectively.

Conclusions: Medullary strain can be used as reference to normalize renal cortical strain. Corticomedullary strain ratio decreases with increasing renal cortical fibrosis. The change of strain ratio on UEI may improve our non–invasive quantitative markers for monitoring the progression of renal cortical fibrosis following renal transplant.

Reference:

[1] Weitzel et al.: Feasibility of Applying Ultrasound Strain Imaging to Detect Renal Transplant Chronic Allograft Nephropathy. Kidney Int Feb, 65(2), pp. 733–736, 2004.

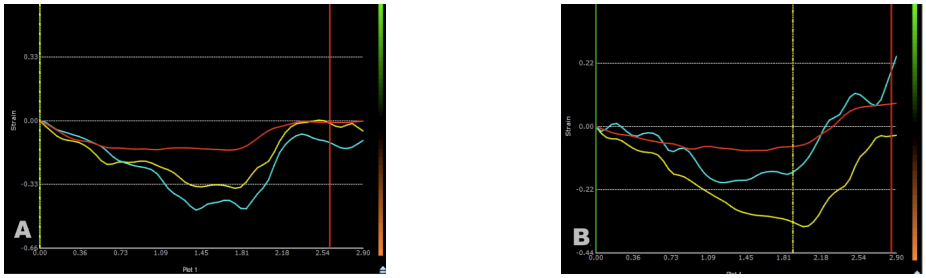

Figure 1: Renal cortical strain (cyan line) and medullary strain (yellow line) are estimated in a case with <5% renal cortical fibrosis in Group 1 (A) and a case with 30% renal cortical fibrosis in Group 2 (B) by using 2–D speckle tracking. The background tissue strain (red line) shows overall compression. The horizontal scale represents fractional strain (multiply by 100 for % strain). One can see the corticomedullary strain ratio is higher in Group 1 than that in Group 2.

* *indicates Presenter*

028 **SINGLE TRACKING LOCATION ARFI ASSESSMENT OF LIVER FIBROSIS PROGRESSION IN A RAT MODEL.**

Etana C Elegbe[1 2], Jonathan Langdon[1,2], Julian Castañeda[1,3], Stephen A McAleavey[1,2].*
[1]Biomedical Engineering Department, University of Rochester, Rochester, NY, USA; [2]Rochester Center for Biomedical Ultrasound, Rochester, NY, USA; [3]Comparative Medicine Department, University of Rochester, Rochester, NY, USA.

Background: As a consequence of the liver's great ability to increase its level of operation in response to the demands of an injury, there is often a significant latent period between the onset of the disease and the clinical symptoms – except in the case of fulminant hepatic failure. At this point however, the disease is usually at an advanced stage and the damage is substantial. Progressive liver fibrosis is a common feature in the majority of chronic liver disease cases [1,2]. Therefore, liver fibrosis stage is considered to be of great prognostic value in the assessment of liver disease [1]. Several studies have shown that there is a connection between the liver tissue mechanical properties and liver fibrosis. Single Tracking Location (STL) ARFI is an elastographic method that estimates shear wave speed, and thus shear modulus, by inducing shear waves in the tissue and tracking its propagation through the region of interest. STL ARFI uses a single tracking line and consequently suppresses speckle–induced biases in the estimates of shear modulus [3]. We investigated the feasibility of Single Tracking Location ARFI as a tool for monitoring and staging the progression of liver fibrosis in an animal model.

Aims: The goal of this work is to demonstrate the feasibility of STL ARFI as a tool in the staging of liver fibrosis *in vivo*. We do this by first successfully inducing liver fibrosis using carbon tetrachloride in an animal model and then monitoring its progression over time. Secondly, we aim to show the correlation between shear modulus measurements made by STL ARFI and the fibrosis stage as assessed by a pathologist and ultimately demonstrate that these measurements can be used to distinguish between normal and fibrotic liver tissue.

Methods: Liver fibrosis is induced in male Sprague Dawley rats via intraperitoneal injections of 1ml/kg of a mixture of 20% carbon tetrachloride in olive oil. The rats are injected three times a week for 9 weeks. The rats in the control group are injected with only olive oil. Two rats each from both the control and diseased groups are imaged twice a week on non–dosing days using a 5.7MHz Siemens Antares linear array ultrasound probe. The rats are anesthetized with a ketamine–xylazine solution. The abdominal region is shaved and depilated to ensure good coupling between the skin and ultrasound probe. The rats are placed in the supine position on a thermal pad and imaged. Ten measurements of the liver tissue shear modulus in a 1cm x 2cm ROI around the transducer focus (2cm) are collected. At the beginning of the following week, blood is drawn from the two rats from the disease group for liver serum tests. After euthanasia, liver samples are then collected and sent to histology for fixing and staining. Blood and liver samples are collected from 2 rats in the control group at the beginning, middle and end of the study. The liver samples are analyzed by a trained pathologist and staged for liver fibrosis using the METAVIR scale.

Results: The shear modulus measurements of the rats in the F0–F3 stages had a mean and standard deviation of 1.23±0.26kPa, 1.90±0.25kPa, 1.76±0.48kPa and 2.69±0.70kPa respectively.

Conclusions: This work demonstrates that STL ARFI can make estimates of liver tissue stiffness in an *in vivo* model. It indicates that this elastographic technique can monitor changes in liver tissue stiffness due to a chronic pathology. These results also suggest the potential for STL ARFI as a tool in the staging of liver fibrosis.

Acknowledgements: This work is funded by NIH grant No. R03 EB016127.

References:

[1] Poynard T, Ngo Y, Perazzo H et al: Prognostic Value of Liver Fibrosis Biomarkers: A Meta–Analysis. Gastroenterol. Hepatol., Vol.7, pp.445–454, 2011.
[2] Massard J, Ratziu V, Thabut D et al.: Natural History and Predictors of Disease Severity in Chronic Hepatitis C. Journal of Hepatology, Vol.44, pp. S19–24, 2006.
[3] Elegbe EC, McAleavey SA: Single Tracking Location Methods Suppress Noise in Shear Wave Velocity Estimation. Ultrasonic Imaging, Vol.35, pp.109–25, 2013.

080 **FEASABILITY OF A NEW TRANSIENT ELASTOGRAPHY EXAMINATION OPTIMIZED FOR SPLEEN STIFFNESS MEASUREMENT.**

C. Bastard[1], D. Festi[2], H. Stefanescu[3], S. Audière[1], L. Sandrin[1], V. Miette[1].*
[1]Echosens, Paris, FRANCE; [2]University of Bologna, Bologna, ITALY; [3]University of Medicine and Pharmacy, Cluj–Napoca, ROMANIA.

Background: Screening for esophageal varices (EV) is recommended in patients with cirrhosis. Indeed, splenomegaly is a common finding in liver cirrhosis, which is the consequence of a portal and splenic congestion with a tissue hyperplasia and fibrosis. These changes might be quantified by transient elastography, which should be a suitable method for the noninvasive evaluation of the presence of esophageal varices. Nevertheless, as the spleen is stiffer than a cirrhotic liver, an optimization of Fibroscan® (Echosens, France) examination is necessary to improve the diagnostic performance.

Aims: The main objective of this study is to evaluate the feasibility and the performances of a new Spleen Stiffness Measurement (SSM) as surrogate noninvasive marker for the presence of esophageal varices in liver cirrhosis patients. This study includes some optimizations (algorithms, depths, shear wave frequency) dedicated to the spleen stiffness assessment.

Methods: The protocol is a multicentric study which will include 300 patients. So far, clinical teams measured spleen stiffness (SSM) by using a research Fibroscan® (FS) platform in 49 consecutive cirrhotic patients who met the inclusion criteria. Patients were also assessed by hepatic venous pressure gradient (HVPG), upper gastroscopy and other biological scores. The dedicated Fibroscan platform generated two transient vibrations (50Hz and 100Hz) at the same measurement point and recorded RF lines. The clinical data obtained at each frequency were reprocessed to apply:

- a Standard Fibroscan Algorithm (SFA) without any modification,
- a Standard Fibroscan Algorithm optimized for spleen depth and stiffness (SFA_optimized),
- a Maximum Likelihood Estimation Algorithm (MLE).

Then, the diagnostic performances were compared.

Results: Intermediate results on 49 patients showed that the new developments for optimizing the SSM are encouraging. The correlation between the grade of EV evaluated by gastroscopy and the MLE result (obtained at 100Hz) was significant (p–value<0,001, Spearman test). Kruskal–Wallis (KW) and Wilcoxon tests showed that MLE and SFA_optimized algorithms were able to discriminate between grade 0 and 3. MLE was also able to discriminate between grade 0 and 2.

Conclusions: The optimization of the Spleen Stiffness Measurement seems encouraging and may increase the diagnostic performance of the Fibroscan® examination to assess the presence and the grades of esophageal varices.

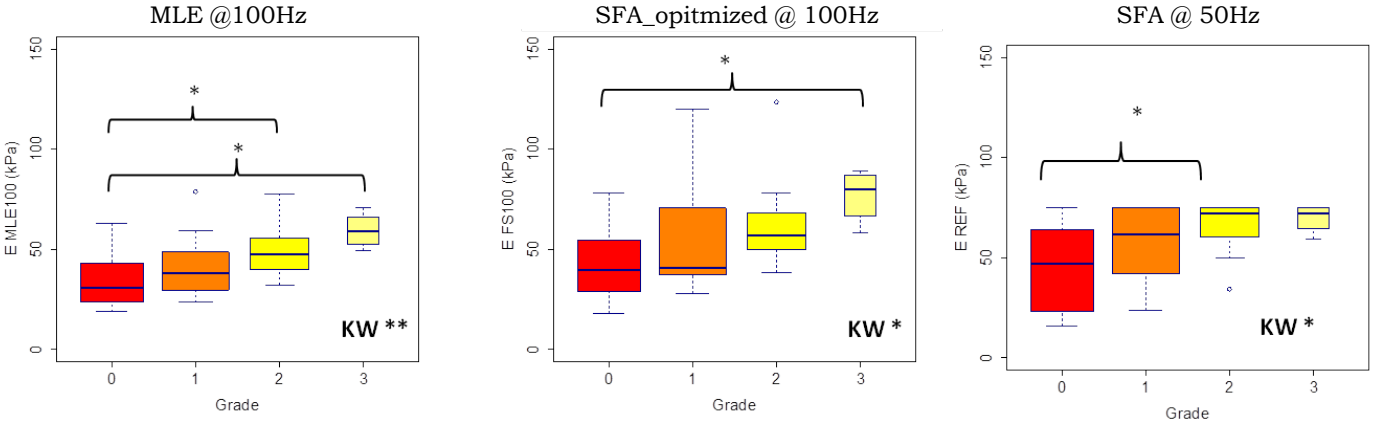

Figure 1: Population independence tested with a Kruskal–Wallis test, and a Wilcoxon test with Bonferroni correction, *:p<0.05, **p<0.01

* *indicates Presenter*

021 **FAST AND TARGETED VISCOELASTIC EVALUATION OF THYROID NODULES: PRELIMINARY *IN VIVO* STUDY.**

Mohammad Mehrmohammadi[1], Pengfei Song[1], Carolina A. Carrascal[1], Matthew W. Urban[1], Matthew. R. Callstrom[1], John C. Morris[1], Shigao Chen[1], James F. Greenleaf[1], Mostafa Fatemi[1], Azra Alizad[1].*

[1]Mayo Clinic College of Medicine, 200 First Street SW, Rochester, MN, 55905, USA.

Background: In 2011, the American Cancer Society reported that the age and gender–adjusted incidence of thyroid cancer has increased faster than that of any other malignancy in recent years. More than 95% of the thyroid nodules are benign and up to 5% may represent intrathyroidal cancers. Conducting biopsies on such a large patient population with benign nodules is a substantial national financial health care burden and is also problematic for patients that undergo biopsy and potentially surgery for benign thyroid nodules. Therefore, the presence of additional complementary diagnostic tools would be important differentiating between benign and malignant nodules.

Aims: In this study, we investigate the feasibility of utilizing two ultrasound–based diagnostic techniques: shear wave dispersion ultrasound vibrometry (SDUV) [1] to quantify both elasticity and viscosity of thyroid nodules and comb–push ultrasound shear wave elastography (CUSE) [2,3] to image elastic properties of thyroid abnormalities and to evaluate the utility of measured parameters to differentiate thyroid nodules in human subjects. SDUV measures shear wave propagation and uses the variation of shear wave speed with frequency, or dispersion, to quantitatively characterize the viscoelastic properties of soft tissue. CUSE is a new shear wave method for fast and robust 2D elasticity imaging. CUSE transmits multiple push beams spaced out like a comb to produce multiple shear wave sources at once so that a 2D full FOV elasticity map can be obtained with only one push–detect acquisition.

Methods: CUSE and SDUV have been implemented on a Verasonics V–1 system (Verasonics, Redmond, WA), which is a fully programmable ultrasound research platform that has 256 independent transmit channels and 128 receive channels. The system is integrated around a software–based beamforming algorithm that performs a pixel–oriented processing algorithm. The performance of the developed CUSE and SDUV techniques were evaluated, in a group of healthy volunteers (n=6) and a group of patients with thyroid abnormalities prior to needle biopsy (n=7). All patient study procedures were conducted according to the protocol approved by Mayo Clinic Institutional Review Board (IRB).

Results: Although further studies on larger population of patients is required to better evaluate the role of the combination of elasticity and viscosity properties of tissue in differentiating various thyroid nodules, our preliminary SDUV results suggests an increase in both shear elasticity (Young's modulus) and shear viscosity in malignant lesions (Figure 1). Therefore, measuring both elasticity and viscosity of thyroid nodules can potentially provide more information for differentiating between benign and malignant nodules. CUSE measurements indicated a clear change in shear wave speed in the regions associated with the nodules compared to the normal background tissue. Moreover, this shear wave speed increment was measured to be much larger in the malignant lesion compared to benign lesions. The latter suggests the potential application of CUSE in human thyroid with large field of view (FOV) and fast frame rate.

Conclusions: Our preliminary results suggest the possibility of gaining a better diagnostic power through measuring viscosity along with elasticity of thyroid nodules. Moreover, the utility of CUSE imaging for human thyroid is demonstrated.

Acknowledgements: This work is supported in part by the grant R01 CA148994 from NIH.

References:

[1] Chen, S., et al.: Shearwave Dispersion Ultrasound Vibrometry (SDUV) for Measuring Tissue Elasticity and Viscosity. IEEE Transactions on Ultrasonics, Ferroelectrics and Frequency Control, 56(1), pp. 55–62, 2009.

[2] Song, P., et al.: Comb–Push Ultrasound Shear Elastography (CUSE): A Novel Method for Two–Dimensional Shear Elasticity Imaging of Soft Tissues. IEEE Transactions on Medical Imaging, 31(9), pp. 1821–1832, 2012.

[3] Song, P., et al.: Comb–Push Ultrasound Shear Elastography (CUSE) with Various Ultrasound Push Beams. IEEE Transactions on Medical Imaging, 2013.

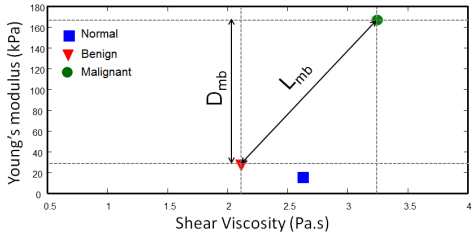

Figure 1: Average Young's modulus (μ_1) vs shear viscosity (μ_2) for normal thyroid, benign and malignant nodules. L_{mb} represents the Euclidian distance between benign and malignant group while D_{mb} represents difference between the respective elasticity's. $L_{mb}>D_{mb}$. This means that the malignant case is farther and hence can be easier discriminated from the benign group if we consider both elasticity and viscosity (L_{mb}) than just the elasticity (D_{mb}) alone.

069 **CROSS–VALIDATION OF ELASTICITY IMAGING USING MAGNETIC RESONANCE ELASTOGRAPHY AND ULTRASOUND SHEAR WAVE ELASTOGRAPHY IN POST–MORTEM MOUSE BRAINS.**

Huan Wee Chan[1,3], Jin Li[1], Craig Cummings[1], Ralph Sinkus[2], Chris Uff[3], Aabir Chakraborty[4], Neil Dorward[3], Simon Robinson[1], Yann Jamin[1], Jeffrey C. Bamber[1].*

[1]Radiotherapy and Imaging Division, Institute of Cancer Research and the Royal Marsden Hospital, Sutton, Surrey, England, SM2 5NG, UK; [2]Imaging Sciences & Biomedical Engineering Division, St. Thomas' Hospital, King's College London, London, England, SE1 7EH, UK; [3]Neurosurgery Department, The National Hospital for Neurology and Neurosurgery, Queen Square, London, England, W1C 3BG, UK; [4]Neurosurgery Department, Southampton General Hospital, Southampton, England, SO16 6YD, UK.

Background: Intra–operative ultrasound shear wave elastography (SWE) has been reported to improve visualisation of brain lesions, specifically epileptogenic lesions, that are subtle or absent on plain magnetic resonance imaging (MRI) [1,2]. Whilst magnetic resonance elastography (MRE) was shown to be a useful pre–operative tool in neurosurgery for predicting tumour consistency [3], ultrasound and magnetic resonance elastography of the brain have never been validated against each other.

Aims: To cross–validate elasticity imaging techniques using MRE and SWE in mouse brains.

Methods: Five anaesthetised nude mice were euthanised with barbiturate via a dorsal tail vein cannula in the scanner prior to MRE acquisition. MRE images were acquired, across 6 coronal planes 300μm apart, with a 7–Tesla microimaging horizontal MRI system (Bruker Instruments, Germany) using 1kHz sinusoidal waves generated by an electromagnetic shaker (Brüel and Kjaer, Denmark) applied to the scalps of the mice. Maps of absolute value of complex shear modulus ($|G^*|$) were reconstructed and mean $|G^*|$ were calculated for an ROI that included the whole brain (Figure 1). For SWE acquisition, performed immediately after MRE, craniotomy was performed to expose the brain prior to imaging with an Aixplorer® (Supersonic Imagine, France) and a 4–15MHz linear array transducer (SL15–4). For each mouse, four coronal section SWE images were acquired and exported to Matlab (The MathWorks Inc., USA) for analysis (Figure 2).

Results: There was good correlation between $|G^*|$ and Young's modulus (YM) (R^2=0.9148), measured with MRE and SWE, respectively (Figure 3), with a slope of the best–fit straight line of about 3.

Conclusions: This preliminary study demonstrated that despite differences in many shear wave properties, brain elasticity measurements made with high resolution MRE correlate well with those measured using clinical SWE, and that $YM \approx 3|G^*|$, as expected for an incompressible medium. With further confirmation, this would appear to demonstrate the potential for combining the methods for neurosurgical planning and intra–operative guidance.

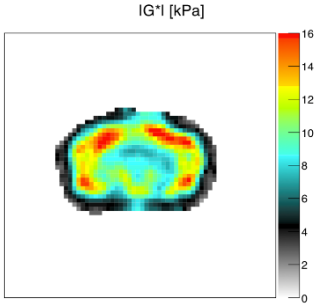

Figure 1: Map of absolute complex shear modulus $|G^*|$ with MRE.

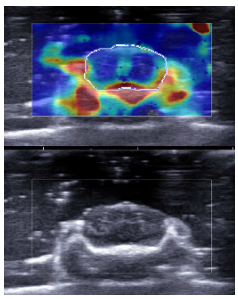

Figure 2: Exported SWE image in Matlab showing freehand selection of region of interest for calculation of YM.

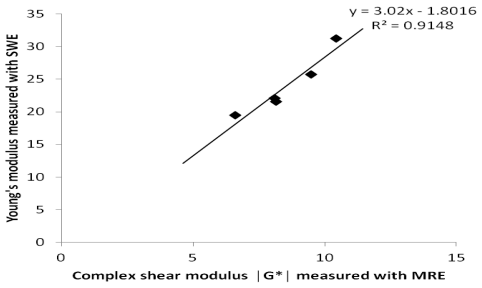

Figure 3: Graph of Young's and absolute shear moduli, measured with SWE and MRE, respectively (the error bars (s.e.m.) are within the size of the markers).

Acknowledgements: This work was supported by a Dorothy Hodgkin Postgraduate Award from the EPSRC, by AstraZeneca, the Institute of Cancer Research and the Royal Free Charity.

References:

[1] Chan HW, et al.: Proc. 11th ITEC, p. 27, 2012.
[2] Chan HW, et al.: Proc. 15th World Congress of Neurosurgery, 2013 (in press).
[3] Murphy MC, et al.: J Neurosurg, 118(3), pp. 643–8, 2013.

* *indicates Presenter*

062 **DYNAMIC OPTICAL COHERENCE TOMOGRAPHY (OCT) BASED AIR JET INDENTATION TO ESTIMATE CORNEAL ELASTIC PROPERTY.**

Li–Ke Wang[1], Jia–Ying Zhang[1,3], Ying Hon[2], Tian–Jie Li[1], Yan–Ping Huang[1], Andrew Lam[2], Yongping Zheng[1].*
[1]Interdisciplinary Division of Biomedical Engineering, [2]School of Optometry, Hong Kong Polytechnic University, Hong Kong, CHINA; [3]Eye Hospital China Academy of Chinese Medical Sciences, Beijing, CHINA.

Background: Corneal elasticity is a key parameter related to the firmness, diopter, even the transparency of cornea, and it is important for distinguishing keratoconus from normal in clinic, especially for keratoconus suspects, considering the severe consequence of keratectasia after corneal refractive surgery. Neither corneal topography nor Pantacam is sensitive enough to pick up such suspects during screening before the surgery. Currently available cornea measurement devices offer corneal elasticity information confounded with the effect of IOP instead of the intrinsic biomechanical property. The material properties of cornea have been evaluated *ex vivo* by inflation tests [1,2], mimicking the change of intraocular pressure (IOP). It is very demanding to have a technology to obtain intrinsic corneal elasticity *in vivo*.

Aims: To develop a dynamic OCT based air jet indentation system to assess the corneal elastic property.

Methods: Based on our earlier study [3], we developed a method to estimate corneal mechanical properties *in vivo* by using air jet indentation (Figure 1). An air pulse with duration of 15ms was generated to deform the cornea at its center location. Meanwhile, OCT was utilized to monitor the dynamic response of the cornea using a transient M–mode with 24000 frames per second of A–line data. The waveforms of air pressure and corneal displacement were recorded to assess the corneal mechanical property. To monitor the test location precisely and conveniently, a CCD camera was added into the probe. Eight silicone phantoms with different elasticity were tested by the system and the results were compared with the result of a traditional indentation test. Corneal elastic property of eight porcine eyeballs was measured under different IOP (ranging from 10–22mmHg) *in vitro* using this system.

Results: The phantom test showed there was a very good correlation between the stiffness values obtained by the current system and the standard indentation test (r=0.996). The mean air jet indentation rate applied on cornea was 30mm/s. The results showed that the porcine corneal stiffness increased with the change of IOP (Figure 2). The initial thickness of porcine cornea was 0.885±0.004mm.

Conclusions: It was demonstrated that it is potential to use the dynamic OCT based air jet system to measure corneal elasticity. In addition, other related parameters of cornea such as initial thickness, corneal deformation and response time were able to be recorded for further analysis. It is important to derive the intrinsic mechanical properties in further studies with the supports from these parameters.

Acknowledgements: This work was partially supported by the Hong Kong Scholar Postdoctoral Fellowship Scheme and National Science Foundation of China Collaboration Scheme (11228411).

References:

[1] Woo SL, et al.: Nonlinear Material Properties of Intact Cornea and Sclera. Exp Eye Res., 14, pp. 29–39, 1972.
[2] Bryant MR, McDonnell PJ: Constitutive Laws for Biomechanical Modeling of Refractive Surgery. J Biomech Eng., 118, pp. 473–481, 1996.
[3] Huang YP, et al.: An OCT–Based Air Jet Indentation System for Measuring Mechanical Properties of Soft Tissues. Meas Sci Tech., 20, p. 1, Article No. 015805, 2009.

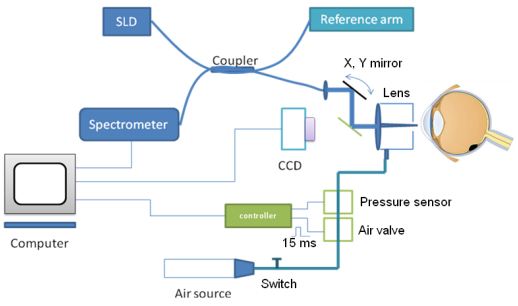

Figure 1: A schematic of OCT based air jet indentation system.

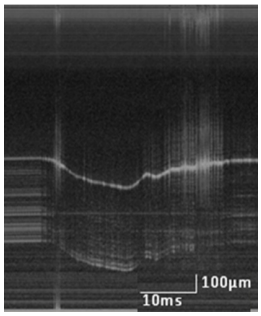

Figure 2: A typical M–mode image.

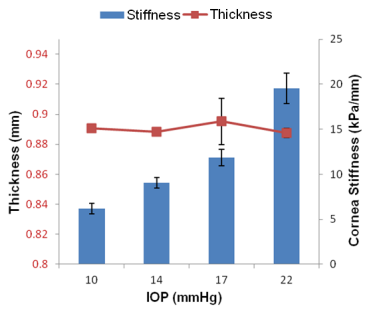

Figure 3: Results of porcine eyeballs *in vitro*.

012 **INVESTIGATING THE EFFECT OF CROSS–LINKING ON THE MECHANICAL PROPERTIES OF PORCINE CORNEAS BY INFLATION TEST.**

Sara Matteoli[1], Antonio Virga[1], Iacopo Paladini[2], Rita Mencucci[2], Andrea Corvi[1].*
[1]Industrial Engineering Department, University of Florence, via di S. Marta 3, 50139, Florence, ITALY;
[2]Medicine and Translational Surgery Department, Eye Clinic, University of Florence, Largo Brambilla 3, 50134, Florence, ITALY.

Background: Corneal cross–linking (CXL) is a clinical technique used to stiffen the corneal tissue using riboflavin (as a photo–sensitizer) and UV–A radiation to increase the formation of covalent intra– and inter–fibrillar by oxidation [1]. This technique is used as a photodynamic treatment of keratoconus, a non–inflammatory corneal dystrophy (usually bilateral) with a frequency of 0.05% in the population. It is a disease characterized by a progressive thinning and ectasia of the stroma, which translates into a conical shape of the cornea resulting in severe visual impairment, which leads to cornea transplantation in approximately 20% of patients [2]. To date, CXL is considered less invasive and much less expensive than corneal transplant. Several studies have reported that CXL may delay or stop progression of keratoconus by improving corneal shape and producing a better quality of vision [3].

Aims: The purpose of the present work was to evaluate the effect of CXL on corneal mechanical characteristics by inflating porcine corneas. All tests were carried out thanks to an experimental apparatus designed for this survey. In particular it has been evaluated the elastic modulus of the corneal tissue to changes in intraocular pressure (up to 80kPa).

Methods: Among the 39 eyes investigated, 14 were subjected to standard CXL (370nm, 3mW/cm^2, 30 minutes) and 25 used as a control sample. The thickness was measured for all corneas through a system Visante OCT, before and immediately after treatment (for cross–linked corneas) and before the inflation test. The latter was performed on corneas stored for 48 hours in a physiological solution. During the tests the intraocular pressure and the radial displacement of the apical cornea were measured. Then, stress–strain curves as well as the elastic modulus, calculated as the slope of the same curves in the ranges of 2–3kPa and 40–60kPa, were evaluated by applying the shell theory.

Results: The investigation on corneal thickness showed a significant reduction (up to 34%) immediately after CXL (P–value<0.001). Stress–strain curves showed a typical behavior of mainly collagen tissues, with an initial phase characterized by high deformability, followed by a phase of stiffening at about 0.5kPa. Statistical analysis showed that the elastic modulus of treated corneas (163±21kPa) calculated in the range of 2–3kPa was significantly higher (P–value=0.001) than that of controls (100±41kPa) with an average increase of about 37%. The same significant increase (P–value<0.001) of the elastic modulus was found in the range of 40–60kPa, with a mean of 3744±518kPa for corneas subjected to CXL and 2590±503kPa for controls, and an average increase of about 31%.

Conclusions: In this study CXL increased corneal stiffness up to 37%. This result is in agreement with previous studies [4,5], which showed a pressure–apical displacement trend similar to that of the present study. Inflation test has proven to be a valuable tool for the investigation of the cornea biomechanics, ensuring the corneal tissue integrity.

References:

[1] F. Raiskup, E. Spoerl: Corneal Crosslinking with Riboflavin and Ultraviolet A. I. Principles. Ocul Surf., 11(2), pp. 65–74, 2013.
[2] S. Hayes, et al.: A Study of Corneal Thickness, Shape and Collagen Organization in Keratoconus using Video Keratography and X–Ray Scattering Techniques. Exp Eye Res, 84(3), pp. 423–434, 2007.
[3] I.M. Beshtawi, et al.: Biomechanical Properties of Corneal Tissue after Ultraviolet–A Riboflavin Crosslinking. J Cataract Refract Surg., 39(3), pp. 451–462, 2013.
[4] S. Kling, et al.: Corneal Biomechanical Changes after Collagen Cross–Linking from Porcine Eye Inflation Experiments. Invest Ophthalmol Vis Sci., 51(5), pp. 3961–3968, 2010.
[5] F. Bao, et al.: Assessment of the *Ex Vivo* Biomechanical Properties of Porcine Cornea with Inflation Test for Corneal Xenotransplantation. J Med Eng Technol, 36(1), pp. 17–21, 2012.

Figure 1: Porcine eye and cornea

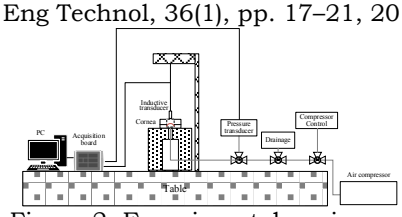

Figure 2: Experimental equipment

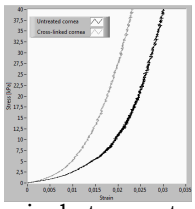

Figure 3: Typical stress–strain curves

* *indicates Presenter*

065 **COMPARISON BETWEEN CRAWLING WAVE SONOELASTOGRAPHY AND STL–ARFI IN BIOMATERIALS.**

Juvenal Ormachea[1], Arthur Salo[2], Amy Lerner[2], Steve McAleavey[2], Benjamin Castaneda[1]*
[1]Pontificia Universidad Católica del Perú, Av. Universitaria 1801, San Miguel, Lima, PERU; [2]University of Rochester, 252 Elmwood Ave., Rochester, NY, 14627, USA.

Background: Crawling Wave Sonoelastography (CWS) and Single Tracking Location Acoustic Radiation Force Impulse (STL–ARFI) are elastographic techniques that estimate the shear wave speed (SWS) generated from mechanical vibration forces or acoustic radiation force (ARF) respectively. Both techniques have been validated independently in tissue mimicking phantoms and soft tissue. However there is a lack of comparison among different techniques in the literature.

Aim: To compare the performance of CWS and STL–ARFI in the estimation of shear wave speed in biomaterials against mechanical measurements (MM).

Methods: Homogeneous elastic and viscoelastic phantoms were made of 10% and 16% gelatin (300 Bloom). Viscoelastic phantoms included 15% castor oil. Measurements using CWS, STL–ARFI and MM were performed at a constant internal temperature phantom. In CWS, two mechanical vibration sources were used to generate crawling waves between 140–360Hz. The method described in [1] was used to estimate the SWS. For STL–ARFI, the method described in [2] was used. Pushing pulses were located 2.1mm apart, and the tracking beam was 1.8mm away. The SWS of the region between the pushing pulses was estimated by cross–correlating the velocity data to attain the arrival time difference. The power spectral density (PSD) is used to estimate the frequency range of STL–ARFI. To compare the estimations of CWS and STL–ARFI, a linear fit was applied to extend the values obtained by CWS [3]. Stress relaxation tests were performed on three samples of each phantom and fit to a Kelvin–Voigt Fractional Derivative (KVFD) model following the methodology in [4]. These MM were considered as ground truth.

Results: Figure 1 shows the SWS maps for the same scanned viscoelastic phantom calculated by (a) CWS and (b) STL–ARFI. The PSD obtained in STL–ARFI indicated a frequency range of 400–1000Hz with a peak at 500Hz. CWS works on a frequency range between 140–360Hz. Figure 2 shows the comparison of the three methods in a range between 140–500Hz.

Conclusions: The experimental results of the three methods are highly congruent, suggesting CWS and STL–ARFI are imaging methods that can be reliably used to investigate viscoelastic properties of biomaterials. CWS and STL–ARFI operate at different and complementary range of frequencies. Moreover, the results of this study contribute to the limited data currently available for comparison of elastographic techniques.

Acknowledgements: This project was supported by Marco Polo Award from PUCP. The authors would like to thank Kevin Parker, Ph.D. for his help and technical support.

References:

[1] Z. Hah, K.J. Parker: Integration of Crawling Waves in an Ultrasound Imaging System. Part 2: Signal Processing and Applications. Ultrasound in Med. & Biol., Vol. 38, pp. 312–323, 2012.
[2] E.C. Elegbe, S.A. McAleavey: Single Tracking Location Methods Suppress Speckle Noise in Shear Wave Velocity Estimation. Ultrason Imaging., Vol. 35, pp. 109–25, 2013.
[3] C.T. Barry, K.J. Parker: Shear Wave Dispersion Measures Liver Steatosis. Ultrasound in Med. & Biol., Vol. 38, pp. 175–182, 2012.
[4] M. Zhang, K.J. Parker: Congruence of Imaging Estimators and Mechanical Measurements of Viscoelastic Properties of Soft Tissues. Ultrasound in Med. & Biol., Vol. 33, pp. 1617–1631, 2007.

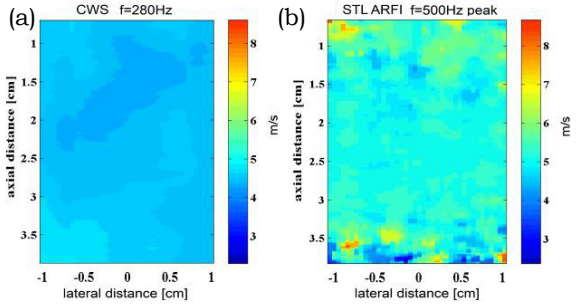

Figure 1: SWS maps estimated with (a) CWS and (b) STL–ARFI.

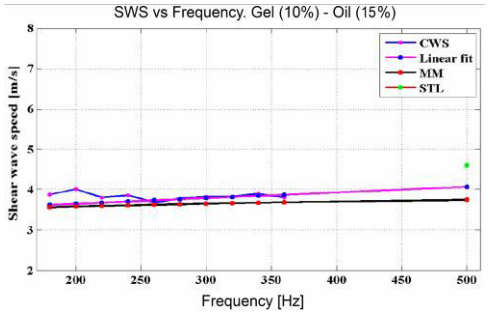

Figure 2: Comparison plot of CWS, STL–ARFI, MM.

* *indicates Presenter*

068 **FINITE ELEMENT ANALYSIS OF SHEAR WAVE PROPAGATION IN SOFT MEDIA WITH PLATE–LIKE GEOMETRY IN A RIGID CONTAINER**

Ramona De Luca[1,2], Jérémie Fromageau[1], Elí Elyas[1], Franco Marinozzi[2], Jeffrey C. Bamber[1].*
[1]Institute of Cancer Research and Royal Marsden Hospital, 15 Cotswold Road, Belmont, Sutton, Surrey, SM2 5NG, England, UK; [2]Mechanical and Aerospace Engineering Department, Sapienza University of Rome, via Eudossiana 18, 00184, Rome, ITALY.

Background: We wish to study shear–like wave propagation in gel layers with a view to understanding the potential of eventually providing a microelastography tool to explore cellular mechanobiology in three–dimensional (3D) cell cultures. This is being done both experimentally, using an optical coherence elastography (OCE) technique [1], which measures the speed of waves generated by a vibrating needle embedded in the gel layer and using finite element (FE) methods. FE methods have already been used to study the propagation of Rayleigh and Lamb waves in thin plate–like samples with free–boundaries, and excellent agreement with analytical theory was found [2]. A more practical situation for 3D cell cultures, however, is when the gel is adhered to a rigid container and is only free at its upper boundary. For this more complex geometry, no analytical solution exists.

Aims: To construct an FE model of a plate–like gel adhered to a rigid plastic base and, using this, to investigate the potential of the above–mentioned OCE method to measure local shear modulus.

Methods: The FE model to simulate OCE experiments was created in MARC/Mentat (MSC Software, Santa Ana, CA, USA). It consisted of a gel plate in a rigid plastic container and a load applied by a shaker coupled with a needle that vibrated through the thickness of the sample. The shaker was excited by a sine–wave burst of five cycles with the central frequency in the range 25–600Hz. To determine the resulting time–varying displacements of the medium, a transient dynamic analysis was carried out and an implicit solver was employed. To reduce computation time, it was assumed that the problem can be modeled using a two–dimensional plane strain formulation. Thus far, the material has been assumed to be purely elastic (no damping) and nearly incompressible (Poisson's ratio is 0.49), with a density of 1000kg/m^3 and a Young's modulus in the range from 1000–25000Pa, according to values measured experimentally in gels. In order to estimate the wave speed, the Akaike information criterion (AIC) method [3] was used to determine pulse time–of–arrival from the time–varying displacement at several points in the middle of the plate. The wave speed was analyzed as a function of three parameters, vibration frequency, gel plate thickness and gel shear modulus. FE simulation results for free–boundary thin layers were also obtained, and compared with the analytical solution, as a validation for the FE model before studying the layer on the rigid substrate.

Results: For the simulated OCE experiment, i.e. with the gel layer on the rigid substrate, good agreement was found between the numerical wave speed estimated using the AIC method and the experimental speed, for example, for a Young's modulus in the range 1.5–12kPa, a gel thickness of 5mm and a vibration frequency of 500Hz, the correlation between the two was 0.99, and the speeds were linearly related with a slope of about 1.1. These preliminary results suggest that simulation is correctly modelling the experimental wave propagation.

Conclusions: The FE model developed, which contains realistic experimental boundary conditions for studying cell cultures, simulates the elastic behavior of a plate–like gel layer on a rigid substrate, providing information useful to understand the range of applicability of, and improve the effectiveness of, the OCE system. It is possible to evaluate the impact of the following factors on the ability to measure the local shear modulus: the effect of the rigid base, the gel thickness, the Young's modulus and the vibration frequency. Further work will be undertaken to do this.

References:

[1] Elyas E, Erler J, Robinson SP, Cox T, Bamber JC: Potential for Quantitative Micro–Elastography using a Multi–Channel Optical Coherence Method. Proc IEEE Ultrasonics Symposium, pp. 2567–2570, Oct. 7–10 2012.
[2] Nenadic IZ, Urban MW, Aristizabal S, Mitchell SA, Humphrey TC, Greenleaf JF: On Lamb and Rayleigh Wave Convergence in Viscoelastic Tissues. Phys Med Biol., 56(20), pp. 6723–6738, 2011.
[3] Li C, Huang L, Duric N, Zhang H, Rowe C: An Improved Automatic Time–of–Flight Picker for Medical Ultrasound Tomography. Ultrasonics, 49, pp. 61–72, 2009.

** indicates Presenter*

078 **A SIMPLE STRAIN MEASUREMENT TECHNIQUE THAT UTILIZES PHOTON ATTENUATION.**

Tareq Alrefae[1].*
[1]Kuwait University, Khaldia, KUWAIT.

Background: Strain is an important quantity in determining elasticity of materials. Knowledge of the amount of elongation or shortening of materials provides key markers that help in assessing its intactness and viability. In addition to being widely available, techniques for strain measurements are diverse. For example, elastography which is applied in biomedical applications utilizes sonogram techniques in determining strain measurements [1]. Another example is that of strain gauges which rely on the sensitivity of electrical properties to changes in length. More examples are found in the literature [2]. To further enrich the library of strain measurement techniques, this work presents a simple method that relies on basic radiation measurements. Specifically, the presented method utilizes photon attenuation, which is described by the following formula [3].

$$I = I_0 e^{-\mu l}$$

Equation (1)

In Equation (1), I_0 is the number of photons striking a sample of length l, I is the number of photons emerging without having interacted in the sample, and μ is the material dependent attenuation coefficient. When this relation is coupled with the normal strain (ε) equation, it becomes easy to theoretically relate strain and radiation intensity, resulting in Equation 2.

$$\varepsilon = \frac{ln\left(\frac{I_0}{I_2}\right)}{ln\left(\frac{I_0}{I_1}\right)} - 1$$

Equation 2

In Equation (2), I_1 and I_2 are the number of photons emerging without having interacted in the sample at lengths l_1 and l_2, respectively.

Aims: The goal of this work is to develop a simple method to measure strain utilizing the radiation feature of photon attenuation.

Methods: Computer simulations that mimic the set–up in Figure 1 are performed. Programming is done using the C++ based GEANT4 toolkit [4], which utilizes Monte Carlo methods to simulate the passage of photons through matter. For better statistics, a relatively large number ($\geq 10^5$) of incoming mono–energetic photons are emitted by the simulated point source, where each photon is tracked throughout its journey. A typical photon journey starts with an emission by the point source and ends with an absorption by, or an escape from, the detector. When a photon reaches the detector, it interacts with its material by one of two modes. The first mode, photoelectric absorption, results in a full energy deposition by the photon inside the detector. The other mode of interaction, Compton scattering, results in a partial energy deposition, after which the photon leaves the detector. A histogram of energy deposition is produced as an output for the simulation. From this output, the number of escaping, non–interacting photons is revealed, after which Equation (2) is applied to calculate the strain.

Results: Figure 2 shows the ratio of the simulated strain to the theoretical strain ($\varepsilon_{sim}/\varepsilon_{th}$), approaching unity as the length of sample increases. Such behavior suggests the validity of the proposed technique for samples with sufficient size. Hence, this size cannot be less than the photon mean free path (λ), which is a function of sample material, and the energy of the photon.

Conclusions: The ability of the proposed technique in measuring strain is demonstrated with computer simulations. The next step is to test this technique experimentally.

References:

[1] Ophir J, Cespedes I, Ponnekanti H, Yazdi Y, Li X: Elastography: A Quantitative Method for Imaging the Elasticity of Biological Tissues. Ultrason Imaging, 13, pp. 111–34, 1991.
[2] Bower AF: Applied Mechanics of Solids. CRS Press, Boca Raton, FL, 2010.
[3] Knoll GF: Radiation Detection and Measurement. Wiley, New York, 2000.
[4] Agostinelli, S., et al.: GEANT4 A Simulation Toolkit. Nuclear Instruments and Methods in Physics Research A, 2003.

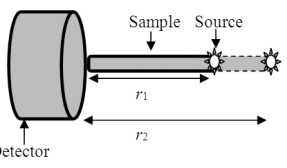

Figure 1: Simulated apparatus.

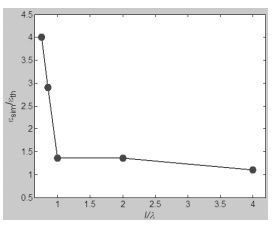

Figure 2: The ratio of simulated strain to theoretical strain ($\varepsilon_{sim}/\varepsilon_{th}$), plotted against sample length (l) in units of photon mean free path (λ).

079 **INVESTIGATION OF A GOLD STANDARD PHANTOM AND MEASUREMENT TECHNIQUE TO ESTIMATE ELASTIC PROPERTIES IN ELASTOGRAPHY.**

Jennifer Oudry[1], Ted Lynch[2], Jonathan Vappou[3], Laurent Sandrin[1], Véronique Miette[1].*
[1]Echosens, Paris, FRANCE; [2]CIRS Inc., Norfolk, Virginia, USA; [3]ICube, CNRS–Université de Strasbourg, Strasbourg, FRANCE.

Background: The development and validation of novel medical imaging modalities based on ultrasound, magnetic resonance, or optics are essential procedures in order to provide clinicians with optimal tools for improving diagnosis and patient monitoring. There is a growing interest in the clinical use of elastographic techniques for both qualifying and quantifying the mechanical properties of soft tissues, in particular in terms of their elastic properties. To this end, ultrasound elastographic phantoms are essential in establishing a set of standards to allow comparisons of these types of systems, evaluate system dependencies and for operator training.

Aims: The goal of this work was to show if there is differences in the evaluation of the elastic properties of phantoms performed by different techniques.

Methods: The shear wave speed and the Young's modulus of Zerdine® material were investigated using three measurement technologies: a common mechanical technique (dynamic mechanical analysis (DMA)) and two elastographic techniques based on shear wave propagation, transient elastography (TE) and shear wave induced resonance (SWIR). In DMA test, the Young's modulus *(E)* was calculated from the complex Young's modulus *(E^*)*. In TE technique, the shear wave speed and Young's modulus were directly measured. In SWIR technique, the Young's modulus was deduced from the magnitude of the complex shear modulus *(G^*)*. Phantoms were assumed to be incompressible, homogeneous, isotropic and linearly elastic. Four tissue–mimicking material formulations were tested with a Young's modulus (*E)* given by the manufacturer ranging between 2–62kPa.

Results: The Young's modulus and the shear wave speed obtained with each studied technique were compared at 50Hz. A statistical study was carried out to evaluate the agreement between measurement methods. As shown in Figure 1, the bias values, estimated by comparing results with known values given by the manufacturer, reached up to 40% depending on the phantom stiffness and the technique used. *t*–test was also performed between techniques; a significant difference was found in the evaluated shear wave speed and Young's modulus means with the different measurement methods.

Conclusions: Results suggest a bias in elastic property measurement which varies with systems. Results highlight the difficulty in finding a reference method to determine and assess the elastic properties of tissue–mimicking materials. The difficulty lies, not only in the choice of the measurement technique, but also in the creation of a gold standard elastography phantom, with its elastic properties and its manufacturing process fully controlled. Thus, there is a clear need to continue to develop elastographic techniques to achieve a consensus in the elastic properties estimation of tissues.

Acknowledgements: The authors thank Anis Hadj Henni from Rheolution Inc., Montréal, Canada for his technical support on the hyper–frequency viscoelastic spectroscopy technique.

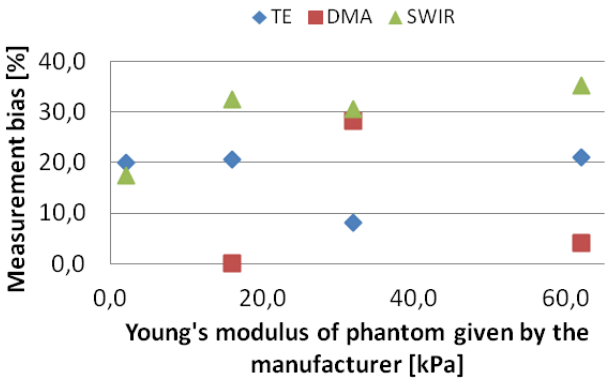

Figure 1: Measurement bias. Resulting Young's modulus at 50Hz were compared to known values given by the manufacturer.

* *indicates Presenter*

030 **PERFOMANCE EVALUATION OF RHEOLOGICAL MODELS APPLIED TO LOCAL CHARACTERIZATION OF BIOMIMETIC MATERIALS IN A CREEP TEST EXPERIMENT.**

Belfor Galaz[1], Rodrigo Acevedo[1].*
[1]Physics Department, University of Santiago of Chile, 3493 Av. Ecuador, Estación Central, Santiago, CHILE.

Background: The use of single (two viscoelastic cells) and continuous (two distributions of viscoelastic cells) bimodal rheological models for a full characterization of viscoelastic behavior of biomimetic materials when are subject to constant stress (creep–test) has been evaluated in a 1D ultrasonic experiment [1]. The implementation to 2D and use as elastography–based diagnostic tool could be limited by the processing time of the curve–fitting process and the noisy characteristics of strain–time curves of soft tissues in clinical conditions [2].

Aims: The goal of this study is to evaluate the performance of different rheological models in terms of the physical description of the time dependency of viscoelastic properties of biomimetic materials and processing time in an ultrasonic imaging creep experiment.

Methods: The experimental setup consists of a water immersion chamber with the biomimetic sample (liquid–saturated polyurethane sponge) placed vertically between the ultrasound probe (Terason 12L5–V) and the load system which is activated by an Arduino platform connected to the ultrasound machine Terason T3000 Advanced (Teratech Corporation, USA). The rf–data are acquired for at least 1 hour. Relative displacement images are computed by a multilevel coarse–to–fine 2D block–matching algorithm, and the corresponding axial strain images are calculated in a cumulative way. The Levenberg–Marquardt method implemented in an open source Matlab–executable C/C++ code (Levmar) is used in the curve–fitting of the models. This process is improved through the control of the damping coefficient and the updating of the model parameters by using the neighbor solutions (good estimates) as an initial guess.

Results: The figure shows the fast characteristic time constant (TC1 in seconds) and determination coefficient (r^2) of the application of the single and continuous bimodal model of Kelvin–Voigt cells to sponge with a circular inclusion (pore–density ratio ~1.03) (pixels in white correspond to mean correlation values bellow 0.85). Apart from some differences in the top region, the TC1 image for the continuous model is homogeneous. The B–mode image shows no inclusion and axial strain (ASE) image (for the last frame) shows only the inclusion background interface.

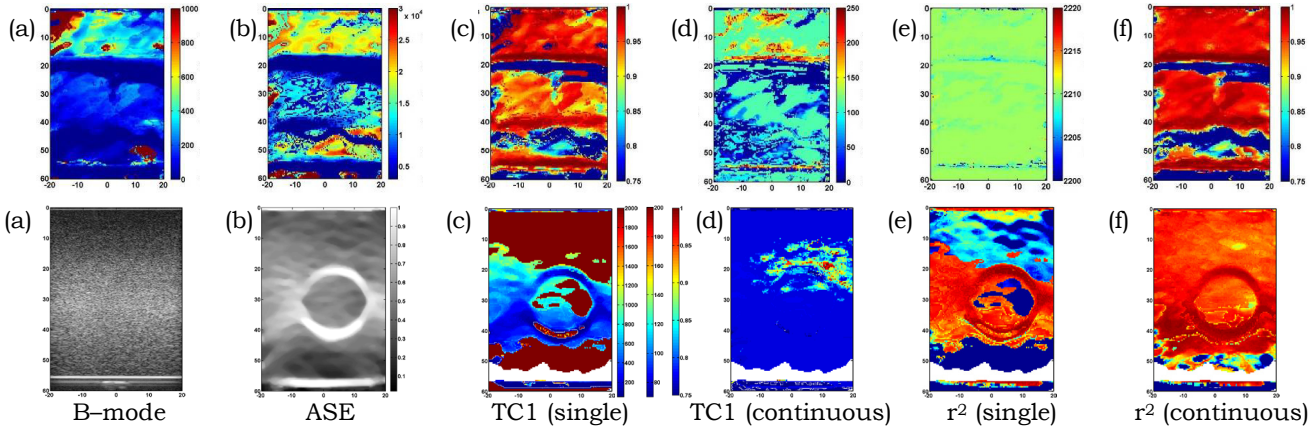

Conclusions: The continuous model appears to be more robust than the single model probably due to the statistical character of the continuous model with an increment in the time processing about 3 times. Study of the relation between the rheological fitted parameters and the poroelastic properties is still necessary.

Acknowledgements: This work is supported by the Fondecyt Initiation project No. 11110289, Chile, PBCT project PSD–54, Chile.

References:

[1] J. J. Ammann, R. Rivera, J. Ophir: Rheological Modeling of the Time–Dependant Behavior of Poroelastic Materials under Creep Test Experiments. Proc. of 5th ITEC, Snowbird, Utah, USA, p. 36, 2006.
[2] S. P. Nair, et al.: Performance Analysis of a New Real–Time Elastographic Time Constant Estimator. IEEE Transactions on Medical Imaging, Vol. 30, No. 2, pp. 497–511, 2011.

** indicates Presenter*

055 **SHEAR WAVE DISPERSION MEASUREMENTS ON TISSUE–MIMICKING PHANTOM AND *EX–VIVO* HUMAN BRAIN.**

Emmanuel Nicolas[1], Samuel Callé[1], Redouane Ternifi[1], Emmanuel Simon[1], Jean–Pierre Remenieras[1].*
[1]UMR Inserm U930, Université François Rabelais, 37032 Tours, FRANCE.

Background: Brain elastography has been recognized as being a promising diagnostic tool. A disease like Alzheimer's slowly replaces normal brain tissue with plaques and neurofibrillary tangles which affect the mechanical properties of cerebral tissue [1].

Aims: Based on results obtained using MRE [2], we propose to test the feasibility of measuring mechanical properties using plane shear wave propagation in a tissue–mimicking phantom using an ultrafast ultrasound imaging system synchronized with an electromechanical actuator. The results are compared to two other rheological methods. The method is then tested on *ex–vivo* human brains.

Methods: The excitation signal used to generate the plane shear wave along the x axis with the actuator has a Gaussian–like waveform. The ultrasound data are recorded along the z axis using Aixplorer (SSI, France) with a 2.8MHz linear probe with 128 elements (custom designed for brain exploration) at a PRF of 5kHz. For each subsample volume along x axis (parallel to the array aperture) at a given depth z, particle velocity $V_z(x,t)$ of the shear wave is estimated using tissue Doppler algorithm with an observation window of 8 samples with 75% overlap, giving a temporal resolution of 0.4ms. The method used to measure phase velocity and attenuation coefficient uses a multi–frequency strategy in the bandwidth 10–150Hz; a 2D frequency–domain approach, using spatial FFT$_s$ of $V_z(x,\omega)$ i.e., $V_z(k_x,\omega)$ is used to estimate the real part of the wave number and least square minimization of log $|V_z(x,\omega)|$ is used to get attenuation. From there, we estimate the complex shear modulus using well–known relations. The measurements are repeated for multiple depths z, allowing a statistically relevant result. Those results are then compared to measurements made with the Rheospectris instrument (Rheolution, Canada), and with classical rheometer coupled with high–frequency rheometer. *Ex–vivo* measurements were conducted, assuming homogeneity of studied areas.

Results: The method discussed here has been validated for the measurement of viscoelastic properties of homogenous phantoms. The values are obtained with a good precision (phase velocity 1.32±0.04m.s^{-1} and attenuation coefficient 52±3Np.m^{-1} at 80Hz). Complex shear modulus is compared between the three methods in Figures 1 and 2. Measurements are in good agreement; we observe similar dispersion evolution, and less than 20% differences overall. *Ex–vivo* measurements conducted on human encephalon give promising results; velocity and attenuation are estimated with the same precision as before. Attenuation is noticeably higher than the phantom. Storage and loss modulus are presented in Figure 3 and 4, for a small area of white matter in a single encephalon. The data can be fitted with a fractional model $K\omega^{\gamma}$.

Conclusions: The plane wave method presented gives good results, given the small error between the different methods. It also gives promising results on real brain tissue. The principal limitation is the homogeneity assumption, which is being addressed in current work by the development of a local inversion algorithm.

Acknowledgements: The authors would like to thank the IFSTTAR (Lyon, France) laboratory for the measurements on the classical rheometer, as well as the anatomy department of the Tours university for the *ex–vivo* encephala.

References:

[1] M.C. Murphy et al.: JMRI, 34, pp. 494–8, 2011. [2] I. Sack et al.: NMR in Biomedicine, 21, pp. 265–71, 2008.

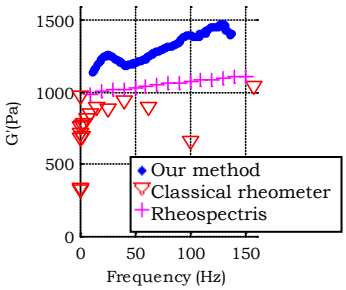

Figure 1: Storage modulus comparison

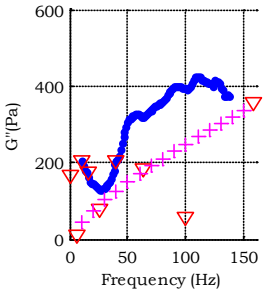

Figure 2: Loss modulus comparison

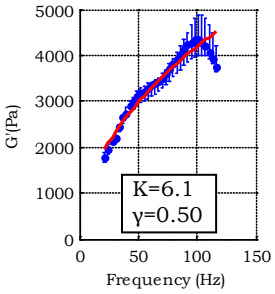

Figure 3: *Ex–vivo G'*

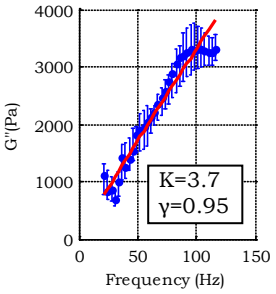

Figure 4: *Ex–vivo G''*

* *indicates Presenter*

027 **OPTICAL COHERENCE ELASTOGRAPHY.**

S Wang[1], J Li[1], S Aglyamov[2], S Emelianov[2], MD Twa[1], KV Larin[1,3].*
[1]University of Houston, Houston, TX, USA; [2]University of Texas, Austin, TX, USA; [3]Baylor College of Medicine, Houston, TX, USA.

Background: Mechanical forces play an important role in the behavior and development at all spatial scales, from cells and their constituents to tissues and organs. Such forces have a profound influence on the health, structural integrity and normal function of cells and organs. Accurate determination of tissue biomechanical properties (e.g., Young's or shear modulus) could help with clinical diagnosis and interpretation of various diseases.

Aims: Optical Coherence Elastography (OCE) is an emerging tool that allows noninvasive assessment of tissue biomechanical properties with high lateral and axial resolution. Here we assessed capability of OCE to quantify very small (micrometer–amplitude) surface mechanical wave propagation in different tissues, including tumors and ocular tissues both *ex vivo* and *in vivo* using a Phase Stabilized Swept Source Optical Coherence Elastography (PhS–SSOCE) system (Figure 1).

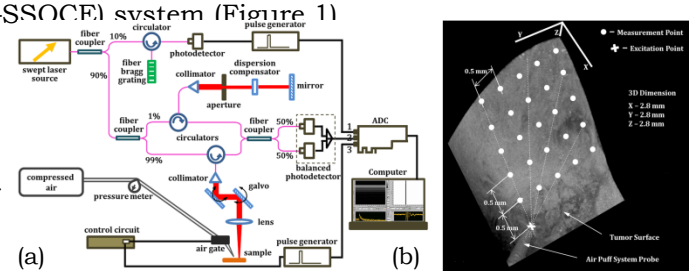

Figure 1: (a) Schematic of PhS–SSOCE system; (b) OCT 3–D image indicating the distribution of excitation and measurement positions across tissue surface.

Methods: Low–amplitude (<10μm) mechanical waves were introduced by focused air puff excitation on tissue surface. Human normal fat and surrounding myxoma tissues were obtained after planned surgical interventions at MDACC. *In vivo* experiments were performed with mice cornea of different ages.

Results: The tissue of myxoma, a type of soft–tissue tumor, turns out to have higher velocity of surface wave (SW) propagation than the normal fat, which can be seen from Figure 2. The SWs group velocity is calculated to be 1.45±0.28m/s and 1.02±0.33m/s for myxoma and normal fat, respectively. Also, we quantified a higher Young's modulus of 7.6±3.0kPa for myxoma compared with 3.5±2.2kPa for normal fat (see Figure 3). *In vivo* experiments with mice cornea of different ages demonstrated that stiffness of the cornea increases with the age from 1–18 months old (as it would normally be expected).

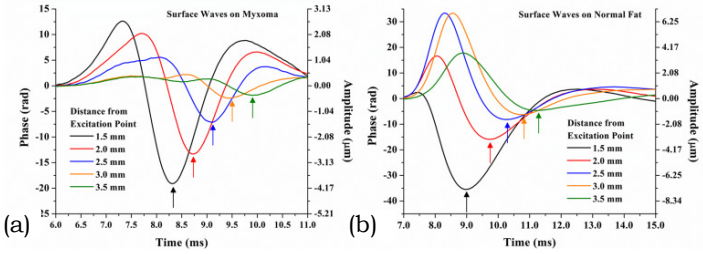

Figure 2: Surface waves recorded at different spatial locations showing time delays detected on (a) myxoma and (b) normal fat.

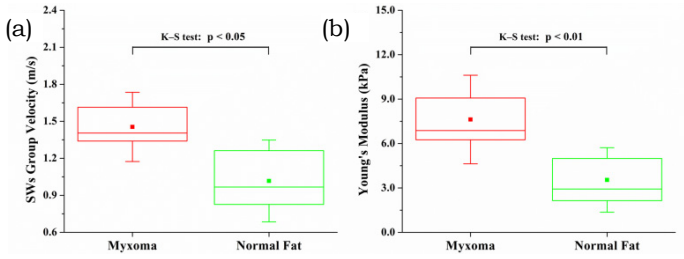

Figure 3: Box plots of (a) the calculated group velocity of SWs and (b) the quantified Young's moduli for myxoma and normal fat. The solid dots and whiskers represent the mean values and standard deviations of data, respectively.

Conclusions: These results demonstrate the OCE system can be useful for the intra–operative detection of soft tissue tumors based on the measurement of their elastic properties. Also, this noninvasive, non–contact measurement technique involves low–force methods of tissue excitation that potentially can be used to assess the biomechanical properties of ocular and other delicate tissues *in vivo*.

Acknowledgements: We acknowledge the funding from NIH grant 1R01EY022362 and Federal Target Program "Scientific and Scientific–Pedagogical Personnel of Innovative Russia" for 2009–2013 Grant 14.B37.21.1238.

* *indicates Presenter*

064 **CRAWLING WAVE SPEED ESTIMATION BASED ON DOMINANT COMPONENT ANALYSIS AM–FM DEMODULATION.**

Renán Rojas[1], Juvenal Ormachea[1], Arthur Salo[2], Paul Rodríguez[1], Amy Lerner[2], Kevin J. Parker[2], Benjamin Castañeda[1].*

[1]Pontificia Universidad Católica del Perú, Av. Universitaria 1801, San Miguel, Lima, PERU; [2]University of Rochester, 252 Elmwood Ave., Rochester, NY, 14627, USA.

Background: Crawling Waves (CrW) were introduced in [1] to quantify tissue elasticity by the shear wave speed caused by two sources oscillating at slightly different frequencies. Shear wave speed was initially estimated by Time of Flight and LFE approaches. In [2], the overall speed for a region of interest is estimated by applying a cosine fit and a cross optimization process. In [3], real–time local speed is estimated via the analytical signal autocorrelation by using a 1–D kernel along the propagation dimension and its relationship with the phase function spatial derivative. Techniques for amplitude and phase demodulation of an analytical signal modeled as a single tone or a sum of harmonics (AM–FM) have been proposed for a variety of medical tasks with high quality results [4,5].

Aims: To estimate the shear wave speed by recovering the dominant signal across frames from a CrW cine loop and estimating the instant spatial frequency along the propagation dimension for the entire projection set using AM–FM techniques.

Methods: (1) A Dominant signal across frames is restored from the ultrasound data by rejecting oscillatory corruptions using a 30–channel Gabor filter bank. (2) A 15–channel Gabor filter bank Dominant Component Analysis [4] is applied to the analytical recovered signal along the propagation dimension, followed by a discrete Quasi–Eigenfunction Approximations [4] demodulation to estimate instant frequency. The large number of channels is due to the fact that no frequency *a–priori* information is considered. Simulations replicating the data high frequency variations and oscillatory corruptions are performed. 10%, 13% and 16% gelatin phantom experiments covering homogenous regions and inclusions are also performed for frequencies between 200–360 Hz.

Results: Results are coherent with the mechanical measurements of homogeneous phantoms, and inclusion shapes are preserved with high contrast. Figure 1 describes the speed estimation mean±st. dev. in contrast with mechanical measurements for a homogeneous phantom. Figure 2 describes the speed estimation for an inclusion phantom. Both results are based on 16% gelatin phantoms.

Conclusions: Accurate shear wave speed estimations under different scenarios are obtained. However, in order to define its applicability, a detailed comparison with the state of the art methods is pending. Finally, since the method focuses on estimating instant frequencies, its framework is a general approach which may be extended to different model dimensions and modalities.

References:

[1] Z. Wu, et al.: Sonoelastographic Imaging of Interference Patterns for Estimation of Shear Velocity Distribution in Biomaterials. The Journal of the Acoustical Society of America, Vol. 120, No. 1 pp. 535–545, 2006.

[2] M. Zhang, et al.: Congruence of Imaging Estimators and Mechanical Measurements of Viscoelastic Properties of Soft Tissues. Ultrasound in Medicine & Biology, Vol. 33, No. 10, pp. 1617–1631, 2007.

[3] K. Hoyt, et al.: Two–Dimensional Sonoelastographic Shear Velocity Imaging. Ultrasound in Medicine & Biology, Vol. 34, No. 2, pp. 276–288, 2008.

[4] J. Havlicek: AM–FM Image Models. PhD dissertation, University of Texas at Austin, 1996.

[5] V. Murray, et al.: Survey of AM–FM Methods for Applications in Medical Imaging. Ibero–American Conference on Trends in Engineering Education and Collaboration, 2009.

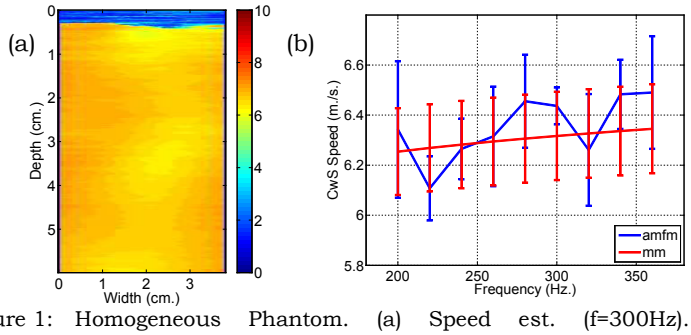

Figure 1: Homogeneous Phantom. (a) Speed est. (f=300Hz). (b) Mean and Std. dev. contrast between AM–FM and M.M.

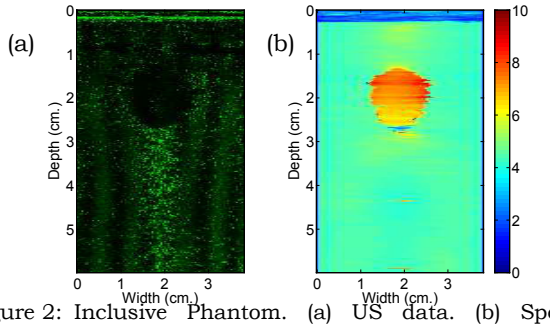

Figure 2: Inclusive Phantom. (a) US data. (b) Speed estimation (f=360Hz).

* *indicates Presenter*

066 **COMBINING AXIAL MEAURES TO ESTIMATE 3D MOTION OVER AN ULTRASOUND VOLUME.**

JM Abeysekera[1], M Honarvar[1], SE Salcudean[1], R Rohling[1].*
[1]Univeristy of British Columbia, Vancouver, BC, CANADA.

Background: Shear modulus estimation from measured displacement is best performed by measuring all three components over a volume. Measuring only one displacement component over a volume can change elasticity estimates by up to 60% compared to 1D motion over a plane [1]. Plain–strain motion reduces the need for 3D measurements, but out–of–plane motion will cause significant errors [2]. A few representative samples of the literature on measuring additional displacement components include beam steering [3], synthetic aperture [4] or intersecting linear array scans [5]. We propose to combine axial measurements from different 4D transducers scanning the same volume from different angles, or, alternatively, a single tracked 4D transducer sequentially scanning a volume from different angles.

Aims: To solve for 3D motion vectors from three volumes of axial motion measurements and to study the effects of scan conversion, interpolation, and calibration on the displacement and elasticity estimates.

Methods: A 300Hz harmonic excitation of a 40×40×40mm^3 cube with a 5mm radius stiff sphere was modeled in FEM. Three volumes were modeled using the geometry of a 4DL14–5/38 transducer (Vermon, Tours, France) and rotated about the center of the cube in 120° increments. A long term goal is to apply this transducer and geometry clinically as a 3D elastography breast cancer system. Time–varying axial displacement measurements were generated by projecting the FEM solution onto the axial directional cosines of each image slice. Zero mean Gaussian noise was added with variance equal to the Cramér–Rao lower bound for partially decorrelated speckle [4]. The overlapping volumes were mapped to a global coordinate system and displacement vectors were found by solving a least squares problem involving a matrix of axial directional cosines and the axial measurements, similar to beam steering methods [3]. Elasticity estimates were obtained by solving a direct, dynamic displacement–pressure FEM inverse problem with sparsity regularization [5]. To simulate calibration error, axial measurements were assumed to have been rotated around a random axis by angle $\Delta\theta$, and shifted by a random vector of magnitude Δt.

Results: The motion field is shown in Figure 1. Elasticity error increases slowly as calibration error increases (Figure 2). The elasticity error without calibration error is caused by inaccuracies in the forward and inverse models, discretization and the three interpolation steps: from FEM mesh to regular grid, image to volume and local to global coordinates. Elasticity error is higher at interfaces of different elasticity, caused by elements crossing the interface representing elasticity with a single value (Figure 3).

Conclusions: The method can reliably solve for dynamic 3D displacement vectors suitable for elasticity estimation. The error in elasticity increases by ~3% for a typical level of calibration error.

Acknowledgements: This work is supported by the Natural Sciences and Engineering Research Council of Canada.

References:

[1] A. Baghani et al.: Proc. MICCAI, pp. 617–624, 2012.
[2] M.M. Doyley: Phys. Med. Biol., Vol. 57, pp. R35–R73, 2012.
[3] U. Techavipoo et al.: IEEE Trans. Med. Imaging, Vol. 23, No. 12, pp. 1479–1489, 2004.
[4] C. Sumi: IEEE Trans. Ultrason. Ferroelectr. Freq. Control, Vol. 55, No. 1, pp. 24–43, 2008.
[5] M. Muller et al.: Proc. IEEE Ultrason. Symp., pp. 672–675, 2007.
[6] W.F. Walker and G.E. Trahey: IEEE Trans. Ultrason. Ferro. Freq. Control, Vol. 42, No. 2, pp. 301–308, 1995.
[7] M. Honarvar et al.: Phys. Med. Biol., Vol. 57, pp. 5909–5927, 2012.

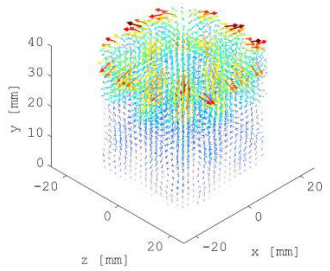

Figure 1: The real part of the displacement phasor vector field solved using three axial measurements with simulated calibration error of 1mm and 3°.

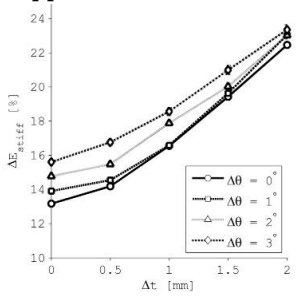

Figure 2: Percent error in elasticity in the stiff inclusion for various levels of calibration error, averaged over 50 trials at each point.

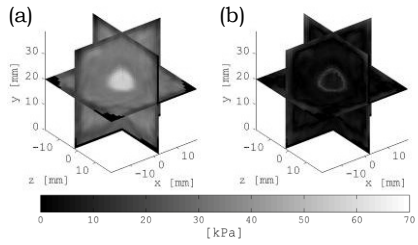

Figure 3: (a) Elasticity estimates using the displacement in Figure 1, and (b) the differences between estimated and true values.

073 **INFERRING STROMAL MICROSTRUCTURE PROPERTIES VIA NONLINEAR ELASTICITY IMAGING.**

Elizabete Rodrigues Ferreira[1], Tengxiao Liu[2], Paul E. Barbone[3], Assad A. Oberai[2], Timothy J. Hall[4].*
[1]University of Minnesota, Minneapolis, MN, USA; [2]Rensselaer Polytechnic Institute, Troy, NY, USA; [3]Boston University, Boston, MA, USA; [4]University of Wisconsin–Madison, Madison, WI, USA.

Background: Breast cancer and other solid tumors are often associated with a desmoplastic reaction, resulting in abnormal fibrous tissue density and microstructure. Second harmonic images (SHG) [1] of breast tissue have revealed that the collagen fiber bundles in healthy glandular tissue are significantly coiled. In benign tumors, they become less coiled, while in malignant tumors they are almost straight and rod–like. It has also been observed that an increasingly invasive phenotype is accompanied by an increase in the concentration of collagen fiber bundles. Altered microstructure in turn leads to altered macroscopic mechanical properties. For example a higher concentration of collagen implies a larger linear elastic modulus, and a decrease in tortuosity would mean a smaller "toe" region in the stress–strain curve [2].

Aims: The aim of this work is to use nonlinear elasticity imaging to recover the microstructural properties of tissue in order to improve medical diagnosis of cancer.

Methods: We use homogenization theory [3] to develop new nonlinear microstructure–based, macroscopic hyperelastic models for biological tissue that contain fiber bundle concentration and tortuosity as parameters. Then, we used these models in conjunction with nonlinear elasticity imaging in order to reconstruct the spatial distribution of the macroscopic tissue parameters from which the averaged microstructural properties of tissue are inferred. Finally, we used displacement measured in benign and malignant tumors to investigate the spatial distribution of recovered microstructural parameters in those tumors.

Results: The new microstructure–based model demonstrates that the crimped collagen fiber bundles observed in healthy tissue have a different macroscopic response when compared to the straight rod–like bundles observed in cancerous tissue as illustrated in the stress–stretch curves below. It is found that the fiber bundle concentration determines the initial elastic modulus, and the fiber bundle tortuosity determines the strain at which the departure from a linear stress–strain behavior takes place. Measured displacement from 10 patients (5 FA and 5 IDC) is used in order to reconstruct the spatial distribution of the macroscopic tissue parameters from which the averaged microstructural properties of tissue are inferred. Preliminary results indicate that fiber bundle tortuosity holds the potential of being able to diagnose cancerous tumors. Indeed, we found out that fiber tortuosity is higher for FA than for IDC (see figures below).

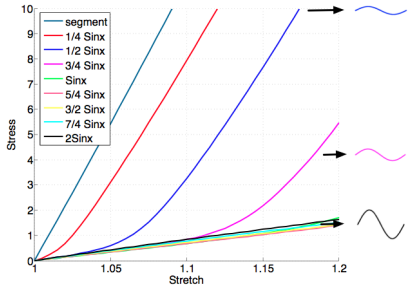

Tortuosity: 1.06 FA

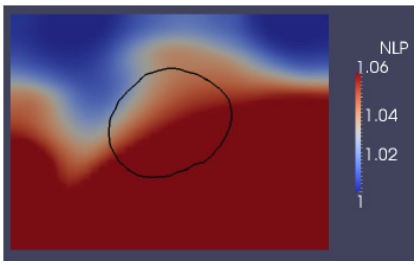

Tortuosity: 1.01 (IDC1)

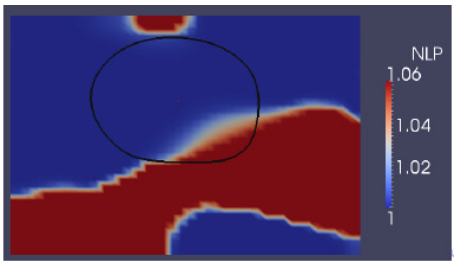

Conclusions: In this study, new constitutive models for collagenous tissue that account for the density and curvature of collagen fibers are developed and implemented in an inverse framework developed by the group in order to determine the spatial distribution of the macroscopic parameters within the tissue, which are directly linked to the average microstructural properties.

Acknowledgements: Support from the NIH (NCI–R01CA140271) and the NSF (Grant No. 50201109) is acknowledged.

References:

[1] G. Falzon, S. Pearson, R. Murison: Analysis of Collagen Fiber Shape Changes in Breast Cancer. Physics in Medicine and Biology, 53, pp. 6641–6652, 2008.
[2] K. Garikipati, S. Göktepe, C. Miehe: Elastica–Based Strain Energy Functions for Soft Biological Tissue. Journal of the Mechanics and Physics of Solids, 56(4), pp. 1693–1713, 2008.
[3] C. Miehe, J. Schröder, M. Becker: Computational Homogenization Analysis in Finite Elasticity: Material and Structural Instabilities on the Micro– and Macro–Scales of Periodic Composites and Their Interaction. Computer Methods in Applied Mechanics and Engineering, 191, pp. 4971–5005, 2002.

* *indicates Presenter*

044 **CELLULAR DISPLACEMENT ESTIMATION USING MITOCHONDRIA IMAGES.**

D. Thomas Seidl[1], Elizabeth Canović[2], Assad A. Oberai[3], Paul E. Barbone[1], Dimitrije Stamenović[2], Michael L. Smith[2].*

[1]Mechanical Engineering Department, [2]Biomedical Engineering Department, Boston University, MA 02215, USA; [3]Mechanical Aerospace and Nuclear Engineering Department, Rensselaer Polytechnic Institute, Troy, NY 12180, USA.

Background: Quantification of cytoskeletal deformation and motion at intracellular length scales is of interest in a number of applications, including measuring cellular mechanical properties. Previously displacement estimates have been acquired by tracking 0.5μm fluorescent microbeads within a cell subjected to an applied deformation. These measurements, along with estimates of cellular traction forces [1] have been used to solve an inverse problem for the mechanical properties of the cell [2]. There are numerous disadvantages to using microbeads as fiducial markers for displacement. First, there are no available means to control the distribution of the beads within a cell, and they at most cover 10% of the total cell area. Secondly, the beads are not always firmly anchored to the cytoskeleton and in some cases are actively transported by cellular machinery. Hence, some bead motion is not consistent with cytoskeletal deformation, introducing error beyond that due to measurement noise. Finally, (and most importantly) the presence of a large number of these beads is damaging to the health (and by plausible extension mechanical properties) of the cell. Another approach is to acquire images of cellular mitochondria and use image registration to estimate displacement. This technique alleviates many of the disadvantages mentioned above, as the mitochondria are immobile, populate a significant portion of the cell, and the fluorescent labeling process has a small to negligible effect on cellular health.

Aims: We aim to evaluate estimates of cellular displacement by finite element based image registration techniques applied to mitochondria stained images.

Methods: NIH3T3 fibroblasts were cultured on soft gel substrates composed of 7.6kPa polyacrylamide. A regular grid (2μm spacing) of fluorescent Alexa–633 (Molecular Probes) dots containing fibronectin was stamped on the gel using soft lithography techniques [1]. The cell binds tightly to these dots and does not otherwise attach to the substrate. A 200nM solution of MitoTracker Green FM (Invitrogen) was applied to the cells to label the mitochondria. Finite element based image registration [3] was used to estimate displacement arising from a known imposed rigid body motion. Fluorescent images were acquired with an Olympus IX81 microscope with x60 water (1 NA) objective and a Hamamatsu Orca R2 camera controlled with Metamorph software.

Results: We were able to compute cellular displacement at least as well as bead tracking methods over a larger region of the cell. Figure 2 implies that displacement estimates at resolutions on the order of 2μm are precise to 0.05μm.

Conclusions: Our results suggest that deformation measurements obtained from mitochondria images are a viable alternative to the use of cytotoxic microbeads.

Acknowledgements: We gratefully acknowledge support from NSF CBET grant 1150467, an Innovation Career Development Professorship from Boston University, NHLBI Grant HL–096005, NCI–R01CA140271 and NSF SI2 grant 1148111.

References:

[1] S. R. Polio, K. E. Rothenberg, D. Stamenović and M. L. Smith: Acta biomaterialia, 8, pp. 82–88, 2012.
[2] E. P. Canović, D.T. Seidl, S.R. Polio, A.A. Oberai, P.E. Barbone, D. Stamenović and M. L. Smith: Biomech Model Mechanobiol, in review, 2013.
[3] M. S. Richards, P.E. Barbone, and A. A. Oberai: Physics in Medicine and Biology, 54.3, p. 757, 2009.

Figure 1: Microbeads

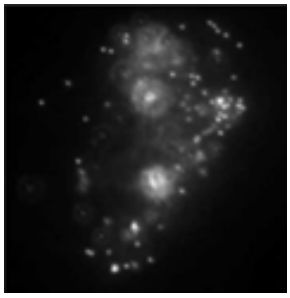

Figure 2:

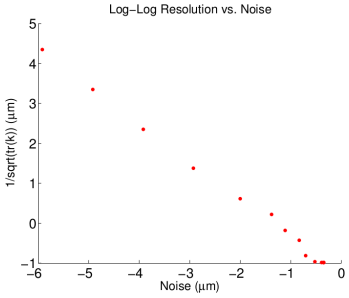

Figure 3: Mitochondria

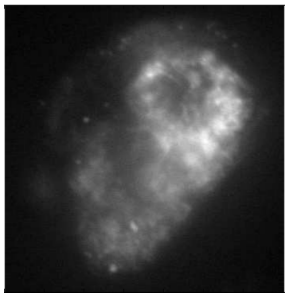

* *indicates Presenter*

082 **QUANTITATIVE ASSESMENT OF SOFT EMBALMED HUMAN CADAVERS WITH ULTRASOUND SHEAR WAVE ELASTOGRAPHY.**

Joyce, Joy[1], Nhan Lee1, Christine Demore[1], Li Cui[1], Shilpa Munirama[2], Sarah Vinnicombe[1], Roos Eisma[1], George Corner[2], Graeme McLeod[2], Sandy Cochran[1].*

[1]University of Dundee, Dundee, Angus, Scotland, UK; [2]Ninewells Hospital & Medical School, Dundee, Angus, Scotland, UK.

Background: A successful development in medical simulation is the use of Thiel–embalmed cadavers, developed by Professor Thiel of the University of Graz, Austria [1]. The use of these soft embalmed cadavers has proven extremely beneficial for training and development of a number of interventional procedures such as ultrasound guided regional anesthesia [2] and laparoscopy [3]. However, there remains a need to quantitatively measure the tissue properties to ensure the validity of imaging, including with elastography.

Aims: The principal aim of this study was to measure tissue elasticity of soft embalmed human cadavers, validated with a known human cohort. A secondary aim was to analyze stiffness against parameters such as gender, age at death and number of days of embalming (DoE).

Methods: With ethical permission, six soft–embalmed cadavers were imaged with ultrasound. Using shear wave elastography, two independent raters undertook 10 repeated measurements of Young's modulus at various sites of interest selected as their stiffness profile is already known *in vivo* [4]. Cadavers were scanned supine using a 4–15MHz linear array transducer (R3.2 Supersonic Imagine, France). Data analysis was performed with the IBM SPSS (Version 20.0, NY, USA) software and NCSS (UT, USA).

Results: (1) Apart from the gastrocnemius muscle, all other tissues correlated well with the *in vivo* data. (2) DoE affected tissue elasticity, signifying that hardening is a function of time during the soft–embalming process. (3) A lack of significant correlation between the age of the cadaver at death and tissue elasticity agrees with findings *in vivo*. (4) It was found that tissues from female cadavers had higher elasticity values than their male counterparts.

Conclusions: We have measured quantitative data demonstrating that soft–embalmed cadavers provide a useful model for evaluation of new ultrasound imaging techniques. This is likely to be of particular use for training and development of interventional techniques such as elastography assisted UGRA, which are not amenable to *in vivo* volunteer access.

Acknowledgements: We would like to express our sincere gratitude to SUPA INSPIRE for funding this work.

References:

[1] Thiel W.: Die Konservierung Ganzer Leichen in Natűrlichen Farben. [The Preservation of the Whole Corpse with Natural Color.]. Ann Anat, 174, pp. 185–95, 1992.

[2] McLeod G, Eisma R, Schwab A, Corner G, Soames R, Cochran S: An Evaluation of Thiel–Embalmed Cadavers for Ultrasound–Based Regional Anaesthesia Training and Research. Ultrasound, 18, pp. 125–9, 2010.

[3] Giger U, Fresard I, Hafliger A, Bergmann M, Krahenbuhl L: Laparoscopic Training on Thiel Human Cadavers: A Model to Teach Advanced Laparoscopic Procedures. Surgical Endoscopy, 22, pp. 901–6, 2008.

[4] Arda K, Ciledag N, Aktas E, Aribas BK, Kose K: Quantitative Assessment of Normal Soft–Tissue Elasticity using Shear–Wave Ultrasound Elastography. AJR American Journal of Roentgenology, 197, pp. 532–6, 2011.

** indicates Presenter*

061 **MAPPING VISCOELASTIC PROPERTIES USING ACOUSTIC RADIATION FORCE**

Mikako Gomyo[1], Kengo Kondo[2], Makoto Yamakawa[3], Tsuyoshi Shiina[1].*
[1]Human Health Sciences Department, Graduate School of Medicine, Kyoto University, Kyoto–City, Kyoto, JAPAN; [2]Center for the Promotion of Interdisciplinary Education and Research, Kyoto–City, Kyoto, JAPAN; [3]Advanced Biomedical Engineering Research Unit, Kyoto–City, Kyoto, JAPAN.

Background: Elasticity and viscosity are important properties of tissue. Numerous methods for measuring and mapping elasticity have been studied and published. However, there is no optimal method for displaying high or low viscosity, though several studies (e.g., [1]) have attempted to map the viscosity distribution.

Aims: This experiment seeks to clearly map viscoelastic properties. A continuous line of acoustic radiation force is used to reduce acquisition time compared to insonification and acquisition by generating a shear wave over a broader area.

Methods: A 10% gelatin phantom with a buried 1% agarose cylindrical inclusion (8mm diameter) is measured using modified a supersonic shear wave imaging system (Supersonic Imagine, Aixplorer, Aix–en–Provence, France). The linear ultrasound probe has 128 elements with a central frequency of 7.5MHz and a frame rate of 5kHz. The region of interest (ROI) is 25.6mm wide and 29.6mm high (Figure 1). Pushing pulses are emitted at every five scan lines, and 32 images are averaged to obtain high quality images of viscoelaatic properties. The phase shift of the generated shear waves is measured to obtain the shear wave speed. Repeating this operation every 10Hz from 100–300Hz yields a shear wave speed graph with frequencies on the abscissa and speeds on the ordinate. This graph is fitted to the Voigt model formula expressed in [2] by the Newton method to evaluate the coefficients of shear elasticity and shear viscosity. Calculating every coordinate value enables mapping these coefficients.

Results: Figure 2 presents the coefficient of shear elasticity, and Figure 3 presents that of shear viscosity. The boundary between gelatin and agarose is recognized clearly in each figure. The mean values of the gelatin phantom (agarose inclusion) obtained by this experiment are a shear elasticity of 5.2kPa (11.1kPa) and a shear viscosity of 0.67Pa·s (4.43Pa·s). The values of shear elasticity measured by mechanical method are 4.8kPa (12.9kPa). It is validated that there is a good correlation between them.

Conclusions: Our method could create a clear and optimal picture of viscosity and elasticity. One remaining problem is acquiring 32 images to obtain the average, which takes about two minutes. Most of the time is spent dealing with for transporting data. In this study, although we thought much of the acquisition of a clear map than the time required, In future work, we will realize real–time processing for imaging with maintaining image quality and conduct experiments on biological tissues and clinical data.

References:

[1] Chia–Lun Yeh, Yae–Lin Sheu, Po–Ling Kuo, and Pai–Chi Li: Tissue Shear Viscosity Measurements using a Spectral Ratio Method. IEEE Trans. Ultrason. Ferroel. Freq. Control, pp. 2555–2558, 2012.
[2] Y. Yamakoshi, J. Sato, and T. Sato: Ultrasonic Imaging of Internal Vibration of Soft Tissue under Forced Vibration. IEEE Trans. Ultrason. Ferroel. Freq. Control, Vol. 17, No. 2, pp. 45–53, 1990.

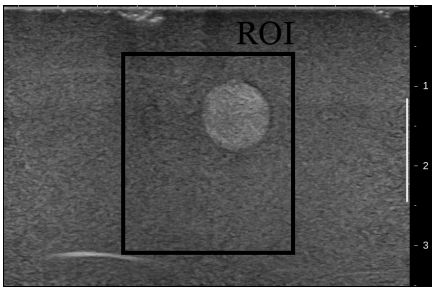

Figure 1: B–mode with ROI

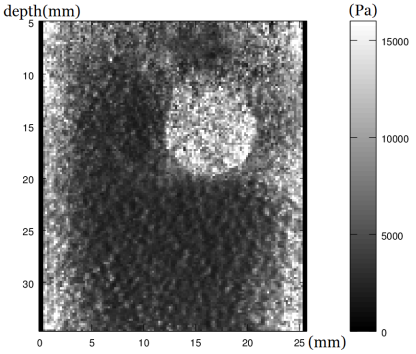

Figure 2: Shear elasticity

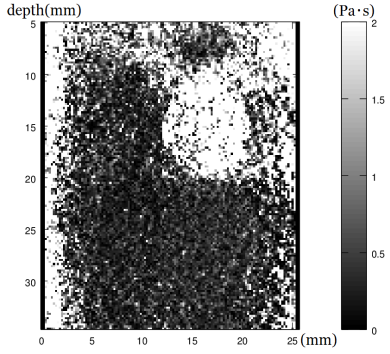

Figure 3: Shear viscosity

Lingfield Park Conference Center Floor Plan

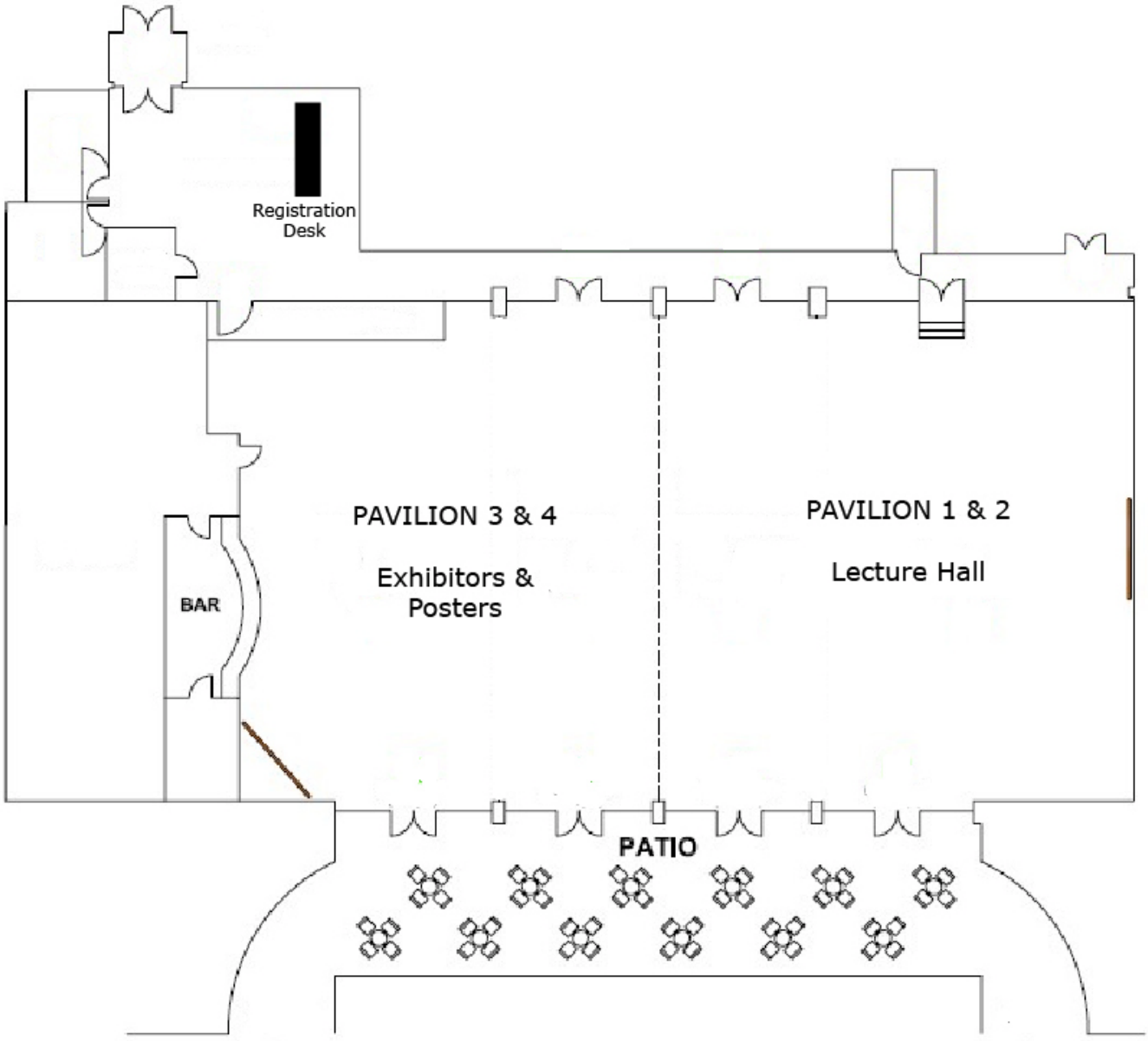

Please Fill Out Both Sides

Conference Evaluation and Questionnaire

OVERALL CONFERENCE

	Poor		Mid		**Excellent**
Overall Conference Evaluation	1	2	3	4	5
General comments/suggestions:					

SCIENTIFIC PROGRAM

	Poor		Mid		**Excellent**
Quality of the Presentations	1	2	3	4	5
Relevance of Presentations to the Conference's Theme	1	2	3	4	5
Time Allotted for Presentations	1	2	3	4	5
Time Allotted for Discussion	1	2	3	4	5
Poster Session	1	2	3	4	5
Tutorials	1	2	3	4	5
Short Presentation Category	1	2	3	4	5
Student Participation	1	2	3	4	5
Equipment Exhibit	1	2	3	4	5
Additional comments/suggestions:					

CONFERENCE MATERIALS

	Poor		Mid		**Excellent**
Printed Proceedings Book	1	2	3	4	5
CD Proceedings	1	2	3	4	5
Other Registration Materials	1	2	3	4	5
CD only or Printed Proceedings Book and CD	CD Only		Proceedings Book and CD		
Additional comments/suggestions:					

CONFERENCE FACILITIES AND SOCIAL PROGRAMME

	Poor		Mid		**Excellent**
Lecture Hall	1	2	3	4	5
Registration Desk	1	2	3	4	5
Meals: Dining facilities	1	2	3	4	5
Conference Lunches	1	2	3	4	5
Conference Dinner and Entertainment	1	2	3	4	5
Coffee Breaks	1	2	3	4	5
Opening Dinner Reception	1	2	3	4	5
Closing Dinner Reception	1	2	3	4	5
Audio–Visual: Screen Visibility	1	2	3	4	5
Sound Level	1	2	3	4	5
Presentation Transition	1	2	3	4	5
Internet Connectivity:	1	2	3	4	5
Additional comments/suggestions:					

Please Fill Out Both Sides

Conference Evaluation and Questionnaire

VENUE AND HOTEL

	Poor		Mid		**Excellent**
Venue: Lingfield, UK and Environs	1	2	3	4	5
Would you return to this city?	Yes		Perhaps		No
Area Attractions	1	2	3	4	5
Hotel: Overall	1	2	3	4	5
Reservations	1	2	3	4	5
Transportation and Accessibility	1	2	3	4	5
Reception and Check–In	1	2	3	4	5
Accommodations	1	2	3	4	5
Facilities	1	2	3	4	5
Parking	1	2	3	4	5
Would you return to this hotel?	Yes		Perhaps		No
Additional comments/suggestions:					

CONFERENCE ADMINISTRATION

	Poor		Mid		**Excellent**
Website	1	2	3	4	5
Registration off–site	1	2	3	4	5
Registration on–site	1	2	3	4	5
Administrative staff	1	2	3	4	5
Correspondence	1	2	3	4	5
Additional comments/suggestions:					

GENERAL INFORMATION

I am a Returning Delegate	Yes		No
I plan to attend the next conference in 2014	Yes	Perhaps	No
and present a paper(s) / poster(s)	Yes	Perhaps	No
Other(s) from my lab would attend the next conference	Yes	Perhaps	No
and he/she / they would present a paper(s) / poster(s)	Yes	Perhaps	No
How did you learn of this conference? (Check all that apply)	☐ Email Announcement		
☐ Internet	☐ Website		
☐ Other	☐ Colleague		
Tutorial Topic Suggestions for next year:			
Additional Comments/suggestions:			

If you would be willing to host the Conference in your city, please give your name to the Conference Staff.
Questions or comments are welcome at any time at <secretariat@elasticityconference.org>
Thank You!